Data for the Ariel space mission and other exoplanet applications 1 Data availability and requirements relevant for the Ariel space mission and other exoplanet atmosphere applications

Katy L Chubb, Séverine Robert, Clara Sousa-Silva, Sergei N Yurchenko, Nicole F Allard, Vincent Boudon, Jeanna Buldyreva, Benjamin Bultel, Athena Coustenis, Aleksandra Foltynowicz, et al.

Data availability and requirements relevant for the Ariel space mission and other exoplanet atmosphere applications

Katy L. Chubb[1,2]★, Séverine Robert[3]†, Clara Sousa-Silva[4,5]‡, Sergei N. Yurchenko[6]§, Nicole F. Allard[7], Vincent Boudon[8], Jeanna Buldyreva[9], Benjamin Bultel[10], Athena Coustenis[11], Aleksandra Foltynowicz[12], Iouli E. Gordon[13], Robert J. Hargreaves[13], Christiane Helling[14,15], Christian Hill[16], Helgi Rafn Hrodmarsson[17], Tijs Karman[18], Helena Lecoq-Molinos[14,15,31], Alessandra Migliorini[19], Michaël Rey[20], Cyril Richard[8], Ibrahim Sadiek[21], Frédéric Schmidt[12], Andrei Sokolov[6], Stefania Stefani[19], Jonathan Tennyson[6], Olivia Venot[17], Sam O. M. Wright[6], Rosa Arenales-Lope[22], Joanna K. Barstow[23], Andrea Bocchieri[24], Nathalie Carrasco[25], Dwaipayan Dubey[22], Oleg Egorov[26], Antonio García Muñoz[27], Ehsan (Sam) Gharib-Nezhad[28], Leonardos Gkouvelis[22], Fabian Grübel[22], Patrick Gerard Joseph Irwin[29], Antonín Knížek[30], David A. Lewis[14], Matt G. Lodge[1], Sushuang Ma[6], Zita Martins[32], Karan Molaverdikhani[22], Giuseppe Morello[33], Andrei Nikitin[26], Emilie Panek[34], Miriam Rengel[35], Giovanna Rinaldi[19], Jack W. Skinner[36,40], Giovanna Tinetti[6], Tim A. van Kempen[37], Jingxuan Yang[29], Tiziano Zingales[38,39]

[1]*University of Bristol, School of Physics, HH Wills Physics Laboratory, Tyndall Avenue, Bristol BS8 1TL, UK*
[2]*Centre for Exoplanet Science, University of St Andrews, North Haugh, St Andrews, KY16 9SS, UK*
[3]*Royal Belgian Institute for Space Aeronomy (BIRA-IASB), Av. Circulaire 3, 1180 Uccle, Belgium*
[4]*Bard College, Institute of Astrophysics and Space Sciences, 30 Campus Rd, Annandale-On-Hudson, NY 12504*
[5]*Institute of Astrophysics and Space Sciences, Rua das Estrelas, 4150-762 Porto, Portugal*
[6]*Department of Physics and Astronomy, University College London, London WC1E 6BT, UK*
[7]*Observatoire de Paris, PSL Research University, 61, Avenue de l'Observatoire, F-75014 Paris, France*
[8]*Lab. ICB, UMR 6303 CNRS / Université de Bourgogne, 9 Av. A. Savary, BP 47870, F-21078 Dijon Cedex, France*
[9]*Institut UTINAM, UMR CNRS 6213, Université de Franche-Comté, 16 Route de Gray, 25030 Besançon cedex, France*
[10]*Université Paris-Saclay, CNRS, GEOPS, 91405, Orsay, France*
[11]*LESIA, Paris Observatory, CNRS, PSL Univ., 5 place Jules Janssen, 92190 Meudon Cedex, France*
[12]*Umeå University, Department of Physics, 901 87 Umeå, Sweden*
[13]*Center for Astrophysics | Harvard & Smithsonian, 60 Garden Street, Cambridge, MA 02138, USA*
[14]*Space Research Institute, Austrian Academy of Sciences, Schmiedlstrasse 6, 8042 Graz, Austria*
[15]*TU Graz, Fakultät für Mathematik, Physik und Geodäsie, Petersgasse 16, A-8010 Graz, Austria*
[16]*International Atomic Energy Agency, Wagramer Strasse 5, Vienna A-1400, Austria*
[17]*Université Paris Cité and Univ Paris Est Creteil, CNRS, LISA, F-75013 Paris, France*
[18]*Institute for Molecules and Materials, Radboud University, Heyendaalseweg 135, 6525 AJ Nijmegen, Netherlands*
[19]*IAPS-INAF, Via Fosso del Cavaliere, 100, 00133, Rome, Italy*
[20]*Université de Reims Champagne-Ardenne, UMR CNRS 7331, BP 1039, F-51687, Reims Cedex 2, France*
[21]*Leibniz Institute for Plasma Science and Technology (INP), Felix-Hausdorff-Straße 2, 17489 Greifswald, Germany*
[22]*Fakultät für Physik, Ludwig-Maximilians-Universität München, Scheinerstraße 1, D-81679 München, Germany*
[23]*School of Physical Sciences, The Open University, Walton Hall, Milton Keynes, MK7 6AA, UK*
[24]*Dipartimento di Fisica, La Sapienza Università di Roma, Piazzale Aldo Moro 5, Roma, 00185, Italy*
[25]*University of Paris-Saclay and ENS Paris-Saclay, LATMOS, 11 bourlevard d'Alembert, 78280 Guyancourt, France*
[26]*V.E. Zuev Institute of Atmospheric Optics SB RAS, 1, Akademician Zuev Sq., Tomsk, 634055 Russia*
[27]*Université Paris-Saclay, Université Paris Cité, CEA, CNRS, AIM, 91191, Gif-sur-Yvette, France*
[28]*Space Science and Astrobiology Division, NASA Ames Research Center, Moffett Field, CA, 94035 USA*
[29]*University of Oxford, Atmospheric, Oceanic and Planetary Physics, Department of Physics, Parks Rd, Oxford OX1 3PU, UK*
[30]*J. Heyrovský Institute of Physical Chemistry, Czech Academy of Sciences, Dolejškova 2155/3, 18223, Prague, Czech Republic*
[31]*Institute of Astronomy, KU Leuven, Celestijnenlaan 200D bus 2401, 3001 Leuven*
[32]*CQE, IMS, Department of Chemical Engineering, Instituto Superior Técnico, Universidade de Lisboa, Portugal*
[33]*Instituto de Astrofísica de Andalucía (IAA-CSIC), Glorieta de la Astronomía s/n, 18008, Granada, Spain*
[34]*Institut d'Astrophysique de Paris (CNRS, Sorbonne Université), 98bis Bd Arago, 75014 Paris, France*
[35]*Max-Planck-Institut für Sonnensystemforschung, Justus-von-Liebig-Weg 3, 37077 Göttingen, Germany*
[36]*Division of Geological and Planetary Sciences, California Institute of Technology, 1200 E. California Blvd., Pasadena, CA, 91125, USA*
[37]*SRON Netherlands Institute for Space Research, Niels Bohrweg 4, 2333 CA, Leiden, the Netherlands*
[38]*Dipartimento di Fisica e Astronomia, Università degli studi di Padova , Vicolo dell'Osservatorio 3, 35122 Padova, Italy*
[39]*INAF, Osservatorio Astronomico di Padova, Vicolo dell'Osservatorio 5, 35122 Padova, Italy*
[40]*Martin A. Fisher School of Physics, Brandeis University, 415 South St, Waltham, MA, 02453, USA*

19 September 2024

ABSTRACT

The goal of this white paper is to provide a snapshot of the data availability and data needs primarily for the Ariel space mission, but also for related atmospheric studies of exoplanets and cool stars. It covers the following data-related topics: molecular and atomic line lists, line profiles, computed cross-sections and opacities, collision-induced absorption and other continuum data, optical properties of aerosols and surfaces, atmospheric chemistry, UV photodissociation and photoabsorption cross-sections, and standards in the description and format of such data. These data aspects are discussed by addressing the following questions for each topic, based on the experience of the "data-provider" and "data-user" communities: (1) what are the types and sources of currently available data, (2) what work is currently in progress, and (3) what are the current and anticipated data needs. We present a GitHub platform for Ariel-related data, with the goal to provide a go-to place for both data-users and data-providers, for the users to make requests for their data needs and for the data-providers to link to their available data. Our aim throughout the paper is to provide practical information on existing sources of data whether in databases, theoretical, or literature sources.

1 INTRODUCTION

1.1 The Ariel space mission

The Ariel space mission is due to launch in 2029. It will measure spectra of exoplanet atmospheres between 0.5 - 7.8 μm (~ 1280 - 20,000 cm^{-1}), with the highest resolving power (R = 100) between 1.95 - 3.9 μm (~ 2500 - 5100 cm^{-1}), undertaking a chemical survey of around 1000 of the planets in our galaxy (Zingales et al. 2018; Venot et al. 2018b; Tinetti et al. 2018). Ariel will be used to constrain elemental abundances in hot gas giant atmospheres (Wang et al. 2023a), as well as allowing for detections of rocky Super-Earth atmospheric signatures (Ito et al. 2022) and the observation of temperate exoplanet atmospheres (Encrenaz et al. 2022). Ariel has inspired various data challenges, such as in retrievals (Barstow et al. 2022) and machine learning (Changeat & Yip 2023; Nikolaou et al. 2023). As highlighted in Tinetti et al. (2021), there is a synergy between Ariel and other exoplanet atmosphere missions; both high-resolution ground-based spectroscopic observations such as the Telescopio Nazionale Galileo (TNG) (Guilluy et al. 2022), and space-based missions such as PLATO (PLAnetary Transits and Oscillations of stars) and TESS (Transiting Exoplanets Survey Satellite) (Kálmán et al. 2023), and JWST (Changeat et al. 2022).

The Hubble Space Telescope (HST) has been widely used in exoplanet science; in particular the coverage of optical and UV regions, for example by the Wide Field Camera 3 WFC3/UVIS and Space Telescope Imaging Spectrograph (STIS) instruments, are important for understanding aerosol properties in exoplanet atmospheres (Wakeford et al. 2020; Fairman et al. 2024). The WFC3 infrared (IR) instrument has been extensively used for IR observations of hot exoplanet atmospheres, particularly for characterising H_2O spectral features which have been detected in abundance in such atmospheres (see, for example, Iyer et al. 2016). The wider spectral coverage and improvement in spectral resolution of both Ariel and JWST compared to HST/WFC3 allows for the improved detection and characterisation of several molecular species in the optical and IR regions (Guilluy et al. 2022). While JWST has a larger telescope than Ariel, allowing for observations of smaller cooler exoplanets using less transits (Changeat et al. 2022), JWST was designed to make observations for many more astronomy fields than only exoplanets. Ariel, on the other hand, will observe simultaneously over a wide wavelength range; it is the first space mission fully dedicated to the study of exoplanet atmospheres and has the unique ability to probe the atmosphere of warm and hot exoplanets with a statistical approach, aiming to observe ~1000 exoplanet atmospheres during its first tier (Tinetti et al. 2021). Ariel is optimised to observe transiting exoplanets, and can be equally or more efficient than JWST for characterising exoplanets orbiting bright stars (see Figure 8-2 of Tinetti et al. 2021). Meanwhile, some of the exoplanets observed by JWST will be used by Ariel for calibration purposes in the first months of observation, and will likely be used to refine the Ariel target list (Edwards et al. 2019a), highlighting the strong synergy between these two missions.

High-resolution spectroscopy utilises cross-correlation techniques to allow for the detection of individual species present at lower abundances than can be observed using the lower resolution observations of spectroscopic missions such as Ariel (Guilluy et al. 2022). The two types of observation together allow for a more complete understanding of an atmosphere (see, for example, Brogi & Line 2019).

Overviews of potential exoplanet targets for Ariel can be found in Edwards et al. (2019a); Edwards & Tinetti (2022). The mission's instrument wavelength coverage is summarised in Table 1. Although the main spectral coverage (besides photometric bands) of Ariel is from 1.1 - 7.8 μm, we consider data which cover the wavelength region from the UV to the far infrared, because of their use in atmospheric models relevant to the Ariel mission and other exoplanet atmosphere applications, such as climate models and analysing observed spectra from complementary exoplanet atmosphere telescopes. To characterise different exoplanet atmospheres, spectra are typically modelled using radiative transfer calculations. These calculations rely on a priori knowledge, often based on assumptions, of a variety of atmospheric processes, such as: molecular absorption and emission, scattering, chemistry, atmospheric dynamics, cloud formation, and atmosphere-surface interaction.

1.2 Atmospheric modelling and retrieval codes

A comprehensive list of exoplanetary retrieval codes (as of March 2023) can be found in MacDonald & Batalha

★ katy.chubb@bristol.ac.uk
† severine.robert@aeronomie.be
‡ csousasilva@bard.edu
§ s.yurchenko@ucl.ac.uk

Table 1. Summary of Ariel instruments and their wavelength coverage and resolving power R=$\frac{\lambda}{\Delta\lambda}$, from Edwards et al. (2019a). AIRS is the Ariel InfraRed Spectrometer, NIRSpec the Near-InfraRed Spectrometer, and VISPhot, FGS1 and FGS2 are photometers (Szabó et al. 2022).

Instrument	Wavelength range (μm)	Wavenumber range (cm^{-1})	R=$\frac{\lambda}{\Delta\lambda}$
VISPhot	0.5 - 0.6	16,667 - 20,0000	
FGS 1	0.6 - 0.81	12,346 - 16,667	Photometric bands
FGS 2	0.81 - 1.1	9091 - 12,346	
NIRSpec	1.1 - 1.95	5128 - 9091	20
AIRS Ch0	1.95 - 3.9	2564 - 5128	100
AIRS Ch1	3.9 - 7.8	1282 - 2564	30

(2023), with updates online[1]. Another detailed overview of radiative transfer and retrieval codes (as of May 2023) can be found in Rengel & Adamczewski (2023). In the Ariel science team, several radiative transfer retrieval packages are available, including ARCiS (Ormel & Min 2019; Min et al. 2020), NEMESIS (Irwin et al. 2008), Pyrat Bay (Cubillos & Blecic 2021), POSEIDON (MacDonald 2023) and TauREx3 (Al-Refaie et al. 2021). They have been compared in the frame of a retrieval challenge for the Ariel mission (Barstow et al. 2022). Table 2 lists a non-exhaustive selection of atmospheric modelling and retrieval codes and their respective repositories used in exoplanetary studies. Whilst these multiple retrieval codes all perform the same basic function – comparing a range of typically one-dimensional, parametric radiative transfer simulations to observed data via a sampling algorithm such as MCMC or nested sampling – they each have slightly different methods for parameterising often complex atmospheric processes. Previous retrieval comparison efforts by Barstow et al. (2020) and Barstow et al. (2022) showcase the agreement between them for simple cases where all codes are able to implement the same parameterisations. However, Barstow et al. (2020) compared a range of cloud parameterisations and showed that whilst the overall conclusions using each method were not in disagreement with each other, the different ways of representing cloud in each model meant that the sensitivity to different aspects of the cloud varied between approaches. Therefore, a multiplicity of retrieval codes is considered to be an asset for the Ariel mission, since each has been written with different priorities in mind. Some codes include more complex chemistry than others (see e.g. Al-Refaie et al. 2022) and others have focused particularly on representation of cloud physics (see e.g. Ormel & Min 2019). Applying multiple retrieval codes to a single dataset is rapidly becoming accepted as field best-practice as it allows these different strengths to be captured and also provides a useful cross-check for cases where solutions may be model dependent (see e.g. Kilpatrick et al. 2018; Lewis et al. 2020; Welbanks & JWST Transiting Exoplanet Community Early Release Science team 2024). Regardless of any differences in parameterisations in these codes used to model exoplanet atmospheres and interpret observations, they all rely on various data inputs crucial for successful analyses of atmospheres, as will be discussed in this paper.

1.3 Paper structure

The intention of this community white paper is to ensure the data necessary to interpret observations from exoplanet atmosphere characterisation missions such as Ariel are up to a standard required for successful analyses, and to allow comparability between analyses (for example, line lists which are complete and accurate at the relevant atmospheric temperatures for all expected species, refractive indices for all aerosol types expected in exoplanet atmospheres, etc). We provide a summary of the types of data typically used by atmospheric retrieval and modelling codes, and we identify potential weaknesses in the data and therefore motivate further research. For different data types, as described below, we will provide an overview of what data is currently: 1) available, 2) typically used, 3) being worked on, and 4) needed. Although the focus is on data required for characterising exoplanet atmospheres related to the Ariel space mission, we also include some discussion on more general data usage in the field of astronomical spectroscopy, for example for broader wavelength regions. We focus on a number of different data types: molecular and atomic line lists (Section 2), molecular and atomic line shapes (Section 3), computed absorption cross-sections and opacities (Section 4), collision induced absorption (CIA) and other continuum data (Section 5), data for aerosols (Section 6), data for atmospheric chemistry models (Section 7), and data required for UV photodissociation or photoabsorption (Section 8). Needs for data standards, meta data, existing rules and associated tools are discussed in Section 9. Current databases providing such data for characterising exoplanet atmospheres are reviewed across the paper in the relevant sections. Our conclusions can be found in Section 10.

The information associated with this paper is made available via the GitHub project[2]. The goal of this platform is to provide a go-to place both for the data-users and for the data-providers, for the users to inform others about their data needs and make requests, and for the data providers to link to the available or inform about their soon-to-be-available data (see Section 10.1).

[1] https://doi.org/10.5281/zenodo.7675743

[2] https://github.com/Ariel-data

Table 2. Examples of typical atmospheric retrieval and modelling codes used by the exoplanetary atmosphere community.

Code	Reference	Link
ARCiS	Min et al. (2020)	https://www.exoclouds.com
ATMO	Tremblin et al. (2015)	https://www.erc-atmo.eu
Helios-r2	Kitzmann et al. (2020)	https://github.com/exoclime/Helios-r2
NASA Planetary Spectrum Generator (PSG)	Villanueva et al. (2018)	https://psg.gsfc.nasa.gov/
NEMESIS	Irwin et al. (2008)	https://nemesiscode.github.io/nemesis.html
NemesisPy	Yang et al. (2023)	https://github.com/Jingxuan97/nemesispy/
petitRADTRANS	Mollière et al. (2019)	https://petitradtrans.readthedocs.io/en/latest/
PICASO	Batalha et al. (2021)	https://natashabatalha.github.io/picaso/
PLATON	Zhang et al. (2020)	https://github.com/ideasrule/platon
POSEIDON	MacDonald (2023)	https://github.com/MartianColonist/POSEIDON
Pyrat Bay	Cubillos & Blecic (2021)	https://pyratbay.readthedocs.io/en/latest/
TauREx3	Al-Refaie et al. (2021)	http://github.com/ucl-exoplanets/TauREx3_public

2 MOLECULAR/ATOMIC LINE LISTS

Molecular and atomic line lists contain information about the frequency and strength of spectroscopic transitions, sometimes referred to as "lines", often accompanied by information on the associated initial and final energy states. When it comes to atomic and molecular line lists, the following factors are important: accuracy, which refers to the frequency or wavelength location of transition lines, and completeness, which refers to both spectral and temperature coverage; i.e. the number of transitions in the latter case. High-resolution spectra ($\frac{\lambda}{\Delta\lambda} \gtrsim 25{,}000$) of exoplanets, typically measured from ground-based instruments, require very accurate line positions to be known, usually over a shorter wavelength range than required for observations from low- to mid-resolution space-based telescopes such as Ariel and JWST. The cross-correlation technique used to analyse observed high-resolution spectra is an efficient tool to characterise exoplanet atmospheres, complementary to observations from space telescopes. It has resulted in numerous detections in exoplanetary atmospheres of hot-Jupiters of molecules and atoms, including CO, H_2O, TiO, HCN, CH_4, NH_3, C_2H_2, OH, VO and CrH, as well Ca, V, Cr, Fe, Ti, Mg, He, K, Na and Li (Guillot et al. 2022; Gandhi et al. 2023).

To interpret the lower-resolution ($\frac{\lambda}{\Delta\lambda} \lesssim 3000$) observations, it is particularly important for overall opacity to be provided by a line list, which requires the line list to be considered complete up to the temperature of the atmosphere being modelled. This metric of completeness is related to the number of spectral line transitions between energy levels which are provided by a line list. There will be transitions between so-called hot bands, for example, which would not be present for a line list computed or based on laboratory measurements at room-temperature, but would be important for characterising the atmospheres of exoplanets at high temperatures of around 1000 K - 2000 K. It is well known that the choice of line list can have a huge impact in interpreting high-resolution spectroscopic observations (see, for example, Serindag et al. 2021; de Regt et al. 2022). Perhaps less intuitive, but the accuracy of line list, especially of the line positions, can be also critical for interpretation of lower-resolution space-based observations, particularly at elevated temperatures > 1000 K (see, for example, Niraula et al. 2022). Therefore it is important that molecular opacitites used in the main stream atmospheric retrieval packages are initially built at the highest resolution ($\frac{\lambda}{\Delta\lambda} \sim 100\,000$) before binning them down to the practical resolution ($\frac{\lambda}{\Delta\lambda} \sim 3000 - 15\,000$) (Chubb et al. 2020a). The aspects of completeness and accuracy for existing molecular line lists will be reviewed below.

2.1 State of the art - Data availability

The main databases which host molecular and atomic line lists are given in Table 3, with more details for a number of the molecular databases found in the subsections below. Of these molecular databases, HITRAN and GEISA provide highly accurate data with the main focus on terrestrial conditions, while the other listed databases typically have more extended coverage, for example covering up to higher temperatures, usually > 1000 K. Table 4 summarises the wavelength and temperature coverage of molecular line lists from some of the main spectral databases. An approximate temperature up to which the line list is considered complete, in terms of completeness of transition data at a given temperature, is given; either hot (≥ 1000 K) or else assumed to be roughly Earth-temperature (≤ 500 K). The latter usually applies to species in the HITRAN database, which was originally designed for terrestrial atmosphere applications. We note that most molecules in the ExoMol database are complete up to at least 3000 K, and hotter for some diatomic species. Some stable diatomic species such as H_2 and HD^+ are even considered complete up to 10,000 K. C_2H_4 is considered complete up to 700 K in both the TheoReTs (Rey et al. 2016a) and ExoMol (Mant et al. 2018) databases; the same applies to HNO_3 (Pavlyuchko et al. 2015) in the ExoMol database, which is also complete up to 700 K. An overview of some molecular and atomic databases (as of September 2022) can also be found in Rengel (2024); additional databases not detailed here include that of JPL Molecular Spectroscopy[3] and the Cologne database for molecular spectroscopy (CDMS)[4].

[3] https://spec.jpl.nasa.gov/
[4] https://cdms.astro.uni-koeln.de/

Atomic line list data can be obtained from various sources such as the NIST[5] (Kramida et al. 2013) and Kurucz[6] (Kurucz 2017) databases, and the Vienna atomic line database (VALD3)[7] (Ryabchikova et al. 2015). The appendix of Grimm et al. (2021) compares the opacities available from these three databases. Atomic partition functions are included in the Kurucz and VALD3 databases, and can also be computed by using various sources such as Irwin (1981). We note that while the Kurucz database is well-used and considered accurate for atomic line lists, the majority of the Kurucz molecular line lists are more approximate than the other line list databases described here.

Figure 1 (left panel) shows a comparison for methane cross-sections computed at 296 K between MeCaSDa (Ba et al. 2013), TheoReTs (Rey et al. 2016b), the latest ExoMol MM line list (Yurchenko et al. 2024d), HITRAN2020 (Gordon et al. 2022) and HITEMP (Hargreaves et al. 2020). These databases are detailed in the subsections below. It can be seen that all databases are very similar at this temperature: the differences are mostly in the "transparency windows" between the strongly absorbing polyads. Transitions in these regions are extremely weak and can be purely extrapolated or even absent; thus, those regions should be considered with care. For example, HITRAN2020 lacks many weak lines, but they are present in HITEMP.

The situation is however very different at high temperatures. This is when the line list completeness or lack of it becomes especially evident and the choice of the line list to be used in retrievals can make a huge difference. In the right display of Fig. 1 we now compare cross-sections of methane generated for $T = 1500$ K. The low temperature line lists HITRAN2020 and MeCaSDa lack the essential absorption practically everywhere, with MeCaSDa being more complete at lower wavenumbers. The so-called "hot line" lists of TheoReTs, ExoMol MM and HITEMP all demonstrate a high level of completeness and generally agree with each across the entire IR region, but also show discrepancies in the near infrared (NIR). The latter are caused by the differences in the theoretical models and essentially reflect the lack of the underlying laboratory data used to constrain these models. Work on the analysis of the experimental spectra of methane in NIR is currently in progress.

2.1.1 Descriptions of molecular databases

2.1.1.1 CaSDa The CaSDa (Calculated Spectroscopic Databases) databases[8] (see Richard et al. 2020, 2024) contain synthetic line lists resulting from fits of the effective Hamiltonian and dipole moment parameters using assigned experimental laboratory spectra. The models used for the calculations are based on the tensorial formalism developed in the Dijon group, as explained in Boudon et al. (2011). Currently, there are 10 CaSDa databases for 10 different molecules, which amount to 39 isotopologues in total. A new database, SiCaSDa, has been released very recently for three isotopologues of SiH_4 (a molecule already observed in the interstellar medium). All these databases are listed in Table 5. For the present topic of exoplanetary spectroscopy, the most relevant ones are, of course, CH_4, C_2H_4 and GeH_4, which are present in the atmospheres of the giant planets of the Solar System. CF_4 and SiF_4 are naturally present in Earth's atmosphere due to volcanic emissions; SiF_4 has been suggested as a possible species on Io by Schaefer & Fegley Jr. (2005) and thus may be relevant in the case of potential volcanic exoplanets; CH_3Cl is present in comets (Hardy et al. 2023) and thus could be of interest for exo-comets (Janson et al. 2023). It was also suggested and explored as a biomarker in exoplanetary atmospheres (Seager et al. 2013). In the near future, the intent is for new data (new bands and new isotopologues, like for instance CH_3D in MeCaSDa) to be added to these databases (Richard et al. 2024), and for further ones to be developed, especially for some molecules of astrophysical interest, like $C_3H_6O_3$ (trioxane that may be relevant for comets, see Richard et al. (2022)).

These databases contain calculated line lists for all spectral regions of these molecules that could be assigned in experimental laboratory spectra and fitted line-by-line using effective Hamiltonians and dipole moments. The databases contain extra information, such as energy levels with all quantum numbers and eigenvectors. When available, different isotopologues data are included in each database. The given accuracy of line positions and intensities is equal to the standard deviation of the fit; extrapolation is limited to only a few rotational quantum number values outside the existing assignment range. The data output is in the 160-character HITRAN2004 format (Rothman et al. 2005). CaSDa use some specific notations for line assignments in the case of CH_3Cl and C_2H_4 since they are based on use of a tensorial formalism similar to that of CH_4. It is also possible to compute absorption cross-sections.

2.1.1.2 ExoMol ExoMol[9] is a provider of the molecular and since 2023 also atomic data necessary for modelling spectroscopy of exoplanets (Tennyson et al. 2024b). The main data products are line lists, with the emphasis on the molecules important for exoplanetary and stellar atmospheres, but also for spectroscopy of planets, comets as well as industrial applications (see Tennyson & Yurchenko 2021). As of today, the ExoMol database contains line lists for 92 molecules and 245 isotopologues, see Table 6 for the current snapshot of the molecular line lists available in ExoMol. Up to the ExoMol 2020 release (Tennyson et al. 2020), the emphasis had been on the completeness of the data in terms of the temperature and wavelength coverage especially aimed at lower to medium resolution exoplanetary studies, usually involving transit spectroscopy, see Table 4. ExoMol line lists are generally constructed to be accurate for resolving power $R \leq 10000$ (Tennyson et al. 2024b), i.e. appropriate for the Ariel and JWST missions. Higher temperatures applications with the atmospheres of hot Jupiters studied by HST instruments being a typical application meant that the line lists had an emphasis on completeness (Yurchenko et al. 2014). Since 2020, the focus of the ExoMol database has shifted to high resolution (HR) applications, i.e. ground-based HR cross-correlation applications. The ExoMol line

[5] https://physics.nist.gov/PhysRefData/ASD/lines_form.html
[6] https://lweb.cfa.harvard.edu/amp/ampdata/kurucz23/sekur.html; http://kurucz.harvard.edu/atoms.html
[7] http://vald.astro.uu.se
[8] https://vamdc.icb.cnrs.fr
[9] www.exomol.com

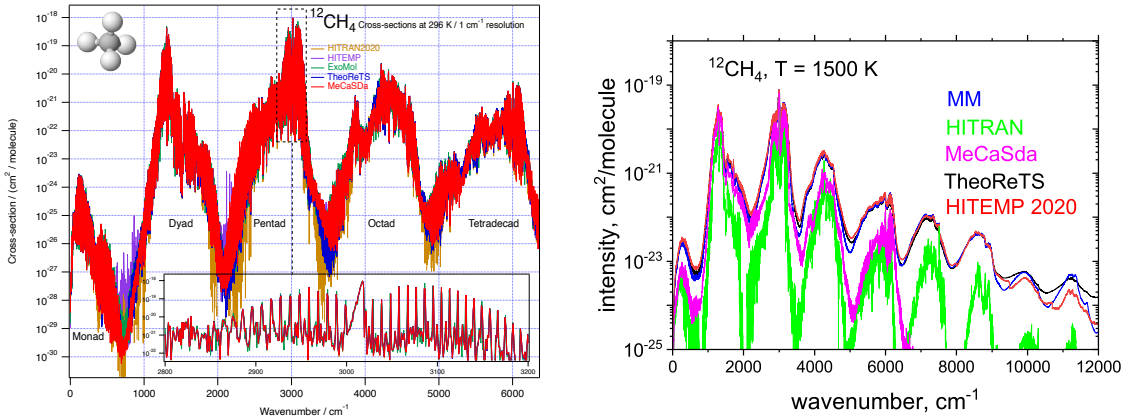

Figure 1. Comparison of $^{12}CH_4$ cross-sections at 296 K (left) and 1500 K (right) in the far and mid-infrared regions for different databases: MeCaSDa (Richard et al. 2020), TheoReTs (Rey et al. 2016b), the ExoMol MM line list (Yurchenko et al. 2024d), HITRAN2020 (Gordon et al. 2022) and HITEMP (Hargreaves et al. 2020).

Table 3. An overview of some line list databases used by the (exo)planetary atmosphere community.

Database	Type of data	Reference	Link
CaSDa	Theoretical line lists up to high temperatures	Richard et al. (2020, 2024)	https://vamdc.icb.cnrs.fr
ExoMol	Theoretical line lists up to high temperatures	Tennyson et al. (2020)	https://exomol.com
GEISA	Accurate line lists for terrestrial conditions	Jacquinet-Husson et al. (2016); Delahaye et al. (2021)	https://geisa.aeris-data.fr
HITEMP	Line lists up to high temperatures	Rothman et al. (2010)	https://hitran.org/hitemp
HITRAN	Accurate line lists for terrestrial conditions	Gordon et al. (2022)	https://hitran.org
Kurucz	Semi-empirical line lists up to high temperatures	Kurucz (1995)	http://kurucz.harvard.edu/molecules.html
MoLLIST	Laboratory line lists up to high temperatures	Bernath (2020)	https://bernath.uwaterloo.ca/molecularlists.php
NASA Ames	Semi-empirical line lists up to high temperatures	e.g. Huang et al. (2023a)	http://huang.seti.org
NIST	Atomic line lists up to high temperatures	Kramida et al. (2013)	https://physics.nist.gov/PhysRefData/ASD/lines_form.html
S&MPO	Spectroscopy and Molecular Properties of Ozone	Tyuterev et al. (2021)	http://smpo.iao.ru
TheoReTs	Theoretical line lists up to high temperatures	Rey et al. (2016b)	https://theorets.tsu.ru
VALD3	Atomic line lists up to high temperatures	Ryabchikova et al. (2015)	http://vald.astro.uu.se

lists are currently being upgraded to the quality of the HITRAN line lists, where the underlying high-resolution data is available. Other conceptual shifts in the ExoMol data structure are the introduction of uncertainties for the line positions to enable the data users to select the lines according with their application needs; provision of UV photoabsorption and photodissociation cross-sections (Pezzella et al. 2022; Tennyson et al. 2023) (see Section 8); broadening due to predissociation (Tennyson et al. 2023; Yurchenko et al. 2024e).

The ExoMol line lists are written as bzip2-compressed ascii files using the two file structure: a States file (.states) and a Transition file (.trans). The States file provides a full description of the (rovibronic) states, including the energy (cm^{-1}), total degeneracy, the total angular momentum, energy uncertainty (cm^{-1}), lifetimes, Lande-g factors as well as the corresponding quantum numbers, with each entry identified by an integer number (State ID). The Transition files provide the Einstein coefficients in the following compact form: i j A_{ij}, where i and j are the upper and lower state IDs, respectively, and A_{ij} is a corresponding Einstein A coefficient (s^{-1}). The quantum numbers in the States file, when available, correspond to the standard spectroscopic convention for a given system, but can also include alternative conventions. This is strongly dependent on how the line lists have been produced.

As part of the ExoMol services, a number of useful tools are provided, including an online cross-sections app, some efficient programs ExoCross and PyExoCross to turn huge line lists into compact temperature and pressure dependent cross-sections (Yurchenko et al. 2018a; Zhang et al. 2024), molecular radiative lifetimes (Owens et al. 2023), molecular specific heats (Wang et al. 2023b) and molecular opacities in four different formats appropriate for a variety of atmospheric retrieval codes (Chubb et al. 2020a); details of the ExoMolOP opacity database are given in Section 4. A detailed Atlas of molecular spectra computed using the ExoMol line lists can be found in Tennyson & Yurchenko (2018), see Fig. 2 as an example, where the ExoAmes (Underwood et al. 2016b) cross-sections of SO_2 are shown.

The majority of the line lists in the ExoMol database have been produced by the ExoMol group using a combination of quantum mechanical calculations based on high-level spectroscopic models (i.e. potential energy surfaces, spin-orbit and other coupling etc.), tuned by fitting to the experimental data and the so-called post-production MARVELisation (Furtenbacher et al. 2007), where some of the computed energies are replaced by experimental values (see Section 2.1.4). Apart from these ExoMol line lists (covering some 70 molecules), the ExoMol database also hosts line lists from other data providers, including a large number of diatomics (Wang et al. 2020b) from the MoLLIST (Molecular Line Lists, Intensities and Spectra) project (Bernath 2020), some of the high-temperature species from HITRAN (HF, HCl, HBr) (Li et al. 2013), and CO from Li et al. (2015). The HITEMP line list for NO (Hargreaves et al. 2019) is

Table 4. An overview of the molecules, wavelength coverage, and temperature coverage for some of the major line lists available from listed databases for the (exo)planetary atmosphere community. See the footnotes to the table for a key of database and wavelength range. Line lists which are considered complete up to ≥ 1000 K are labelled with (*H*), and all others are generally assumed to be complete up to ~ 500 K. A few exceptions are noted in the text.

Molecule	λ range	Database
AlCl	IR, Vis, UV	Ex(*H*),Ku(*H*),Mo(*H*)
AlF	IR, Vis, UV	Ex(*H*),Ku(*H*),Mo(*H*)
AlH	IR, Vis, UV	Ex(*H*),Ku(*H*),Mo(*H*)
AlO	IR, Vis, UV	Ex(*H*)
AsH_3	IR	Ex
BeH	IR, Vis, UV	Ex(*H*)
C_2	IR, Vis, UV	Ex(*H*),Ku(*H*)
C_2H_2	IR	Ex(*H*),HI
C_2H_4	IR	Ex,HI,Th, SDa
C_2H_6	IR	HI
C_2N_2	IR	HI
C_4H_2	IR	HI
C_3	IR	Ex(*H*)
CaF	IR, Vis, UV	Ex(*H*),Mo(*H*)
CaH	IR, Vis, UV	Ex(*H*),Mo(*H*)
CaO	IR, Vis, UV	Ex(*H*)
CaOH	IR,Vis	Ex(*H*)
CF_4	IR	HI,SDa,Th
CH	IR, Vis, UV	Ex(*H*),Ku(*H*),Mo(*H*)
CH^+	IR, Vis, UV	Ex(*H*)
CH_2	IR	Th(*H*)
CH_3	IR	Ex(*H*),Th(*H*)
CH_3Br	IR	HI
CH_3Cl	IR	Ex(*H*),HI,SDa,Th
CH_3CN	IR	HI
CH_3F	IR	Ex,HI,Th
CH_3I	IR	HI
CH_3OH	IR	HI
CH_4	IR, NIR	Ex(*H*),HI,HT(*H*),Th(*H*),SDa(*H*)
ClO	IR	HI
$ClONO_2$	IR	HI
CN	IR, Vis, UV	Ex(*H*),Ku(*H*),Mo(*H*)
CO	IR	Ex(*H*),HI,HT(*H*)
CO_2	IR	Am,Ex(*H*),HI,HT(*H*)
$COCl_2$	IR	HI
COF_2	IR	HI
CP	IR	Ex(*H*)
CrH	NIR	Ex(*H*),Mo(*H*)
CS	IR	Ex(*H*),HI
CS_2	IR	Am,HI
FeH	NIR	Ex(*H*),Mo(*H*)
GeH_4	IR	HI,SDa,Th
H_2	IR, Vis, UV	Ex(*H*),HI(*H*)
H_2CO	IR	Ex(*H*),HI,Th
H_2CS	IR	Ex(*H*)
H_2O	IR	Ex(*H*),HI,HT(*H*)
H_2O_2	IR	Ex(*H*),HI
H_2S	IR	Ex(*H*),HI
H_3^+	IR	Ex(*H*)
H_3O^+	IR	Ex(*H*)
HBO	IR	Ex(*H*)
HBr	IR	Ex(*H*),HI(*H*)
HCl	IR	Ex(*H*),HI(*H*)
HCN	IR	Ex(*H*),HI
HC_3N	IR	HI
HCOOH	IR	HI
HDO	IR	Ex(*H*),HI
HD^+	IR	Ex(*H*)
HeH+	IR	Ex(*H*)
HF	IR	Ex(*H*),HI(*H*)
HI	IR	Ex(*H*),HI(*H*)
HNO_3	IR	Ex,HI
HO_2	IR	HI
HOBr	IR	HI
HOCl	IR	HI
KCl	IR	Ex(*H*)
KF		Ex(*H*),Mo(*H*)
KOH	IR	Ex(*H*)
LaO	Vis,UV	Ex(*H*),Mo(*H*)
LiCl	IR	Ex(*H*),Mo(*H*)
LiF	IR	Ex(*H*),Mo(*H*)
LiH	IR	Ex(*H*)
LiH^+	IR	Ex(*H*)
LiOH	IR	Ex(*H*)
MgF	IR, Vis, U	Ex(*H*),Mo(*H*)
MgH	IR, Vis, U	Ex(*H*),Mo(*H*)
MgO	IR, Vis, U	Ex(*H*)
N_2	IR,UV	Ex(*H*),HI
N_2O	IR	Am,Ex(*H*),HI,HT(*H*)
NaF		Ex(*H*),Mo(*H*)
NaH	IR, Vis, UV	Ex(*H*)
NaCl	IR	Ex(*H*)
NaO	IR, Vis, UV	Ex(*H*)
NaOH	IR	Ex(*H*)
NF_3	IR	HI,Th
NH	IR, Vis, U	Ex(*H*),Ku(*H*),Mo(*H*)
NH_3	IR	Ex(*H*),HI
NO	IR, Vis, U	Ex(*H*),HI,HT(*H*)
NO^+	IR	HI
NO_2	IR	HI,HT(*H*)
NS	IR	Ex(*H*)
O_2	IR, Vis, UV	HI
O_3	IR	HI,SM
OCS	IR	Am,Ex(*H*),HI
OH	IR, Vis, UV	Ex(*H*),HI,HT(*H*),Mo(*H*)
OH^+	IR, Vis, UV	Ex(*H*),Mo(*H*)
PH	IR, Vis, UV	Ex(*H*)
PH_3	IR	Ex(*H*),HI,Th(*H*)
PN	IR	Ex(*H*)
PO	IR	Ex(*H*)
PS	IR	Ex(*H*)
S_2	UV	HI
ScH	IR, Vis, UV	Ex(*H*)
SF_6	IR	HI,SDa,Th
SH	IR, Vis, UV	Ex(*H*),Mo(*H*)
SiF_4	IR	SDa
SiH	IR, Vis, UV	Ex(*H*),Ku(*H*)
SiH_2	IR	Ex(*H*)
SiH_4	IR	Ex(*H*),Th,SDa
SiO	IR, Vis, UV	Ex(*H*),Ku(*H*)
SiO_2	IR	Ex(*H*)
SiH	IR, Vis, UV	Ex(*H*)
SiS	IR	Ex(*H*)
SO	IR, Vis, UV	Ex(*H*),HI
SO_2	IR	Am,Ex(*H*),HI
SO_3	IR	Ex(*H*),HI
TiH	Vis	Ex(*H*),Mo(*H*)
TiO	IR, Vis, UV	Ex(*H*),Mo(*H*),Ku(*H*)
VO	IR, Vis, UV	Ex(*H*)
YO	IR, Vis, UV	Ex(*H*)
ZnO	IR, Vis, UV	Ex(*H*)
ZrO	IR, Vis, UV	Ex(*H*)

Databases: Am=NASA Ames; Ex=ExoMol; HI=HITRAN; HT=HITEMP; Mo=MoLLIST; Ku=Kurucz; SDa=TFSiCaSDa, MeCaSDa, TFMeCaSDa, GeCaSDa, SiCaSDa, ECaSDa; SM=S&MPO; Th=TheoReTS; see Table 3.
λ ranges: UV = 0.1 - 0.4 μm; Vis = 0.4 - 0.8 μm; IR ≥ 0.8 μm.

Table 5. Calculated molecular absorption lines in the CaSDa databases.

HITRAN ID	Molecule	DB name	Isotopologues	Total nb. of lines	Relevant for Ariel
06	CH_4	MeCaSDa	3	12,988,898	*
24	CH_3Cl	ChMeCaSDa	2	12,152	
30	SF_6	SHeCaSDa	4	491,500	
38	C_2H_4	ECaSDa	1	96,397	*
42	CF_4	TFMeCaSDa	1	258,208	*
52	GeH_4	GeCaSDa	5	60,878	*
–	RuO_4	RuCaSDa	9	30,205	
–	SiF_4	TFSiCaSDa	3	210,401	*
–	UF_6	UHeCaSDa	8	110,129	
–	SiH_4	SiCaSDa	3	20,090	*

Table 6. An overview of the line lists provided by ExoMol, www.exomol.com

Molecule	Reference	Molecule	Reference	Molecule	Reference
AlCl	Yurchenko et al. (2023a)	H_2CS	Mellor et al. (2022)	NH_3	Coles et al. (2019b)
AlF	Yousefi & Bernath (2018)	H_3^+	Bowesman et al. (2023)	$^{15}NH_3$	Yurchenko et al. (2024a)
AlH	Yurchenko et al. (2024e)	H_3O^+	Yurchenko et al. (2020b)	NO	Wong et al. (2017)
AlO	Patrascu et al. (2015)	HBO	Li et al. (2024)	NO	Qu et al. (2021)
AsH_3	Coles et al. (2019a)	HBr	Coxon & Hajigeorgiou (2015)	NS	Yurchenko et al. (2018b)
BeH	Darby-Lewis et al. (2018)	HCCH	Chubb et al. (2020b)	OCS	Owens et al. (2024a)
C_2	Yurchenko et al. (2018d)	HCl	Li et al. (2013)	OH	Brooke et al. (2016)
C_2	Brooke et al. (2013)	HCN/HNC	Barber et al. (2014)	OH^+	Hodges et al. (2018)
C_2H_4	Mant et al. (2018)	HD	Amaral et al. (2019)	P_2H_2	Owens & Yurchenko (2019)
C_3	Lynas-Gray et al. (2024)	HD^+	Amaral et al. (2019)	PF_3	Mant et al. (2019)
CaF	Hou & Bernath (2018)	HDO	Mizus et al. (2024)	PH	Langleben et al. (2019)
CaH	Yadin et al. (2012)	HeH^+	Amaral et al. (2019)	PH_3	Sousa-Silva et al. (2015)
CaH	Owens et al. (2022a)	HF	Coxon & Hajigeorgiou (2015)	PN	Semenov et al. (2024)
CaO	Yurchenko et al. (2016)	HNO_3	Pavlyuchko et al. (2015)	PO	Prajapat et al. (2017)
CaOH	Owens et al. (2022a)	HS	Yurchenko et al. (2018b)	PS	Prajapat et al. (2017)
CH	Masseron et al. (2014)	KCl	Barton et al. (2014)	ScH	Lodi et al. (2015)
CH_3	Adam et al. (2019)	KF	Frohman et al. (2016)	SH	Gorman et al. (2019)
CH_3Cl	Owens et al. (2018b)	KOH	Owens et al. (2021)	SiH	Yurchenko et al. (2018c)
CH_3F	Owens et al. (2018a)	LaO	Bernath et al. (2022)	SiH_2	Clark et al. (2020)
CH_4	Yurchenko & Tennyson (2014)	LiCl	Bittner & Bernath (2018)	SiH_4	Owens et al. (2017)
CH^+	Pearce et al. (2024)	LiF	Bittner & Bernath (2018)	SiN	Owens et al. (2022a)
CH_4	Kefala et al. (2024)	LiH	Coppola et al. (2011)	SiO	Yurchenko et al. (2022)
CN	Syme & McKemmish (2021)	LiH^+	Coppola et al. (2011)	SiO	Kurucz (2011)
CO	Li et al. (2015)	LiOH	Owens et al. (2024b)	SiO_2	Owens et al. (2020)
CO_2	Yurchenko et al. (2020a)	MgF	Hou & Bernath (2017)	SiS	Upadhyay et al. (2018)
CP	Ram et al. (2014)	MgH	Owens et al. (2022a)	SO	Brady et al. (2024)
CrH	Chowdhury et al. (2006)	MgH	Gharib-Nezhad et al. (2013)	SO_2	Underwood et al. (2016b)
CS	Paulose et al. (2015)	MgO	Li et al. (2019)	SO_3	Underwood et al. (2016a)
FeH	Wende et al. (2010)	N_2	Western et al. (2018)	TiH	Burrows et al. (2005)
H_2	Roueff et al. (2019)	N_2O	Yurchenko et al. (2024c)	TiO	McKemmish et al. (2019)
$H_2{}^{16}O$	Polyansky et al. (2018)	NaCl	Barton et al. (2014)	VO	McKemmish et al. (2016)
$H_2{}^{17,18}O$	Polyansky et al. (2017)	NaF	Frohman et al. (2016)	VO	Bowesman et al. (2024)
H_2CO	Al-Refaie et al. (2015)	NaH	Rivlin et al. (2015)	YO	Yurchenko et al. (2024b)
H_2O_2	Al-Refaie et al. (2016)	NaO	Mitev et al. (2022)	YO	Yurchenko et al. (2019)
H_2S	Azzam et al. (2016)	NaOH	Owens et al. (2021)	ZrO	Perri et al. (2023)
H_3^+	Mizus et al. (2017)	NH	Perri & McKemmish (2024)		

based on the ExoMol NOname line list (Wong et al. 2017), combined with other data.

2.1.1.3 HITRAN and HITEMP The HITRAN molecular spectroscopic database has been a go-to source of molecular data for 50 years (Rothman 2021). HITRAN, an acronym of high-resolution transmission, was primarily established to model the radiative transfer through the Earth's atmosphere and consequently included line-by-line parameters to model the dominant terrestrial absorbers. Over the years, as observations, experiments, and analytical techniques have improved, the HITRAN database has been regularly updated and expanded to accommodate state-of-the-art molecular parameters from the microwave through to the near UV spectral range. Papers describing quadrennial editions of the database typically receive thousands of citations. HITRAN2020 (Gordon et al. 2022) – the most recent edition of the database – features a compilation of line-by-line parameters, both experimentally-derived and calculated, for 55

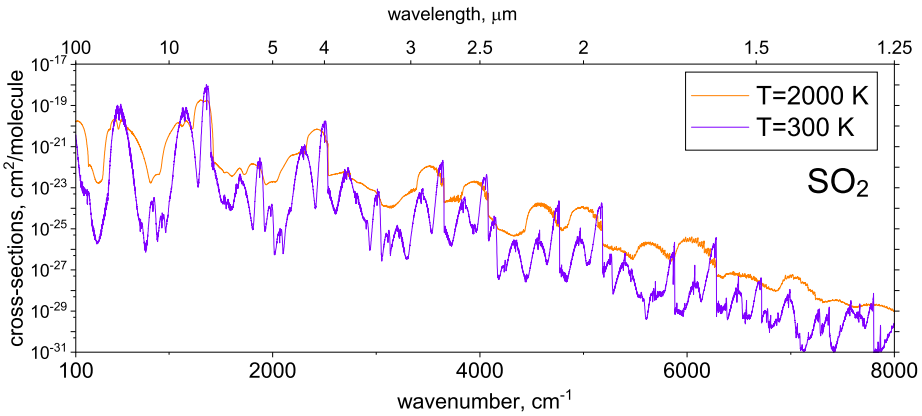

Figure 2. ExoMol Spectral Atlas (Tennyson & Yurchenko 2018): Cross-sections of SO_2 computed with the ExoMol line ExoAmes (Underwood et al. 2016b).

molecules and is freely available from HITRAN*online*[10]. Table 1 of Gordon et al. (2022) provides a summary of the spectral coverage and the number of lines included in HITRAN for each isotopologue of every molecule. Each transition in HITRAN includes the line position, intensity, lower-state energy, line shape parameters, and assignment information that are necessary for calculating the absorption of a transition at a given temperature and concentration. HITRAN line-by-line parameters are provided at a reference temperature of 296 K with intensities that account for the typical natural abundance on Earth. Alongside Voigt line shape parameters for air- and self-broadening (i.e., the broadening due to the terrestrial atmosphere and pure gas, respectively), recent editions of HITRAN have also accommodated parameters for high-level line shapes and broadening parameters that are applicable to planetary atmospheres other than Earth. This includes atmospheres dominated by H_2/He, CO_2 (Wilzewski et al. 2016; Tan et al. 2022), and H_2O (Tan et al. 2019). A summary of the additional broadening available via the HITRAN database is provided in Table 7.

In addition to line-by-line parameters, HITRAN also provides experimental absorption cross-sections for over 300 molecules for which no reliable quantum mechanical models exist (Kochanov et al. 2019) (see Section 2.1.3.1), collision-induced absorption data for a variety of collisional complexes (Karman et al. 2019) (see Section 5), aerosol properties (see Section 6), and water vapor continuum data (Mlawer et al. 2012) (see Section 5). HITRAN also provides auxiliary data necessary for carrying out calculations of spectra at different thermodynamic conditions, including Total Internal Partition Sums (Gamache et al. 2017; Gamache et al. 2021). The HITRAN Application Programming Interface, HAPI (Kochanov et al. 2016), allows one to efficiently download HITRAN data and carry out calculations of spectral absorption, emission, and transmission. HITRAN provides line lists for a small number of species which are considered complete up to high temperatures of around 4000–5000 K: HF, HCl, HBr, HI, and H_2 (Li et al. 2013).

HITEMP (Rothman et al. 2010) is in principle updated alongside the HITRAN database and is specifically aimed at modelling high-temperature ($\gtrsim$ 1000 K) environments

[10] www.hitran.org

Table 7. Reference sources for Voigt line broadening parameters available in HITRAN, in addition to air- and self-broadening which are provided for every line. W16 refers to Wilzewski et al. (2016), T19 to Tan et al. (2019), T22 to Tan et al. (2022), D18 to Dudaryonok & Lavrentieva (2018), L20 to Lavrentieva & Dudaryonok (2020), and self refers to self-broadening parameters (see Gordon et al. 2022).

HITRAN ID	Molecule	Broadening Parameters H_2	He	H_2O	CO_2
1	H_2O	–	–	Self	–
2	CO_2	T22	T22	T19	T22
4	N_2O	–	T22	T19	T22
5	CO	T22	T22	T19	T22
6	CH_4	–	–	T19	–
7	O_2	–	–	T19	–
9	SO_2	W16	W16	–	D18
11	NH_3	W16	W16	T19	W16
13	OH	T22	T22	–	–
14	HF	W16	W16	–	W16
15	HCl	W16	W16	–	W16
19	OCS	T22	T22	–	L20
20	H_2CO	T22	T22	–	T22
23	HCN	T22	T22	–	–
26	C_2H_2	W16	W16	–	W16
28	PH_3	T22	T22	–	–
31	H_2S	T22	T22	T19	T22
45	H_2	Self	–	–	–
52	GeH_4	T22	–	–	–

where HITRAN data cannot be reliably applied. This includes the atmospheres of stars, brown dwarfs, and planets at elevated temperatures, such as hot Jupiters, hot super-Earths, or Venus. At the moment HITEMP provides line lists for eight molecules (H_2O, CO_2, N_2O, CO, CH_4, NO, NO_2, OH) and is consistent with HITRAN where possible, but typically includes a substantial proportion of calculated *ab initio* or semi-empirical parameters. These additional lines account for hot bands, and other transitions that are negligible (i.e., extremely weak) at terrestrial temperatures and therefore not included in the HITRAN line list. While the number of lines required for each molecule can reach billions, one goal of HITEMP has been to remain practical to use in line-by-line radiative transfer calculations. Therefore, the underlying *ab initio* line lists are analyzed and filtered

to reduce the number of lines necessary for each molecule, as demonstrated for the addition of CH_4 (Hargreaves et al. 2020) to HITEMP.

In summary, HITRAN and HITEMP both provide essential input parameters for many radiative transfer codes. These data are used for a variety of applications, including the modelling of exoplanet atmospheres at high-resolution.

2.1.1.4 NASA Ames database The database from NASA Ames uses the "Best Theory + Reliable High-Resolution Experiment (BTRHE)" strategy (Huang et al. 2021) to provide accurate and complete line lists for species such as SO_2 (5 isotopologues up to 500 K) (Huang et al. 2015, 2016), CO_2 (up to 3000 K) (Huang et al. 2023a), NH_3 (Huang et al. 2022b), N_2O (Huang et al. 2023b), OCS, CS_2 and their isotopologues. The most recent NASA Ames releases include hot line lists are for the four most abundant isotopologues of CO_2 ($^{12}C^{16}O_2$, $^{13}C^{16}O_2$, $^{16}O^{12}C^{18}O$, and $^{16}O^{12}C^{17}O$) (Huang et al. 2022a) and extensive room temperature line lists for N_2O with its 12 isotopologues (Huang et al. 2023b). The ExoMol SO_2 line list (Underwood et al. 2016b) was also produced jointly with NASA Ames. Some of the earlier NASA Ames line lists were formatted using the HITRAN-like line-by-line ascii format, while the more recent line lists are provided in the ExoMol-like format with two parts, states and transitions. Although these are ascii files, for transitions (Einstein coefficients and states IDs), NASA Ames uses a simple compacting scheme based on representing real numbers as integers. The line lists can be accessed online[11].

2.1.1.5 TheoReTS Precise knowledge of high-energy molecular states and intensities of rovibrational transitions is essential for the modelling of various planetary atmospheres as well as for the understanding of spectral properties, even in extreme dynamical and temperature conditions. This clearly demonstrates the need of having consistent line-by-line spectroscopic databases, with a large coverage in terms of both wavelengths and temperatures. Because of their completeness, variational calculations are well designed for the modelling of planetary atmospheres, unlike traditional spectroscopic effective models for which wavenumber extrapolation beyond the range of observed data turns out very limited. Within that context, the TheoReTS (Theoretical Reims-Tomsk Spectral data) project (Rey et al. 2016b) – whose philosophy closely follows that of ExoMol (Tennyson et al. 2020) – was born in 2016[12]. For the construction of accurate variationally-computed molecular line lists allowing a complete description of the main spectral features, highly-optimised numerical methods and symmetry tools for solving the nuclear-motion equation as well as high-level *ab initio* calculations are required.

The TheoReTS line lists are simple ascii files with three columns: ν_{ij}, S_{ij}, E_{low}. For ease of use, quantum numbers and symmetry labels can be provided upon request using a HITRAN-like format. In addition, variational energy levels can be also replaced by rotation-vibration levels computed from empirical effective Hamiltonians whose parameters are fitted to experimental data, as in the case of methane (Rey et al. 2018). This ensures almost the same quality as HITRAN2020 (Gordon et al. 2022) for the line positions of cold bands while many new hot bands can be accurately predicted. For modelling hot exoplanets and brown dwarfs, a methane line list for the HITEMP (Hargreaves et al. 2020) spectroscopic database was constructed using the TheoReTS predictions (Rey et al. 2017; Wong et al. 2019). Moreover, in order to facilitate the manipulation of the so-called quasi-continuum formed by billions of lines (e.g. due to line lists of heavy molecules at high-temperatures), a set of super-lines can be generated at different temperatures to drastically reduce the total number of lines by several orders of magnitude (Rey et al. 2016b).

In its current form, TheoReTS contains line lists for 9 molecules (CH_4, PH_3, SF_6, C_2H_4, CF_4, GeH_4, SiH_4, CH_3F, NF_3) and 28 isotopologues. New line lists will be released in 2024, either by improving the existing ones or by including new ones for both *semirigid* and *nonrigid molecules* (Rey et al. 2023). Among the next candidates of primary importance – potentially relevant for the study of exoplanetary atmospheres are CH_2, CH_3, NH_3, H_2CCN, H_2NCN, CH_3Cl, C_3H_4, H_2O_2, CCl_4, CH_3CN or C_2H_6 that will be gradually uploaded in TheoReTS. The construction of comprehensive line lists is now being revisited using a novel methodology developed in Reims to derive *ab initio* effective models (Rey 2022), combining the small dimensionality of the spectroscopic polyad models and the completeness of the variational calculation. Fine-tuning of the *ab initio*-based spectroscopic parameters allows matches to observed data to be made without much computational effort, unlike a refinement procedure of the PES which is generally more demanding. Effective parameters plan to be shared in the upgraded version of TheoReTS.

2.1.2 *Laboratory spectroscopy measurements*

As might be expected, the vast majority of laboratory studies have been undertaken with terrestrial applications in mind, and these studies form the basis for many of the line lists discussed throughout this section. Laboratory studies not only provide empirical measurements of critical parameters such as line positions, intensities, broadening coefficients, and temperature dependencies (e.g., see Gordon et al. 2022, which overviews experimental works included for HITRAN2020), but they are also used to refine and develop theoretical models, they are essential for constraining calculated parameters, and they are often used directly as is the case for absorption cross-section measurements (see Section 2.1.3.1). However, the experimental conditions of manystudies, such as pressure and temperature, are not always directly applicable to non-terrestrial planetary environments, which means spectroscopic parameters derived from them have limitations when applied elsewhere. Within our Solar System there are atmospheric temperatures, pressures, and constituents that are beyond those encountered in the Earth's atmosphere. Moreover, the variety of exoplanet atmospheres that are already accessible to transit measurements, via JWST observations or high-resolution ground-based observations (and those that will be observed by the near-future Ariel mission), mean that the experimental requirements far exceed atmospheric environments previously studied and necessitate a range of planetary-applicable lab-

[11] https://huang.seti.org/ and https://data.nas.nasa.gov/ai3000k
[12] https://theorets.tsu.ru/ and https://theorets.univ-reims.fr/

oratory measurements to better model these observations (Fortney et al. 2019).

The value of experimental spectroscopy for characterizing planetary atmospheres cannot be overstated. However, this section is not meant to be a comprehensive overview of the history of spectroscopic works, but instead aims to provide a summary of recent experimental measurements that highlight key techniques, spectroscopic parameters, and molecules currently being investigated for planetary applications.

2.1.2.1 Experimental data for Solar System planets

Experimental data can support both the study of our Solar System bodies and contribute significantly to the understanding of exoplanet spectroscopy.

The advent of the ESA Venus Express mission to Venus and the NASA/Juno and ESA/JUICE missions to the Jovian system pushed the interest on new laboratory experiments to study the properties of CO_2 at high temperatures and pressures, to simulate the Venusian case, and H_2 and H_2+He mixtures as representative of collision induced absorption (CIA) in Jupiter's atmosphere. For example, two different experimental apparatus have been used to obtain the spectra representative of Venus (Stefani et al. 2013) and Jupiter (Snels et al. 2021), due to the different pressure and temperature values covered. In the case of Venus, CO_2 spectra were obtained in the 1-10 μm spectral band (Stefani et al. 2022a,b), exploring temperature and pressure values according to a real Venus vertical profile (Seiff et al. 1985). An example is shown in Figure 3. For the Jupiter case, collision induced absorption (CIA) coefficients of H_2 and H_2-He were measured (see Section 5). Furthermore, empirical absorption cross-sections for key absorption species observed in the atmospheres of Gas Giant planets have traditionally been implemented in retrievals when line lists were incomplete, as done for CH_4 in the visible (Karkoschka 1994). Moreover, numerous experimental measurements of broadening parameters applicable to planetary atmospheres (e.g., H_2, He, CO_2, and H_2O) and their temperature dependencies have been combined into functional forms by Wilzewski et al. (2016) and Tan et al. (2022) to populate these parameters in spectroscopic databases.

Titan, with its complex atmosphere, has motivated data-focused experiments for decades (e.g. McKellar 1989; de Vanssay et al. 1995; Curtis et al. 2008; Sung et al. 2013; Hewett et al. 2020), valuable not just for the analysis of the Saturnine moon but for studies of the early Earth and its exoplanetary analogues. These studies reflect the need for spectroscopic data of hydrocarbons and other organic molecules in nitrogen-rich environments and have already significantly improved our understanding of the opacities of CH_3D and C_2H_6 for instance (He et al. 2022b; Hörst et al. 2008; Vuitton et al. 2019).

2.1.2.2 High-temperature experimental measurements

Experimental measurements are relatively sparse outside of the terrestrial temperature range, but there have been some efforts to address this for planetary applications in recent years. In particular, we focus on the spectral region covered by Ariel at elevated temperatures, due to the atmospheric temperatures found in the proposed exoplanet target lists (Edwards et al. 2019a; Edwards & Tinetti 2022). Laboratory studies at high temperatures consistent with hot planetary atmospheres (i.e., above room temperatures and typically up to ~1000–2000 K), using a variety of experimental techniques, have provided crucial data for exoplanetary studies. However, acquiring spectra at high temperatures is challenging, primarily because of the physical properties of laboratory equipment, but also due to decomposition of the sample molecule, which can lead to reaction products contaminating observations.

Many existing experimental line lists have been built upon spectra recorded with Fourier transform spectrometers (FTS) and typically span the infrared region. These measurements provide relatively wide spectral coverage (e.g. multiple vibrational modes) at high spectral resolution ($\lesssim 0.01$ cm^{-1}). It is common to couple Fourier transform spectrometers with cells capable of reaching elevated temperatures. Analyses from these measurements have provided new insight for line positions (Hargreaves et al. 2012, for NH_3), intensities (Georges et al. 2019, for CH_4), line shape parameters (Delahaye et al. 2016, for H_2O), and absorption cross-sections (Beale et al. 2016, for C_3H_8) sufficient for accurate retrievals of planetary conditions. Complementary to FTS, cavity ring down spectrometers (CRDS) are capable of providing similar frequency accuracy to FTS, but the increased effective path provided by the cavity results in much higher sensitivity for weak transitions. This high sensitivity makes CRDS well-suited to weaker 'window' regions of molecular absorption that are difficult to study with other methods. For example, line parameters obtained for weak CH_4 transitions in the NIR (Campargue et al. 2023) can be included in spectroscopic databases directly or used to refine line positions in future iterations of *ab initio* line lists. Moreover, CRDS measurements enable constraints to be applied to the water vapor continuum (Koroleva et al. 2023) , which is essential for accounting for the total water absorption through long path lengths (see Section 5). Laser-based techniques, for example, have been able to probe limited spectral regions at even higher resolutions comparable with millimeter rotational studies (e.g. $\Delta\nu < 1.0\times10^{-6}$ cm^{-1}). More recently, frequency combs have enabled highly accurate spectroscopic studies to be acquired over moderately large spectral regions, which can now include whole vibrational bands. For example, comb spectroscopy has been used for measurements of high-temperature spectra of H_2O (Schroeder et al. 2017; Rutkowski et al. 2018), CH_4 (Malarich et al. 2021), and CO_2 (Cole et al. 2023) in the 6250–7570 cm^{-1} range. Water spectra measured in a premixed methane/air flat flame (Rutkowski et al. 2018) were assigned using the MARVELised POKAZATEL line list, while H_2O (Schroeder et al. 2017) and CH_4 (Malarich et al. 2021) spectra measured in a range of temperatures and sub-atmospheric pressures were used to assess the accuracy of current editions of HITRAN and HITEMP databases. The CO_2 spectra were measured at pressures up to 25 bar to test and improve line mixing models and their temperature dependence (Cole et al. 2023). Another development relevant for high-temperature applications is the optical-optical double resonance spectroscopy with continuous-wave pump and comb probe, which allows measurement and assignment of hot-band transitions with sub-Doppler resolution without the need to heat the sample (Foltynowicz et al. 2021b; Silva de Oliveira et al. 2024). This technique has so far been used to measure and assign hot band transitions in the $3\nu_3 \leftarrow \nu_3$ range of CH_4 (Foltynowicz et al.

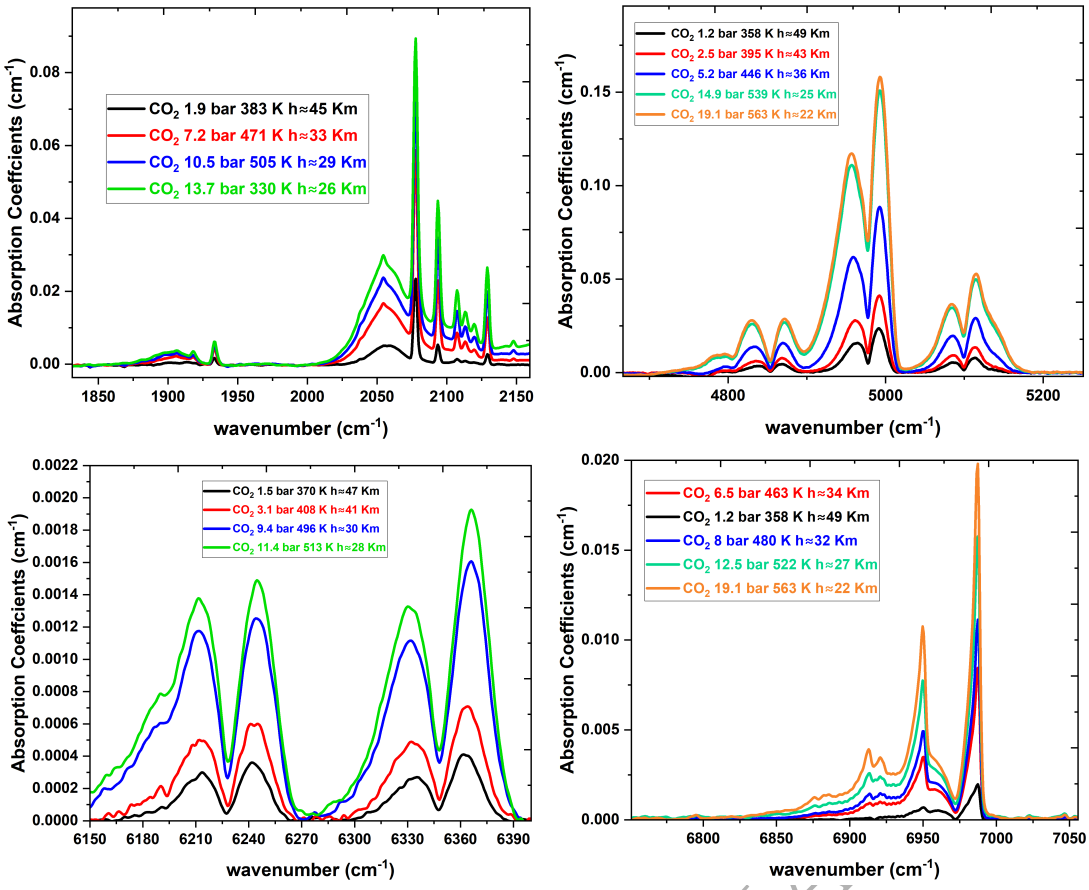

Figure 3. Measured spectra of CO_2 at different temperatures and pressures relevant to the atmosphere of Venus, from Stefani et al. (2013).

2021a; Silva de Oliveira et al. 2024), finding good agreement with the TheoReTS predictions (Rey et al. 2014a; Hargreaves et al. 2020). See Section 2.1.2.3 for a detailed spotlight overview of frequency comb spectroscopy for planetary applications.

In addition to providing measurements of line positions, intensities, and line shape parameters, broadband FTS measurements of high-temperature gases enclosed in a heated tube cell (up to ~1500 K) can also provide essential testing of the accuracy of current line lists available in the literature, such as for the CO_2 line list in HITEMP (Bharadwaj & Modest 2007; Alberti et al. 2015). Such measurements have also provided valuable absorption cross-sections that can be used for atmospheric characterisation when line lists have been incomplete for planetary studies (e.g. Nassar & Bernath 2003, for CH_4). In addition, spectra obtained from high-enthalpy sources (Georges et al. 2019) and oxyacetylene torches with temperatures up to 3000 K (Coheur et al. 2005), or time-resolved spectroscopy in glow discharges (Pastorek et al. 2022, and references therein), can be used to investigate combustion environments and non-local thermodynamic equilibrium (non-LTE) conditions (Dudás et al. 2023). Spectroscopic parameters obtained from these studies can then been used to constrain theoretical line lists, improving the accuracy throughout. While FTS measurements combined with tube furnaces apparatus have formed the bulk of many studies at high temperatures, often laser based analyses are used in high-temperature remote sensing applications of combustion processes (Tancin et al. 2020). Combining laser spectroscopy techniques with shock-tube apparatus enables sensitive measurements at higher temperatures and pressures (Ding et al. 2019; Strand et al. 2019; Tancin & Goldenstein 2021; Chakraborty et al. 2024), which can be difficult to reach with tube furnaces. In addition, these techniques can also be combined with frequency combs to provide accurate measurements at high-temperature that cover broad spectral ranges, such as recent investigations for the line-positions of CH_4(Pinkowski et al. 2021; Malarich et al. 2021).

Spectroscopic studies of atomic transitions and diatomic molecules at high temperatures have historically taken advantage of the Sun's photosphere (~5800 K), providing accurate line positions. For example, telluric-free, high-resolution Solar spectra recorded from orbiting satellites have been used to extend laboratory studies, as done for CH (Melen et al. 1989; Colin & Bernath 2010), NH (Ram & Bernath 2010), and OH (Melen et al. 1995; Bernath & Colin 2009; Civiš et al. 2023); similarly Barton et al. (2013) used extensive sunspot spectra due to Campbell et al. (1995) to help create an extensive SiO line list. This can provide key measurements of spectral lines positions for molecules that are difficult to measure in the laboratory. A recent review of middle-to-near IR emission spectra of four simple astrophysically relevant molecular radicals, OH, NH, CN and CH, was given by Civiš et al. (2023). In addition, key diatomic species that characterise spectra of brown dwarfs are also expected to be present in exoplanet atmospheres. These molecules are

challenging for theoretical calculations, and measurements of line positions and intensities are essential for improving models. Semi-empirical line lists have been developed for these molecules by analysing archived high-temperature, high resolution spectra, such as carried out for FeH (Hargreaves et al. 2010), and MgH (Shayesteh et al. 2007; Gharib-Nezhad et al. 2013; Hinkle et al. 2013; Owens et al. 2022a), and TiO (Cameron & Bernath 2022). These semi-empirical works have often been directly implemented into brown dwarf (Bailey & Kedziora-Chudczer 2012) and exoplanet (Mukherjee et al. 2023) atmospheric models to improve characterisation.

Water is a key molecule for our atmosphere, and has been prominent in exoplanet observations since early transmission spectra (Tinetti et al. 2007; Swain et al. 2009). The water line lists discussed above have relied on numerous experimental studies to accurately determine spectroscopic parameters (e.g. positions, intensities, line shapes, broadening coefficients, pressure shifts, temperature dependencies), and to refine assignments. Indeed, some of the current theoretical line lists of H_2O suitable for high temperature analyses have their origin in earlier works that identified new transitions of high-temperature water vapor on the Sun (Wallace et al. 1995; Polyansky et al. 1997; Viti et al. 1998). Some examples of recent high-temperature water vapor studies that use FTS (Zobov et al. 2008; Alberti et al. 2015), scanned laser spectroscopy (Melin & Sanders 2018; Melin et al. 2020) and frequency comb studies (Schroeder et al. 2017; Rutkowski et al. 2018) have all helped to refine spectroscopic parameters for H_2O line lists and to constrain *ab initio* calculations. Hot (1723 K) laboratory studies have also been used to test and confirm the accuracy of the available line lists (Melin et al. 2020).

Small polyatomic molecules such as ammonia and methane can have complex infrared spectra when observed at high resolution, and spectroscopic analyses at high temperatures provide opportunities for extending rovibrational assignments (Barton et al. 2015). Simplified empirical line lists have been produced by analysing multiple measurements at a variety of different temperatures, as done for NH_3 (Hargreaves et al. 2012) and CH_4 (Beale et al. 2017; Ghysels et al. 2018; Malarich et al. 2021). These simplified line lists lack spectroscopic assignments but constitute empirical line positions, intensities, and lower-state energies, and are capable of reproducing the experimental spectra over the temperature range of the studies and can be used to characterize brown dwarf and exoplanet atmospheres. Analyses of these line lists can then be performed to determine line assignments and constrain calculated parameters. Furthermore, the measured spectra can be converted into experimental absorption cross-sections (Wong et al. 2019) that can themselves be used as input data to planetary models in place of line lists, or can be used to compared the accuracy of multiple high temperature line lists as done for CH_4 (Hargreaves et al. 2020). Measurements of absorption cross-sections up to temperatures of 1600 K (Es-sebbar & Farooq 2014; Alrefae et al. 2014; Wong et al. 2019), become particularly necessary for molecules when no complete line lists exists (also Section 2.1.3.1).

Each edition of the HITRAN database incorporates a substantial proportion of experimentally-derived parameters and readers are directed toward the paper describing HITRAN2020 (Gordon et al. 2022, and references therein) for a summary of relevant spectroscopic experimental studies that apply to molecules given in Table 4. In addition, it should be noted that the MARVEL (measured active rotation-vibration energy levels) methodology (Furtenbacher et al. 2007) (see Section 2.1.4), which is used to empirically correct energy levels of *ab initio* line lists (e.g. Yurchenko et al. 2022), is built upon an extensive survey of experimental measurements, and readers are also directed to each work for a summary of relevant literature.

It is worth stressing that experimental measurements can be particularly challenging for reactive (or toxic) species, especially at high temperatures, which can limit the availability of parameters. In most cases, the absolute intensities are not available experimentally for species and therefore relying on the theory is the only option. It is therefore not uncommon for some spectroscopic parameters, including intensities (and associated lifetimes) as well as pressure-broadening (Tan et al. 2022), to be based only on limited laboratory measurements for some molecules (e.g. H_2 broadening of CO_2).

2.1.2.3 Spot-light: Frequency comb-based spectroscopy

This section presents a deeper dive into different aspects of frequency comb spectroscopy with the emphasis on its potential for providing spectroscopic data for exoplanetary spectroscopic studies.

Recent advancements in frequency comb sources and comb-based spectroscopic techniques (Gohle et al. 2007; Foltynowicz et al. 2011; Maslowski et al. 2016; Kowzan et al. 2016; Coddington et al. 2016; Changala et al. 2016; Weichman et al. 2019; Ycas et al. 2018; Krzempek et al. 2019; Muraviev et al. 2020; Foltynowicz et al. 2021b) have provided new opportunities for broadband precision molecular spectroscopy. The combination of large bandwidth, high spectral resolution, and high frequency accuracy provided by frequency combs make them ideal sources for high-precision measurements of spectroscopic molecular parameters. Such high-resolution measurements are an essential component to improving the accuracy of theoretically derived line lists (see Sections 2.1.2.2 and 2.1.4). Frequency combs can either be used directly as light sources for broadband high-resolution spectroscopy (which is referred to as direct frequency comb spectroscopy) or as references to calibrate the frequency axis of tunable-laser-based spectrometers (referred to as comb-referenced spectroscopy). While the simultaneous spectral coverage of most frequency combs cannot yet compete with incoherent sources, the spectral resolution of comb-based spectrometers is orders of magnitude better than that of an FTS spectrometer based on an incoherent light source, allowing the measurement of undistorted line profiles at low pressures with sub-MHz accuracy on line positions. Moreover, the spectral and spatial coherence of the combs make possible the use of path length enhancement methods, such as multi-pass cells (Adler et al. 2010a) and cavities (Adler et al. 2010b), to increase the absorption sensitivity and detect weak absorption bands. Comb-referenced cavity-enhanced tunable-laser-based spectrometers provide even better absorption sensitivity and - when combined with saturation spectroscopy - line positions with kHz accuracy.

Below we give an overview of precision measurements using direct frequency comb spectroscopy and comb-referenced spectroscopy, with a focus on measurements that led to new line lists or substantial improvement of exist-

ing ones for different molecules. We note that an exhaustive coverage of all measurements involving frequency combs is beyond the scope of this work.

Table 8 summarises a selection of experimental line lists obtained from measurements using different direct frequency comb spectroscopy techniques. Most of these measurements were performed at room temperature using direct absorption in multi-pass cells or enhancement cavities. Many of the works provided also line intensities, and pressure broadening and shift parameters. Three of the room temperature line lists have already been used to update the databases, namely the ν_4 band region (3000–3160 cm^{-1}) of CH_3I (Sadiek et al. 2020) and the ν_1+ν_3 band region (2110–2200 cm^{-1}) of CS_2 (Karlovets et al. 2020) were used in updates to the HITRAN2020 database (Gordon et al. 2022), and the ν_6 and ν_4 band region (1250–1380 cm^{-1}) of H_2CO measured by Germann et al. (2024) was used to improve the accuracy of the ExoMol line list for H_2CO (Al-Refaie et al. 2015; Al-Derzi et al. 2021).

To study complex molecules, whose spectra are unresolved at room temperature, buffer gas cooling has been implemented to reduce the number of populated rotational and vibrational states. Combining buffer gas cooling with cavity-enhanced comb spectroscopy allowed the measurement of rotationally resolved spectra of nitromethane (CH_3NO_2), naphtalene ($C_{10}H_8$), adamantane ($C_{10}H_{16}$), and hexamethylenetetramine ($C_6N_4H_{12}$) (Spaun et al. 2016), and vinyl bromide (CH_2CHBr) (Changala et al. 2016) in the 2850–3070 cm^{-1} range, as well as the buckminster fullerene (C_{60}) in the 1180–1190 cm^{-1} range (Changala et al. 2019).

Cavity-enhanced comb spectroscopy has also been combined with velocity-modulation to measure four bands of a molecular ion HfF^+ in the 11500–13000 cm^{-1} range (Cossel et al. 2012). Finally, the time-resolved capabilities of comb spectroscopy have been used to measure high-resolution spectra of trans- and cis-DOCO transients (products of the OD + CO reaction) in the OD stretch region 2380–2750 cm^{-1} (Bui et al. 2018), as well as the pressure broadening of absorption lines of the short-lived CH_2OO Criegee intermediate (Luo 2020) in the 1217–1287 cm^{-1} range.

Table 9 summarises a selection of experimental line lists obtained from measurements using different comb-referenced spectroscopy techniques. Many works using comb-referenced cavity-enhanced techniques in the near-infrared provided transition frequencies for overtone and combination bands with kHz level accuracy for, e.g., H_2O (Chen et al. 2018; Kassi et al. 2018; Tóbiás et al. 2020; Tóbiás et al. 2024), CO_2 (Reed et al. 2021; Guo et al. 2021; Fleurbaey et al. 2023), CO (Mondelain et al. 2015; Wang et al. 2021) and CH_4 (Votava et al. 2022). In the mid-infrared, sub-MHz and kHz level accuracy was obtained for the fundamental bands of CH_4 (Kocheril et al. 2018), N_2O (Knabe et al. 2013; Ting et al. 2014; AlSaif et al. 2018), CHF_3 (Vicentini et al. 2020), and CH_3OH (Santagata et al. 2019) using saturation and Doppler-broadened spectroscopy in absorption cells, and for CH_4 using sub-Doppler cavity-enhanced spectroscopy (Okubo et al. 2011; Abe et al. 2013). Three of these works have already been used for updating the databases and are included as part of HITRAN2020 (Gordon et al. 2022). This includes line positions for the 3←0 and 4←0 bands of CO (Mondelain et al. 2015) and the ν_3 region of CH_4 (Abe et al. 2013), with the work of Fleurbaey et al. (2021) included in a fit for line positions of the 1.27 μm band of O_2. Line intensities were provided only by a couple of works using CRDS in the Doppler-limited regime, since saturation spectroscopy often does not yield absolute intensities.

2.1.3 Alternative parameterisations

2.1.3.1 Absorption cross-section measurements Determining an accurate line list for a large proportion of known molecules is not practical, or possible, due to the complexity of assigning congested spectra (Sousa-Silva et al. 2019; Zapata Trujillo & McKemmish 2022a,b, 2023). In such instances, numerous individual lines typically blend into unresolved spectral bands. However, these molecules can still form strong detectable features in atmospheric spectra, and their spectroscopic signatures are required in retrieval frameworks for detection, in addition to improving the retrieval accuracy of planetary characteristics or other atmospheric species. To provide this necessary data, it is common practice to carefully measure experimental absorption cross-sections. These measurements are required to cover the expected temperature and pressure conditions of the appropriate planetary atmosphere, as well as including the appropriate broadening gases (e.g. H_2, He, N_2, etc) at a resolution that provides sufficient details.

Cross-sections are not just restricted to the infrared or visible wavelength regions; many valuable cross-sections which cover the UV region are regularly employed in Earth observations, for example. There are many cross-sections included in the HITRAN database that cover the UV and visible regions, such as SO_2 and O_3. While this section will mainly discuss infrared and visible absorption cross-sections due to the relevance for Ariel, UV absorption cross-sections are also important for exoplanet atmosphere models used to inform our understanding of observed planets. UV cross-sections also have special continuum features related to photodissociation and photoabsorption effects; see Section 8 where we discuss these separately.

The Pacific Northwest Nation Laboratory (PNNL) produced a large catalogue (Sharpe et al. 2004) of infrared absorption cross-sections for many chemical compounds recorded at 1.0 atm with a Fourier transform spectrometer at temperatures of 5, 25 and 50°C. Species included compounds that were difficult to measure in the laboratory. These cross-sections are no longer available from PNNL directly, but the majority of these measurements are now included as part of the HITRAN database (Gordon et al. 2022). The HITRAN database provides experimental absorption cross-sections of over 300 molecules (Kochanov et al. 2019), in addition to the line-by-line molecules described above. HITRAN also regularly expands the available data with each new edition (Gordon et al. 2022).

It should be noted that many chemical compounds have been measured due to signatures appearing in Earth observation measurements. For example, chlorine-containing compounds (e.g. chlorofluorocarbons) are intensely monitored because their reactions in the atmosphere lead to the depletion of stratospheric ozone. Therefore, the temperature and pressure coverage of absorption cross-sections is regularly expanded for improved accuracy of retrievals, for example, using Fourier transform measurements of the molecule contained in a cold cell (Harrison 2018).

Table 8. Molecular line lists obtained from direct frequency comb spectroscopy measurements using different methods: DCS - dual comb spectroscopy; FTS - Fourier transform spectroscopy; Vernier - Vernier spectroscopy; VIPA - spectrometers based on virtually imaged phased array; PAS - photoacoustic spectroscopy; OODR - optical-optical double resonance spectroscopy; CE - cavity enhanced. The spectral coverage and temperature range are also indicated; RT - room temperature. All works listed here provided line positions, and some, indicated in the 'Parameters' column, provided also intensities, S, self, air and reaction matrix broadening parameters, $\gamma_{\rm self}$, $\gamma_{\rm air}$, $\gamma_{\rm p}$, and self shift parameters, $\delta_{\rm self}$.

Molecule	Range [cm^{-1}]	Range [μm]	Method	T [K]	Parameters	Reference
H_2O	6800–7200	1.39 - 1.47	DCS	296-1300	$\gamma_{\rm self}$, $\gamma_{\rm air}$	Schroeder et al. (2017)
	6250–6670	1.50 - 1.60	CE FTS	1950	S	Rutkowski et al. (2018)
CO_2	5064–5126	1.95 - 1.97	CE Vernier	RT	S, $\gamma_{\rm self}$	Siciliani de Cumis et al. (2018)
	6800–7000	1.43 - 1.47	DCS	495-977	line mixing	Cole et al. (2023)
N_2O	1250–1310	7.63 - 8.00	FTS	RT		Hjältén et al. (2021)
CO	6310–6365	1.57 - 1.58	CE VIPA	RT	$\gamma_{\rm self}$, $\delta_{\rm self}$	Kowzan et al. (2019)
	2040–2230	4.48 - 4.90	FTS	RT		Nishiyama et al. (2024)
CH_4	1250–1380	7.25 - 8.00	FTS	RT	S	Germann et al. (2022)
	2900–3050	3.28 - 3.45	DCS	RT		Baumann et al. (2011)
	5870–6130	1.63 - 1.70	DCS	RT		Zolot et al. (2013)
	5900-6100	1.64 - 1.69	OODR	111		Foltynowicz et al. (2021a)
	5910-5980	1.67 - 1.69	OODR	RT		Silva de Oliveira et al. (2024)
	6770–7570	1.32 - 1.48	DCS	296-1000	$\gamma_{\rm self}$, $\delta_{\rm self}$	Malarich et al. (2021)
$^{13}CH_4$	1250–1380	7.25 - 8.00	FTS	RT	S	Germann et al. (2022)
$^{14}CH_4$	2910–3110	3.22 - 3.44	PAS	RT		Karhu et al. (2019)
H_2CO	1250–1380	7.25 - 8.00	FTS	RT	S	Germann et al. (2024)
$H^{13}CN$	6390–6535	1.53 - 1.56	DCS	RT	S	Guay et al. (2018)
C_2H_2	6430–6630	1.51 - 1.56	DCS	RT		Zolot et al. (2013)
CH_3I	3000–3160	3.16 - 3.3	FTS	RT	S	Sadiek et al. (2020)
	2930–3160	3.16 - 3.57	FTS	RT	S	Hjältén et al. (2023)
CS_2	2110–2200	4.55 - 4.74	DCS	RT	S	Karlovets et al. (2020)
HfF^+	11500–13000	0.77 - 0.87	CE VIPA	823		Cossel et al. (2012)
CH_3NO_2	2940–3090	3.24 - 3.40	CE FTS	10-20		Spaun et al. (2016)
CH_2CHBr	3023–3033	3.30 - 3.31	CE FTS	10-20		Changala et al. (2016)
DOCO	2380–2750	3.64 - 4.20	CE FTS	RT		Bui et al. (2018)
C_{60}	1180–1190	8.40 - 8.47	CE FTS	150		Changala et al. (2019)
CH_2OO	1217–1287	7.77 - 8.22	DCS	RT	$\gamma_{\rm p}$	Luo (2020)
CH_2Br_2	2960–3120	3.21 - 3.38	FTS	RT		Sadiek et al. (2023)

Other planets of the Solar System (and their moons) contain many trace gases, which are typically retrieved using experimental absorption cross-sections. For example, Titan, with its rich hydrocarbon atmosphere, requires cross-section measurements of nitrogen broadened species at low temperatures (e.g. Sung et al. 2013; Sung et al. 2018; Vuitton et al. 2019). Similarly, H_2 and He broadened measurements are required for the Jovian planets (e.g. Sung et al. 2016a; Dodangodage et al. 2020). It is expected that some of these species will be present at elevated temperatures in warm Gas Giant exoplanetary atmospheres (Fleury et al. 2023), therefore recent studies have also provided experimental absorption cross-sections at elevated temperatures (e.g. Alrefae et al. 2014; Hargreaves et al. 2015; Beale et al. 2016; Bernath & Fernando 2021; Adil et al. 2023).

The limited number of absorption cross-section measurements for specific temperatures and pressures makes them less flexible than line lists. However, techniques have been developed to interpolate between measurements with polynomial coefficients (Buehler et al. 2022) as well as producing pseudo-line lists (Steffens et al. 2023). Each technique does not identify quantum mechanical transitions, as is the case for spectroscopic line lists (see earlier in Section 2), but instead empirical parameters are determined that can reproduce the absorption cross-section intensity over the range of measurements. However, care should be taken when extrapolating these techniques to conditions beyond those used from the initial studies.

Ariel will cover the ~2500–5000 cm^{-1} (~2 - 4 μm) region at a resolving power of 100 (see Table 1), which spans the spectral range where key molecular functional groups (e.g. C-H stretch at ~ 3000-3300 cm^{-1}) exhibit strong absorption. The majority of the absorption cross-sections described above and included in HITRAN have spectral features within this region. Some of these molecules have already been proposed as biosignatures (Zhan et al. 2021) or technosignatures (Haqq-Misra et al. 2022), due to their distinct spectral features and limited pathways for synthesis. Indeed, it was in this spectral range that the recent tentative detection of dimethyl sulphide (DMS or $(CH_3)_2S$) was made from transit spectra of K2-18b recorded using JWST (Madhusudhan et al. 2023) and absorption cross-sections in HITRAN.

Polycyclic aromatic hydrocarbons (PAHs) and tholins are known to contribute significantly to the optical properties of Solar System planetary spectra (Abdel-Shafy & Mansour 2016; Zhao et al. 2018). They have an optical slope similar to cloud/hazes, potentially causing a degeneracy in the interpretation of spectral data caused by aerosols (see Section 6, and, for example, Figure 1 of Ercolano et al. (2022)). Ercolano et al. (2022) explore the detectability of PAHs observed with Ariel (Tinetti et al. 2018) and Twinkle (Edwards et al. 2019b), finding there is

Table 9. Molecular line lists obtained from comb-referenced spectroscopy measurements using different methods: CRDS - cavity ring down spectroscopy; NICE-OHMS - noise-immune cavity enhanced optical heterodyne molecular spectroscopy; CRSS - comb-referenced saturation spectroscopy, DAS - direct absorption spectroscopy; CEAS - cavity enhanced absorption spectroscopy, NICE-VMS - noise-immune cavity enhanced velocity modulation spectroscopy. The spectral coverage of each is also indicated.

Molecule	Band	Range [cm^{-1}]	Range [μm]	Method	Reference
$H_2^{16}O$	(013 ← 000)	12,621 - 12,665	0.789 - 0.792	CRDS	Chen et al. (2018)
	(101 ← 000)	7164 - 7185	1.391 - 1.396	CRDS	Kassi et al. (2018)
	(200 ← 000)	7000 - 7350	1.36 - 1.43	NICE-OHMS[a]	Tóbiás et al. (2020); Diouf et al. (2022) Tóbiás et al. (2024)
$H_2{}^{17}O$	(200 ← 000)[b]	7228 - 7289	1.37 - 1.38	NICE-OHMS	Melosso et al. (2021)
$H_2{}^{18}O$	(200 ← 000)	7000 - 7350	1.36 - 1.43	NICE-OHMS[a]	Diouf et al. (2021); Tóbiás et al. (2024)
H_2O[c]	Several[d]	8041 – 8633	1.15 - 1.24	CRDS	Koroleva et al. (2023)
$^{12}C^{16}O_2$	(30012 ← 00001)	6170 – 6370	1.57 - 1.62	CRDS	Reed et al. (2021)
	(30013 ← 00001)				
	(30012 ← 00001)[d]	6170 – 6370	1.57 - 1.62	CRDS	Guo et al. (2021)
	(20012 ← 00001)	4830 – 5010	1.99 - 2.07	CRDS	Fleurbaey et al. (2023)
	(20013 ← 00001)				
	(01111 ← 01101)	2306 – 2312	4.33 - 4.34	CRSS	Galli et al. (2013)
$^{14}C^{16}O_2$	(00011 ← 00001)	2190 – 2250	4.44 - 4.57	CRDS	Galli et al. (2011)
N_2O	$3\nu_1$	6518 - 6578	1.52 - 1.53	CRDS	Liu et al. (2019)
	$3\nu_1$	6518 - 6578	1.52 - 1.53	DAS	Iwakuni (2022)
	ν_3	2190 – 2210	4.52 - 4.57	DAS	Knabe et al. (2013)
	ν_3	2130 - 2270	4.41 - 4.69	CRSS	Ting et al. (2014)
	ν_1	1250 - 1310	7.63 - 8.00	DAS	AlSaif et al. (2018)
N_2O[e]	– [d]	8320 – 8620	1.16 - 1.20	CRDS	Karlovets et al. (2021, 2022)
CO	(7 ← 0)[d]	14300 - 14500	0.689 - 0.699	CRDS	Balashov et al. (2023)
	(3 ← 0)	6170 - 6420	1.56 - 1.62	CRDS	Mondelain et al. (2015)
	(3 ← 0)	6170 - 6420	1.56 - 1.62	CRDS	Kowzan et al. (2017)
	(3 ← 0)	6170 - 6420	1.56 - 1.62	CRDS	Wang et al. (2021)
	(4 ← 0)[d]	8206 - 8465	1.18 - 1.22	CRDS	Bordet et al. (2021)
CH_4	$2\nu_3$	6015 – 6115	1.64 - 1.66	CRDS	Votava et al. (2022)
	ν_3	2890 - 3120	3.21 - 3.46	CEAS	Okubo et al. (2011); Abe et al. (2013)
	ν_3	2890 - 3120	3.21 - 3.46	CRSS	Kocheril et al. (2018)
O_2	B band[d]	14539 – 14550	0.687 - 0.688	CRDS	Domysławska et al. (2020)
	(0,0)[d]	7800 – 7960	1.26 - 1.28	CRDS	Fleurbaey et al. (2021)
$H^{13}CN$	$2\nu_3$	6390 – 6536	1.53 - 1.56	CRSS	Hrabina et al. (2022)
D_2H^+	ν_1	2588 – 2930	3.41 - 3.86	NICE-VMS	Markus et al. (2019)
CHF_3	ν_5	1156 - 1160	8.62 - 8.65	CRSS	Vicentini et al. (2020)
CH_3OH	ν_5	970 - 973	10.29 - 10.30	CRSS	Santagata et al. (2019)
Benzene	ν_{11}	675 - 689	14.5 - 14.8	DAS	Lamperti et al. (2020)

[a]: Assisted with spectroscopic networks; [b]: Hyperfine-resolved; [c]: Six isotopologues; [d]: Intensities provided; [e]: Five isotopologues

a possibility of detection. Dubey et al. (2023) investigate the formation processes of various PAHs on the thermalised atmospheres of hot Jupiter exoplanets, and found that planets with an effective temperature of around 1300 K are the most promising targets for investigating PAHs, particularly for atmospheres with a high carbon-to-oxygen ratio (C/O) and high metallicity. A follow-up study by Grübel et al. (MNRAS, submitted) focuses on the inter-comparison of different cloud/haze, PAHs and tholin models while retrieving the best case scenario for a particular planet, Wasp-6 b. The cross-sections presented by Ercolano et al. (2022), based on calculations of Draine & Li (2007), represent a combined effect observed from a collection of crystalline PAHs. These cross-sections are consistent with observations of the interstellar medium (ISM) and thus presumably originate from a diverse PAH mixture. Given the sheer amount of different molecules, they currently represent the most convenient way to implement PAHs in atmospheric retrievals. The NASA Ames PAH IR Spectral Database is a source of cross-section data for PAHs (Boersma et al. 2014; Bauschlicher et al. 2018; Mattioda et al. 2020)[13], offering extensive data on thousands of PAHs, although primarily for the identification within interstellar emission spectra rather than for their detection in exoplanetary atmospheres.

2.1.3.2 Vibrational frequency calculations The computation of a full ro-vibrational line list for one species can be very time consuming, and often takes years to produce. There has thus been work on computing the vibrational spectra for a large number of species, and then adding rotational sub-structure (for example using software such as PGOPHER (Western 2017)), in order to indicate where prominent spectral features are expected. Root mean square errors of such computations are typically on the order of 15 - 25cm^{-1} (Zapata Trujillo & McKemmish 2022b), with higher order computational chemistry or laboratory-derived data required to be incorporated for higher accuracies. There are some notable absorption features in the observed spectra of some exoplanet atmospheres, for example in WASP-39b's

[13] https://www.astrochem.org/pahdb/

atmosphere at 4.56 μm as observed by JWST (Alderson et al. 2023), which have yet to be identified among the species with available ro-vibrational spectra. There is benefit in identifying potential species or types of species which could fit such features, which could then give incentive for more detailed work into the full ro-vibrational spectra. The computation of such vibrational frequencies for large numbers of molecules is facilitated by studies into the best practice for appropriate model chemistry choices for harmonic frequency calculations, such as Zapata Trujillo & McKemmish (2022b, 2023). VIBFREQ1295 (Zapata Trujillo & McKemmish 2022a) is a database of vibrational frequency calculations. RASCALL (Rapid Approximate Spectral Calculations for ALL) (Sousa-Silva et al. 2019) is an approach which can simulate spectra consisting of approximate band centres and qualitative intensities for a huge number of species. The approximate spectra for a large number of phosphorus-bearing species was computed by Zapata Trujillo et al. (2021), building upon the RASCALL database by using quantum chemistry to improve on the accuracy of the approximate spectra for these species.

In addition, computations are available which focus on the vibrational spectra of nanoclusters, such as $(TiO_2)_n$, which can be important for exoplanet atmosphere models or observations in the IR (Sindel et al. 2023). Vibrational frequencies of other nanoclusters have been computed, such as $(VO)_n$ up to $n = 10$ (Lecoq-Molinos et al. 2024), $(VO_2)_n$ up to $n = 10$ (Lecoq-Molinos et al. 2024), $(V_2O_5)_n$ up to $n = 4$ (Lecoq-Molinos et al. 2024), Ti_xO_y (Jeong et al. 2000) and $(MgO)_x$ (Chen et al. 2014).

2.1.4 *How high-resolution laboratory spectroscopy can help improve the accuracy of theoretically computed line lists*

There are several ways in which laboratory spectroscopy can contribute to the data needs of exoplanetary atmospheric studies, some of which are already in active use and some require more investment. The most common and efficient methodology of the production of spectroscopic data is semi-empirical, in which molecular spectra are first measured at given laboratory conditions (temperature, pressures, wavelength range etc), analysed and then inter- or extrapolated to conditions dictated by the retrieval frameworks. A typical example illustrating the need for such extrapolations is that most of the existing experimental molecular spectra have been recorded at, or close to, the ambient atmospheric conditions on Earth, i.e. room temperature and pressure, and for specific spectroscopic ranges dictated by the experimental setup. A typical retrieval procedure, on the other hand, requires a broad range of temperatures, pressures and wavelengths, on dense grids of the corresponding values (for example, pressures between at least 1×10^{-5} - 100 bar, and temperatures ~100 K - 3000 K). This is achieved by representing the experimental data in some functional forms, so-called spectroscopic models, of different complexity and extrapolation power.

This is a powerful, well established procedure, which is however very hungry for experimental data. Some molecules have almost no spectra measured, especially those corresponding to extreme conditions such as suggested for the atmospheres of the so-called Lava planets, including SiO_2, KOH, NaOH and MgOH (Schaefer et al. 2012; Tennyson & Yurchenko 2017). Apart from the mainstream atmospheric molecules, such as those described in Section 2.1.2.2, with relatively accessible spectra, there is a serious lack of analysed laboratory spectra for a large number of molecules at higher temperatures and lower wavelengths.

The so-called effective Hamiltonians (such as used by CaSDa) based on Taylor-type expansions with respect to the angular momenta with a large set of empirical spectroscopic constants provide very accurate description of the experimental spectra (usually recorded at room temperature) but with rather limited extrapolation power (e.g. to higher temperatures and especially to higher energies). These methods usually benefit from an extensive rotational coverage of individual vibrational bands in a given spectroscopic regions and thus are ideally suitable for the analysis of the FTS-like broad band techniques, as mentioned above. The so-called empirically adjusted *ab initio* techniques (employed by ExoMol, ThoReTS and NASA Ames) are based on the empirical refinement of the underlying inter-nuclear *ab initio* spectroscopic properties, such e.g. potential energy surfaces (PES). These methods hugely benefit from analysed laboratory data (line positions and energies), ideally with an extensive coverage of the vibrational excitations at the lowest rotational excitations to minimise the coupling between the rotational and vibrational degrees of freedom. Put simply, experimental information on vibrations is especially important to increase the quality of the extrapolation of the empirical model, while the rotational information is more useful for interpolation and benchmarking of the models. These type of empirical techniques are less accurate than effective Hamiltonians when it comes to matching the experiment, but are very powerful when extrapolating to higher temperatures and even higher energies.

The MARVEL (measured active rotation-vibration energy levels) (Furtenbacher et al. 2007) process involves analysing high-accuracy laboratory measured spectra to get out experimentally-determined energy levels. These energy levels are then used in theoretically computed line lists to improve the accuracy of all transitions which involve those levels. In the case of the ExoMol database, the MARVEL process has been applied to molecular line lists for species such as C_2H_2 (Chubb et al. 2018a), TiO (McKemmish et al. 2017), H_2CS (Mellor et al. 2022), C_2 (Furtenbacher et al. 2016; McKemmish et al. 2020), CaOH (Wang et al. 2020a), H_2S (Chubb et al. 2018b), NH_3 (Al-Derzi et al. 2015; Furtenbacher et al. 2020), AlO (Bowesman et al. 2021), H_2CO (Al-Derzi et al. 2021; Germann et al. 2024), H_3^+ (Bowesman et al. 2022), OCS (Xu & Tennyson 2024) as well as ongoing efforts to refine the line list of PH_3. Due to new laboratory data becoming available, the MARVEL process for improving the accuracy of theoretial line lists need to be assessed periodically. The opacities computed from line lists therefore also ideally need recomputing periodically, as the accuracy and coverage of line lists improve (see Section 4).

Regardless of the method used to improve the accuracy of theoretically computed line lists, their key common feature is the strong dependence on experimental laboratory data. Even the best modern *ab initio* methods, except perhaps of very limited systems, do not have the required quality to be used in atmospheric applications and need to be either completely constructed from scratch, such as for the Effective Hamiltonians, by fitting the corresponding expansion, so-called spectroscopic, parameters or refined, such as for

the *ab initio* methods, by fitting the corresponding analytic descriptions of the spectroscopic models to the experimental data.

Our general appeal to the experimental spectroscopists who would like to engage with exoplanetary atmospheric studies is to talk to the atmospheric modelers about their direct needs in terms of the species, temperature and wavelength coverage and also talk to the line list providers about their needs in terms of the vibrational and rotational coverage.

2.2 Data used by retrieval codes

Owing to the importance of the line lists for atmospheric retrievals, it would not be an exaggeration to say that all, or close to all, the line lists discussed throughout this section, have already been or are in the process of being included in the main (exo-)planetary retrieval frameworks. It is the usual practice of exoplanetary atmospheric modelers to implement new line lists or important updates into their retrieval programs periodically; this usually involves building molecular opacities in the form of cross-sections or k-tables. Details on opacities used in various retrieval codes can be found in Section 4.

2.3 What's being worked on?

(i) **ExoMol:** at the time of writing, the following line lists are in progress by the ExoMol project (see Section 2.1.1.2), either as new species or improvements/updates to existing line lists; diatomics: OH, PN, CO, CH, CS, OH^+, NO^+, NiH, CrH, AlF, BH, ZrS; triatomics in IR: HCN, HOD; triatomics (electronic): HCN; larger polyatomic (IR): C_2H_2, C_2H_6. MARVEL studies for N_2O isotopologues (see Tennyson et al. (2024a) for $^{14}N_2^{16}O$), CO_2 (see Ibrahim et al. (2024); Alatoom et al. (2024), CO, HCN/HNC, HCO^+, BH, CS_2, C_2H_4 and $^{15}NH_3$ are being performed as well as updates to $^{14}NH_3$, HCCH, and inevitably, water.

(ii) **TheoReTS:** line lists for several species including CH_2, CH_3, NH_3, H_2CCN, H_2NCN, CH_3Cl, C_3H_4, H_2O_2, CCl_4, CH_3CN or C_2H_6 are being worked on, and will be gradually uploaded to the TheoReTS database (see Section 2.1.1.5).

(iii) **CaSDa:** the CaSDa database is working on producing new IR data for the existing species listed in Table 5, including new bands and new isotopologues (e.g. for CH_3D). They also plan to develop new line lists for species such as SiH_4 and $C_3H_6O_3$ (see Section 2.1.1.1).

(iv) **NASA Ames:** line lists for sulphur-bearing species OCS and CS_2 (see Section 2.1.1.4).

(v) **HITRAN and HITEMP:** Work toward the next edition of the HITRAN database is underway, which will include works highlighted in the HITRAN2020 paper (Gordon et al. 2022) and additional recent literature. Examples include expanding the 3800-4800 cm^{-1} region of NH_3, the addition of new molecules such as S_2 (Gomez et al. 2024).

(vi) **Non-LTE conditions:** although most studies of exoplanet atmospheres assume species to be in local thermodynamic equilibrium (LTE), effects arising from non-LTE conditions are known to be important in Earth's upper atmosphere, as well as in the atmospheres of other Solar System planets. In the most accurate treatment, non-LTE radiative transfer calculations determine the populations of all the atomic and molecular states involved by considering the relevant species' rates with respect to radiative decay and collisional excitation, de-excitation as well as potentially ionisation and other processes (Wright et al. 2022). However, complete data sets are rarely available for this purpose; even for the Non-LTE of H atoms, some of the collisional data are not so well known. In particular, data for collisions of H atoms with heavy particles (atoms/molecules) are lacking (Muñoz & Schneider 2019). Studies such as Wright et al. (2022) are working towards improving data and models for non-LTE effects in exoplanet atmospheres. In a recent work, García Muñoz et al. (2024) also considered non-LTE effects and emphasised the importance of H_2O-H_2O excitation collisions, especially for the vibrational modes of the molecule.

(vii) **Vibrational modes of molecular clusters:** vibrational spectra from DFT calculations are in progress for species such as $(TiO)_n$ clusters up to n = 10 and $(SiO)_n$ clusters up to n = 20 (Lecoq-Molinos, in prep.).

(viii) **Quantum computing approaches:** *ab initio* line list parameters are currently calculated using modern high-performance computers, particularly crucial for line lists containing millions to billions of transitions. However, the algorithms used can become computationally intensive and time consuming, scaling with the complexity of the molecule and temperature coverage. Quantum computers could be an alternative solution, even though fault-tolerant quantum computers are unlikely to be available in the immediate future. Variational Quantum Algorithms (VQAs) and, in particular, Variational Quantum Eigensolvers (QVEs) are promising class of algorithms to estimate the eigenstates and the corresponding eigenvalues of a given Hamiltonian (Cerezo et al. 2020; Tilly et al. 2022). This kind of technology demonstrates the potential, from a theoretical point of view, to describe the electronic structure of complex molecules faster. In the near future, a quantum speedup would be ideal to describe precise line lists (Innan et al. 2023).

2.4 Data needs: What's missing and urgent?

The main molecules expected to be observed by Ariel and JWST are the usual atmospheric suspects, H_2O, CO_2 and CH_4, as well as the recently detected SO_2. The line lists for these species are generally in a good shape both in terms of temperature completeness and in terms of accuracy, at least as far as space-based observations in the IR are concerned. This applies to other potentially detectable, common atmospheric absorbers such as NH_3, HCN, N_2O, NO, C_2H_2 etc. While the existing data for these species should be at a high level of readiness for the majority of low-to-medium resolution studies including JWST or Ariel, not all line lists extend to low enough wavelengths to cover the entire range observed by these telescopes - see, for example, the wavelength ranges in Tables 7 - 15 of Chubb et al. (2020a) for a number of high-temperature line lists and should be considered when interpreting observed spectra which includes a wavelength region not covered by a given line list. Not taking this into account could cause some biases in analyses which extend beyond the wavelength range of current line lists. Extending current line lists into the optical is therefore very important. Less mainstream or more exotic molecules are not at such a good readiness level, some of which we re-

view in the following. The line lists for high resolution (HR) applications require even more work. With some exceptions, such as H_2O or CO_2 in the mid-IR, HR applications demand further improvement of the quality and quantity of the laboratory data at high temperatures for most of the molecules. The data needs discussed below are mostly for the IR and optical regions as directly imposed by to the observational and associated retrieval coverage of Ariel and JWST. However, the data needs in shorter wavelengths, UV and even far-UV, are dictated by the atmospheric chemistry models (see Section 7).

(i) **Species occurring in JWST studies:** The recent potential detection of CS_2 in the exoplanetary atmosphere of TOI-270d (Holmberg & Madhusudhan 2024; Benneke et al. 2024) is an example of a molecule requiring improvement of the spectral coverage of associated molecular data, highlighting the need for line lists of sulphur species such as CS_2 up to high temperatures. The recent observation of SO_2 in the atmosphere of hot gas giant exoplanet WASP-39 b (Tsai et al. 2023; Powell et al. 2024) and in the atmosphere of warm Neptune WASP-107 b (Dyrek et al. 2024) prompted an increase in interest in sulphur species, with theoretical studies such as Janssen et al. (2023) predicting the importance of them also in hot rocky exoplanet atmospheres. The SO_2 line list of Underwood et al. (2016b) is considered complete up to high temperatures of ~2000 K in the wavelength range it covers, but only covers wavelengths down to 1.25 μm. This will lead to an underestimation of opacity in the wavelength region below 1.25 μm for model atmospheres including SO_2. The main reason for the lack of wavelength coverage of the line list is that the quantum chemistry computations used for computing a high-temperature line list can become extremely computationally extensive with increasing energy (decreasing wavelength), especially for molecules composed of more and heavier atoms. Considering the recent SO_2 detections in exoplanet atmospheres, having a high temperature line list extending to lower wavelengths is a high priority.

(ii) **Ti- and V-bearing species:** Hoeijmakers et al. (2020) predict significant concentrations of gas-phase TiO_2, VO_2, and TiS in the atmosphere of hot Jupiter exoplanet WASP-121b. These could be important absorbers, potentially accessible both by the high and low resolution observational methods, which currently do not have any available ro-vibrational (IR) or rovibronic (Vis and UV) line lists.

(iii) **Species relevant to lava planets:** recent studies suggested that modelling the atmospheric properties of hot-Super Earth (lava) exoplanets require different types species to be considered, including KOH, NaOH, SiO_2, CaOH, FeO, MgO, MgOH (Schaefer et al. 2012; Tennyson & Yurchenko 2017; Mahapatra et al. 2017). There have therefore been calls for line lists for these species spanning the IR and visible spectral region. We note these calls have been somewhat addressed and there are now available line lists from ExoMol for KOH and NaOH (IR) (Owens et al. 2021), SiO_2 (IR) (Owens et al. 2020), CaOH (IR, Vis) (Owens et al. 2022b), MgO (IR, UV) (Li et al. 2019). Theoretically, FeO is particularly challenging; there are more than fifty low-lying electronic states (Sakellaris et al. 2011; Tennyson & Yurchenko 2017).

(iv) **Carbon and hydrocarbon species:** for example, C_3 which can be important for high-temperature carbon atmospheres (Aringer et al. 2009). An ExoMol IR line list for C_3 has just been completed (Lynas-Gray et al. 2024). Martin-Drumel et al. (2023) report recent laboratory work on the infrared spectra of C_3, with a combined fit of available infrared and optical laboratory data performed using the PGOPHER (Western 2017) package; these and other data were used as input for a MARVEL study (Tennyson 2024). Molecular line lists are required for the following hydrocarbon species, in IR for direct retrievals and at shorter wavelengths for atmospheric chemistry modellings (see more in Section 7). C_4H is considered to be important in the upper atmosphere of low-metallicity objects (Bilger et al. 2013). Allene (CH_2CHCH) and propyne (CH_3CCH) are isomers of one another which have both been detected on Titan (Lombardo et al. 2019; Nixon et al. 2013). Propene has also been observed on Earth (Blake et al. 1996), and is expected on Saturn (Moses et al. 2000). There are some known cross-sections for propene (Bernath et al. 2023), including some hosted by the HITRAN database (Sung et al. 2018), but not a line list.

(v) **PAHs:** can be important for Earth and Titan-like atmospheres (López-Puertas et al. 2013). As previously mentioned, one of the main sources of PAH cross-sections is the NASA Ames PAH database (Boersma et al. 2014; Bauschlicher et al. 2018; Mattioda et al. 2020)[14], which is tailored for characterising species in the cold temperatures of the ISM. To be able to fully comprehend the abundance and role of PAHs on exoplanets, there is a need for new PAH opacities to be calculated or measured over a broad parameter space of environmental conditions and easily implementable for retrieval applications. This necessity extends beyond the infrared spectrum, as the availability of temperature-dependent UV cross-sections is quite limited (see Section 8 for the availability of UV PAH photionisation and photoabsorption cross-sections).

(vi) **Species relevant to Archean atmospheres:** another special type of exoplanetary atmosphere with special data requirements are archean atmospheres, necessitating line lists for species including HC_3N (Rimmer et al. 2019, 2021).

(vii) **Molecular ions:** Bourgalais et al. (2020) performed laboratory experiments to help identify ions observable by Ariel in the upper atmospheres of sub-Neptunes. Their results pointed towards H_3O^+ and H_3^+ being the most promising. Partly as a consequence of this study ExoMol provides IR line lists for H_3O^+ (Yurchenko et al. 2020b) and H_3^+ (Mizus et al. 2017; Bowesman et al. 2023). The ExoMol database also provides line lists for a number of other ions including CH^+ (Pearce et al. 2024), OH^+ Hodges & Bernath (2017); Hodges et al. (2018) and HeH^+ (Amaral et al. 2019) covering a very broad wavelength range. Other potentially important ions for which there are no suitable line lists at present include HCO^+, N_2H^+ and H_2O^+, as well as NO^+ which is the dominant molecular ion in the Earth's ionosphere.

(viii) **Radicals:** such as OH, HO_2, C_2H, CH_2, C_3H_3, NH_2, N_2H_3 are known to be important on Earth (Seinfeld & Pandis 2016), Mars (McElroy & Donahue 1972), Titan (Wilson & Atreya 2004), and other planetary atmospheres (Catling & Kasting 2017). Out of these species, the required molecular data are only in a good shape for OH. There are high quality (accurate and complete) rovibronic data for OH applicable for IR and UV studies (Bernath 2020;

[14] https://www.astrochem.org/pahdb/

Mitev et al. 2024). Construction of an IR line list for CH_2 is in progress as part of TheoReTs.

(ix) **Line lists are needed** extending into the UV and optical. Extension down to the UV is needed for all major species such as, H_2O, CO_2, CO, OH, CH_4, HCN, N_2, NH_3, C_2H_2, C_2H_4, C_2H_6, H_3^+, H_2^+, H_3O^+, OH^+, SO, SH, H_2S, SO_2, OCS, S_2, CS. See Section 8 for further discussion on UV photoabsorption and photodissociation data. In some of these cases (such as HCN, NH_3, C_2H_2, C_2H_4, C_2H_6, H_3O^+, H_2S, SO_2, OCS), data in the optical as well as the UV is also lacking or only partially covered for line lists which are appropriate up to high temperatures. Extending even just down to the optical region is even more pressing for direct use of these line lists in interpreting and modelling Ariel and JWST observations. We note that spectroscopic measurements of excited states of some of these species in the UV region are available in the literature, for example for NH_3 from Langford et al. (1998). See Section 2.1.4 for a discussion on how measured data such as these can be used to compute an accurate and complete line list up to high temperatures.

(x) **Isotopologues:** Very recently Lew et al. (2024) used JWST to detect isotopologues of CO. Similar studies have been performed on cool stars from the ground (Pavlenko et al. 2020b,a); such isotope-resolved studies have the potential to provide a lot of extra information about atmospheres. Some atoms have more than one isotope with relatively large terrestrial abundances, e.g. Cl is 75% ^{35}Cl and 25% ^{37}Cl. In other cases, isotopic abundances can be very different from Solar abundances, e.g. Mg and C. The importance of H means that even if deuterium (D) is a minor fraction, D containing molecules such HD, HOD and CH_3D can be highly abundant. We note that all these species have different symmetry to the parent (unsubstituted) molecule which means that the spectra of the two species differ significantly. The ExoMol data base provides line lists for HOD (Voronin et al. 2010) and the weak IR spectrum of HD (Amaral et al. 2019), while CH_3D has been considered by TheoReTs (Rey et al. 2014b). Lines for isotopically substituted species which do not break their symmetry are straightforward to compute given a spectroscopic model for the parent molecule, and this done routinely by ExoMol; methods to improve the accuracy of these line lists have been developed (Polyansky et al. 2017; McKemmish et al. 2024). A list of natural (terrestrial) abundances of various species included in the HITRAN database can be found online[15], as well as elemental isotopic compositions from NIST[16].

(xi) **Vibrational modes of molecular clusters:** Köhn et al. (2021) point out that the onset of cloud formation may be observable through vibrational bands of $(TiO_2)_4$, $(TiO_2)_5$, and $(TiO_2)_6$, potentially via the Mid-Infrared Instrument on JWST or the Extremely Large Telescope's mid-IR imager, but more complete line-list data are required first. We note that the full quantum chemical computation of line lists for such large clusters is challenging, and so may require computations of vibrational frequencies only, at least as a starting point. There is some discussion on this in Section 2.1.3.2. We note some vibrational data for TiO_2 nanoclusters have recently been computed (Sindel et al. 2023).

[15] https://hitran.org/docs/iso-meta/
[16] http://physics.nist.gov/Comp

3 LINE SHAPES: MOLECULAR AND ATOMIC

3.1 Theoretical approaches to line-shape parameters: Molecules

The Voigt profile. In order to simulate a spectrum of a single molecule at given pressure and temperature, three main components are required; line position, line intensity and line profile. In this section, the latter is reviewed. The most popular line profile used in the majority of atmospheric applications (and beyond) is the Voigt profile. It refers to the so-called "intermediate" pressure regime and accounts for collision (pressure) and Doppler (thermal motion) broadenings considered as statistically independent processes and has been the standard for high-resolution line-by-line modelling of infrared molecular absorption (Armstrong 1967). The Voigt profile represents a convolution of the associated Lorentzian and Gaussian profiles, representing the collisional and Doppler effects, and tends to these two shapes in the limiting cases of high and low gas densities, respectively. The Voigt profile has no closed analytical form and is often related to the complex probability function. Several special numerical algorithms exist in the literature for efficient evaluation of the Voigt profile (Humblicek 1982; Kuntz 1997), see the recent computational and numerical comparison by Zhang et al. (2024); some numerical approaches allow one to take advantage of the convolution of the entire spectrum at once (van den Bekerom & Pannier 2021). While for the Doppler contribution, the corresponding (half) line width γ_D is a simple function of the molecular mass, gas temperature and the line positions (frequency):

$$\gamma_D = \sqrt{\frac{2N_A k_B T \ln 2}{M}} \frac{\tilde{\nu}_{fi}}{c}, \quad (1)$$

there is no simple analytic description of the line (half) width γ_L, defining the Lorentzian contribution, at least in the general case. The molecular parameters γ_L strongly depend on the system (the molecule and the perturbing partner), as well as on the gas conditions, i.e. pressure and temperature. Together with the line positions $\tilde{\nu}$, transition probabilities (e.g. oscillator strength gf or Einstein A coefficients), the Lorentzian width (usually half-width-at-maximum, or HWHM) γ_L are an integral part of spectroscopic databases. They are typically obtained empirically either through direct measurements with different level of parametric modelling or semi-empirically, where a more sophisticated theory tuned to available experimental data is involved such as, e.g., the semi-empirical approaches (Bykov et al. 2004) representing a simplification of the Robert-Bonamy formulae to Anderson-type expressions with fitted correction-factor parameters or modified complex Robert-Bonamy calculations (Ma et al. 2007) with adjusted atom-atom interaction parameters. Application of fully first-principles methods are currently limited to simple system or low temperatures (Wcisło et al. 2021).

The pressure-broadening of spectral lines corresponding to pure *rotational* (microwave, MW) and *rovibrational* (infrared, IR) transitions is mainly governed by inelastic collisions (De Lucia & Green 1988) and exhibit (except for light perturbers such as hydrogen and helium) strongly pronounced dependence on the rotational quantum number J.

Apart from the line broadening effect, collisions also affect the line positions by introducing the so-called line shift δ. These are also provided by the spectroscopic databases, especially those focusing on high resolution applications,

such as terrestrial, planetary (Sung & Varanasi 2005), Solar and in some cases stellar, but so far have not featured very much in the low-mid resolution spectroscopy of exoplanets, as would be applicable to the Ariel mission. It is also noteworthy that ro-vibrational line shifts are typically smaller than the associated line widths by some orders of magnitude.

In the context of the Ariel mission, the temperature and pressure dependencies of line widths are crucial. For Voigt line widths γ (in $\mathrm{cm}^{-1}\mathrm{atm}^{-1}$), the following power law is almost always assumed:

$$\gamma(T) = \gamma_0(T_{\mathrm{ref}}, P_{\mathrm{ref}}) \left(\frac{T_{\mathrm{ref}}}{T}\right)^n \frac{P}{P_{\mathrm{ref}}}, \quad (2)$$

where T_{ref} and P_{ref} are some reference temperature and pressure (e.g. 1 atm and 296 K, respectively). Then the parameters γ_0 (reference value of HWHM) and n (temperature exponents) are tabulated by the databases for each perturber. This model works quite well for many molecular systems but for a given set of parameters it can deviate when a description of a large range of temperatures is required.

The Lorentzian (and therefore Voigt) as an isolated line profile model is known to fail in the far wings, always leading to an overestimation of the opacity at high pressure, especially for the systems with closely spaced lines (Hartmann et al. 2008, Chapter IV), e.g. in heavier molecules. As a work-around, a cut-off the far wings at some distance from the centre of the line is applied. The common standards are to use a 25 cm^{-1} cut-off, employed by HITRAN, ExoMol and now also by MAESTRO (Molecules and Atoms in Exoplanet Science: Tools and Resources for Opacities) (Gharib-Nezhad et al. 2024). A detailed analysis of line-wing profiles and cutoffs in the context of exoplanet atmospheres, including the Voigt profile, can be found in Gharib-Nezhad et al. (2024).

Beyond the Voigt line profile. Recent experimental studies powered by the development of experimental techniques in the last few decades have demonstrated the importance of the departure of the line shape description from the simple Voigt profile model, at least for high resolution applications. This motivated the spectroscopic databases also to provide parameters for more accurate profile models. One of such departures is due to the effect of collisional (Dicke) line narrowing.

The line narrowing can be described either as a reduction of the Doppler component (velocity-changing collisions resulting in molecular confinement) or the dependence of the collisional relaxation rates on the relative molecular speed. In the first case, velocity-changing collisions are often considered as strong (no memory effects, Maxwell-Boltzmann re-distribution of velocities after each collision) and the most frequently used associated profile is that of Rautian & Sobel'man (1966, 1967), although the soft-collision model (light perturbers, many collisions required to modify significantly the active-molecule velocity) developed by Galatry (1961) is used by some researchers too. It is now understood that both mechanisms can be important across any pressure regimes, from very low to very high (D'Eu et al. 2002).

In the second case, the speed-dependence (SD) of the collisional relaxation rates dominates the line narrowing and the corresponding models forming the so-called Speed-Dependent Voigt (SDV) profiles. The most accurate description of the dependence on the absolute absorber's speed (Berman 1972; Pickett 1980) is by the hypergeometric confluent function (hgSDV model), which however, leads to high computational costs. As a more practical approach, a modification of hgSDV based on the mean quadratic speed (Rohart et al. 1994; Köhler et al. 1995; Rohart et al. 2007) is used (qSDV model, often referred to as simply SDV), for which an efficient numerical-calculation algorithm is available (Boone et al. 2007).

Both mechanisms, with the velocity-changing collisions and with the speed dependence viewed as independent, are accounted for in "combined" line-shape models, such as Speed-Dependent Rautian (SDR) or Speed-Dependent Galatry (SDG) profiles. The partial correlation of these effects is considered by the partially Correlated quadratic-Speed-Dependent Hard-Collision profile (pCqSDHCP), developed by Tran et al. (2013) (called the Hartmann-Tran profile or HTP profile) and recommended for high resolution spectroscopy in a IUPAC Technical Report (Tennyson et al. 2014). Parameters for this advanced profile have been incorporated into the HITRAN database (Gordon et al. 2022) since 2016 for the hydrogen molecule as well as some transitions of water vapor and molecular oxygen. The line narrowing effects, being routinely used in high-resolution terrestrial and planetary applications, have not been considered in the mainstream exoplanetary spectroscopic studies yet, and likely first requires studies to demonstrate the impact of such line profiles on different atmospheric models.

Another important deficiency of the common line profile methodology used in spectral modelling is due to the breakdown of the isolated lines approximation. This phenomenon, also caused by molecular collisions, is associated with the so-called line-mixing or line-interference effect. While the line narrowing effects are mostly noticeable at lower pressure (well below 1 atm for most gases), line-mixing usually becomes relevant at higher pressure when individual lines start to broaden and overlap. Line-mixing effects can be especailly significant in the line wings regions where intensity is never truly zero, and there is always some degree of overlapping with others lines. Because of this effect, the intensity in the wings of a band falls off faster than predicted by the sum of Lorentzians (see figures in Hartmann et al. 2010). To a lesser extent, the troughs between individual lines or branches can also be affected. In practice, as stated above, cross-sections calculations employ sums of Voigt profiles with certain wing cut-offs, say ± 25 cm^{-1} from line centres. Such treatment bypasses a proper account of line-mixing and prevents overestimation of absorption away from band centres which would come from addition of billions of line wings (recall that the wings of the Voigt profile fall off as Lorentzians $\propto \omega^{-2}$ and not exponentially). However, such cut-offs may lead to another non-physical situation, where the calculated cross-sections between strong bands end up being exactly zero. In reality, line-mixing would cause a sub-Lorentzian shape that far enough from strong absorption bands would contribute to continuum absorption (see Section 5 for a discussion on continuum absorption). An in-depth discussion of wing cut-offs is presented in Gharib-Nezhad et al. (2024). An empirical method of far-wing corrections involving χ-factors is discussed in the following sections.

At higher pressure where even line cores significantly overlap, line-mixing can lead to a noticeable intensity redistribution within a branch or an entire band. This is known

to happen for closely spaced lines in Q-branches and band heads even at sub-atmospheric pressures, and these features may appear stronger and more narrow than one would expect from the sum of isolated lines. This presents potential interest for more reliable confirmation of molecular species' detection, where features like these are often the most noticeable. The case of very high pressure has been considered before in order to describe the deep venusian atmosphere (Filippov et al. 2013; Buldyreva et al. 2013). In such conditions, the rotational structure is entirely collapsed and the band shape differs significantly from the sum of individual spectral lines. This is relevant to modelling of radiative transfer in hot dense atmospheres.

Proper analysis of line-mixing is complicated, and usually a perturbative approach is taken on a band-by-band basis for the most intense bands. At present, line-mixing is not typically implemented in suites for producing opacities for exoplanetary atmospheric retrievals, although these effects may become more important with newer instruments that can probe high-pressure regions of around 1 - 10 bar.

Calculations of line widths and shifts.

The needs of MW/IR pressure-broadened line widths and pressure-induced line shifts for atmospheric applications motivated an extensive development of theoretical methods. The most developed and commonly accepted hypothesis of the impact approximation completed by various choices for the translational dynamics gave birth to semi-classical (Anderson 1949; Tsao & Curnutte 1962), classical (Gordon 1966), and quantum-mechanical (Baranger 1958a; Shafer & Gordon 1973) approaches. Besides, there are statistical approaches, e.g. Margenau (1935), whose two-particle static limit is the opposite case to the impact approximation. Static limit works well for low molecular velocities (negligible rate of change of intermolecular interactions) and is applicable at large frequency detunings, i.e. in the far spectral wings which are hardly observable at IR wavelegths. Therefore, approaches based on the impact approximation remain major tools for predicting collisional line-shape parameters. High computational cost and absence of refined potential-energy surfaces (PES) set limits to the use of quantum-mechanical methods as soon as polyatomic/"exotic" molecular pairs and/or high temperatures are concerned.

Quantum-mechanical approaches. The most rigorous method, close coupling (CC), is usually applied to predict parameters of purely rotational transitions at room temperature, and only some studies address hot environments. Such data, provided the vibrational contribution to line-broadening is small, can technically be reused for other lines in the infrared. Certain simplifications of this formalism, such as the coupled-states (CS) approximation (used, for example, in Thibault et al. 2011), the infinite-order sudden (IOS) approximation (Goldflam et al. 1977), and the nearest neighbour Coriolis coupling (NNCC) (Yang et al. 2018; Selim et al. 2022) can make calculations more manageable while preserving the accuracy in the high-temperature limit for most lines in the band. The main issue of quantum-mechanical approaches at higher temperatures is that the number of rotational functions needed to construct a complete basis grows too fast, making calculations of the scattering matrix impractical. A useful feature of quantum-mechanical approaches is that they allow estimating parameters of beyond-Voigt profiles mentioned above. Semiclassical approaches can provide the Lorentzian component of the profile, and with some extra work, the speed-dependence parameters. If all the parameters of the extended Hartmann-Tran profile are required, one could employ the generalised Hess approach along with CC for the scattering matrix computation. This has been done recently for H_2 and HD with helium as the perturber (Wcisło et al. 2021; Stankiewicz et al. 2021) up to 1000 K.

Semi-classical approaches. The need for accurate potential energy surfaces (PES) and long-time statistics accumulation also disadvantage purely classical computations. As a result, advanced semi-classical approaches are typically employed, such as the formalism of Robert and Bonamy (Robert & Bonamy 1979) and its fully complex implementation (Lynch et al. 1996) further supplied by exact trajectories (Buldyreva et al. 1999), a corrected average over the perturber's states (Antony et al. 2006; Ma et al. 2007) and an account for line coupling (Ma et al. 2013). In cases where large volumes of line-shape data are to be produced with a minimal CPU cost, the semi-empirical method (Bykov et al. 2004) is used which represents a simplification of the Robert-Bonamy expressions to the Anderson-Tsao-Curnutte forms with a correction factor with empirically fitted parameters. Although some experimental values are necessary, the adjusted model parameters are practically temperature-independent and can be used for calculations at other required temperatures (not too low to keep the validity of the trajectory notion).

Machine Learning. Given the high volume of line broadening data that is required to model the effects of various different exoplanet compositions, machine learning appears to provide a practical approach to the problem. Recently Guest et al. (2024) have completed an initial machine learning study of air-broadening based on data in the HITRAN database. Studies which look at the effect of changing the broadener are underway.

UV and visible frequency ranges. Spectra which involve transitions between electronic states (i.e. rotation-vibration-electronic or rovibronic transitions), typically between the ground and an excited electronic state, occur, with some exceptions, in the UV and/or visible region. In these cases, the line broadening due to predissociative effects can dominate the collisional (pressure) broadening by some orders of magnitude. These broadening are caused by the associated lifetimes of *quasi-bound* transitions decreased. A new data format has recently been proposed to capture (Tennyson et al. 2023) and use (Yurchenko et al. 2023b) the predissociative line broadening in spectroscopic databases.

In the case of rovibronic transitions between *bound* low-lying vibrational levels of electronic states, available measurements show *no* well pronounced J-dependencies in the collisional broadening of rovibronic transitions. The absence of rotational dependence of the collisional (pressure) broadening means that rotational energy transfer is of minor importance and the broadening parameters are mainly influenced by elastic collisions. For such transitions line widths and line shifts have the same orders of magnitude. As mentioned by Margenau (1936), lines of rovibronic (bound-bound) transitions are broadened and shifted similarly to atomic lines of a similar type and a similar energy jump. Indeed, the first theoretical approaches to pressure-induced line widths/shifts used the model of a classical oscillating radiator whose phase is modified during collision by a random amount, leading thus, via Fourier-integral analysis, to

a "dispersion" (Lorentz) profile. For example, Lindholm (1945) and Foley (1946) successfully developed such theories. Foley (1946), in particular, argued that non-adiabatic effects are small for atoms due to large gaps between their electronic levels but can occur for molecular IR transitions because of similar energy differences between the rotational levels of the radiator and perturber. Detailed analyses of some representative one-term interactions (dipole-dipole, quadrupole-quadrupole and dispersive) in the framework of phase-shift theory were made by Mizushima (1951) who also considered velocity averaging and derived line-width and line-shift expressions (intended for microwave transitions) with explicit temperature dependencies. These expressions served as a basis for the power law of Eq. (2). Later, Hindmarsh et al. (1967) accounted additionally for short-range repulsive forces via a Lennard-Jones 12-6 potential model but for simplicity conducted their derivation with the mean-thermal-velocity approximation. Temperature dependence of collisional broadening and shifts of atomic and molecular rovibronic lines has been also addressed by Cybulski et al. (2013). Quantum-mechanical adiabatic approaches were initiated by Jablonski (1937, 1945) who assumed the gas to be a very large "molecule" and calculated the stationary states of internal motion. A unified model relying on the Franck-Condon principle and containing both impact and quasistatic limits was proposed by Szudy & Baylis (1975). The authors retrieved the expressions of Lindholm (1945) and Foley (1946) in the classical limit and suggested also a first-order correcting term leading to line shapes with an asymmetry effect.

When there is an interaction with one or more dissociative states, i.e., predissociations, the broadening can vary significantly due to a variation in the lifetimes of the excited states. The broadening in this case is a manifestation of such interaction with the continuum. The extent of the line broadening (or lifetime of the state in question) derives from the strength of the predissociation, i.e., the strength of the coupling between the bound excited states and the dissociative states. Typically non-radiative lifetimes of electronically excited states are ca. 10^{-8}s which result in widths of 5×10^{-4} cm^{-1}. For lifetimes of 10^{-13} s the linewidth will be 50 cm^{-1} which will result in the rotational structure disappearing. For nonradiative lifetimes shorter than 10^{-15} s, the vibrational structure disappears and will resemble a continuum. These types of predissociation-induced line broadenings have been well documented experimentally for over half a century (see chapter 7.4.2 in Lefebvre-Brion & Field (2004)).

3.2 Theoretical approaches to line-shape parameters: Atoms

The broadening of alkali lines by rare gases is a problem which has been extensively investigated in experimental and theoretical work (Allard & Kielkopf 1982; Burrows & Volobuyev 2003; Allard et al. 2016, 2019; Peach et al. 2020; Allard et al. 2023, 2024). A theory of spectral line broadening has been developed to calculate neutral atom spectra given the interaction and transition moments for relevant states of the radiating atom with other atoms in its environment. Within this framework it is possible to compute the complete spectrum with a unified approach. Unlike impact theories of line broadening which predict a Lorentzian line or the approximation methods of Szudy & Baylis (1975, 1996) the unified theory of Allard et al. (1999) provides an accurate spectrum from the line centre to the extreme wing. Complete details and the derivation of the theory are given by Allard et al. (1999). The approach is based on quantum theory of spectral line shapes by Baranger (1958b,c) with an adiabatic representation to include the degeneracy of atomic levels.

The spectrum $I(\Delta\omega)$ can be written as the Fourier transform (FT) of the dipole autocorrelation function Φ(s),

$$I(\Delta\omega) = \frac{1}{\pi} Re \int_0^{+\infty} \Phi(s) e^{-i\Delta\omega s} ds \,, \tag{3}$$

where $\Delta\omega$ is the angular frequency difference from the unperturbed centre of the spectral line. The autocorrelation function Φ(s) is calculated with the assumptions that the radiator is stationary in space, the perturbers are mutually independent, and in the adiabatic approach the interaction potentials give contributions that are scalar additive. This last simplifying assumption allows the total profile $I(\Delta\omega)$ to be calculated when all the perturbers interact, as the FT of the $N^{\rm th}$ power of the autocorrelation function ϕ(s) of a unique atom-perturber pair. Therefore,

$$\Phi(s) = (\phi(s))^N \,, \tag{4}$$

that is to say, the interperturber correlations are neglected. For a perturber density n_p,

$$\Phi(s) = e^{-n_p g(s)}, \tag{5}$$

where decay of the autocorrelation function with time leads to atomic line broadening. When n_p is high, the spectrum is evaluated by computing the FT of Eq. (5). The real part of $n_p g(s)$ damps $\Phi(s)$ for large s but this calculation is not feasible when extended wings have to be computed at low density because of the very slow decrease of the autocorrelation function. An alternative is to use the expansion of the spectrum $I(\Delta\omega)$ in powers of the density described in Royer (1971). For the implementation of alkali lines perturbed by helium and molecular hydrogen in atmosphere codes, the line opacity is calculated by splitting the profile into a core component described with a Lorentzian profile, and the line wings computed using an expansion of the autocorrelation function in powers of density. The impact approximation determines the asymptotic behavior of the unified line shape correlation function. In this way the results are applicable to a more general line profile and opacity evaluation for the same perturbers at any given layer in the photosphere or planetary atmosphere.

In Allard et al. (2019) the use of a density expansion in the opacity tables is reviewed. When the expansion is stopped at the first order it is equivalent to the one-perturber approximation. Previous opacity tables were constructed to third order allowing us to obtain line profiles up to $N_{\rm He}/N_{\rm H_2}$=10^{19} cm^{-3}. The new tables are constructed to a higher order allowing line profiles to $N_{\rm He}/N_{\rm H_2}$=10^{21} cm^{-3}.

3.3 State of the art - Data availability

3.3.1 Molecular line profiles

Voigt parameters: it is now recognised in the (exo-)atmospheric community that Earth's conditions with the oxygen and nitrogen as the main collisional broadeners are not default ones, especially for hot Jupiter exoplanets, where

hydrogen and helium dominate molecular collisions. Although, as noted below, broadening parameters are becoming available for a small number of systems which deviate from the Voigt profile, the vast majority of available data are for Voigt broadening parameters. Even so, collisional broadening parameters which are required for computing Voigt profiles are missing or incomplete for a larger number of the relevant molecules (see Section 2) and are therefore in practice substituted by crude "guestimates" when generating molecular opacities for the subsequent use in the radiative transfer calculations. Indeed, computing opacities without line profiles is meaningless, i.e. "something" is always better than "nothing", but the errors involved are usually difficult to quantify. The impact of using incorrect broadening parameters was shown by Niraula et al. (2022, 2023) to impact retrieved exoplanet properties.

HITRAN now includes different broadening species applicable to planetary atmospheres, as shown in Table 7. The addition of these parameters to the database is carried out by searching the literature for accurate experimental measurements, which can be fit to a rotationally-dependent function (see Wilzewski et al. 2016; Tan et al. 2019, 2022). This enables the functions to be applied to the high-temperature line lists of databases such as ExoMol and HITEMP. These broadeners are representative of the typical species in the (exo-)atmosphere under study: a mix of H_2 and He for gas giants, CO_2 for rocky planets and H_2O for tropical atmospheric scenarios (or water-dominated atmospheres). The temperature dependence of line broadening parameters has also recently been under investigation. Indeed line shapes are described by different parameters such as the pressure broadening and pressure shift coefficients and their respective dependence on temperature; this applies to both molecules and atoms. The species and broadeners for which Voigt broadening parameters are currently available in the ExoMol database can be found online[17]. A complete set of air-broadening parameters have been generated using machine learning (Guest et al. 2024) and a large number of broadening parameters based on the theory of Buldyreva et al. (2022) have also been added recently.

Empirical χ-factor corrections: Solar System applications have shown that the Voigt profile, tending to a Lorentz profile with increasing pressure, is not applicable for high-pressure conditions where a sub-Lorentzian profile needs to be used (Bézard et al. 2011). The pressure is so high in the lower layers of the atmosphere that the line-interference (intensity-transfer, also called line mixing) effects, in particular line (and, therefore, band) wings, need to be accurately modeled. For now, the band shapes obtained in the impact-approximation (Markov) limit of collisional-broadening theory (which is invalid for large detunings from the band centre) are empirically corrected via so-called χ-factors, as, e.g., Tonkov et al. (1996); Bézard et al. (2011) for CO_2 on Venus and the recent confirmation by laboratory measurements (Mondelain et al. 2022, 2023). Empirical χ-factor corrections were also used to model far-wing absorption for CO_2 at high pressures and temperatures (Tran et al. 2011; Cole et al. 2023), CH_4 (Tran et al. 2011) and H_2O (Tran et al. 2011). The artificial χ-factors as well as the forced re-normalisation procedure in the impact-approximation models become unnecessary if a non-Markovian approach operating with a frequency-dependent relaxation matrix and a symmetric metric in the line space is employed (Buldyreva & Daneshvar 2013; Filippov et al. 2013), but the collision-induced absorption (while relevant) should be correctly modelled; see Section 5. Even for correctly modelling methane absorption in the cold ice giant atmospheres, for example, having more precise line profiles can be important.

Double-power law: Gamache & Vispoel (2018) suggested to correct Eq. (2) by adding a supplementary power term (so-called double-power law), with an analogous two-term expression for the shifts, in order to model line widths and shifts over large temperature intervals with the same parameters' sets. So far, this has been applied to the H_2O-CO_2 collisional system, with respective parameters published in Régalia et al. (2019), to CO_2-H_2O reported in (Vispoel & Gamache 2024), and to He-broadening of H_2 and HD (Wcisło et al. 2021; Stankiewicz et al. 2021).

The importance of laboratory measured broadening parameters: as mentioned earlier in this section, accurate laboratory broadening measurements are critical for the production of rotationally-dependent broadening parameters, many of which have been compiled in the HITRAN database (see Table 7). A few examples of laboratory measurements of broadening coefficients to study Earth, Mars, Jupiter and other planetary compositions for key absorbers include Smith et al. (2014); Sung et al. (2020); Devi et al. (2016); Lavrentieva & Dudaryonok (2020). Available measurements that are relevant to high-temperature atmospheres, are not all necessarily relevant to high-metallicity atmospheres (e.g. Gharib-Nezhad et al. 2019; Yousefi et al. 2021; Baldacchini et al. 2001; Goldenstein et al. 2013), or are only limited to a small spectral region. Further details can be found in Hartmann et al. (2018). Nevertheless, such measurements in the laboratory are an important component of compiling broadening parameters for a large range of species, spectral regions, broadening species, temperatures, and pressures.

3.3.2 *Atomic line profiles*

Na and K: the resonance line doublets of atoms such as Na and K can have a large impact on the spectra of exoplanets and Brown Dwarfs, as demonstrated by, for example, Allard et al. (2019) and Whiteford et al. (2023). Such strong lines as these require detailed computations to model the line profile and wings far from the line centre. Typically works such as Allard et al. (2016) for K perturbed by H_2[18], Allard et al. (2024) for K perturbed by He[19], Allard et al. (2019) for Na perturbed by H_2[20], Allard et al. (2023) for Na perturbed by He[21], or Burrows & Volobuyev (2003) for Na and K perturbed by a mixture of H_2 and He, are used in the computation of opacities for exoplanet and Brown Dwarf

[17] https://exomol.com/data/data-types/broadening_coefficients/

[18] https://cdsarc.u-strasbg.fr/viz-bin/qcat?J/A+A/589/A21

[19] https://cdsarc.cds.unistra.fr/viz-bin/cat/J/A+A/683/A188

[20] http://cdsarc.u-strasbg.fr/viz-bin/qcat?J/A+A/628/A120

[21] https://cdsarc.cds.unistra.fr/viz-bin/cat/J/A+A/674/A171

atmospheres. See also Sharp & Burrows (2007) for empirical estimates used for other atomic (and molecular) line broadening parameters.

For the strongest atomic lines (K, Na, He) individual line absorption can dominate the entire observed spectroscopic region and very accurate shapes are mandatory, as described above. For others (Fe, Ca, Mg etc.), the atomic features are less intense and can be very dense, comparable to the molecular lines. In this case, the spectra are less sensitive to the individual lines. We do not go in detail here on these other species, and instead focus only on Na and K which are most relevant to high-temperature exoplanet atmospheres due to their extensive line wings.

3.4 Data used by retrieval codes

As previously highlighted in this section, the vast majority of atmospheric modelling and retrieval codes use the Voigt profile as the current standard for temperature- and pressure-broadened opacities.

The broadening parameters used for computing opacities (either on-the-fly or pre-computed; see Section 4) will have an impact on the resulting radiative transfer models (e.g. Anisman et al. 2022a; Gharib-Nezhad & Line 2019). It is important to compute (or choose, if pre-computed) opacities which are relevant for the atmosphere which is being modelled, both in terms of temperature and pressure, and also what the main broadening species are (e.g. H_2/He-dominated, H_2O-dominated, CO_2-dominated atmospheres). Often broadening data are supplied alongside line lists, which may then be typically used in the computation of opacities. One of the main differences between opacity computations is the extent out to which the line wings are calculated from the line centre (see, for example, Gharib-Nezhad et al. 2024). The ExoMolOP database (Chubb et al. 2020a) employs the line profiles of Allard et al. (2016) and Allard et al. (2019) in computing the resonance line opacities of K and Na, respectively, broadened by H_2. For the molecular opacity Voigt line profiles in the ExoMolOP database, averaged-J broadening parameters for H_2 and He broadening were used for those species with available data at the time, as outlined in Table 2 of Chubb et al. (2020a). The Voigt line wings were computed up to 500 Voigt widths from the line centres, up to a maximum cutoff of 25 cm^{-1}. The EXOPLINES database (Gharib-Nezhad et al. 2021) uses a Voigt profile with a variable line-wing cutoff depending on the pressure (30 cm^{-1} for P ≤ 200 bar and 150 cm^{-1} for P > 200 bar), but note the lack of available broadening coefficients for the species they compute opacities for (including a number of metal hydrides). They therefore estimated parameters to use in a similar way to Chubb et al. (2020a), based on the similarity between molecular symmetry or dipole moments that these absorbers have with the available Lorentz coefficients. Some works, such as Gharib-Nezhad & Line (2019) and Anisman et al. (2022a) use opacities which were computed assuming H_2O-broadening parameters, extracted from the HITRAN2020 database (Gordon et al. 2022). The opacities computed for the Helios-r2 retrieval code (Kitzmann et al. 2020; Grimm et al. 2021) are computed using a Voigt profile. The impact of the spectral line wing cut-off has been recently reviewed by Gharib-Nezhad et al. (2024), with the recommendation for the following line wing cut-offs to be used for current computations using the Voigt profile: 25 cm^{-1} for P ≤ 200 bar and 100 cm^{-1} for P > 200 bar.

3.5 What's being worked on?

Machine learning approaches: so far, the theoretical methods used for line broadening are very limited in what they can realistically provide, in terms of the molecular species, spectral ranges and temperature coverage. Machine learning (ML) represents an attractive alternative to fill the existing data gaps in broadening data due to its relative simplicity, which has been recently explored to produce air broadening data in the ExoMol data base (Guest et al. 2024). Considering the success of ML in a wide range of applications and the fast progress in the development of ML techniques, the work in this direction will continue.

(Vib)rotational line-shape parameters: the extreme conditions experienced by most observable exoplanets (high temperatures and huge levels of ionisation) lead to the formation of "exotic" species whose spectroscopic parameters are often impossible to measure in standard laboratory experiments. A significant number of required perturbers and non-existing empirical PESs to practice "standard" theoretical approaches described in Section 3.1. Therefore, for a rough J-independent theoretical estimate for IR/MW line width (in $cm^{-1}atm^{-1}$), the following expression for the Lorentzian HWHM has been recently suggested (Buldyreva et al. 2022):

$$\gamma_{\rm L} = 1.7796 \cdot 10^{-5} \frac{m}{(m-2)} \frac{1}{\sqrt{T}} \sqrt{\frac{m_a + m_p}{m_a m_p}} d^2, \qquad (6)$$

where only the index $m = 2(q-1)$ of the leading long-range interaction $V \sim R^{-q}$, the active- and perturbing-molecule masses m_a, m_p and the kinetic diameter of the molecular pair $d = (d_a + d_b)/2$ are required at the input temperature T. Besides the neutral active molecules, Eq. (6) holds also for ionic absorbers. It has been employed to produce line-width data (Buldyreva et al. 2024b) for more than fifty active species (and their isotopologues) self-perturbed and perturbed by He, Ar, O_2, H_2, N_2, CO, CO_2, NO, H_2O, NH_3 and CH_4 at the reference temperature of 296 K. These new data are progressively integrated into ExoMol as new files of ExoMol Diet (Barton et al. 2017) and into the definition .def files for all line lists of a considered molecule.

Rovibronic line-shape parameters: the same goal of providing at least approximate values of line-shape parameters for electronic transitions in hot-temperature active molecules concerned by Ariel has initiated recently a study (Buldyreva et al. 2024a) revisiting classical phase-shift theory. Besides a general analysis for arbitrary molecular pairs (including the points on the temperature dependence and Maxwell-Boltzmann averaging over relative velocities), improvements of the potential and trajectory descriptions were attempted. Detailed calculations, based on specially computed state-of-the-art PESs, were done for some representative molecular pairs (NO and OH perturbed by N_2 and Ar, selected because of available experimental data). As intended, for the considered molecular partners the calculated line-shape parameters were found to be consistent with measurements within 30–40% in wide temperature ranges (300–3000 K). Although this phase-theory approach requires knowledge of the isotropic interaction PESs associated with the excited and ground radiator's states, it has

a much lower computational cost with respect to quantum-mechanical methods which, in addition, become unpractical at high temperatures.

3.6 Data needs: What's missing and urgent?

In general, we would advocate for a consistent set of parameters which cover an adequate spectral range for each species of importance. This includes species which require new or improved line lists in Section 2.4. The need for the accurate treatment of line broadening effects in atmospheric retrievals is known to play an important role in atmospheric models, and more so with emerging observational facilities, regardless of if they are space-based (lower resolution) such as JWST and Ariel or ground-based (high resolution) such as the VLT or ELT (Hedges & Madhusudhan 2016). Studies such as Gharib-Nezhad & Line (2019), Niraula et al. (2022), and Anisman et al. (2022a) highlight the impact of using different broadening species for computing spectral line shapes on model atmospheric spectra, indicating that incorrect line shapes will likely lead to biases when analysing observed spectra. Gharib-Nezhad & Line (2019) find that emission spectra are particularly affected by incorrect broadening parameters, with the differences observed highly dependent on the pressure-temperature structure of the atmosphere. There will be an impact on the radiative balance and thermal structure of the atmosphere. In the frame of the Ariel mission, the requirement of a consistent set of parameters which cover an adequate spectral range for each species of importance is a challenging request as Ariel aims to observe about 1000 exoplanets ranging from Jupiters and Neptunes down to super-Earth size in the visible and the infrared with its meter-class telescope (Edwards et al. 2019a). This implies very different broadeners and pressure and temperature conditions. Line shapes accurate at high temperature, up to 2500 K, are high up on the list. This includes temperature exponents of the line parameters as temperature dependent line mixing effects for the main molecular species at least. The most important broadeners to be considered remain the usual suspects; H_2, He, CO_2 and H_2O.

(i) **Species occuring in JWST studies:** see the first point in Section 2.4, with line broadening parameters also required up to high temperatures for the listed species.

(ii) **Species relevant to lava planets:** the broadening for molecules important in lava planet environments require very different types of line-broadening to other commonly studied planets, which are generally not currently available (see, for example, Tennyson & Yurchenko 2017). This includes species such as KOH, NaOH, SiO_2, CaOH, FeO, MgO, MgOH (Schaefer et al. 2012; Tennyson & Yurchenko 2017; Mahapatra et al. 2017), whose spectra will be broadened by exotic molecules.

(iii) **H_2 and He broadeners at high temperatures:** there has been significant progress recently in the provision of line broadening parameters for H_2/He dominated atmospheres such as of hot Jupiters or hot Neptunes. Even so, it should be acknowledged that while many species in HITRAN have broadening parameters for terrestrial-relevant molecules, H_2 and He broadening parameters are not available for some important species such as CH_4.

(iv) **N_2 broadening:** it is known from studies of the Solar System that broadening by N_2 is required for the remote sensing of Titan (He et al. 2022b). Currently, N_2 is not separated from "air" in HITRAN, but is included as a broadening gas for many absorption cross-sections included in HITRAN that have been observed in Titan's atmosphere.

(v) **Species relevant to heavy atmospheres:** the availability of broadening data with species such as CO_2 and H_2O as broadeners is also relatively limited (see e.g. Table 7).

(vi) **Rotational- and vibrational-dependence:** while the rotational (J)-dependence is often not known for many species (see, e.g., Gharib-Nezhad et al. 2021), the vibrational dependence is even less studied but generally considered to be less important, see Guest et al. (2024) for example.

(vii) **Beyond Voigt profiles:** introducing a new line profile, such as Hartmann-Tran (see Section 3.1), implies introducing new line parameters. This complicates the release of parameters and recipes to the community. Efforts are made, and for instance, HAPI[22] (Kochanov et al. 2016) enables any user to choose a set of adequate line parameters depending on the atmospheric conditions of their spectra. Nevertheless, issues arise when the available parameters do not entirely cover the required spectral range and different datasets need to be combined. This results in a lack of traceability and poor reliability on the retrievals' results. We would therefore advocate for a consistent set of parameters which cover an adequate spectral range. Note that the various representations of the profiles are not orthogonal fits so the parameters cannot be used reliably in other functional forms.

(viii) **Line mixing:** A recent overview of line mixing, which causes potentially large deviations from a Voigt profile at high pressures, can be found in Gharib-Nezhad et al. (2024). We are not aware of any exoplanetary models which currently allow for the effects of line mixing, but these effects may become more important with newer instruments that can probe high-pressure regions of around 1 - 10 bar.

(ix) **Deuterated species:** deuterated molecular species are targeted in the (exo-)planetary community to infer planetary evolution. Typical targets for these kinds of investigation are hydrocarbons and water: C_2HD, CH_3D, and HDO (Villanueva et al. 2022) all have the property that they have different symmetry to their parent isotopologue. Broadening parameters for these species are important but the change of symmetry means the usual practice of transferring broadening parameters between isotopologues will not work for these cases.

(x) **Atomic species:** line parameters for atomic species are generally not readily available (with the previously noted exceptions of the strong Na and K doublets broadened by H_2 and He), which can lead to uncertainties in the calculated cross-sections. As shown in Grimm et al. (2021), the use of a Voigt profile for atomic lines is not always suitable. For instance the wings of autoionisation lines are more appropriately described by a so-called Fano profile (Fano 1961), which decreases much faster than a Voigt profile. Using a Voigt profile for these lines will result in an overestimate of the absorption, creating an artificial continuum. Other problematic lines for atomic species are resonance lines, where using a normal Voigt profile can also lead to over- or underestimated absorption.

(xi) **Limitations of experimental studies on some species:** as noted in Section 2.1.2.2, experimental measurements can be particularly challenging for reactive (or toxic) species, especially at high temperatures, which can limit the

[22] https://hitran.org/hapi/

availability of parameters. It is therefore not uncommon for some spectroscopic parameters, such as pressure-broadening (Tan et al. 2022), to be based only on limited laboratory measurements for some molecules. For example, inorganic salts are very difficult to sublimate and keep in the gas phase. These molecules, where possible, could be targets of theoretical studies instead.

The lack of the line shape data also means the lack of understanding of their importance on the atmospheric characterisation. More work, both experimental and theoretical is required.

4 COMPUTED CROSS-SECTIONS AND OPACITIES

Line lists (see Section 2) give all the information required (such as upper and lower energy levels, transitions, and typically either Einstein-A coefficients or intensities at a reference temperature) to generate a cross-section at a given temperature and pressure. Line lists will have a maximum temperature up to which they are considered complete; cross-sections computed above these temperatures will have opacity missing. This is because hot band transitions between energy levels of higher energy than are populated for the maximum line list temperature will not be taken into account. When computing cross-sections various choices need to be made, such as what line list, line profile, line-wing cut-off, and broadening parameters to use (see Sections 2 and 3). These will partly be determined by the requirements of the cross-sections being computed: will they be used for modelling Earth-like planets, in which case a line list such as HITRAN might be the most appropriate, or hotter exoplanets, in which case a line list computed or measured up to high temperatures is more appropriate, such as those provided by databases such as HITEMP (Rothman et al. 2010), ExoMol (Tennyson et al. 2020), or TheoReTs (Rey et al. 2016b). If the cross-sections are for modelling or retrieving atmospheric properties of a hot gas giant exoplanet, then the atmospheric composition will be typically dominated by H_2 and He. The choice of broadening parameters in Section 3 will thus be H_2 and He for such atmospheres, whereas for a planet with a heavier atmosphere, heavier broadening species such as H_2O or N_2 will be more appropriate. Partition functions are also required for computing cross-sections; these are typically included as part of a line list (see Section 2), with tools such as TIPS (Gamache et al. 2021) available for computing partition functions for the HITRAN2020 database. Studies such as Niraula et al. (2022) and Niraula et al. (2023) highlight how different choices, including line lists, broadening coefficients, and far-wing behaviours, can impact interpretations of observed spectra. Niraula et al. (2023) explore the impact of opacity choices on the atmospheric properties of the JWST NIRSpec/G395H transmission spectra of WASP-39 b (Alderson et al. 2023). Both Niraula et al. (2022) and Niraula et al. (2023) conclude that the incompleteness and inaccuracy of line lists is the biggest issue in the accurate retrieval of atmospheric properties from observations. Niraula et al. (2022) find strong biases due to incorrect line broadening assumptions, with the effects due to incomplete knowledge of far line wings greater for super-Earths than warm-Jupiters. They find the strongest biases, however, are due to using a line list which is incomplete at the atmospheric temperature being probed (i.e. using HITRAN instead of HITEMP or ExoMol for a hot Jupiter exoplanet atmosphere). Villanueva et al. (2024) present comparison tests designed for the exoplanetary community, in order to identify the effects of different input data choices, such as opacity format and line list source.

Opacity files are typically provided as either: 1) high-resolution cross-sections, 2) sampled cross-sections, or 3) correlated-k coefficients, also known as k-tables. The general process is to compute high-resolution cross-sections (typically with a grid spacing of around 0.1 cm^{-1} or 0.01 cm^{-1}, or R = $\frac{\lambda}{\Delta\lambda}$ ~ 1,000,000) for a grid of temperatures and pressures (typically spanning pressures of at least ~1×10^{-5} - 100 bar, and temperatures ~100 K - 3000 K), and then, usually for reasons of computational feasibility, to either sample these cross-sections at a lower resolution ($\frac{\lambda}{\Delta\lambda}$ ~ 10,000 - 20,000), or compute k-tables at $\frac{\lambda}{\Delta\lambda}$ ~ 300 - 5000, if the application is for lower-resolution applications such as characterising Ariel or lower-resolution JWST observations. These resolutions are approximately equivalent to one another for achieving the same accuracy when used in an atmospheric modelling or retrieval code. The general principle of k-tables is to order spectral lines within a given spectral bin, producing a smooth cumulative distribution function to represent opacity, which can then be more efficiently sampled than cross-sections being sampled without any ordering of the spectral lines, with less loss of opacity for the same resolving power (see, for example, Min 2017; Chubb et al. 2020a; Leconte 2021, for further details).

Super-lines: very large line lists can contain billions of lines between millions of energy level states, for example the latest ExoMol CH_4 line list consists of over 50 billion transitions between 9 million states (Yurchenko et al. 2024d). The computation of opacities from such large line lists can benefit from techniques such as the super-lines method (Rey et al. 2016b; Yurchenko et al. 2017; Tennyson et al. 2020), which yields a vast improvement in computational speed when computing high-resolution cross-sections. Either line intensities can be computed at a given temperature, and then the intensities of all lines within a specified spectral bin summed together to create a so-called super-line. If a high enough resolving power, such as R = $\frac{\lambda}{\Delta\lambda}$ ~ 1,000,000, is used for the creation of the super-lines then the overall opacity will be conserved (Yurchenko et al. 2017; Tennyson et al. 2020; Chubb et al. 2020a). Alternatively, some line lists, such as the CH_4 line lists of ExoMol (Yurchenko et al. 2017) and TheoReTs (Rey et al. 2014a, 2016b), are already partitioned into a large set of relatively weak lines and a small set of important, stronger lines. When computing opacities, the weaker lines can be combined into a set of super-lines (or effective lines as done for CH_4 in HITEMP (Hargreaves et al. 2020)), with broadening of the stronger lines treated individually. Irwin et al. (2019) employed a similar "pseudo continuum" approach when employing the NH_3 line list of Coles et al. (2019b) to analyse the visible spectrum of Jupiter, finding a great increase in efficiency with very little loss of accuracy.

4.1 State of the art - Data availability

There are some programs which have been developed by line list producers to generate cross-section data

from line lists, such as ExoCross[23] (Yurchenko et al. 2018a) and pyExoCross[24] (Zhang et al. 2024) (ExoMol), and HAPI (HITRAN)[25] (Kochanov et al. 2016). Other tools have been developed by line list users, such as HELIOS-K[26] (Grimm & Heng 2015), Exo-k[27] (Leconte 2021), RADIS[28] (Pannier & Laux 2019; van den Bekerom & Pannier 2021) and others (Min 2017). Various databases are available which have made use of tools such as these to compute opacities. Each will have their own set of assumptions and choices used when computing the opacities, depending on the intended applications: some databases provide high resolution cross-sections and some sampled cross-sections or k-tables (see the introduction to this section), often formatted for direct use in a particular atmospheric retrieval or modelling code. Some codes, which employ a so-called line-by-line method, work directly from line lists, and so do not require these opacity files. In such an approach assumptions about line broadening are made by the user at the time of running the code and so it can be considered to be more flexible, however it can become computationally unfeasible for atmospheric retrievals which cover a large range of pressures, temperatures, and wavelengths. Table 10 gives a non-exhaustive list of opacity databases employed by typical codes used to compute models or run retrievals relevant for the Ariel space mission, along with other applications. Some additional notes on these databases are given in Section 4.2. It is important, although not always the case, for modelling and retrieval studies to report on the opacities they use and either cite or explain the assumptions that went into computing those opacities. This allows for traceability and for analyses to be reproducible.

4.2 Data used by retrieval codes

Molecular opacities (cross-sections and k-tables) are now included in many radiative transfer codes and associated libraries, such as those listed in Table 2. The opacity databases listed in Table 10 are available online and although some are formatted with specific retrieval or modelling codes in mind, they can generally be adapted for more general use or for different codes. ExoMolOP (Chubb et al. 2020a) has k-tables and cross-sections for currently around 80 species in the ExoMol database formatted for direct input into TauREx3 (Al-Refaie et al. 2021), ARCiS (Ormel & Min 2019; Min et al. 2020), NEMESIS (Irwin et al. 2008), petitRADTRANS (Mollière et al. 2019) (see Table 2). The EXOPLINES (Gharib-Nezhad et al. 2021), Gandhi2020 (Gandhi et al. 2020), MAESTRO (Batalha et al. 2022) and DACE (Grimm et al. 2021) databases/compilations all contain high-resolution cross-sections for various pressures and temperatures. These can be sampled down to a smaller desired resolution for practical use, or converted to k-tables. Various tools currently exist for this, including Exo-k[29] (Leconte 2021), with more tools expected to be become openly available in the near future. We note there are various file formats used for storing opacity data which are often different for different retrieval codes; popular choices include HDF5 (Mollière et al. 2019; Al-Refaie et al. 2021), pickle (Al-Refaie et al. 2021), or FITS (Min et al. 2020).

The need to interpret observational spectra covering a wide range of atmospheric conditions robustly and benchmark them across various studies inspired the creation of the MAESTRO (Molecules and Atoms in Exoplanet Science: Tools and Resources for Opacities) database. MAESTRO is a NASA-supported, open opacity service accessible to the community through a web interface[30]. Primary aims of the MAESTRO project are to incorporate the most up-to-date line lists, establish community standards for computing opacity data (see, e.g., Gharib-Nezhad et al. 2024), and offer insights and guidance on assumptions and limitations regarding data relevancy and completeness, particularly concerning different atmospheric compositions. The overall goal is to create one uniform and standard database for opacities. MAESTRO currently hosts high-resolution data from various sources such as EXOPLINES (Gharib-Nezhad et al. 2021) and ExoMolOP (Chubb et al. 2020a), which span a large range of pressures, temperatures, and wavelengths. The ExoMolOP data hosted by the MAESTRO database are the high-resolution cross-sections which were used to compute the k-table or sampled cross-section files mentioned above. There is an option for opacity-producers to submit data to MAESTRO via GitHub[31].

We note the importance of checking opacity files for their original line list source to check their accuracy, spectral coverage, and see what temperature they are suitable to be used up to; see Section 2 for a discussion of completeness of the line lists for different species, which depends on the temperature up to which a line list is considered complete.

4.3 What's being worked on?

Opacities need to be updated periodically as new line lists become available or are updated; work is in progress to keep these databases up-to-date, including adding important isotopologues to ExoMolOP. The MAESTRO database is also expanding, with new species and isotopologues to be added in due course. With existing instruments such as HST/UVIS and potential future instruments such as the Habitable Worlds Observatory (HWO), comes the requirement for opacity data which spans into the UV region, starting around 0.1 - 0.2μm. Work is ongoing to compute opacities down to these wavelengths for the species which already have some UV data available, and for future line lists which are in progress. Such opacities will be incorporated into databases such as ExoMolOP and MAESTRO.

4.4 Data needs: What's missing and urgent?

(i) **External updates and advances:** as mentioned at the start of this section, there are many variables and assump-

[23] https://github.com/Trovemaster/exocross
[24] https://github.com/ExoMol/PyExoCross
[25] https://hitran.org/hapi/
[26] https://github.com/exoclime/HELIOS-K
[27] https://perso.astrophy.u-bordeaux.fr/~jleconte/exo_k-doc/index.html
[28] https://github.com/radis/
[29] https://perso.astrophy.u-bordeaux.fr/~jleconte/exo_k-doc/index.html
[30] https://science.data.nasa.gov/opacities/
[31] https://github.com/maestro-opacities/submit-data

Table 10. An overview of some typical opacity databases designed for the (exo)planetary atmosphere community.

Database	Types of data	Reference	Link
DACE	Many molecular and atomic cross-sections, 0.01 cm^{-1} spacing	Grimm et al. (2021)	https://dace.unige.ch/opacityDatabase/
ExoMolOP	Sampled cross-sections and k-tables for many molecules	Chubb et al. (2020a)	https://exomol.com/data/data-types/opacity/
EXOPLINES	High-resolution cross-sections for selected species	Gharib-Nezhad et al. (2021)	https://doi.org/10.5281/zenodo.4458189
Gandhi2020	High-resolution cross-sections for 6 molecules, 0.01 cm^{-1} spacing	Gandhi et al. (2020)	https://osf.io/mgnw5/?view_only=5d58b814328e4600862ccfae4720acc3
MAESTRO	High-resolution cross-sections from various sources	Batalha et al. (2022)	https://science.data.nasa.gov/opacities/

tions that are made when computing opacities. As new and improved data become available (line lists, broadening parameters, theoretical knowledge), then opacities will ideally need to be recomputed to keep to date with the latest advances. The requirements of new instruments will also have an impact here; opacities for use in characterising atmospheres observed with JWST, for example, need to be at higher resolution than those for use in characterising observations of the same planets using HST or Spitzer. Theoretical advances in line shape theory could also impact new opacities. As mentioned above, opacities which extend into the UV are also needed.

(ii) **Heavy and other atmosphere applications:** a focus on heavier atmospheres will require opacities tailored differently (*i.e.* different broadening parameters) to those for lighter gas giant atmospheres. In addition, stellar atmospheres also have their own requirements (e.g. Cristallo et al. 2007).

(iii) **Isotopologues:** although there are exceptions and updates are being made, opacities and line lists can be focused on the main isotopologues of a species only. For some species, however, isotopologues are more important than in others; for example natural elemental abundances of $^{79}Br/^{81}Br$ and $^{35}Cl/^{37}Cl$ require molecules containing these elements to be formed from cross-sections combined from a combination of the two main isotopologues. There is also some interest in observing different isotopologues in exoplanet (and brown dwarf) atmospheres (Mollière & Snellen 2019; Barrado et al. 2023), which require accurate opacities to be computed for a variety of individual isotopologues for species of interest.

5 COLLISION INDUCED ABSORPTION (CIA) AND CONTINUUM DATA

5.1 Collision induced absorption (CIA)

Collision-Induced Absorption (CIA) arises as broad features in atmospheric spectra due to additional spectral absorption occurring during collisions between pairs of species, with the interactions inducing a dipole moment. Symmetric molecules, such as O_2, N_2, H_2 do not possess any permanent or vibrationally induced electric dipole and are thus microwave and IR inactive, although even if extremely weak, magnetic dipole and electric quadrupole moments can contribute to the absorption. Nevertheless, significant absorption is induced through the creation of a transient dipole via intermolecular interactions during their collisions. This process enables one to reveal the presence of nonpolar species in the atmosphere by detecting collision induced supramolecules signatures. CIA in dense gases was discovered in 1949 by Crawford and Welsh in the infrared range (Crawford et al. 1949). Almost immediately after this discovery, it was realized that CIA of electromagnetic radiation should be important in just about any cool and dense environment, including atmospheres of solar and extrasolar planets (Trafton 1964; Mayor & Queloz 1995), cool white dwarfs (Shipman 1977; Mould & Liebert 1978; Bergeron et al. 1995; Saumon & Jacobson 1998), brown dwarfs (Burgasser et al. 2006; Geballe et al. 2009), cool main sequence stars (Linsky 1969; Hansen & Sterl Phinney 1998), and so-called first stars (Rees 1976; Bromm & Larson 2004; Bromm et al. 2009; Ripamonti & Abel 2004; Loeb 2010).

The term "collision-induced absorption" is usually used to refer to any bimolecular absorption that is absent from the isolated molecules but reveals itself as a result of intermolecular interaction (Vigasin & Mokhov 2017). To understand this process theoretically, a detailed statistical analysis of the wide range of thermally exciting interacting molecules that make up molecular pairs is needed. Three categories of molecular pairs, all related to a range of the potential energy surface of the associated van der Waals complex, can be distinguished: true bound, metastable and free pairs. The simultaneous presence of bound–bound (dimer), bound–free, free–bound and free–free (collisional) transitions in collision-induced processes makes the spectral analysis and the theoretical treatment very complex.

For decades, CIA has been known to contribute significantly to the transmission of radiation in the Earth's atmosphere, primarily via N_2-N_2, N_2-O_2, and O_2-O_2 (Farmer & Houghton 1966; Rinsland et al. 1981, 1982), as well as to play a crucial role in the radiation budget of other planets (Tipping & Poll 1985). Different molecular pairs have been identified as major contributors to the opacity of planetary atmospheres, such as H_2-H_2, H_2-He in gas giant planets (Richard et al. 2012), O_2-CO_2 and CO_2-CO_2 in Venus' atmosphere (Gruszka & Borysow 1997) and H_2-N_2, N_2-CH_4 in Titan's (Borysow & Tang 1993). In the Solar System, the H_2 dimer has been detected on Jupiter and Saturn from the comparison between satellite measurements and laboratory absorption spectra recorded by McKellar (1988). Several ionic complexes were also identified for example in the E-ring of Saturn, where the successive solvation of sodium cations by water was proposed to assign the observed mass spectrum (Postberg et al. 2009) H_2-H_2 and H_2-He collision-induced absorption (CIA) are considered as a thermometer to measure the thermal structure of the upper tropospheres of the gas giants (Conrath et al. 1998). The opacity of Jupiter in the far infrared is dominated by the CIA of H_2–H_2 and H_2–He (Trafton 1964; Borysow et al. 1984; Richard et al. 2012), making them vital components of not only the solar system gas giant planets but also Jupiter-like exoplanetary atmospheres. The importance of CIA warming in exoplanets was highlighted in (Ramirez & Kaltenegger 2017) in the context of rocky planets with H_2-dominated atmospheres. Furthermore, the impact of CIA on the radiative budget has been demonstrated in the atmospheres of Earth

and Super-Earth mass exoplanets with with H_2-enriched atmospheres (Pierrehumbert & Gaidos 2011). Other molecular pairs, including CO_2 have been studied to assess the impact of CIA on the surface temperature and to draw conclusion on the climate and habitability of of early Mars (Turbet et al. 2019, 2020; Godin et al. 2020). These CIA signatures are expected in spectra of hot Jupiters (Bell et al. 2024) too. During their campaign of measurements, Turbet et al. (2019) showed the disagreement between experimental data and the theoretical *ab initio* calculations of Wordsworth et al. (2017). Sufficient wavenumber coverage and appropriate temperature ranges for the data are necessary for the CIA effect to be included. When it comes to symmetric molecules, such as H_2 or O_2, the CIA contribution is the only way to quantify the density of these molecules, bearing in mind that their absorption coefficients depend on the square density (see, e.g., Richard et al. 2012).

5.2 Continuum

Continuum absorption is a process, and therefore dataset, which is typically presented as distinct from CIA. There are two main contributions which make up continuum absorption data: 1) excess opacity due to far line wings (see Section 3), and 2) dimer absorption, i.e. the absorption due to molecules which collide and become loosely bonded; to date this is most commonly associated with water (Ptashnik et al. 2011b; Shine et al. 2016).

There is potentially some community consensus lacking on how the continuum absorption and CIA processes are distinguished in experiment and calculations, and how they are treated numerically in radiative transfer codes. In some cases (see Section 5.3.2) continuum data contains some CIA absorption also, so care needs to be taken to not double count these contributions. We note the temperature coverage of continuum data is limited.

Probably the most well used source of continuum data, particularly for terrestrial applications and Earth-like planets, is the water vapour continuum. The continuum is a source of opacity which should be included in addition to line-by-line molecular absorption of H_2O (and other species, where necessary and available). It is typically tailored to be used alongside a particular opacity source; e.g. the MT_CKD continuum data (Mlawer et al. 2012; Mlawer et al. 2023) is designed to work alongside opacities computed from the HITRAN line list with a 25 cm^{-1} Voigt line wing cut-off. This is due to the continuum data making up for the excess opacity due to far line wings.

5.3 State of the art - Data availability

5.3.1 *Collision induced absorption (CIA)*

The primary source for CIA data is the HITRANonline website[32], where coverage for the number of pairs of species is greatest. Another compilation of CIA data can be found via the Laboratoire de Météorologie Dynamique Generic GCM (LMDG) online repository[33] (see, e.g., Charnay et al. 2021), which can be found via the Exo-k website[34]. For hot Jupiters, with a H_2- and He-dominated atmosphere, H_2-H_2, H_2-He, and He-He are the most important sources of CIA to be included. However for Earth-like or heavier atmospheres, a wider range of species will need to be considered.

Table 11 summarises the current status of CIA data available in the HITRAN database. An overview of the transitions and pairs of species included at the time of the 2019 update of the HITRAN CIA parameters can be found in Karman et al. (2019), with updates for the 2020 release of the HITRAN database outlined in Gordon et al. (2022). Table 11 shows the coverage and limitations of the current state of CIA data for the species where data exists and also the wavenumber regions and temperatures for which this data is applicable. It can be seen that the coverage of CIA data for heavy molecules is seriously lacking, which could have an impact on the modelling efforts of super-Earth atmospheres. CIA data for H_2-H_2 and H_2-He were originally motivated by the Solar System gas giants (Fletcher et al. 2018), but the wide increase in temperature coverage was due to the interest in higher temperature exoplanet atmospheres such as hot Jupiters (Borysow 2002). Light molecular systems are generally less complicated to model and measure, which could also explain the more complete wavelength and temperature coverage of data for lighter species. Higher mass molecular systems with many degrees of freedom, on the other hand, are more challenging to understand. Classical molecular dynamics simulations were used for CH_4-CO_2 (Fakhardji et al. 2022) and compared to measurements (Turbet et al. 2019). The agreement was good but the limitations of the model were highlighted.

The accurate spectroscopic parameters obtained from the comb-referenced spectroscopy measurements of O_2 by Fleurbaey et al. (2021) in Table 9, combined with other CRDS measurements (Mondelain et al. 2019; Kassi et al. 2021), were recently utilised (Adkins et al. 2023) for fitting a parameterised representation of the theoretical calculations by Karman et al. (2018) for O_2-O_2 and O_2-N_2 collision-induced absorption.

5.3.2 *Continuum*

There are various databases and literature which provide continuum data, such as the MT_CKD (Mlawer-Tobin-Clough-Kneizys-Davies) database[35] (Mlawer et al. 2012; Mlawer et al. 2019). Both self (due to the interaction of the species with itself) and foreign (due to interaction with the species with another species in air) continuum data are available. The MT_CKD water vapor continuum was recently made available through HITRANonline (Mlawer et al. 2023). H_2O continuum data is also available from the CAVIAR project (Ptashnik et al. 2011a; Shine et al. 2016). Anisman et al. (2022b) performed a recent analyses of the impact of continuum data in exoplanet atmospheres and showed that its inclusion led to potential observable shifts in the transit depth in the region of 60 ppm for planets with water-rich atmospheres. Original sources of continuum data measured in the laboratory include works such as Baranov et al. (2008); Odintsova et al.

[32] https://hitran.org/cia
[33] https://web.lmd.jussieu.fr/~lmdz/planets/LMDZ.GENERIC/datagcm/continuum_data
[34] https://perso.astrophy.u-bordeaux.fr/~jleconte/exo_k-doc/where_to_find_data.html
[35] https://github.com/AER-RC/MT_CKD

Table 11. Collision induced absorption (CIA) data sets available from HITRANonline with the wavenumber and temperature ranges for which they provide coverage, and the citations for the original sources.

System	ν_{range}/cm^{-1}	λ_{range}/μm	T_{min}/K	T_{max}/K	Reference
H_2–CH_4 (equilibrium)	0 - 1,946	> 5.14	40	400	Borysow & Frommhold (1986a)
H_2–CH_4 (normal)	0 - 1,946	> 5.14	40	400	Borysow & Frommhold (1986a)
H_2–H_2	20 - 10,000	1 - 500	200	3,000	Abel et al. (2011); Fletcher et al. (2018)
H_2–H	100 - 11,000	0.9 - 100	1,000	2,500	Gustafsson & Frommhold (2003)
H_2–He	20 - 20,000	0.5 - 500	200	9,900	Abel et al. (2012)
He–H	50 - 11,000	0.9 - 200	1,500	10,000	Gustafsson & Frommhold (2001)
N_2–H_2	0 - 1,886	> 5.3	40	400	Borysow & Frommhold (1986b)
N_2–He	1 - 1,000	10 - 10,000	300	300	Bar-Ziv & Weiss (1972)
N_2–N_2	0 - 5,000	> 2	70	330	Karman et al. (2015); Baranov et al. (2005) Lafferty et al. (1996); Hartmann et al. (2017) Sung et al. (2016b); Chistikov et al. (2019)
N_2–air	1,850 - 5,000	2 - 5.4	228	330	Baranov et al. (2005); Lafferty et al. (1996) Hartmann et al. (2017); Menoux et al. (1993)
N_2–H_2O	1,930 - 2,830	3.5 - 5.2	250	350	Hartmann et al. (2018)
O_2–CO_2	12,600 - 13,839	0.7 - 0.8	296	296	Vangvichith et al. (2009)
O_2–N_2	1,300 - 13,840	0.7 - 7.7	193	296	Baranov et al. (2005); Lafferty et al. (1996) Thibault et al. (1997); Orlando et al. (1991) Menoux et al. (1993); Maté et al. (1999) Tran et al. (2006); Karman et al. (2018)
O_2–O_2	1,150 - 29,800	0.3 - 8.7	193	293	Baranov et al. (2004); Maté et al. (1999) Thibault et al. (1997); Orlando et al. (1991) Tran et al. (2006); Karman et al. (2018) Tran et al. (2006); Karman et al. (2018) Spiering & van der Zande (2012); Spiering et al. (2011) Thalman & Volkamer (2013); Kassi et al. (2021) Adkins et al. (2023)
O_2–air	1,300 - 13,839	0.7 - 7.7	193	300	Maté et al. (1999); Spiering & van der Zande (2012) Thibault et al. (1997); Orlando et al. (1991) Tran et al. (2006); Karman et al. (2018) Drouin et al. (2017)
CO_2–CO_2	1 - 3,250	3.1 - 10,000	200	298	Gruszka & Borysow (1997); Baranov & Vigasin (1999) Baranov (2018)
CO_2–H_2	0 - 2,000	> 5	200	350	Wordsworth et al. (2017)
CO_2–He	0 - 1,000	> 10	300	300	Bar-Ziv & Weiss (1972)
CO_2–CH_4	1 - 2,000	5 - 10,000	200	350	Wordsworth et al. (2017)
CO_2–Ar	0 - 300	> 33	200	400	Turbet et al. (2020) Odintsova et al. (2021)
CH_4–He	1 - 1,000	> 10	40	350	Taylor et al. (1988)
CH_4–Ar	1 - 697	14.3 - 10,000	70	296	Samuelson et al. (1997)
CH_4–N_2	0 - 1379	> 7.3	40	400	Finenko et al. (2021, 2022)
CH_4–CH_4	0 - 990	> 10.1	200	800	Borysow & Frommhold (1987)

(2020). As well as H_2O, the MT_CKD continuum model also includes contributions from the so-called foreign continuum involving carbon dioxide, ozone, nitrogen and oxygen (Mlawer et al. 2012). It includes a number of collision-induced continuum absorption bands, so care needs to be taken not to double count when including both continuum and collision induced absorption (CIA) data (Mlawer et al. 2012).

Although we do not go into detail here, we note that other continuum opacities, such as H^-, can be important for characterising hot gaseous exoplanet atmospheres. For example, opacity data was computed and implemented into retrieval codes used in the observational study of Lewis et al. (2020) using data from John (1988). Retrieval analysis found evidence for significant amounts of H^- in the atmosphere of hot Jupiter HAT-P-41b, thought to be produced through a combination of photochemical and collisional processes (Lewis et al. 2020). Evidence for H^- was also found by Mikal-Evans et al. (2022) in the atmosphere of ultra-hot gas giant exoplanet WASP-121b and by Arcangeli et al. (2018) for very hot gas giant exoplanet WASP-18b.

5.4 Data used by retrieval codes

5.4.1 Collision induced absorption (CIA)

Collision induced absorption data is readily usable in retrieval codes such as ARCiS, TauREx3, petitRADTRANS, and others mentioned in Table 2. The HITRAN formatted data (.cia) provides a basis for including CIA data[36] (Karman et al. 2019). As noted above, CIA including H_2 and He is commonly included in the atmospheric modelling of hydrogen and helium rich atmospheres and the corresponding data is distributed with the default data sets for retrieval codes such as TauREx3 and ARCiS. Additional species can be included in the modelling and retrieval

[36] https://hitran.org/data/CIA/CIA_Readme.pdf

codes as they become available or are updated, following the HITRAN format to maximise interoperability. Though data format does not pose a major limitation, restricted wavelength range coverage for the CIA data poses constraints on modelling where CIA between additional species is considered.

The HITRAN CIA format supports different sets of absorption data for the same pair of species but for varying temperatures. While this is provided in some data sets, it relies on implementation in the retrieval code or downstream processing library in order to query based on temperature. This is not always supported.

5.4.2 *Continuum*

Anisman et al. (2022b) modelled the effects of including vs not including continuum data for H_2O on examples of low-mass temperate exoplanet transmission spectra using TauREx3 (Al-Refaie et al. 2021). The effect of continuum cross-sections exhibit an inverse relationship with temperature, so are most important for use in modelling atmospheres with temperatures at or close to Earth's.

As previously mentioned, one aspect of using continuum models such as MT_CKD is that they rely on specific line wings being used for computations of corresponding molecular cross-sections. For example, the MT_CKD model assumes that a line wing cutoff of 25 cm^{-1} is used, otherwise there can be double counting of the wing contribution (see, for example, Gharib-Nezhad et al. 2024).

5.5 What's being worked on?

Collision induced absorption (CIA) coefficients of H_2 and H_2-He have been recently measured in the 3600-5500 cm^{-1} (~1.8-2.8μm) spectral range in order to characterise Jupiter's atmosphere (Vitali et al. 2024). These are shown in Figure 4, covering pressure values from 10 mbar to 70 bar and temperature values of 120 - 500 K. It is important to have up-to-date CIA measurements, even for H_2-H_2 and H_2-He where there is already data available (see Table 11), either to expand the wavelength region or to compare the newer measurements to previous measurements or theoretical models present in the literature. As was highlighted in Section 5.1, the CIA of H_2–H_2 and H_2–He contribute significantly to the opacity of Jupiter, and therefore Jupiter-like exoplanets (Trafton 1964; Borysow et al. 1984; Richard et al. 2012).

CIA laboratory measurements have also been published recently from groups in Grenoble (Fleurbaey et al. 2022). There is a simulation chamber for absorption spectroscopy in planetary atmospheres in INAF (Snels et al. 2021); see Fig. 5. In terms of species, molecular systems related to Venus and Early Mars are mostly being targeted, i.e. CO_2-H_2O and CO_2-CO_2.

Theoretical work is planned for molecular systems related to Jupiter-like planets.

5.6 Data needs: What's missing and urgent?

5.6.1 *Collision induced absorption (CIA)*

(i) **Data for additional CIA species:** CIA data is currently unavailable for many pairs of species that are thought to be important in exoplanetary atmospheres, for example N_2 is currently the only available species for collisions with H_2O (see Table 11). H_2O, and other species such as CO_2 and CH_4 have been detected multiple times in exoplanet atmosphere spectra with JWST. CIA data for these molecules or combinations including them is crucial for a correct interpretation of the spectra especially in the search for biosignatures (Malaterre et al. 2023).

(ii) **Wavelength coverage:** much of the data that is available is limited to bands at wavelength ranges outside the window observed by Ariel (see Table 11 for an overview of current coverage of CIA data). The broad CIA features will, however, impact the shape of the Ariel observed spectra. In Jupiter's spectra, some CIA contributions are visible between 2 and 2.5 microns (López-Puertas et al. 2018) which is lower in wavelength than the data available for many other pairs. Without taking CIA into account, it is possible that major uncertainties on the retrieved values will remain.

(iii) **Temperature dependence:** data is often available only at room temperature, and the extension to higher temperatures is desirable, especially for modelling hot Jupiters and lava planets. We note some work has been done towards this, e.g. Stefani et al. (2018) for CO_2, along with data for H_2-H_2, H_2-H, H_2-He, He-H, detailed in Table 11.

(iv) **Isotopologues:** CIA data coverage does not currently extend far in the consideration of isotopologues; generally the main isotopologue is taken for theoretically derived data, while the terrestrial ratios are used for experimentally derived data. The potential impact of a variation in isotopologues for CIA is small, meaning isotopologue data is less urgent than for the above mentioned pairs, though it is potentially relevant for the HD-H_2 pair (Karman et al. 2019).

5.6.2 *Continuum*

(i) **Species other than H_2O:** although the MT_CKD database contains some other species such as CO_2, O_3, N_2, and O_2, the main focus of continuum absorption has been on H_2O. (Exo)planets with atmospheres dominated by species other than H_2O have a particular need for continuum data.

(ii) **Temperature dependence:** continuum absorption data for H_2O is currently only available below temperatures of 500 K, so there is not available data to use for modelling exoplanets with higher temperature atmospheres. We do note, however, that the impact of the H_2O continuum absorption on spectra decreases as the temperature increases (Anisman et al. 2022b), so this is not thought to be of urgent concern for the community.

6 AEROSOLS AND SURFACES

It is well known that the types of cloud or haze particles, collectively known as aerosols, in the atmospheres of exoplanets will have an effect on their observed transmission or emission spectra (Wakeford & Sing 2015; Pinhas & Madhusudhan 2017; Min et al. 2020; Ma et al. 2023; Taylor & Parmentier 2023), and their albedo (Muñoz & Isaak 2015; Fraine et al. 2021; Barrientos et al. 2023; Chubb et al. 2023), through the cloud particle's absorption and scattering properties. Generally, haze particles are smaller than cloud particles and are formed via photochemistry, which is a disequilibrium process with stellar UV leading to the formation of solid particles. Clouds, on the other hand, are formed via equilibrium processes which involve condensation and rainout.

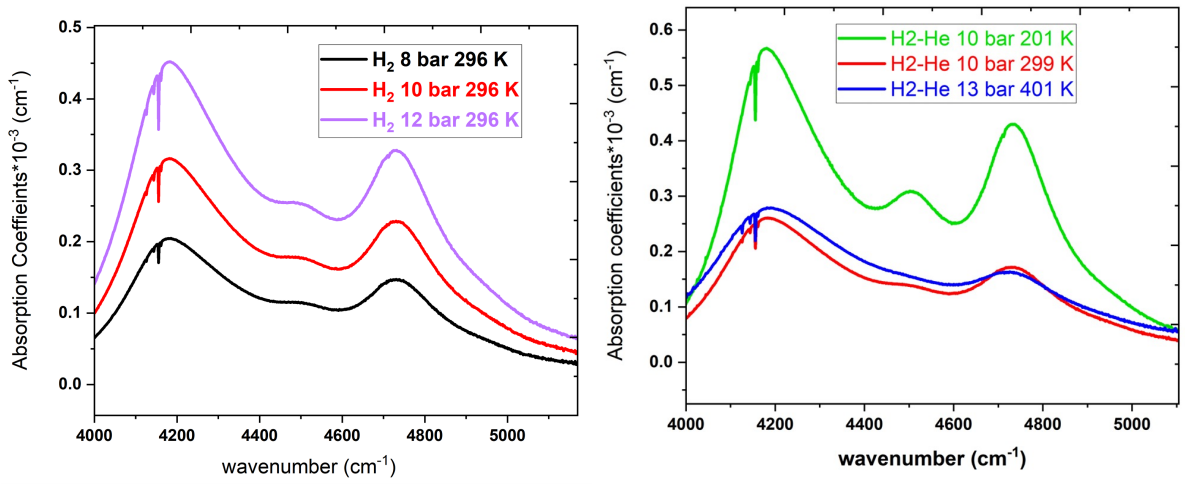

Figure 4. Left: H_2 CIA coefficients at different pressures (8, 10, 12 bars) and room temperature (296 K). Right: H_2-He CIA coefficients at different pressures (10, 13 bars)) and temperatures (201, 299, 401 K). (Vitali et al. 2024)

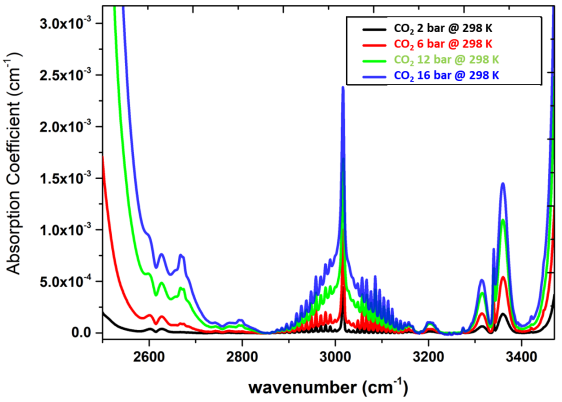

Figure 5. The absorption spectra of 16.03 amagat of carbon dioxide at 243 and 323 K, demonstrating a number of CIA bands, recorded with PASSxS, after subtraction of the strong contributions of the ν_3 fundamental band at 2350 $cm^{-1}$and a weaker Fermi doublet ($\nu_3 + \nu_1, \nu_3 + 2\nu_2$) around 3700 cm^{-1}, as well as contributions of the $^{16}O^{12}C^{18}O$ isotopomer (Snels et al. 2021).

Gao et al. (2021) give an overview of the state of knowledge (as of February 2021) of exoplanet aerosols as determined from observations, modeling, and laboratory experiments. Wavelength-dependent, and ideally also temperature-dependent, refractive indices, also known as optical constants, are required to compute the scattering and absorption coefficients of clouds and hazes (aerosols) for use in exo-planetary atmosphere models. Thermochemical data are also required for predicting which aerosol species are expected to be present at various altitudes and horizontally across a given exoplanet atmosphere. Typically the outputs from global circulation models (GCMs), such as pressure-temperature profiles as a function of longitude and latitude across the planet (see, e.g. Lee et al. 2021; Cho et al. 2021; Schneider et al. 2022; Skinner & Cho 2022; Skinner et al. 2023; Changeat et al. 2024, for details on GCMs and complex atmospheric dynamics) are used as a basis for kinetic cloud models which then predict which particles will condense at different locations of the atmosphere (see, e.g. Ackerman & Marley 2001; Helling et al. 2008; Gao et al. 2020b; Roman et al. 2021; Rooney et al. 2022; Helling et al. 2023). Usually some assumptions need to be made, such as initial elemental abundances available for condensing, and the strength of vertical atmospheric mixing, for example. Due to the importance of optical and UV data for understanding aerosol properties in exoplanet atmospheres, it has been suggested by Fairman et al. (2024) and Wakeford et al. (2020) that one should complement JWST observations with one from HST.

Similarly, planetary surfaces can be modelled by a simple reflectance model (for instance using linear mixing) (Cui et al. 2018), but also by radiative transfer modelling using optical constants, similar to the approach for Solar System planets (Hapke 1993; Andrieu et al. 2015). In both contexts, already existing databases contain relevant and useful sources but in many cases new measurements would be desirable (see Section 6.4). Here we outline some typical sources of currently available data for these different applications.

6.1 State of the art - Data availability

6.1.1 Refractive Indices

Codes which compute the scattering and absorption properties of a particle or a surface require the refractive index to be known. The real and imaginary part of the refractive index relates to the scattering and absorption properties of the material, respectively. The refractive indices of aersols are complex numbers which are intrinsically dependent on the individual compositions of the aerosols (see, for example, Di Biagio et al. 2019). If modelling an atmospheric layer consisting of different types of aerosol materials, or modelling mixed-material aerosol particles, then the refractive indices are often mixed using effective medium theory (see, for example, Mishchenko et al. 2016).

As well as there being variation with wavelength, there is also some temperature dependence with refractive indices. This has been demonstrated by Zeidler et al. (2015) for olivine and enstatite up to 973 K and by Zeidler et al. (2013) for corundum, spinel, and α-quartz up to 900 K. It can be seen by such studies that the vibrational band peaks shift slightly and their shapes change with temperature, which

could be enough to lead to some incorrect conclusions when trying to fit models to observed spectra. The reason for these changes is that at higher temperatures, vibrational transitions will tend to occur between higher states with slightly lower energetic differences, and the states will be broadened by vibrational mode interactions (Zeidler et al. 2015). This causes broader and redshifted bands with increasing temperature; see, for example, Figures 2 - 7 of Zeidler et al. (2015). We note that data for high temperatures are typically not currently available for many species, and so room temperature data are often used for characterising higher temperature planetary atmospheres, potentially causing biases in analyses.

Table 12 gives the wavelength and temperature range of the available refractive indices of various materials from different sources. We note this table is not exhaustive, and it is useful to search in the various databases and compilations mentioned below for additional species of interest. Studies which predict which cloud or haze species are present in various exoplanet atmospheres (see, for example, Ackerman & Marley 2001; Helling et al. 2008; Gao et al. 2020b; Rooney et al. 2022; Helling et al. 2023) are useful as references for species to include in atmospheric models.

Databases which compile the optical properties of various materials include:

Heidelberg-Jena-St.Petersburg-Database of Optical Constants (HJPDOC)[37] (Henning et al. 1999; Jäger et al. 2003) and **Database of Optical Constants for Cosmic Dust**[38] provide optical properties (refractive index, reflectivity, transmittance) of analog materials of cosmic dust in the wavelength range from the UV to far IR mainly produced in Astrophysical Institute and University Observatory (AIU) Jena but also from open sources, including papers, reports, dissertations, where these data were derived. Users of the database are requested to cite the original sources of data.

Aerosol Refractive Index Archive (ARIA)[39] is a comprehensive collection of refractive index datasets of typical aerosol particles covering broad spectroscopic ranges. It contains both the original experimental and interpolated (mostly from very low to room temperature) values, intended to be used in light scattering parameters by the Oxford Mie Code.[40]

HITRAN2020 database[41] (Gordon et al. 2022) provides refractive indices from visible to millimeter spectral ranges for many types of species including aerosol particles, required for calculation of extinction, scattering, and absorptive properties of atmospheric particles aiming at terrestrial and planetary (low temperature) applications.

Optical Constants database (OCdb)[42] (see, e.g. Drant et al. 2024) provides optical constants of organic refractory materials (i.e. tholins, laboratory analogs of photochemical hazes) and ices relevant to planetary and astrophysical environments from peer-reviewed sources. The data provided mostly correspond low temperatures.

Open-source database of optical constants `refractiveindex.info`[43] (Polyanskiy 2024) is another recent resource of optical data from publicly available sources such as scientific publications and material datasheets published by manufacturers.

Texas A&M University dust 2020 database (TAMUdust2020) (Saito et al. 2021) compiles the optical properties of irregularly shaped aerosol particles, such as dust aerosol and volcanic ash particles, for a wide range of values of the size parameter, the index of refraction, and the degree of sphericity. The data are produced using state-of-the-art light scattering calculations and validated with laboratory/in-situ measurements.

Original sources of refractive index data include those of works such as Henning et al. (1995); Jäger et al. (2003); Dorschner et al. (1995); Zeidler et al. (2011); Drant et al. (2024). A number of species are also included in Palik's handbook of optical constants (Palik 2012).

Refractive indices as a function of wavelength for different species thought to be present in exoplanetary atmospheres have been compiled in various works, such as Lavvas & Koskinen (2017); Kitzmann & Heng (2017); Min et al. (2020); Lietzow & Wolf (2022). Kitzmann & Heng (2017) provide a rather extensive compilation of wavelength-dependent refractive indices (real and imaginary components; see their Table 1 for species and sources) which are stored at the associated GitHub page for the LX-MIE mie-scattering tool[44]. Similarly, the wavelength-dependent refractive indices used in Wakeford & Sing (2015) can be downloaded from the author's webpage[45], although some updates have become available since this early compilation.

Anisotropic crystalline particles have refractive indices which depend on the direction of propagation of incident light with respect to the particle's axes of symmetry. The complex refractive indices related to light perpendicular to the main symmetry axis are often named ordinary, while the others are labelled extraordinary. These complex indices should typically be averaged over the three (x, y, z) axes of the particle for use in atmospheric codes. It is not always clear if available indices have already been mixed, but they may be labelled either ordinary/extraordinary, or by their x, y, z axes. Where indices have been averaged is often noted in compilations such as Kitzmann & Heng (2017) (see their Table 1).

Although the refractive indices data in these databases exist for very broad spectroscopic ranges, from microwave to far UV, for a given species the coverage is usually rather limited, see for example Table 12. A broad spectral range coverage of the optical properties is crucial to understand the role of aerosols in (exoplanet) atmospheric retrievals via radiative transfer models. In the context of the Ariel spectroscopic range, the IR data are especially urgent, but broader ranges are also required for atmospheric chemistry models involved in the retrievals. Due to the lack of the laboratory or in-situ measurements, it is common and especially important for exoplanet atmosphere applications to use interpolations to obtain continuous data (see, for example, Kitzmann & Heng 2017).

The Granada-Amsterdam light scattering

[37] https://www2.mpia-hd.mpg.de/HJPDOC/
[38] https://www.astro.uni-jena.de/Laboratory/OCDB/
[39] http://eodg.atm.ox.ac.uk/ARIA/
[40] https://eodg.atm.ox.ac.uk/MIE/
[41] https://hitran.org/aerosols/
[42] https://ocdb.smce.nasa.gov
[43] https://refractiveindex.info/
[44] https://github.com/exoclime/LX-MIE
[45] https://stellarplanet.org/science/condensates/

database[46] (Muñoz et al. 2012) contains experimental scattering matrices as functions of the scattering angle of samples of small irregular particles. These are laboratory experiments typically performed at two optical wavelengths. Laboratory data such as these are important to be able to benchmark theoretical codes, particularly those which model the scattering matrices of irregularly shaped particles. Available codes for computing complex dust particle opacities, both for spherical and fractal shapes, include optool (Dominik et al. 2021)[47], the discrete-dipole-approximation code ADDA (Yurkin & Hoekstra 2011)[48], the T-matrix codes (Mackowski & Mishchenko 1996)[49] and CORAL (Lodge et al. 2023)[50]. Other well-used codes include PyMieScatt[51] (Sumlin et al. 2018), which can deal with both direct and inverse Mie calculations.

6.1.2 *Thermochemical data*

Thermochemical data is required as input to kinetic cloud models of exoplanet atmospheres, for example in the computation of bulk growth processes for a particular species as a function of pressure and temperature, which requires gas-surface reactions (Helling 2021). There are several thermochemical properties of interest for astrophysical studies, including the Gibbs free energies of formation, the change in enthalpy, or the entropy (Lecoq-Molinos et al. 2024). Chemical and cluster data for all the species that take part in the cloud formation process are required for complete atmospheric models. Particularly, cluster data is crucial to model the nucleation process and the formation of cloud condensation nuclei (CCN). Databases, including the NIST-JANAF Thermochemical tables (Chase 1998)[56] and the other databases listed in Section 7.1.1 contain thermochemical data but rarely cluster data. As noted by Helling (2021), laboratory data are often not available, and so thermochemical data for various species can also be computed. For example, thermochemical data for TiO_2 nanoclusters have been recently computed by Sindel et al. (2022a,b), and for V_xO_y clusters by Lecoq-Molinos et al. (2024). These data are appropriate for use in modelling the formation of cloud condensation nuclei in exoplanet atmospheres. A variety of other sources for thermochemical data exist. For example, for TiO_2 data is provided by Jeong et al. (2000); Lee et al. (2015); Sindel et al. (2022b), with Jeong et al. (2000) also providing information about other intermediate Ti_xO_y structures, including their vibrational frequencies. For SiO and SiO_2 thermochemical data are available from works such as Bromley et al. (2016); Flint & Fortenberry (2023). For MgO, Köhler et al. (1997) provide thermochemical data, and Chen et al. (2014) provide cluster structures and vibrational spectra for $(MgO)_x$ (but not thermochemical data directly). Other species with thermochemical data include silicon carbide (Gobrecht et al. 2017), KCl (Rose & Berry 1992), silicates (Goumans & Bromley 2012), magnesium and calcium aluminates (Gobrecht et al. 2023), aluminium oxides (Gobrecht et al. 2022, 2018; Lam et al. 2015; Patzer et al. 2005), and Fe-bearing species (Chang et al. 2013; Ding et al. 2009).

Condensation curves (or vapour pressure curves), which indicate the thermal stability of a species, are necessary inputs into codes which predict the expected cloud materials present in an exoplanet's atmosphere based on it's pressure and temperature structure, typically found via global climate models (GCMs). Condensation curves appropriate for modelling exoplanet atmospheres up to high temperatures are available from a number of sources, with those for some typical species thought to be important in exoplanet atmospheres given in Table 13. Gao et al. (2020b)[57] give expressions for condensation curves from a number of different sources, including some of those mentioned in Table 13.

For cooler atmospheres, such as those in our solar system, ices are formed when gaseous species become supersaturated. The altitudes where the saturation occurs is a function of the mixing ratio of the species in question and the atmospheric temperature. Species dependent condensation curves will therefore vary with season and latitude, for example in the case of benzene in Titan, the latitudinal dependence is particularly evident in the fall at the poles where the decrease in stratospheric temperature is more dramatic and leads to an increase in the mole fractions. Barth (2017) extrapolated high-temperature vapor pressure data of benzene (C_6H_6) to lower temperatures to calculate benzene condensation curves. Their results predicted benzene and HCN to condense at near identical altitudes for the temperature profiles. However, Dubois et al. (2021) measured the equilibrium vapor pressure of pure crystalline benzene (C_6H_6) at temperatures relevant to Titan. Their measurements indicated that the prior extrapolations from literature values underestimated the vapor pressure. Feeding their laboratory data into a microphysical model, Dubois et al. (2021) showed that C_6H_6 polar cloud particles form first at higher altitudes and continue to exist at all latitudes down to the saturation point of HCN at slightly lower altitudes where co-condensation of C_6H_6 and HCN is possible. This is because the larger measured vapor pressure of C_6H_6 allows for larger ice particles that continue to grow deeper down in the troposphere, beyond the condensation point of HCN. It is therefore important for accurate condensation curve data to be available across a wide range of temperatures for a large number of species relevant to (exo)planetary and solar system atmospheres.

Notable sources for condensation curve formulae which can be used in atmospheric models include Visscher et al. (2006), who give approximations for condensation curves of various sulphur- and phosphorus-bearing species, and Visscher et al. (2010) for iron- silicon- and magnesium-bearing species. Morley et al. (2012) compute condensation curves for Cr, MnS, Na_2S, ZnS, and KCl, for use in characterising brown dwarf atmospheres, based on the thermochemical models of Visscher et al. (2006, 2010). Wakeford et al. (2016) give expressions for equilibrium condensation temperatures as functions of pressure and metal-

[46] https://www.iaa.csic.es/scattering/list/index.html
[47] https://github.com/cdominik/optool.git
[48] https://github.com/adda-team/adda.git
[49] https://www.giss.nasa.gov/staff/mmishchenko/tmatrix/
[50] https://github.com/mglodge/CORAL.git
[51] https://pymiescatt.readthedocs.io/en/latest/
[56] https://janaf.nist.gov/
[57] https://github.com/natashabatalha/virga/blob/master/virga/pvaps.py

Table 12. Sources used for the real (n) and imaginary (k) parts of the refractive indices of a selection of species of various materials typically used in (exo)planetary atmosphere models of clouds and hazes (aerosols). The temperature range is left blank in cases where we assume the data is not higher than room temperature.

Material	Form	Name	Wavelength range (μm)	Temperature range (K)	Reference
Al_2O_3	Crystalline	Corundum	0.03 - 10		Palik (2012)
Al_2O_3	Crystalline	Corundum	6.7 - 10,000	300 - 928	Zeidler et al. (2013)[a]
Al_2O_3	Amorphous	Corundum	0.2 - 12		Koike et al. (1995)[a]
Al_2O_3	Amorphous	Corundum	7.8 - 500		Begemann et al. (1997)[a]
$C_xH_yN_z$	Solid	Tholins	0.02 - 920		Khare et al. (1984)[b]
KCl	Crystalline	Potassium chloride	0.22 - 167		Querry & Wieliczka (1988)
Fe	Metallic	Iron	0.1 - 100,000		Palik (2012)
Fe_2O_3	Solid	Hematite	0.1 - 1000		Triaud (2005)[d]
Fe_2SiO_4	Crystalline	Fayalite	0.4 - 10,000		Unpublished[a]
FeO	Amorphous	Wustite	10 - 510	10 - 300	Henning et al. (1995)
FeS	Crystalline	Troilite	20 - 480	10 - 300	Pollack et al. (1994)
$MgAl_2O_4$	Crystalline	Spinel	6.7 - 10,000	300 - 928	Zeidler et al. (2013)[a]
Mg_2SiO_4	Amorphous	Forsterite	0.2 - 950		Jäger et al. (2003)
Mg_2SiO_4	Crystalline	Forsterite	2 - 100	50 - 295	Suto et al. (2006)
MgO	Cubic	Magnesium oxide	0.2 - 625		Palik (2012)
$MgSiO_3$	Amorphous (glass)	Enstatite	0.2 - 500		Dorschner et al. (1995)[e]
$MgSiO_3$	Amorphous (sol-gel)	Enstatite	0.2 - 1000		Jäger et al. (2003)[e]
$MgSiO_3$	Crystalline	Enstatite	2 - 98		Jaeger et al. (1998)
SiO_2	Crystalline	Quartz	0.05 - 8.4		Palik (2012)
SiO_2	Crystalline	Quartz	6.25 - 10,000	300 - 928	Zeidler et al. (2013)
SiO	Amorphous	Silicon oxide	0.05 - 100		Palik (2012)
TiO_2	Crystalline	Rutile	0.4 - 10		Zeidler et al. (2011)
TiO_2	Crystalline	Anatase	0.4 - 10		Zeidler et al. (2011)

[a]: *Available via the Database of Optical Constants for Cosmic Dust*[52]
[b]: *Available via the HITRAN2020 database*[53] *(Gordon et al. 2022)*
[c]: *Available via the refractiveindex.info database of optical constants*[54] *(Polyanskiy 2024)*
[d]: *Available via the Aerosol Refractive Index Archive (ARIA)*[55]

[e]: *Jäger et al. (2003) use the sol-gel method, and Dorschner et al. (1995) a melting and quenching technique; a comparison between the two is made in Jäger et al. (2003).*

licity for various Al- and Ti-bearing species. Appendix A of Ackerman & Marley (2001) provides relations for saturation vapour pressures of a few species, such as NH_3, H_2O, Fe, and $MgSiO_3$ (enstatite). For NH_3 they fit measurements tabulated in the CRC Handbook of Chemistry and Physics (Weast 1971). For H_2O they make use of data from Buck (1981), and from Barshay & Lewis (1976) for Fe and enstatite.

Section 3.2 of Woitke et al. (2018), along with their supplementary document (Woitke et al. 2017), give a detailed comparison of condensed phase data from either the NIST-JANAF database (Chase 1998) or the geophysical SUPCRTBL database[58] (Johnson et al. 1992; Zimmer et al. 2016). They offer comparisons of 121 species, and find good agreement for all species apart from anorthite, $CaAl_2Si_2O_8$. These data are used in Woitke et al. (2018) to compute vapour pressure curves, with an example for Fe shown in their Figure D.1.

Figure 4 of Gail et al. (2013) illustrates the importance of using the most up-to-date measurements for vapour pressure curves, as they compare their experimentally determined data for SiO with data from Nuth-III & Ferguson (2006) and Schick (1960). There is a considerable difference between the curves shown for SiO, with the newer measured data allowing SiO to be present in solid form up to higher temperatures than the older data. It is recommended that any users of thermochemical data such as condensation curves cite the sources of their data to allow for comparisons and for re-analysis in the case of newer data being produced. A thorough investigation into the reliability of the data used for condensation curves of species important for characterising (exo)planetary atmospheres such as those mentioned here, including additional newer measurements, would be a worthwhile endeavour, useful for assessing which species are expected in the atmospheres of current and future observations.

[58] https://models.earth.indiana.edu/supcrtbl.php

Table 13. Example of sources used for vapour pressure/condensation curves of various materials typically thought to be important in exoplanet atmospheres, particularly those at higher temperatures such as hot Jupiters.

Material	Reference	Note
Al_2O_3	Wakeford et al. (2016)	Following the approach of Visscher et al. (2010)
$CaTiO_3$	Wakeford et al. (2016)	
KCl	Morley et al. (2012)	
Fe	Visscher et al. (2010)	
Fe_2O_3	Sharp & Huebner (1990)	Coefficients for a large number of condensed species are given in Table 2b
Fe_2SiO_4	Sharp & Huebner (1990)	
FeO	Sharp & Huebner (1990)	
FeS	Woitke et al. (2018)	Equation inside GGchem source code
$MgAl_2O_4$	Woitke et al. (2018)	Equation inside GGchem source code
Mg_2SiO_4	Visscher et al. (2010)	
$MgSiO_3$	Visscher et al. (2010)	
SiO_2	Grant et al. (2023)	
SiO	Gail et al. (2013)	Older data from Nuth-III & Ferguson (2006); Schick (1960)
TiO_2	Woitke & Helling (2004)	Powell et al. (2018) give this formula rewritten in different units

6.1.3 *Measured cloud and haze production in the laboratory*

Atmospheric chamber experiments can be used to simulate the atmospheres of Solar System bodies, in order to study haze formation, and measure transmittance and reflectance spectra. This has been done for Titan (He et al. 2022a; Imanaka et al. 2004), Triton (Moran et al. 2022), and early Earth (DeWitt et al. 2009; Hörst et al. 2018b); in such studies many haze properties can be measured, such as production rate, bulk composition, molecular composition, and their transmission and reflectance from the optical to the near-infrared. The latter is done with Fourier Transform Infrared (FTIR) Spectroscopy. In the case of He et al. (2022a), they provide a set of optical constants of Titan haze analogs in the wavelength range 0.4 - 3.5 μm. Similar atmospheric chamber experiments have been used to study the formation of water ice clouds on Mars (Phebus et al. 2011), organic aerosols in anoxic and oxic atmospheres of Earth-like exoplanets (Gavilan et al. 2018), precursors to haze formation in cool exoplanet atmospheres (He et al. 2019), and to explore haze production in super-Earth and mini-Neptune atmospheres (Hörst et al. 2018a).

Several groups contribute to databases of refractive indices using different laboratory setups, such as COSmIC at NASA Ames (Sciamma-O'Brien et al. 2023), PAMPRE at LATMOS (Gavilan et al. 2018; Drant et al. 2024), and John Hopkins University (He et al. 2022a). Previous work on Titan haze analogs revealed that the setup conditions likely affect the analog's composition and thus their refractive indices (see, e.g., Brassé et al. 2015). Further laboratory experiments are important to fully understand the composition of different solid particles and their resulting optical properties.

6.1.4 *Surface reflectance*

For terrestrial exoplanets and exomoons, the bottom boundary layer of the atmosphere must be considered as the surface. Table 14 summarises the most important databases of surface reflectance in Planetary Science. They encompass Earth natural rocks analogues, but also synthetic materials in the lab (such as ices), meteorites and in-situ samples measured back in Earth, such as the Moon or Ryugu asteroid. The reflectance spectrum of Phobos was measured from 0.4 - 4.75 μm by Wargnier et al. (2023). The dataset from in-situ measurements of reflectance in planetary science is usually scattered and unfortunately, such a database is missing.

Reflectance measurements can be done over several wavelength ranges, but also for different observation geometries (incidence and emergence angles), leading to BiDirectionnal Reflectance Distribution Function (BRDF). Laboratory measurements can also be done for various surface properties (such as grain size, grain shape, compaction, roughness) but also various kinds of mixtures (such as linear geographic mixture, intimate mixture, intra-grain mixture).

The databases which contain information on observation geometries and the nature of the samples do not always contain optical constants, as can be seen by Table 14. Additionally some databases contain characterisation of the samples using other methods of investigations (Raman spectroscopy, petrological description, X-ray diffraction, Laser Induced Breakdown Spectroscopy, X-ray fluorescence or electron microprobe analysis). The SSHADE (Solid Spectroscopy Hosting Architecture of Databases and Expertise) (Schmitt et al. 2018) database regroups several databases. It provides spectral and photometric data obtained by various spectroscopic techniques including reflectance spectroscopy. The measured samples include ices, pure minerals, rocks, organic and carbonaceous materials as well as liquids. They are either synthetic, natural samples from Earth or other planetary bodies such as (micro-)meteorites or lunar soils. Additional characterisations of the samples are not systematically done but optical constants are often available and observation geometries are generally given. The USGS-Speclab (Kokaly et al. 2017) database regroups spectra measured with laboratory, field, and airborne spectrometers, acquired on samples of specific minerals, plants, chemical compounds, and man-made

materials. It also contains mathematically computed mixtures. The RELAB database regroups spectroscopic data acquired on pure minerals, natural and synthetic samples. The ECOSTRESS database (Meerdink et al. 2019) regroups data acquired on natural and man-made materials. The Mineral and Rock Sample Database University of Winnipeg (Cloutis 2015) contains data acquired on pure minerals and natural or synthetic mixtures. Finally, the PTAL (Planetary Terrestrial Analogue Library, Dypvik et al. 2021) regroups data acquired on whole rocks. Additional characterisation are systematically done by multiple techniques.

6.2 Data used by retrieval codes

There are a number of exoplanetary atmospheric modelling and retrieval codes which include the effects of solid-state aerosol species in their radiative transfer calculations, and thus require wavelength-dependent, and ideally also temperature-dependent, refractive index data (e.g. Wakeford & Sing 2015; Pinhas & Madhusudhan 2017; Min et al. 2020; Ma et al. 2023; Taylor & Parmentier 2023). The LRS instrument onboard JWST, covering ~ 5 - 12.5 μm, allows for observations of vibrational-mode aerosol signatures which are commonly found in this wavelength region; for example quartz clouds were inferred in hot Jupiter WASP-17 b by Grant et al. (2023) (using optical constants of crystalline SiO_2 at 928 K from Zeidler et al. 2013) and silicate clouds ($MgSiO_3$, SiO_2 and SiO) have been inferred in hot Neptune WASP-107 b by Dyrek et al. (2024).

Many retrieval codes have their own built-in library of refractive indices, the option to directly include pre-computed cloud opacities, or both. See for example Table 1 of Min et al. (2020) for species included in atmospheric modelling and retrieval code ARCiS, with the option to read in your own refractive index data and use the code to compute either spherical or irregularly shaped particles (Min et al. 2005) of a defined particle size distribution. petitRADTRANS (Mollière et al. 2019) also has a list of built-in cloud opacities[59], with the option to add more. There are also available add-ons which can be coupled with existing retrieval codes. For example, *YunMa* is an exoplanet cloud simulation and retrieval package (Ma et al. 2023) which can be coupled to the TauREx3 platform to retrieve microphysical cloud properties in exoplanet atmospheres.

Typically in cases of databases and compilations, the original citation for the measured or computed refractive indices is mentioned. It is important these citations are also included in any atmospheric modelling or retrieval works, as there may be future updates for particular species. Works such as Zeidler et al. (2015) highlight the importance of this; they show temperature-dependence has an impact on the refractive indices and therefore the spectral features which are included in atmospheric models for enstatite and olivine.

The refractive indices determined by using different techniques can differ from one another; for example in the case of amorphous $MgSiO_3$ (see Table 12) Jäger et al. (2003) use the sol-gel method, and Dorschner et al. (1995) use melting and quenching technique; a comparison between the two is made in Figure 4 of Jäger et al. (2003).

[59] https://petitradtrans.readthedocs.io/en/latest/content/available_opacities.html

Surfaces are often neglected but some retrievals propose to include surface reflectance measurements by linear mixing (Cui et al. 2018). More advanced radiative transfer modelling will be used, based on optical constants, for instance using the Hapke model (Hapke 1993). Surface reflection is also an important component of studies such as Stam (2008); Fauchez et al. (2017); Trees & Stam (2022), who consider the reflection spectra of a planet's atmosphere and surface (if there is one), including polarisation state; these studies are particularly useful for modelling the observations of future instruments such as the Habitable Worlds Observatory (HWO) (Vaughan et al. 2023).

6.3 What's being worked on?

Ongoing laboratory experiments (see, for example, setups described in works such as Deguine et al. 2020; Drant et al. 2024; He et al. 2024) are essential for measuring new refractive indices, exploring photochemical pathways, and verifying theoretical calculations related to aerosols in planetary and exoplanet atmospheres. He et al. (2024), for example, recently measured the density and optical properties of organic haze analogues generated in water-rich exoplanet atmosphere experiments, for use in characterising observations from JWST. Gao et al. (2021), who give an overview of the state of knowledge (as of February 2021) of aerosols for exoplanet atmospheres, highlight the importance of ongoing laboratory experiments and development of theoretical methods. A recent review by Sciamma-O'Brien et al. (2024) further highlights the importance of measured optical constants of laboratory aerosols for interpreting JWST observations.

As mentioned in Section 6.1.3, there are several groups with different laboratory setups who are working on measuring the optical properties of different aerosol analogs. Collaborations are currently ongoing between LATMOS (Gavilan et al. 2018; Drant et al. 2024) and NASA Ames (Sciamma-O'Brien et al. 2023) to compare optical properties found with different laboratory setups. Such collaborations will provide more complete data sets and help better understand implications for future observations. Work is ongoing to combine different laboratory spectroscopic measurements in order to provide continuous data of refractive indices across a broad spectral range covering the ranges of JWST and Ariel; see, for example, He et al. (2024) and Drant et al. (2024) for current examples of this.

For condensation curve data, work is ongoing from groups such as those at NASA Ames, where three groups are working independently to address the different properties and optical constants required for accurate condensation curves.

6.4 Data needs: What's missing and urgent?

(i) **Wavelength coverage:** as shown in Table 12, the available data for a number of aerosols do not have the wavelength-coverage required to cover the observational range of Ariel (0.5 - 7.8 μm) and/or other telescopes related to exoplanet atmospheres such as JWST (~ 0.6 - 28.5 μm, with the LRS instrument covering ~ 5 - 13 μm). We also note that refractive indices are important for modelling reflectance spectra of exoplanets and their atmospheres, includ-

Table 14. Sources for the reflectance data of various materials typically used in (exo)planetary surface models.

Name	Reflectance	Optical constants	Link
SSHADE	X	X	https://www.sshade.eu/
USGS-Speclab	X		https://crustal.usgs.gov/speclab/
RELAB	X		https://sites.brown.edu/relab/relab-spectral-database/
ECOSTRESS	X		https://speclib.jpl.nasa.gov
Mineral and Rock Sample Database University of Winnipeg	X		https://www.uwinnipeg.ca/c-tape/sample-database.html
PTAL	X		http://erica.uva.es/PTAL/

ing albedo in the visible region (see, for example, Krenn et al. 2023; Chubb et al. 2023).

(ii) **Temperature-dependence:** As mentioned above, the main spectral features of aerosols which could be observed in exoplanet atmospheres using JWST, for example, may be shifted at high-temperatures in comparison to room-temperature (Zeidler et al. 2013, 2015), making high-temperature measurements of refractive indices of high priority. Zeidler et al. (2013, 2015) demonstrate the temperature-dependence of optical properties (i.e. refractive indices) of aerosol particles such as enstatite and olivine which are expected in typical hot gas giant exoplanets. Zeidler et al. (2015) demonstrate the vibrational bands of olivine and enstatite becoming broader and redshifted with increasing temperature; see, for example, their Figures 2 - 7. It is assumed a similar effect will be found in other species, however there are no available studies on temperature dependence for the vast majority of refractive indices and most are therefore only available for terrestrial temperatures. Obtaining newer high temperature data for a wide range of other species important in higher temperature atmospheres would greatly aid in the analysis of observed spectra from missions such as JWST and Ariel. Reflectance spectra and refractive indices above 500 - 600 K are also important for surfaces, but at such high temperatures are usually not available.

For ices, important for characterising cooler solar system bodies, three types of temperature effects are usually considered (Schmitt et al. 1998): (i) Phase transitions upon heating, irreversible for some cases, can lead to profound changes in spectral features. (2) Thermal annealing, also associated with irreversible reorganisation of amorphous to more ordered structure resulting in a progressive shift and narrowing of the bands. (3) Thermal contraction of the crystal and phonon-phonon interactions can lead to a change of the spectroscopic bands with a complex temperature behaviour depending on many factors including the solid structure, phase etc, with the bandwidth generally increasing on heating. This change is reversible upon temperature.

For cooler Solar system conditions, the temperature dependence of the refractive index have been studied, e.g. by Warren & Brandt (2008); Biermann et al. (2000). The temperature dependence of the refractive index of H_2O has been investigated recently by He et al. (2022c) between 30 K and 160 K (see their Figure 7). These results for water and other small molecules are available in the Leiden Ice Database for Astrochemistry - LIDA (Rocha et al. 2022). From what we know about ices, there is a clear temperature dependence which for H_2O results in a roughly 10% increase from 30 K to 160 K (He et al. 2022c).

Like for the majority of the data types considered in this work, more laboratory studies, especially at warmer conditions, are needed for refractive indices.

(iii) **A guide on what tools to use:** computing cloud opacities from refractive index data requires some additional assumptions, including the shape of the cloud particles, and whether the particles are mixed composition. For example, Mie computations are fast but only applicable for spherical particles, while the discrete dipole approximation (DDA) (Draine & Flatau 1994) or *T*-matrix method (Mackowski & Mishchenko 1996) are very accurate for non-spherical particles which can be composed of multiple materials, but also computationally expensive. There are some methods which lie between these extremes, allowing for the computation of scattering and absorption coefficients for non-spherical particle shapes, at a lower cost but typically also lower accuracy that DDA. For example the Distribution of Hollow Spheres (DHS) method (Min et al. 2005) is thought to be a good compromise between accuracy and speed, with the option to choose a degree of irregularity of the particles. The DHS method has been used in studies such as Dyrek et al. (2024). There is also the modified mean field theory (MMF) method, designed for computing opacities of dust aggregates (Tazaki & Tanaka 2018). Photochemical hazes are well described by mean field approximations, as the solid particles produced by photochemistry coagulate at relatively high pressures in the atmosphere and form fractal aggregates of spherical particles (Botet et al. 1997). The Fractal Meanfield Scattering Code of Botet et al. (1997), available on GitHub[60], can be used to get the optical properties of fractal aggregates using refractive indices and fractal dimension as inputs. A recent study by Lodge et al. (2023) investigates the differences which result in the use of the Mie, MMF, and DDA approaches, and demonstrates that using a lower resolution for DDA can also be a good compromise in terms of accuracy and speed. There has been a call amongst some users of atmospheric modelling and retrieval codes for some simple tools to create and read-in cloud opacities. There are two approaches here: either the code reads in refractive indices and particle sizes, and uses Mie theory or similar (DHS is available as part of the ARCiS (Min et al. 2020) code, for example) to compute opacities on the fly; or pre-computed grids of opacities for various species, particle sizes, and shapes, can be read in. Codes such as YunMa (Ma et al. 2023) assume spherical particle sizes. For surfaces, simple linear mixing of pure component spectra can be easily surpassed by more advanced radiative

[60] https://github.com/storyofthewolf/fractal_optics_coreshell.git

transfer models, such as Hapke's (Hapke 1993). The effect of the surface texture (compacity, roughness, grain size) should be also taken into account if the actual data contains sufficient information to retrieve these parameters.

(iv) **Amorphous vs crystalline forms:** there is some discussion in the literature over whether crystalline or amorphous structures are expected under certain situations. It is thought that condensates are typically crystalline if their condensation timescale is faster than their annealing timescale, and amorphous if the opposite is true. This is because in the former case the condensates can rearrange quickly enough to form the crystalline structure, but if the condensation occurs much faster then the formed condensate will be amorphous (Gail & Sedlmayr 1999; Herbort et al. 2020). Grant et al. (2023) demonstrate the impact of choosing either amorphous or crystalline structures for their refractive indices of solid-state SiO_2, with some resulting small differences between their retrieved spectra of WASP-17 b. It is therefore important for refractive indices for both crystalline and amorphous forms to be available for models. Helling (2021) calls for opacity data for condensates across large wavelengths ranges and crystalline species, along with opacity modelling for non-spherical and charged cloud particles.

(v) **Additional species:** it has been noted by members of the community that sulphuric acid-based aerosols are of interest but are missing from the list of available aerosol refractive indices.

(vi) **Condensation curves:** these are required for all species in order to correctly predict their presence in exoplanet atmospheres, over a large range of pressures and temperatures. As mentioned above, Figure 4 of Gail et al. (2013) illustrates the considerable difference between condensation curves of SiO using different measured data, with the newer measurements allowing SiO to be present in solid form up to higher temperatures than the older ones. This highlights the importance of laboratory data for cloud modelling.

(vii) **In-situ measurements of reflectance:** as noted in this section, these data are available from different sources (see Table 14), but not available in one easily accessible database.

(viii) **Cloud nucleation parameters:** constraints on the surface tension, contact angles and similar parameters are required for the description of cloud nucleation (Arfaux & Lavvas 2024). These are typically used even for non-molecular condensates, which are characterised by the absence of the corresponding condensing species in the gas phase e.g. $MgSiO_3$ and Na_2S (Arfaux & Lavvas 2024), thus a better understanding of the heterogeneous mechanisms at play for these cases is also needed.

(ix) **Laboratory data to aid understanding of the coupling of haze and clouds:** it is becoming more evident with the latest observations that the coupling of haze and clouds is important (see, for example, Arfaux & Lavvas 2024). To better understand this coupling, experiments that investigate the potential of haze particles acting as nucleation sites for the condensation of anticipated condensates in exoplanet atmospheres are needed.

7 ATMOSPHERIC CHEMISTRY

Data required for atmospheric chemistry models appropriate for exoplanet atmospheres primarily include thermochemical data for equilibrium networks, and collision and reaction rates for kinetic networks.

7.0.1 *Equilibrium chemistry*

There are a variety of codes designed to model chemical equilibrium in atmospheres, including exoplanet atmospheres. For example, ACE (Agúndez et al. 2012, 2020), FastChem[61] (Stock et al. 2018, 2022), and GGchem[62] (Woitke et al. 2018) all work by minimising the Gibbs free energy of the system for a given pressure and temperature. The minimisation of Gibbs free energy requires thermochemical data as input. Many codes make use of the algorithm of Gordon & Mcbride (1994) to compute the free energy minimisation.

Here we give a little more context to what data are required for codes such as these. Each species is characterised by two sets of thermochemical coefficients, that can be in a 7-format or in a 9-format. The 9-format, being a more recent one, permits more accurate calculations. There is a set for the "high-temperature" range and another one for the "low-temperature" range. For each of these ranges, thermochemical properties of each species in the Normal Conditions Enthalpy (h^0) and Entropy (s^0) can be calculated thanks to the NASA polynomials. For the 7-format, the expressions are:

$$\frac{h^0(T)}{RT} = a_1 + \frac{a_2 T}{2} + \frac{a_3 T^2}{3} + \frac{a_4 T^3}{4} + \frac{a_5 T^4}{5} + \frac{a_6}{T} \tag{7}$$

$$\frac{s^0(T)}{R} = a_1 \ln T + a_2 T + \frac{a_3 T^2}{2} + \frac{a_4 T^3}{3} + \frac{a_5 T^4}{4} + a_7. \tag{8}$$

The polynomials corresponding to the 9-format are slightly different:

$$\frac{h^0(T)}{RT} = -a_1 T^{-2} + a_2 T^{-1} \ln T + a_3 + \frac{a_4 T}{2} + \frac{a_5 T^2}{3} + \frac{a_6 T^3}{4} + \frac{a_7 T^4}{5} + \frac{b_1}{T} \tag{9}$$

$$\frac{s^0(T)}{R} = -\frac{a_1 T^{-2}}{2} - a_2 T^{-1} + a_3 \ln T + a_4 T + \frac{a_5 T^2}{2} + \frac{a_6 T^3}{3} + \frac{a_7 T^4}{4} + b_2. \tag{10}$$

With these two quantities calculated, the Gibbs Free Energy of the system can be calculated:

$$G_{sys} = \sum_l^L (h_l^0(T) - T s_l^0(T) + RT \ln \frac{P}{P^0} + RT \ln N_l) \times N_l \tag{11}$$

The sets of N_l that will minimise this equation (the Gibbs Free Energy of the system) will correspond to the composition at thermochemical equilibrium. Some databases which gather equilibrium thermodynamic coefficients for large sets of species are listed in Section 7.1.1.

[61] https://github.com/exoclime/FastChem
[62] https://github.com/pw31/GGchem

7.0.2 Disequilibrium chemistry

In addition to equilibrium chemistry, some codes include disequilibrium chemistry processes (i.e. quenching induced by vertical mixing, photodissociation, condensation and evaporation, surface deposition, outgassing and atmospheric escape) that control the atmospheric chemical composition (i.e. García Muñoz 2007; Moses et al. 2011; Venot et al. 2012, 2020; Tremblin et al. 2016; Rimmer & Helling 2016; Tsai et al. 2017; Al-Refaie et al. 2022). These codes require data adapted to the type of exoplanets studied. For instance, for warm exoplanets, such as hot Jupiters, data which are validated/measured/calculated at high temperatures are necessary. The data are: chemical schemes, that is to say a list of hundreds to thousands of reactions, with the associated reaction rates, but also physico-chemical data for photodissociations (UV absorption cross-sections and quantum yields). Thermodynamic data are also necessary to calculate reverse reactions rates.

7.1 State of the art - Data availability

7.1.1 Equilibrium chemistry

The C/H/O/N (CHON) chemical species included in ACE (Agúndez et al. 2012, 2020) are mainly sourced from Gordon & Mcbride (1994), Atkinson et al. (2004, 2006, 2007) and Bounaceur et al. (2010), with some constants computed using THERGAS (Muller et al. 1995). ACE is commonly used in conjunction with chemical kinetic models by Venot et al. (2012, 2020) and in the more recently rewritten Python version FRECKLL (Al-Refaie et al. 2022). FastChem (Stock et al. 2018, 2022) sources their thermochemical data from the NIST-JANAF database (Chase 1998)[63]. A version of FastChem has recently been released which includes equilibrium condensation and rainout (Kitzmann et al. 2023), and comes with a python interface. GGchem (Woitke et al. 2018) uses multiple sources of thermochemical data, with new species continuously added to the data files on the GitHub page. The sources for their chemical data comes from (Barklem & Collet 2016), NIST-JANAF (Chase 1998) and Tsuji (1973). Appendix C of Woitke et al. (2018) includes a comparison of the molecular equilibrium constants collected from various sources; the full comparison data can be found at Worters et al. (2017). A graphical comparison of mineral Gibbs free Energy data can also be found at Woitke et al. (2017). Other sources of thermochemical data include the Burcat database (Burcat et al. 2005)[64] and Sharp & Huebner (1990). Recently, Wang et al. (2023b) provided NASA polynomials for 464 molecules with an emphasis on those species which are important for exoplanets.

7.1.2 Disequilibrium chemistry

Concerning chemical schemes, one major difficulty is to get data corresponding to the temperature of exoplanets. Due to long-standing studies of Solar System bodies, most of the chemical schemes developed for planetology are valid for low-temperature medium (e.g. Atreya & Gu (1994); Moses et al. (2005, 2018); Dobrijevic et al. (2014, 2016)). However, in the combustion domain, many studies regarding chemical kinetics at high temperatures have been performed in the last few decades and can be relevant for modeling the atmospheres of exoplanets (e.g. Cathonnet et al. (1982); Kéromnès et al. (2013); Burke et al. (2016)). Based on this fact,Venot et al. (2012, 2015, 2020) and Veillet et al. (2024) have developed and updated reliable chemical schemes validated through combustion experiments for CHON species. These schemes have been validated on a large range of temperatures and pressures, typically 500–2500 K and 10^{-6}–100 bar, thanks to comparisons with many experimental datasets (Veillet et al. 2024). This range of validation is probably adequate, as the chemical composition of the upper part of the atmosphere, which might in certain cases be at lower temperatures than 500 K, is mainly governed by photolysis processes and/or vertical mixing-induced quenching. Even if those have not been validated with the same methodology as the aforementioned ones, chemical schemes with sulphur have also been developed and presented in various studies, such as Zahnle et al. (2016), Tsai et al. (2021), and Hobbs et al. (2021). The network of Tsai et al. (2021) was recently used to contextualise the photochemically produced SO_2 feature detection in the atmosphere of hot Jupiter WASP-39 b (Tsai et al. 2023). Other disequilibrium chemical schemes tailored for exoplanets include the STAND network (Rimmer & Helling 2016), which includes effects of UV photochemistry, cosmic ray chemistry and lightning-driven chemistry, and the network of Moses et al. (2010) which uses thermochemical/photochemical kinetics and transport models. ExoREL (Hu 2019, 2021) is a code to compute disk-averaged reflected-light spectra at any planetary phase, taking into account the radiative properties of clouds and their feedback on planetary albedo.

Databases such as the JPL Chemical Kinetics and Photochemical Data database[65], the KInetic Database for Astrochemistry (KIDA) database[66] (Wakelam et al. 2012), the NIST chemical kinetic database[67], and the UMIST Database for Astrochemistry (UDfA)[68] (Millar et al. 2024) are all sources of kinetic and photochemical data. KIDA provides evaluations of reaction rates and uncertainties, and contains chemical schemes used in planetology. Concerning UV photochemical data, very few data exist at high temperatures. Venot et al. (2013); Venot et al. (2018a) studied experimentally the thermal dependency of carbon dioxide and its impact on atmospheric composition and Fleury et al. (2023) studied the one of C_2H_2. Grosch et al. (2015) measured UV absorption cross-sections of sulphur-containing compounds at elevated temperatures. See Section 8 for details on UV photodissociation and photoabsorption cross-sections.

7.2 Data used by retrieval codes

7.2.1 Equilibrium chemistry

Many of the aforementioned equilibrium chemistry codes are included in various atmospheric modelling and retrieval codes, such as TauREx3 (Al-Refaie et al. 2021) where ACE

[63] https://janaf.nist.gov/janbanr.html
[64] http://garfield.chem.elte.hu/Burcat/burcat.html
[65] https://jpldataeval.jpl.nasa.gov/index.html
[66] https://kida.astrochem-tools.org/
[67] https://kinetics.nist.gov/kinetics/
[68] http://udfa.ajmarkwick.net

is included as standard with the option to include others using the plugin feature of TauREx 3.1, and ARCiS (Ormel & Min 2019; Min et al. 2020), where GGchem (Woitke et al. 2018) is fully integrated. FastChem (Stock et al. 2018, 2022) is the main chemical model used in the HELIOS radiative transfer code (Malik et al. 2017; Kitzmann et al. 2020). Other codes such as petitRADTRANS (Mollière et al. 2019) and Exo-REM (Baudino et al. 2015) include self-written chemical routines. For example, easyCHEM is a self-written Gibbs free energy minimizer which is included in petitRADTRANS and described in Mollière et al. (2017). Al-Refaie et al. (2022) compares computed atmospheric spectra of a hot gas giant exoplanet using some of the available equilibrium chemistry codes plugged into TauREx3; ACE (Agúndez et al. 2012, 2020), FastChem (Stock et al. 2018), GGchem (Woitke et al. 2018), and also GGchem with condensation included. Jaziri et al. (2024) explore the reliability of 1D equilibrium chemistry models to predict the composition of 3D exo-atmospheres with simulated transmission spectra of Ariel and JWST observations. They use the ACE chemical scheme in the TauREx retrieval code. ATMO (Tremblin et al. 2015; Tremblin et al. 2016) is a radiative/convective equilibrium code which is coupled to the CHNO-based chemical network of Venot et al. (2012).

7.2.2 *Disequilibrium chemistry*

In addition to equilibrium chemistry, some atmospheric retrieval codes explicitly parameterise the disequilibrium chemistry process of quenching. For example, Kawashima & Min (2021) outlines the disequilibrium chemistry scheme included in atmospheric retrieval and modelling code ARCiS (Ormel & Min 2019; Min et al. 2020), which includes vertical mixing of CH_4, CO, H_2O, NH_3, N_2, and CO_2. ARCiS uses thermochemical data collated as part of GGchem (mentioned above; Woitke et al. 2018), along with some extra species sourced from Burcat et al. (2005) and Ruscic et al. (2005). Recently, a step forward has been made with TauREx3 using the kinetic code FRECKLL (Full and Reduced Exoplanet Chemical Kinetics distiLLed) as a plugin (Al-Refaie et al. 2022), in order to perform retrievals taking into account chemical kinetics. The kinetic network included in FRECKLL is based on the chemical scheme of Venot et al. (2020). VULCAN is another open source chemical kinetics code for exoplanetary atmospheres, written in python (Tsai et al. 2017). Their paper describes the rate coefficients and thermodynamic data used in the network. ATMO (Tremblin et al. 2015; Tremblin et al. 2016) includes a kinetic chemical network, as well as the equilibrium chemistry network described above. HyDRA (Gandhi & Madhusudhan 2017) is a disequilibrium retrieval framework for thermal emission spectra of exoplanetary atmospheres.

7.3 What's being worked on?

A chemical scheme validated through combustion experiment coupling CHON species to sulphur species is currently in progress and should be published in 2024 (Veillet et al., in prep). There is currently work underway to include P and S in CHON chemical schemes, using ab initio methods. Sticking coefficients of gas phase molecules onto solid atmospheric haze are currently in progress and should be published in 2024 (Perrin et al. in prep). Several UV absorption cross sections (NH_3, HCN, SO_2) are currently under study at LISA with their own UV platform and will be published in the coming years (Collado et al. in prep).

7.4 Data needs: What's missing and urgent?

(i) **Rocky exoplanets:** data for rocky exoplanets require chemical networks that include many different species, which can be much more complex than what is usually the case for hydrogen-dominated atmospheres. These species include KOH, NaOH, SiO_2, CaOH, FeO, MgO, MgOH, as outlined in works such as Tennyson & Yurchenko (2017) and Herbort et al. (2020)

(ii) **Reaction rates for various different molecules:** Helling (2021) call for more thermochemical data, particularly reaction rates, for elements other than CHON(S). This has been pointed out by others, for example for phosphine (Bains et al. 2021), which is applicable to Venus as well as exoplanet atmospheres; for chlorine-bearing species which would be helpful for Mars; and species such as TiO and VO for high-temperature exoplanet atmospheres. Other elements which ideally would be included in chemical schemes include Si, Mg, Na, K, Ca, and Al (Fortney et al. 2019).

(iii) **Reaction rates for ions:** ion chemistry may affect the deeper layers of the atmosphere through, for example, the formation of haze. The ionosphere is also relevant because it connects with the upper atmospheres and therefore with the long-term evolution of the planet's composition.

(iv) **Reaction rate coefficients at a variety of pressures and temperatures:** Reaction rates must therefore be known at temperatures ranging from ~ 30 K to above 3000 K, and because the deep atmospheric layers are chemically mixed with the layers probed by spectroscopic observations, at pressures up to about ~ 100 bar.

(v) **Condensation:** some codes, such as GGchem (Woitke et al. 2018) and the latest version of FastChem (Kitzmann et al. 2023), already include condensation. Expanding more codes to explicitly include condensation and including additional elements in chemical networks will be useful to fully characterise where the elements of an atmosphere will go under chemical equilibrium conditions.

(vi) **Gas-particle processes:** when aerosol particles are present in the atmosphere, gas-particle chemistry has been shown to influence not only the particles, but also the atmospheric content (Cavalié et al. 2023; Petera et al. 2023, and Knížek et al. in prep.). For that purpose, sticking coefficients of gas components on solid particles are largely missing.

8 UV PHOTODISSOCIATION/PHOTOABSORPTION DATA

The need for a description of molecular absorption in the ultraviolet (UV) region is motivated mainly by the following two reasons: 1) direct observations in the UV, which are not in the Ariel instrumental range but are of relevance to a number of existing, past, or potential future instruments; the WFC3/UVIS instrument on board the Hubble Space Telescope (HST) (200 - 1000 μm), the Galaxy Evolution Explorer (GALEX) (135 - 280 nm) (Viswanath et al. 2020), the Far Ultraviolet Spec-

troscopic Explorer (FUSE) (90.5 – 119.5 nm) (Moos et al. 2004), Cassini Ultra-violet Imaging Spectrograph (UVIS) (55.8-190 nm) (Esposito et al. 2004), and the Habitable Worlds Observatory (HWO) future mission concept; and 2) utilisation in atmospheric chemistry calculations for considering the chemical consequences of photodissociation, see Section 7. For example, improving the cross-section data of H_2O in the the vacuum ultraviolet (VUV, ~100 - 200 nm) leads to significant changes in the outcome of photochemistry: for an abiotic habitable planet with an anoxic, CO_2–N_2 atmosphere orbiting a Sun-like star, it enhances the OH production which in turn suppresses a broad range of species in anoxic atmospheres (Ranjan et al. 2020), including H_2 and CH_4. This is just one mechanism, clearly showing the sensitivity of the models to UV cross-sections and thus highlighting the critical need for laboratory data used photochemical models, whether from measurements or calculations. The impact of the strong variation of CO_2 absorption cross-sections with temperature on abundance and photodissociation rates of many species (CO2, CH_4, NH_3) was demonstrated by Venot et al. (2018a).

The special but typical feature of molecular spectra in the UV/VUV wavelength region is their continuum. Their featureless character is due to the dissociative effects in the high energy/low wavelength region. It is this type of spectra produced by transitions to or from states above a dissociation limit and caused by the dissociation that we mainly discuss in this section. Photoabsorption includes both bound–bound transitions (these appear as either sharp lines or continuum) and bound–free photodissociation (continuum) transitions, see, e.g., Pezzella et al. (2021); Tennyson et al. (2023). Bound-bound transitions which result in sharp lines are often included as part of a line list which extends into the UV region (see Section 2). These types of spectra can be completely featureless for transitions to the continuum (from bound states to fully unbound, or dissociative states, e.g. HF above 100-160 nm (Pezzella et al. 2022)) or mostly consisting of sharp lines (from bound to bound or quasi-bound states, e.g. MgH in the A-X band at 0.5 μm (Owens et al. 2022a)), or anything in between (Pezzella et al. 2022). Both continuum absorption and photodissociation need to be represented as cross-sections rather than the lines of a typical line list, as they are continuum processes.

This creates challenges not only for the production of UV spectral data but also for its provision and format. For the featureless UV spectra, it is natural to provide data in the form of temperature dependent cross-sections. This is the format of the MPI-Mainz UV/VIS Spectral Atlas[69] (Keller-Rudek et al. 2013) and Leiden[70] (Heays et al. 2017; Hrodmarsson & Van Dishoeck 2023) databases. In cases where the cross-sections are dominated by the continuum, the pressure effect is considered to be negligible, but it is noteworthy that in cross-sections dominated by resonances to Rydberg and valence states, high pressures can significantly affect the absorption cross-sections. Such effects have been observed in NO where transitions to Rydberg states were significantly broadened and shifted up until 1000 bar where the Rydberg states have all but vanished from the spectrum (Miladi et al. 1975, 1978). However, most UV spectra comprise a mixture of the bound-bound transitions (sharper lines) and continuum.

8.1 State of the art - Data availability

One of the main sources of photodissociation cross-sections of molecules is the Leiden database[71] which provides photodissociation and photoionisation cross-sections for 116 atoms and molecules of astrochemical interest collected from the literature, both experimental and theoretical (Heays et al. 2017; Hrodmarsson & Van Dishoeck 2023). The photodissociation thresholds and threshold products provided by this database are summarised in Table 15, and the provided photoionisation thresholds summarised in Table 16 for molecules at low (interstellar/terrestrial) temperatures. The PHIDRATES website[72] provides a set of tools to calculate photoionisation, photodissociation, and photodissociative ionisation rate coefficients (Huebner et al. 1992). There is also the MPI-Mainz UV/VIS Spectral Atlas[73] (Keller-Rudek et al. 2013), where experimental temperature dependent cross-sections for a larger number of molecules are provided. We note, however, that there are some limitations in terms of temperature-dependence and wavelength coverage of the data in cross-section databases such as these, so it is worth checking the range of temperatures covered by the cross-sections for each species of interest.

In the past few years, there have been multiple VUV cross-sections (photoabsorption and photoionisation) measured at the VUV DESIRS beamline at the SOLEIL synchrotron facility in France (Nahon et al. 2012). Absolute photoabsorption cross-sections have been measured using a Fourier-transform absorption cell (de Oliveira et al. 2016) where multiple species have been measured such as OH (Heays et al. 2018), CO (Hakalla et al. 2016; Lemaire et al. 2018), S_2 (Stark et al. 2018), SO (Heays et al. 2023), and others. Absolute photoionisation cross-sections of radical species have been measured with the double-imaging photoelectron photoion (i2PEPICO) instrument DELICIOUS3 (Garcia et al. 2013) where the radicals were produced continuously in a stable manner with a flow tube (Garcia et al. 2015). This has allowed the measurements of photoionisation cross setions of species such as OH (Harper et al. 2019), NH_2 (Harper et al. 2021), SH (Hrodmarsson et al. 2019), and others. In the frame of the EXACT project[74] VUV absorption cross-sections are also measured experimentally. The first species studied was carbon dioxide (Venot et al. 2013; Venot et al. 2018a).

Regarding computations of photoionisation or photoabsorption, the XCHEM code has recently been used to compute the photoionisation of H_2O (Fernández-Milán et al. 2023), and also the valence-shell photoionisation of CO_2 (Pranjal et al. 2024). Photoabsorption cross-sections for atmospheric volatile organic compounds (VOCs) have

[69] https://www.uv-vis-spectral-atlas-mainz.org/uvvis/
[70] https://home.strw.leidenuniv.nl/~ewine/photo/index.html
[71] https://home.strw.leidenuniv.nl/~ewine/photo/index.html
[72] https://phidrates.space.swri.edu/
[73] https://www.uv-vis-spectral-atlas-mainz.org/uvvis/
[74] https://www.anr-exact.cnrs.fr/

Table 15. Photodissociation thresholds and threshold products in the Leiden database (Heays et al. 2017; Hrodmarsson & Van Dishoeck 2023).

Species	Photodis. products	Thresh Photodis	Species	Photodis. products	Thresh Photodis	Species	Photodis products	Thresh Photodis
AlH	Al + H	392	CO_2	CO + O	227	NH_2CHO	NH_3 + CO	208
C_2	C + C	193	CS	C + S	168	NH_3	NH + H_2	301
C_2H	C_2 + H	253	CS_2	CS + S	278	NO	N + O	191
C_2H_2	C_2H + H	217	H_2	H + H	274	NO_2	NO + O	398
C_2H_3	H_2CC + H	1240	H_2^+	H + H^+	290	NaCl	Na + Cl	293
C_2H_4	C_2H_2 + H_2	258	H_2CO	H_2 + CO	361	NaH	Na + H	606
C_2H_5	C_2H_4 + H	260	H_2CS	H_2 + CS	313	O_2	O + O	242
C_2H_5OH	C_2H_5O + H	208	H_2O	H + OH	242	O_2^+	O + O^+	186
C_2H_6	C_2H_5 + H	287	H_2O_2	OH + OH	556	O_3	O_2 + O	1180
C_3	C_2 + C	268	H_2S	H + SH	318	OCS	CO + S	280
C_3H_3	C_3H_2+ H	300	HC_3H	l-C_3H + H	400	OH	O + H	279
C_3H_7OH	C_3H_7O + H	208	HC_3N	H + C_3N	244	OH^+	O^+ + H	247
CH	C + H	358	HCN	H + CN	243	PH	P + H	398
CH^+	C + H^+	303	HCO	H + CO	2037	PH^+	P^+ + H	369
CH_2	C + H	417	HCO^+	H + CO^+	145	S_2	S + S	283
CH_2^+	CH^+ + H	204	HCOOH	H + HCOO	333	SH	S + H	345
CH_3	CH + H_2	271	HCl	H + Cl	279	SH^+	S^+ + H	320
CH_3CHO	HCO + CH_3	342	HCl^+	H + Cl^+	267	SO	S + O	233
CH_3OCH_3	CH_3O + CH_3	196	HF	H + F	211.4	SO2	O + SO	219
CH_3OCHO	HCO + CH_3	248	HNC	H + CN	165	SiH	Si + H	417
CH_3CN	CH_2CN + H	308	HNCO	NH + CO	333	SiH^+	Si^+ + H	391
CH_3NH_2	CH_3NH + H	244	HO_2	H + O_2	476	SiO	Si + O	150
CH_3OH	CH_3O + H	280	LiH	Li + H	579	c-C_3H	C_3 + H	289
CH_3SH	CH_3S + H	331	MgH	Mg + H	623	c-C_3H_2	c-C_3H + H	284
CH_4	CH_3 + H	277	N_2	N + N	127	SiO	Si + O	150
CH_4^+	CH_3^+ + H	1031	N2O	N_2 + O	735	l-C_3H	C_3 + H	379
CN	C + N	160	NH	N + H	362	l-C_3H_2	l-C_3H + H	320
CO	C + O	110	NH^+	N^+ + H	281	l-C_4	C_3 + C	263
CO^+	C^+ + O	149	NH_2	NH + H	314	l-C_4H	C_4 + H	267
–	–	–	–	–	–	l-C_5H	C_5 + H	348

Table 16. Ionisation thresholds in the Leiden database (Heays et al. 2017; Hrodmarsson & Van Dishoeck 2023).

Species	Thresh Photoion	Species	Thresh Photoion	Species	Thresh Photoion	Species	Thresh Photoion
Al	207	CH_3OH	113	HCO	152	O_2	103
AlH	156	CH_3SH	131	HCOOH	110	O_3	99
C	110	CH_4	98	HCl	97	OCS	111
C_2	102	CN	87	HF	77.5	OH	95
C_2H	107	CO	88	HNC	103	P	118
C_2H^-	412	CO_2	90	HNCO	108	PH	122
C_2H_2	109	CS	110	HO_2	109	Rb	297
C_2H_3	147	CS_2	123	K	286	S	120
C_2H_4	118	Ca	203	Li	230	S_2	133
C_2H_5	153	Ca^+	104	LiH	152	SH	119
C_2H_5OH	119	Cl	96	Mg	162	SO	120
C_2H_6	108	Co	158	Mn	167	SO_2	100
C_3	102	Cr	183	N	85	Si	152
C_3H_3	143	Fe	158	N_2	79	SiH	156
C_3H_7OH	123	H	91	N_2O	96	SiO	108
C_2H^-	348	H^-	1470	NH	92	Ti	182
C_6H^-	327	H_2	82	NH_2	111	Zn	132
CH	117	H_2CO	114	NH_2CHO	121	c-C_3H	129
CH_2	119	H_2CS	135	NH_3	122	c-C_3H_2	136
CH_3	126	H_2O	98	NO	134	l-C_3H	136
CH_3CHO	121	H_2O_2	117	NO_2	127	l-C_3H_2	119
CH_3OCH_3	127	H_2S	119	Na	241	l-C_4	116
CH_3OCHO	113	HC_3H	139	NaH	179	l-C_4H	129
CH_3CN	102	HC_3N	107	Ni	162	l-C_5H	168
CH_3NH_2	135	HCN	91	O	91	–	–

been computed by Prlj et al. (2020, 2022), using a combination of time-dependent and time-independent methods. Ndengué et al. (2023) explore the temperature dependence of the electronic absorption spectrum of NO_2 up to 2200 K, down to a wavelength of 0.25 μm (up to 40,000 cm^{-1}) by combining *ab initio* methods with high-resolution experiments. Xue et al. (2020) utilise machine learning methods for the computation of absorption cross-sections in the visible and UV wavelength region, including benzene. Machine learning algorithms for the computation of electronically excited states are also utilised by Sršeň & Slavíček (2021) and Sršeň et al. (2023).

Collections of theoretical UV cross-sections of PAHs are available online[75] (Malloci et al. 2007) and measurements of the cross-sections of cationic PAHs (Zhen et al. 2016; Wenzel et al. 2020) have been used recently by Berné et al. (2022) to show the importance of up-to-date experimental measurements to understand the contribution of the ionisation of PAH cations to a variety of environments.

The ExoMol database has started providing photoabsorption and photodissociation data, see Tennyson et al. (2023). This will include UV line lists (bound-bound transitions only), UV photoabsorption cross-sections (bound-continuum only) and separately full temperature dependent photoabsorption cross-sections (all together). The data are produced with essentially the same computational ExoMol-methodology used for production of line lists, see Section 2.1.1.2, i.e. a mixture of first-principle quantum-mechanical calculations and empirical refinement, see Pezzella et al. (2021). As in the case of the line lists, the advantage of theoretical spectra is in the completeness at higher temperatures. ExoMol also provides hosting for experimental VUV/UV cross-sections of molecules, see Fateev et al. (2023). The recent AloHa AlH line list gives an example of the treatment of mixed spectral lines and continuum absorption in UV (Yurchenko et al. 2024e) while Pezzella et al. (2022) gives an example of photodissociation cross-sections.

Absolute VUV branching ratios (sometimes known as quantum yields) of molecules are generally not very well known, in part due to the experimental difficulties of measuring them. Rotationally resolved absolute photodissociation branching ratios of small molecules like CO (Ranjan et al. 2020; Gao et al. 2020a, 2013), CO_2 (Lu et al. 2014), N_2 (Song et al. 2016; Shi et al. 2017), and others have been obtained using two tunable VUV laser systems. Other advancements have been in the use of VUV free electron lasers such as the one in the Dalian Light Source in China, where VUV photodissociation branching ratios have been measured for species such as H_2S (Zhou et al. 2020), CS_2, and OCS along with even more recent results of H_2O (Chang et al. 2023; Wogan et al. 2024). There are more recent measurements in the context of exoplanet atmospheres that are noteworthy such as recent measurements of ethane (C_2H_6) (Chang et al. 2020) considering its relevance to both Hycean atmospheres and Enceladus. As the sizes of molecules grow, the fragmentation patterns become more difficult to disentangle. In the case of C_2H_6, there are seventeen different fragmentation channels available at the Lyα limit, each other with different sets of fragmentation products which can be formed in various electronically excited states.

Regarding the electronically excited species, to a zeroth order approximation the electronic fluorescence proceeds faster than the collision frequency in the atmosphere in question. The validity of this approximation is dependent on the pressure and temperature of the relevant environments but typically non-dissociative fluorescence lifetimes of small molecules are of the order of one to a few microseconds. For environments where collision rates and these fluorescence rates are comparable, collisions with electronically excited species should not be neglected because they could lead to different photochemical paradigms that are currently neglected in most atmospheric models. For example, when H_2O is photodissociated from the D state, OH is formed in the electronically excited A state which has a fluorescent lifetime of 1 microsecond (Livingston Large & Kliewer 2024).

8.2 What's being worked on?

(i) ExoMol is working on producing temperature-dependent UV photoabsorption and photodissociation data for a variety of molecules including OH, SO and HCN.

(ii) Recently, acetylene has been measured (Fleury et al. 2023) and more data are to be published soon (Fleury et al. in prep), as part of the EXACT project[76], where UV absorption cross-sections are measured experimentally. The EXACT project aims to measure UV absorption cross-sections at high temperatures for many species, using their experimental setup at LISA.

(iii) VUV photoabsorption cross-sections and VUV Photoionisation cross-sections are currently being studied for a number of molecules at the DESIRS beamline at the SOLEIL synchrotron facility in France. Current efforts involve sulphur-containing species; photoabsorption cross-section of CS and C_2 will be measured and the photoionisation cross-sections of sulphur containing radicals such as CCS will be investigated.

(iv) PAHs: similar to the recent experimental work of Chowdhury et al. (2024) on the cyanonaphthalenes, the photoionisation of a large sample of neutral PAHs of varying sizes and symmetries are being investigated (Hrodmarsson et al. in prep) to improve previous experimental data on PAH photoabsorption data from the 1990's (Verstraete et al. 1990; Tobita et al. 1994; Jochims et al. 1996; Jochims et al. 1997, 1999) currently in use to describe the contribution of neutral PAHs to the gas heating in the ISM. At the LISA laboratory, UV absorption cross sections for several molecules of atmospheric importance are currently under study. A future instrumental direction at LISA is to construct a double VUV laser system with a VMI spectrometer that will be dedicated to measuring VUV branching ratios of molecules of interest to exoplanet atmospheres.

8.3 Data needs: What's missing and urgent?

(i) **Photoabsorption cross-sections at high temperatures:** Fortney et al. (2019) (a collaborative Astro2020 Science White Paper) expressed the need for photoabsorption

[75] http://astrochemistry.ca.astro.it/database/pahs.html

[76] https://www.anr-exact.cnrs.fr/

cross-sections measurements and their temperature dependency in the VUV wavelength range (115 - 230 nm) for molecules such as N_2, O_2, O_3, H_2O, CO, CO_2, CH_4, NH_3, TiO, VO, HCN, C_2H_2, H_2S, PH_3.

(ii) **Branching ratios:** Despite a huge progress in laboratory provision of branching ratios, e.g. Burkholder et al. (2020), more data for atmospheric studies is needed (Jenkin et al. 2019; Gao et al. 2020a).

(iii) **Non-LTE:** most photodissociation cross sections come from the study of molecules in thermal equilibrium. However, there it is generally accepted that the upper atmospheres of most observable exoplanets are not thermal and so Non-LTE cross sections will be needed.

9 DATA STANDARDS

9.1 Principles of and need for data standards

Standards for the description of atomic and molecular data are crucial for their effective use in the study of exoplanet atmospheres. The successful adoption of a set of standards for the description of species, quantum states and spectroscopic processes facilitates interoperability between simulation codes, data exchange between researchers, the long-term preservation of data and automatic processing of data, for example through Application Programming Interfaces (APIs).

In any discussion about data standards a distinction must be made between metadata and data formats. All datasets are associated, implicitly or explicitly, with some set of conventions for describing metadata: the context, applicability, provenance, physical units and additional information which give meaning to the raw numbers of the data themselves. The format in which these numerical data are provided may vary between databases (depending, for example, on the size of the data sets). However, an interoperable ecosystem of databases must adopt standardised, unambiguous and machine-readable metadata conventions to allow comparison and aggregation across data sets.

Modern database services aspire to conform to so-called FAIR principles of data curation (Wilkinson et al. 2016); in brief, FAIR data are:

- Findable: associated with globally unique and persistent identifiers; registered in a searchable, online resource.
- Accessible: retrievable through a standardised protocol.
- Interoperable: associated with metadata in a formal, well-described representation.
- Reusable: clearly-licensed and documented, with detailed provenance and rich metadata attributes providing context to the data.

In the context of atomic and molecular data, the adoption of these principles can be realised as follows

- Atomic and molecular species and states should be specified using common identifiers.
- Data sets, such as line lists and cross-sections, should be assigned globally unique identifiers and be locatable through these identifier using online services.
- Where data sets are updated, older versions should be permanently available, identified and time-stamped.
- All numerical data should be associated with clear metadata describing its format, physical units and limits of applicability (for example, valid temperature or pressure range).
- Digital Object Identifiers (DOIs) should be attached to data sets to permanently identify the origin of the data; typically such DOIs will refer to the data's associated publication, such as a journal article.

9.2 Focus on Interoperability: VAMDC and other services

The Virtual Atomic and Molecular Data Centres (VAMDC) consortium (VAMDC 2014-; Albert et al. 2020) is a group of research institutes that share a common technical and political framework for the distribution and curation of atomic and molecular data. The goal of the consortium is to build a software infrastructure allowing the linking and searching of multiple databases through a common data format ("XSAMS") and query language ("VSS2"). The VAMDC has built a platform (the "portal") for the simultaneous search of, at the time of writing, 38 databases and the aggregation of matching data sets. It now is concerned with further developing data standards, promoting collaboration in data production and evaluation, and in broadening its scope beyond spectroscopy and plasma physics. As machine learning matures and becomes more widely-adopted, the VAMDC is also exploring the application of artificial intelligence to its data services, to facilitate, for example, data transformation and visualisation and to assist with the validation and aggregation of data.

An up-to-date summary of the current status of the VAMDC and its database nodes can be found in the report of its most recent annual meeting, held as a Technical Meeting of the International Atomic Energy Agency in November 2023 (Hill 2023).

9.3 What's being worked on?

The PyValem software library (PyValem 2024) provides a framework of Python routines for parsing standardised, text-based representations of atomic and molecular species and states; the syntax of these representations is largely adopted by the HITRAN and ExoMol databases, and is fully implemented in the CollisionDB database (Hill et al. 2024; CollisionDB 2024) of plasma collisional processes. In addition to providing a common language for referring to species and states, this library can also perform a degree of validation on its input, for example by ensuring that quantum numbers are valid and reactions conserve stoichiometry and charge.

Several of the resources described in this paper expose an API for the automated querying and retrieval of atomic and molecular data; in addition to the VAMDC portal service outlined above, there are well-documented APIs for the HITRAN, ExoMol and CollisionDB databases; the software tools for interacting with these APIs are either already available or under active development.

The MAESTRO database, introduced in Section 4.2, is under ongoing development. It aims to create one uniform and standardised database for opacities useful in the characterisation of exoplanet atmospheres, and to aid in the establishment of community standards for computing opacity data (see, e.g., Gharib-Nezhad et al. 2024).

9.4 Data standards needs: What's missing and urgent?

At the time of writing there are several competing standards for describing atomic and molecular species; whilst some of these are widely-adopted in some areas of chemistry and physics (for example, SMILES (Weininger 1988), or InChI / InChIKey strings (Heller et al. 2015)), there is no entirely satisfactory and easy-to-use standard for small molecules, particularly metal hydrides, in the context of astrophysical spectroscopy.

As described above, the line lists required of even relatively small molecules for spectroscopic modelling at elevated temperatures can become very large, with over 10^{10} individual transitions contributing the observable spectra. Therefore, database services supporting the asynchronous retrieval of large data files are needed. New software tools are required for the visualisation, validation, extraction and, potentially, reduction of such data sets. These tools should allow for the interconversion between popular data formats (XSAMS, HITRAN, ExoMol, and so on) and must be tested and maintained on a regular basis. In addition to improving usability, these tools can also perform the important function of validating the integrity of the data by checking for format consistency and data completeness.

A further issue is the complexity of the quantitative description of line broadening effects: this necessitates a flexible data model that can be applied to multiple databases; at present different approaches are taken by those databases that contain broadening data sets.

10 CONCLUSION

In this white paper we have focused on a number of different data types: molecular and atomic line lists (Section 2), molecular and atomic line shapes (Section 3), computed cross-sections and opacities (Section 4), collision induced absorption (CIA) and other continuum data (Section 5), data for aerosols (Section 6), data for atmospheric chemistry models (Section 7), and data for UV photodissociation or photoabsorption (Section 8). Needs for data standards, metadata, existing rules and associated tools were discussed in Section 9. For each data type we have focused on: data availability, what data is typically used by atmospheric modelling and retrieval codes, what is missing and urgent, and what is currently being worked on. Of course the information provided in this paper is not comprehensive, but we have tried to give an overview for each data type for both data users and data providers.

We also note that there are some important data topics relating to exoplanet atmospheres which we do not address in this particular paper. For example, accurate data regarding stellar spectra are important for photochemistry (see Section 7) and UV photodissociation processes (see Section 8). The secondary eclipse measurement of a transiting exoplanet gives information on the emission and reflection spectra. These measurements are presented as a ratio of planetary flux to stellar flux, and therefore also require an accurate stellar flux model. We note there are some resources for theoretical models of stellar spectra such as the Kurucz-Castelli grids of models[77] (Heiter et al. 2002; Castelli & Kurucz 2004), models from the SVO (Spanish Virtual Observatory) [78], which provides data for 70 collections of theoretical spectra and observational templates, and the PHOENIX stellar models[79] (Husser et al. 2013). The Virtual Planet Laboratory regroups data from various publications[80], and there are additional sources of stellar spectra available from the MUSCLES survey of 11 low-mass, planet-hosting stars[81] (France et al. 2016). We refer to works such as Gandhi & Madhusudhan (2017), Shulyak et al. (2020) and Rackham et al. (2023) for further information on the topic of stellar spectra for use in characterising exoplanet atmospheres.

Although the primary focus of the working group who initiated this white paper is for data needs appropriate for the Ariel space mission, we do discuss data for e.g. spectral regions which fall outside the observing window of Ariel. Such regions can be very useful for theoretical models which inform predictions for target planets for the Ariel mission, or for observations which are complementary to those planned by Ariel. Many of these data needs will be shared by all those in the exoplanet atmosphere community, not only those working directly on preparing for the Ariel space mission.

10.1 Ariel-data GitHub platform

The description of the data associated with this paper and the Ariel mission in general is available at GitHub via the project https://github.com/Ariel-data. The goal of this platform is to provide a go-to place both for the data-users and data-providers, for the users to highlight their data needs and make requests, and for the data providers to link to the available data. As an open access tool, GitHub provides huge advantages of forming direct dialogues between these sides of the community, where the modelers can make their shopping-lists for the data producers to start planning their calculations or experiments, even for those who are currently not directly involved in the Ariel consortium or in the field of exoplanetary science in general.

We invite everyone to test and make use of this system.

11 DATA AVAILABILITY

The data discussed in this paper will be available for access at GitHub via the project https://github.com/Ariel-data, which was created as a platform to bridge the two communities, data-providers and data-users. As an open platform, for the users, it provides an efficient way to communicate their needs, while the data providers can use it to make their work more visible. Any data-related GitHub "issues" raised for the attention of the Ariel Working-Group will be visible to the entire community of the lab data providers, from experimentalists to theoreticians.

[77] http://kurucz.harvard.edu/grids.html

[78] http://svo2.cab.inta-csic.es/theory/newov2/index.php

[79] https://phoenix.astro.physik.uni-goettingen.de/

[80] https://vpl.uw.edu/models/spectral-database-tools/

[81] https://archive.stsci.edu/prepds/muscles/

12 ACKNOWLEDGEMENTS

We thank the comprehensive efforts of the Reviewers for a number of constructive comments through the paper. The ExoMol project is supported by the European Research Council (ERC) under the European Union's Horizon 2020 research and innovation programme through Advance Grant numbers 883830 (ExoMolHD).
K.L.C was funded by UK Research and Innovation (UKRI) under the UK government's Horizon Europe funding guarantee as part of an ERC Starter Grant [grant number EP/Y006313/1].
S.Y. acknowledges funding by STFC Projects No. ST/Y001508/1.
S.R. acknowledges funding by the Belgian Science Policy Office (BELSPO) through the FED-tWIN program (Prf-2019-077 - RT-MOLEXO) and through financial and contractual support coordinated by the ESA Prodex Office (PEA 4000137943, 4000128137).
A.F. acknowledges funding by the Knut and Alice Wallenberg Foundation (KAW 2020.0303) and the Swedish Research Council (2020-00238).
This research was supported by the Excellence Cluster ORIGINS which is funded by the Deutsche Forschungsgemeinschaft (DFG, German Research Foundation) under Germany's Excellence Strategy - EXC-2094 - 390783311.
A.V.N. and O.E. acknowledge the support from the Russian Scientific Foundation (RSF, No. 22-42-09022).
M.R. acknowledges support from the French ANR TEMMEX project (Grant 21-CE30-0053-01) and from the Romeo computer center of Reims Champagne-Ardenne.
F.S. acknowledges support from the "Institut National des Sciences de l'Univers" (INSU), the "Centre National de la Recherche Scientifique" (CNRS) and "Centre National d'Etudes Spatiales" (CNES) through the "Programme National de Planétologie".
T. Zi acknowledges NVIDIA Academic Hardware Grant Program for the use of the Titan V GPU card and the support by the CHEOPS ASI-INAF agreement n. 2019-29-HH.0 and the Italian MUR Departments of Excellence grant 2023-2027 "Quantum Frontiers".
Ch. H and H.L.M. acknowledge funding from the European Union H2020-MSCA-ITN-2019 under grant agreement no. 860470 (CHAMELEON).
O.V. acknowledges funding from the ANR project 'EXACT' (ANR- 21-CE49-0008-01) and the Centre National d'Études Spatiales (CNES). This work was also supported by CNES, focused on Ariel, through 'EXACT'.
J.K.B. is supported by an STFC Ernest Rutherford Fellowship, grant number ST/T004479/1.
A.M. (Alessandra Migliorini) acknowledges funding from the Italian Space Agency (ASI) contract with the National Institute for Astrophysics (INAF) n. 2018-22-HH.0.1-2020.
I.S. acknowledges the support by DFG (DFG, German Research Foundation) – project No. SA 4483/1–1.
M.R. acknowledges the support by the DFG priority program SPP 1992 "Exploring the Diversity of Extrasolar Planets" (DFG PR 36 24602/41).
A.K. (Antonín Knížek) acknowledges support from grant no. 24-12656K by the Czech Science Foundation and the ESA Prodex project under PEA 4000129979.
I.E.G and R.J.H acknowledge funding support through NASA grant 80NSSC23K1596 and NASA PDART grant 80NSSC24K0080.
Z.M. acknowledges, through Centro de Química Estrutural, the financial support of Fundação para a Ciência e Tecnologia (FCT) for the projects UIDB/00100/2020 and UIDP/00100/2020, and through Institute of Molecular Sciences, the financial support of FCT for the project LA/P/0056/2020.
A.B. was supported by the Italian Space Agency (ASI) with *Ariel* grant n. 2021.5.HH.0.
N.C. thanks the European Research Council for funding via the ERC OxyPlanets project (grant agreement No. 101053033).

REFERENCES

Abdel-Shafy, H. I. & Mansour, M. S., 2016. A review on polycyclic aromatic hydrocarbons: Source, environmental impact, effect on human health and remediation, *Egypt. J. Pet.*, **25**, 107–123.
Abe, M., Iwakuni, K., Okubo, S., & Sasada, H., 2013. Accurate transition frequency list of the ν_3 band of methane from sub-doppler resolution comb-referenced spectroscopy, *J. Opt. Soc. Am.*, **30**, 1027–1035.
Abel, M., Frommhold, L., Li, X., & Hunt, K. L. C., 2011. Collision-induced absorption by H_2 pairs: From hundreds to thousands of kelvin, *J. Phys. Chem. A*, **115**, 6805–6812.
Abel, M., Frommhold, L., Li, X., & Hunt, K. L. C., 2012. Infrared absorption by collisional H_2-He complexes at temperatures up to 9000 K and frequencies from 0 to 20,000 cm^{-1}, *J. Phys. Chem.*, **136**, 044319.
Ackerman, A. S. & Marley, M. S., 2001. Precipitating condensation clouds in substellar atmospheres, *ApJ*, **556**, 872.
Adam, A. Y., Yachmenev, A., Yurchenko, S. N., & Jensen, P., 2019. A Variationally Computed IR Line List for the Methyl Radical CH_3, *J. Phys. Chem. A*, **123**, 22.
Adil, M., Giri, B. R., Elkhazraji, A., & Farooq, A., 2023. Mid-IR absorption spectra of C1-C4 alkyl acetates at high temperatures, *J. Quant. Spectrosc. Radiat. Transf.*, **300**, 108522.
Adkins, E. M., Karman, T., Campargue, A., Mondelain, D., & Hodges, J. T., 2023. Parameterized model to approximate theoretical collision-induced absorption band shapes for O_2-O_2 and O_2-N_2, *J. Quant. Spectrosc. Radiat. Transf.*, **310**, 108732.
Adler, F., Maslowski, P., Foltynowicz, A., Cossel, K. C., Briles, T. C., Hartl, I., & Ye, J., 2010a. Mid-infrared Fourier transform spectroscopy with a broadband frequency comb, *Opt. Express*, **18**, 21861–21872.
Adler, F., Thorpe, M. J., Cossel, K. C., & Ye, J., 2010b. Cavity-enhanced direct frequency comb spectroscopy: Technology and applications, *Annu. Rev. Anal. Chem.*, **3**, 175–205.
Agúndez, M., Venot, O., Iro, N., Selsis, F., Hersant, F., Hébrard, E., & Dobrijevic, M., 2012. The impact of atmospheric circulation on the chemistry of the hot Jupiter HD 209458b, *A&A*, **548**, A73.
Agúndez, M., Martínez, J. I., de Andres, P. L., Cernicharo, J., & Martín-Gago, J. A., 2020. Chemical equilibrium in AGB atmospheres: successes, failures, and prospects for small molecules, clusters, and condensates, *A&A*, **637**, A59.
Al-Derzi, A. R., Furtenbacher, T., Tennyson, J., Yurchenko, S. N., & Császár, A. G., 2015. MARVEL analysis of the measured high-resolution spectra of $^{14}NH_3$, *J. Quant. Spectrosc. Radiat. Transf.*, **161**, 117–130.
Al-Derzi, A. R., Tennyson, J., Yurchenko, S. N., Melosso, M., Jiang, N., Puzzarini, C., Dore, L., Furtenbacher, T., Tóbiás, R., & Császár, A. G., 2021. An improved rovibrational linelist of formaldehyde, $H_2^{12}C^{16}O$, *J. Quant. Spectrosc. Radiat. Transf.*, **266**, 107563.
Al-Refaie, A. F., Yurchenko, S. N., Yachmenev, A., & Tennyson, J., 2015. ExoMol line lists - VIII: A variationally computed line list for hot formaldehyde, *MNRAS*, **448**, 1704–1714.

Al-Refaie, A. F., Polyansky, O. L., Ovsyannikov, R. I., Tennyson, J., & Yurchenko, S. N., 2016. ExoMol line lists XV: A hot line-list for hydrogen peroxide, *MNRAS*, **461**, 1012–1022.

Al-Refaie, A. F., Changeat, Q., Waldmann, I. P., & Tinetti, G., 2021. TauREx 3: A fast, dynamic, and extendable framework for retrievals, *AJ.*, **917**, 37.

Al-Refaie, A. F., Changeat, Q., Venot, O., Waldmann, I. P., & Tinetti, G., 2022. A comparison of chemical models of exoplanet atmospheres enabled by TauREx 3.1, *ApJ*, **932**, 123.

Alatoom, D., Ibrahim, M. T. I., Furtenbacher, T., Csaszar, A. G., Alghizzawi, M., Yurchenko, S. N., Azzam, A. A. A., & Tennyson, J., 2024. MARVEL analysis of high-resolution rovibrational spectra of $^{16}O^{12}C^{18}O$, *J. Comput. Chem.*.

Albert, D., Antony, B. K., Ba, Y. A., et al., 2020. A Decade with VAMDC: Results and Ambitions, *Atoms*, **8**, 76.

Alberti, M., Weber, R., Mancini, M., Fateev, A., & Clausen, S., 2015. Validation of HITEMP-2010 for carbon dioxide and water vapour at high temperatures and atmospheric pressures in 450-7600 cm^{-1} spectral range, *J. Quant. Spectrosc. Radiat. Transf.*, **157**, 14–33.

Alderson, L., Wakeford, H. R., Alam, M. K., Batalha, N. E., et al., 2023. Early release science of the exoplanet WASP-39b with JWST NIRSpec G395H, *Nature*, **614**, 664–669.

Allard, N. F. & Kielkopf, J. F., 1982. The effect of neutral nonresonant collisions on atomic spectral lines, *Rev. Mod. Phys.*, **54**, 1103.

Allard, N. F., Royer, A., Kielkopf, J. F., & Feautrier, N., 1999. Effect of the variation of electric-dipole moments on the shape of pressure-broadened atomic spectral lines, *Phys. Rev. A*, **60**, 1021.

Allard, N. F., Spiegelman, F., & Kielkopf, J. F., 2016. K-H_2 line shapes for the spectra of cool brown dwarfs, *A&A*, **589**, A21.

Allard, N. F., Spiegelman, F., Leininger, T., & Mollière, P., 2019. New study of the line profiles of sodium perturbed by H_2, *A&A*, **628**, A120.

Allard, N. F., Myneni, K., Blakely, J. N., & Guillon, G., 2023. Temperature and density dependence of line profiles of sodium perturbed by helium, *A&A*, **674**, A171.

Allard, N. F., Kielkopf, J. F., Myneni, K., & Blakely, J. N., 2024. New theoretical study of potassium perturbed by He and a comparison to laboratory spectra, *A&A*, **683**, A188.

Alrefae, M., Es-sebbar, E.-t., & Farooq, A., 2014. Absorption cross-section measurements of methane, ethane, ethylene and methanol at high temperatures, *J. Mol. Spectrosc.*, **303**, 8–14.

AlSaif, B., Lamperti, M., Gatti, D., Laporta, P., Fermann, M., Farooq, A., Lyulin, O., Campargue, A., & Marangoni, M., 2018. High accuracy line positions of the ν_1 fundamental band of $^{14}N_2{}^{16}O$, *J. Quant. Spectrosc. Radiat. Transf.*, **211**, 172–178.

Amaral, P. H. R., Diniz, L. G., Jones, K. A., Stanke, M., Alijah, A., Adamowicz, L., & Mohallem, J. R., 2019. Benchmark Rovibrational Linelists and Einstein A-coefficients for the Primordial Molecules and Isotopologues, *ApJ*, **878**, 95.

Anderson, P. W., 1949. Pressure broadening in the microwave and infra-red regions, *Phys. Rev.*, **76**, 647–662.

Andrieu, F., Doute, S., Schmidt, F., & Schmitt, B., 2015. Radiative transfer model for contaminated rough slabs, *Applied Optics*, **54**, 9228.

Anisman, L. O., Chubb, K. L., Changeat, Q., Edwards, B., Yurchenko, S. N., Tennyson, J., & Tinetti, G., 2022a. Cross-sections for heavy atmospheres: H_2O self-broadening, *J. Quant. Spectrosc. Radiat. Transf.*, **283**, 108146.

Anisman, L. O., Chubb, K. L., Elsey, J., Al-Refaie, A., Changeat, Q., Yurchenko, S. N., Tennyson, J., & Tinetti, G., 2022b. Cross-sections for heavy atmospheres: H_2O continuum, *J. Quant. Spectrosc. Radiat. Transf.*, **278**, 108013.

Antony, B. K., Gamache, P. R., Szembek, C. D., Niles, D. L., & Gamache, R. R., 2006. Modified complex robert–bonamy formalism calculations for strong to weak interacting systems, *Mol. Phys.*, **104**, 2791–2799.

Arcangeli, J., Désert, J.-M., Line, M. R., Bean, J. L., Parmentier, V., Stevenson, K. B., Kreidberg, L., Fortney, J. J., Mansfield, M., & Showman, A. P., 2018. H- opacity and water dissociation in the dayside atmosphere of the very hot gas giant WASP-18b, *ApJL*, **855**, L30.

Arfaux, A. & Lavvas, P., 2024. Coupling haze and cloud microphysics in WASP-39b's atmosphere based on JWST observations, *MNRAS*, p. stae826.

Aringer, B., Girardi, L., Nowotny, W., Marigo, P., & Lederer, M. T., 2009. Synthetic photometry for carbon rich giants* - I. Hydrostatic dust-free models, *A&A*, **503**, 913–928.

Armstrong, B., 1967. Spectrum line profiles: The Voigt function, *J. Quant. Spectrosc. Radiat. Transf.*, **7**, 61–88.

Atkinson, R., Baulch, D. L., Cox, R. A., Crowley, J. N., Hampson, R. F., Hynes, R. G., Jenkin, M. E., Rossi, M. J., & Troe, J., 2004. Evaluated kinetic and photochemical data for atmospheric chemistry: Volume I - gas phase reactions of O_x, HO_x, NO_x and SO_x species, *Atmos. Chem. Phys.*, **4**, 1461–1738.

Atkinson, R., Baulch, D. L., Cox, R. A., Crowley, J. N., Hampson, R. F., Hynes, R. G., Jenkin, M. E., Rossi, M. J., Troe, J., & Subcommittee, I., 2006. Evaluated kinetic and photochemical data for atmospheric chemistry: Volume II - gas phase reactions of organic species, *Atmos. Chem. Phys.*, **6**, 3625–4055.

Atkinson, R., Baulch, D. L., Cox, R. A., Crowley, J. N., Hampson, R. F., Hynes, R. G., Jenkin, M. E., Rossi, M. J., & Troe, J., 2007. Evaluated kinetic and photochemical data for atmospheric chemistry: Volume III - gas phase reactions of inorganic halogens, *Atmos. Chem. Phys.*, **7**, 981–1191.

Atreya, S. K. & Gu, Z. G., 1994. Stability of the Martian atmosphere: Is heterogeneous catalysis essential?, *J. Geophys. Res.*, **99**, 13133–13146.

Azzam, A. A. A., Yurchenko, S. N., Tennyson, J., & Naumenko, O. V., 2016. ExoMol line lists XVI: A Hot Line List for H_2S, *MNRAS*, **460**, 4063–4074.

Ba, Y. A., Wenger, C., Surleau, R., Boudon, V., Rotger, M., Daumont, L., Bonhommeau, D. A., Tyuterev, V. G., & Dubernet, M.-L., 2013. MeCaSDa and ECaSDa: Methane and ethene calculated spectroscopic databases for the virtual atomic and molecular data centre, *J. Quant. Spectrosc. Radiat. Transf.*, **130**, 62–68, HITRAN2012 special issue.

Bailey, J. & Kedziora-Chudczer, L., 2012. Modelling the spectra of planets, brown dwarfs and stars using VSTAR, *MNRAS*, **419**, 1913–1929.

Bains, W., Petkowski, J. J., Seager, S., Ranjan, S., Sousa-Silva, C., Rimmer, P. B., Zhan, Z., Greaves, J. S., & Richards, A. M. S., 2021. Phosphine on Venus cannot be explained by conventional processes, *Astrobiology*, **21**, 1277–1304.

Balashov, A. A., Bielska, K., Li, G., Kyuberis, A. A., Wójtewicz, S., Domysławska, J., Ciuryło, R., Zobov, N. F., Lisak, D., Tennyson, J., & Polyansky, O. L., 2023. Measurement and calculation of CO (7–0) overtone line intensities, *J. Chem. Phys.*, **158**, 234306.

Baldacchini, G., D'Amato, F., Buffa, G., Tarrini, O., De Rosa, M., & Pelagalli, F., 2001. Temperature dependence of foreign gas broadening and shift of the aQ(9, 9) transition line of ammonia, *J. Quant. Spectrosc. Radiat. Transf.*, **68**, 625–633.

Baranger, M., 1958a. General impact theory of pressure broadening, *Phys. Rev.*, **112**, 855–865.

Baranger, M., 1958b. Simplified Quantum-Mechanical Theory of Pressure Broadening, *Phys. Rev.*, **111**, 481–493.

Baranger, M., 1958c. Problem of Overlapping Lines in the Theory of Pressure Broadening, *Phys. Rev.*, **111**, 494–504.

Baranov, Y., Lafferty, W., & Fraser, G., 2005. Investigation of collision-induced absorption in the vibrational fundamental bands of O_2 and N_2 at elevated temperatures, *J. Mol. Spectrosc.*, **233**, 160–163.

Baranov, Y. I., 2018. Collision-induced absorption in the region of the ν_2+ν_3 band of carbon dioxide, *J. Mol. Spectrosc.*, **345**, 11–16.

Baranov, Y. I. & Vigasin, A. A., 1999. Collision-induced absorption by CO_2 in the region of ν_1, $2\nu_2$, *J. Mol. Spectrosc.*, **193**, 319–325.

Baranov, Y. I., Lafferty, W. J., & Fraser, G. T., 2004. Infrared spectrum of the continuum and dimer absorption in the vicinity of the O_2 vibrational fundamental in O_2/CO_2 mixtures, *J. Mol. Spectrosc.*, **228**, 432–440.

Baranov, Y. I., Lafferty, W. J., Ma, Q., & Tipping, R. H., 2008. Water-vapor continuum absorption in the 800-1250cm^{-1} spectral region at temperatures from 311 to 363 K, *J. Quant. Spectrosc. Radiat. Transfer*, **109**, 2291–2302.

Barber, R. J., Strange, J. K., Hill, C., Polyansky, O. L., Mellau, G. C., Yurchenko, S. N., & Tennyson, J., 2014. ExoMol line lists – III. An improved hot rotation-vibration line list for HCN and HNC, *MNRAS*, **437**, 1828–1835.

Barklem, P. S. & Collet, R., 2016. Partition functions and equilibrium constants for diatomic molecules and atoms of astrophysical interest, *A&A*, **588**, A96.

Barrado, D., Mollière, P., Patapis, P., et al., 2023. $^{15}NH_3$ in the atmosphere of a cool brown dwarf, *Nature*, **624**, 263–266.

Barrientos, J. G., MacDonald, R. J., Lewis, N. K., & Kaltenegger, L., 2023. In search of the edge: A Bayesian exploration of the detectability of red edges in exoplanet reflection spectra, *ApJ*, **946**, 96.

Barshay, S. S. & Lewis, J. S., 1976. Chemistry of primitive solar material, *Annu. Rev. Astron. Astrophys.*, **14**, 81–94.

Barstow, J. K., Changeat, Q., Garland, R., Line, M. R., Rocchetto, M., & Waldmann, I. P., 2020. A comparison of exoplanet spectroscopic retrieval tools, *MNRAS*, **493**, 4884–4909.

Barstow, J. K., Changeat, Q., Chubb, K. L., Cubillos, P. E., Edwards, B., MacDonald, R. J., Min, M., & Waldmann, I. P., 2022. A retrieval challenge exercise for the Ariel mission, *Exp. Astron.*, **53**, 447–471.

Barth, E. L., 2017. Modeling survey of ices in Titan's stratosphere, *Planet Space Sci.*, **137**, 20–31.

Barton, E. J., Yurchenko, S. N., & Tennyson, J., 2013. ExoMol Molecular linelists – II. The ro-vibrational spectrum of SiO, *MNRAS*, **434**, 1469–1475.

Barton, E. J., Chiu, C., Golpayegani, S., Yurchenko, S. N., Tennyson, J., Frohman, D. J., & Bernath, P. F., 2014. ExoMol Molecular linelists – V. The ro-vibrational spectra of NaCl and KCl, *MNRAS*, **442**, 1821–1829.

Barton, E. J., Yurchenko, S. N., Tennyson, J., Clausen, S., & Fateev, A., 2015. High-resolution absorption measurements of NH_3 at high temperatures: 500-2100 cm^{-1}, *J. Quant. Spectrosc. Radiat. Transf.*, **167**, 126–134.

Barton, E. J., Hill, C., Czurylo, M., Li, H. Y., Hyslop, A., Yurchenko, S. N., & Tennyson, J., 2017. The ExoMol pressure broadening diet: H_2 and He line-broadening parameters, *J. Quant. Spectrosc. Radiat. Transf.*, **203**, 490–495.

Bar-Ziv, E. & Weiss, S., 1972. Translational Spectra Due to Collision-Induced Overlap Moments in Mixtures of He with CO_2, N_2, CH_4, and C_2H_6, *J. Phys. Chem.*, **57**, 34–37.

Batalha, N., Rooney, C., & MacDonald, R., 2021. natasha-batalha/picaso: Release 2.2 (v2.2.0), 10.5281/zenodo.5093710, *Zenodo*.

Batalha, N., Lewis, N., Chubb, K., Freedman, R., Gharib-nezhad, E., Gordon, I., Hargreaves, R., MacDonald, R., Sousa-Silva, C., Tennyson, J., Valenti, J., & Yurchenko, S., 2022. MAESTRO: Building access and community standards for opacity data at the onset of next-generation atmosphere observations, in *Bulletin of the American Astronomical Society*, vol. 54, p. 102.371.

Baudino, J.-L., Bézard, B., Boccaletti, A., Bonnefoy, M., Lagrange, A.-M., & Galicher, R., 2015. Interpreting the photometry and spectroscopy of directly imaged planets: a new atmospheric model applied to beta pictoris b and SPHERE observations, *A&A*, **582**, A83.

Baumann, E., Giorgetta, F. R., Swann, W. C., Zolot, A. M., Coddington, I., & Newbury, N. R., 2011. Spectroscopy of the methane ν_3 band with an accurate midinfrared coherent dual-comb spectrometer, *Phys. Rev. A*, **84**, 062513.

Bauschlicher, C. W., Ricca, A., Boersma, C., & Allamandola, L. J., 2018. The NASA Ames PAH IR Spectroscopic Database: Computational Version 3.00 with Updated Content and the Introduction of Multiple Scaling Factors, *ApJS*, **234**, 32.

Beale, C. A., Hargreaves, R. J., & Bernath, P. F., 2016. Temperature-dependent high resolution absorption cross sections of propane, *J. Quant. Spectrosc. Radiat. Transf.*, **182**, 219–224.

Beale, C. A., Hargreaves, R. J., Coles, P., Tennyson, J., & Bernath, P. F., 2017. Infrared absorption spectra of hot ammonia, *J. Quant. Spectrosc. Radiat. Transf.*, **203**, 410–416.

Begemann, B., Dorschner, J., Henning, T., Mutschke, H., Gürtler, J., Kömpe, C., & Nass, R., 1997. Aluminum oxide and the opacity of oxygen-rich circumstellar dust in the 12-17 micron range, *ApJ*, **476**, 199.

Bell, T. J., Crouzet, N., Cubillo, P. E., Kreidberg, L., et al., 2024. Nightside clouds and disequilibrium chemistry on the hot Jupiter WASP-43b, *Nature Astronomy*, **8**, 879–898.

Benneke, B., Roy, P.-A., Coulombe, L.-P., Radica, M., et al., 2024. JWST reveals CH_4, CO_2, and H_2O in a metal-rich miscible atmosphere on a two-Earth-radius exoplanet.

Bergeron, P., Saumon, D., & Wesemael, F., 1995. New Model Atmospheres for Very Cool White Dwarfs with Mixed H/He and Pure He Compositions, *ApJ*, **443**, 764–779.

Berman, P. R., 1972. Speed-dependent collisional width and shift parameters in spectral profiles, *J. Quant. Spectrosc. Radiat. Transf.*, **12**, 1331–1342.

Bernath, P. & Fernando, A. M., 2021. Infrared absorption cross sections for hot isobutane in the CH stretching region, *J. Quant. Spectrosc. Radiat. Transf.*, **269**, 107644.

Bernath, P. F., 2020. MoLLIST: Molecular Line Lists, Intensities and Spectra, *J. Quant. Spectrosc. Radiat. Transf.*, **240**, 106687.

Bernath, P. F. & Colin, R., 2009. Revised molecular constants and term values for the X $^2\Pi$ and B$^2\Sigma^+$ states of OH, *J. Mol. Spectrosc.*, **257**, 20–23.

Bernath, P. F., Dodangodage, R., & Liévin, J., 2022. S-type Stars: LaO Line List for the B $^2\Sigma^+$ - X $^2\Sigma^+$ Band System, *J. Mol. Spectrosc.*, **933**, 99.

Bernath, P. F., Dodangodage, R., Zhao, J., & Billinghurst, B., 2023. Infrared absorption cross sections for propene broadened by N_2 (450-1250 cm^{-1}) and by H_2 (2680-3220 cm^{-1}), *J. Quant. Spectrosc. Radiat. Transf.*, **296**, 108462.

Berné, O., Foschino, S., Jalabert, F., & Joblin, C., 2022. Contribution of polycyclic aromatic hydrocarbon ionization to neutral gas heating in galaxies: model versus observations*, *A&A*, **667**, A159.

Bézard, B., Fedorova, A., Bertaux, J.-L., Rodin, A., & Korablev, O., 2011. The 1.10- and 1.18-μm nightside windows of Venus observed by SPICAV-IR aboard Venus Express, *Icarus*, **216**, 173–183.

Bharadwaj, S. P. & Modest, M. F., 2007. Medium resolution transmission measurements of CO_2 at high temperature—an update, *J. Quant. Spectrosc. Radiat. Transf.*, **103**, 146–155.

Biermann, U. M., Luo, B. P., & Peter, T., 2000. Absorption Spectra and Optical Constants of Binary and Ternary Solutions of H_2SO_4, HNO_3, and H_2O in the Mid Infrared at Atmospheric Temperatures, *J. Phys. Chem. A*, **104**, 783–793.

Bilger, C., Rimmer, P., & Helling, C., 2013. Small hydrocarbon molecules in cloud-forming brown dwarf and giant gas planet atmospheres, *MNRAS*, **435**, 1888–1903.

Bittner, D. M. & Bernath, P. F., 2018. Line Lists for LiF and LiCl in the X $^1\Sigma^+$ Ground State, *ApJS*, **235**, 8.

Blake, D. R., Chen, T.-Y., Smith Jr., T. W., Wang, C. J.-L., Wingenter, O. W., Blake, N. J., Rowland, F. S., & Mayer, E. W., 1996. Three-dimensional distribution of nonmenthane hydrocarbons and halocarbons over the northwestern Pacific during the 1991 Pacific Exploratory Mission (PEM-West A), *JGR-Atm*, **101**, 1763–1778.

Boersma, C., Bauschlicher, C. W., Ricca, A., Mattioda, A. L., Cami, J., Peeters, E., de Armas, F. S., Saborido, G. P., Hudgins, D. M., & Allamandola, L. J., 2014. The NASA Ames PAH IR spectroscopic database version 2.00: updated content, web site, and on(off)line tools, *ApJS*, **211**, 8.

Boone, C., Walker, K., & Bernath, P., 2007. Speed-dependent Voigt profile for water vapor in infrared remote sensing applications, *J. Quant. Spectrosc. Radiat. Transf.*, **105**, 525–532.

Bordet, B., Kassi, S., & Campargue, A., 2021. Line parameters of the 4-0 band of carbon monoxide by high sensitivity cavity ring down spectroscopy near 1.2 μm, *J. Quant. Spectrosc. Radiat. Transf.*, **260**, 107453.

Borysow, A., 2002. Collision-induced absorption coefficients of H_2 pairs at temperatures from 60 K to 1000 K, *A&A*, **390**, 779–782.

Borysow, A. & Frommhold, L., 1986a. Theoretical Collision-induced Rototranslational Absorption Spectra for the Outer Planets: H_2-CH_4 Pairs, *ApJ*, **304**, 849.

Borysow, A. & Frommhold, L., 1986b. Theoretical Collision-induced Rototranslational Absorption Spectra for Modeling Titan's Atmosphere: H_2–N_2 Pairs, *ApJ*, **303**, 495.

Borysow, A. & Frommhold, L., 1987. Collision-induced Rototranslational Absorption Spectra of CH_4-CH_4 Pairs at Temperatures from 50 to 300 K, *ApJ*, **318**, 940.

Borysow, A. & Tang, C., 1993. Collision Induced Absorption of N_2-CH_4 for Modeling Titan's Atmosphere, in *AAS/Division for Planetary Sciences Meeting Abstracts #25*, vol. 25, p. 25.12.

Borysow, A., Moraldi, M., & Frommhold, L., 1984. Modelling of collision-induced absorption spectra, *J. Quant. Spectrosc. Radiat. Transf.*, **31**, 235–245.

Botet, R., Rannou, P., & Cabane, M., 1997. Mean-field approximation of Mie scattering by fractal aggregates of identical spheres, *Appl. Opt.*, **36**, 8791–8797.

Boudon, V., Champion, J.-P., Gabard, T., Loëte, M., Rotger, M., & Wenger, C., 2011. Spherical top theory and molecular spectra, in *Handbook of High-Resolution Spectroscopy*, vol. 3, pp. 1437–1460, eds Quack, M. & Merkt, F., Wiley, Chichester, West Sussex, United Kingdom.

Bounaceur, R., Herbinet, O., Fournet, R., Glaude, P.-A., Battin-Leclerc, F., Pires da Cruz, A., Yahyaoui, M., Truffin, K., & Moreac, G., 2010. Modeling the Laminar Flame Speed of Natural Gas and Gasoline Surrogates, in *SAE 2010 World Congress & Exhibition*, SAE International.

Bourgalais, J., Carrasco, N., Changeat, Q., Venot, O., Javanović, L., Pernot, P., Tennyson, J., Chubb, K. L., Yurchenko, S. N., & Tinetti, G., 2020. Ions in the thermosphere of exoplanets: Observational constraints revealed by innovative laboratory experiments, *ApJ*, **895**, 77.

Bowesman, C. A., Shuai, M., Yurchenko, S. N., & Tennyson, J., 2021. A high resolution line list for AlO, *MNRAS*, **508**, 3181–3193.

Bowesman, C. A., Akbari, H., Hopkins, S., Yurchenko, S. N., & Tennyson, J., 2022. Fine and hyperfine resolved empirical energy levels for VO, *J. Quant. Spectrosc. Radiat. Transf.*, **289**, 108295.

Bowesman, C. A., Mizus, I. I., Zobov, N. F., Polyansky, O. L., Sarka, J., Poirier, B., Pezzella, M., Yurchenko, S. N., & Tennyson, J., 2023. ExoMol line lists - L: High-resolution line lists of H_3^+, H_2D^+, D_2H^+ and D_3^+, *MNRAS*, **519**, 6333–6348.

Bowesman, C. A., Qu, Q., McKemmish, L. K., Yurchenko, S. N., & Tennyson, J., 2024. ExoMol line lists – LV: Hyperfine-resolved molecular line list for vanadium monoxide ($^{51}V^{16}O$), *MNRAS*, **529**, 1321–1332.

Brady, R. P., Yurchenko, S. N., Tennyson, J., & Kim, G.-S., 2024. ExoMol line lists – LVI. The SO line list, MARVEL analysis of experimental transition data and refinement of the spectroscopic model, *MNRAS*, **527**, 6675–6690.

Brassé, C., Muñoz, O., Coll, P., & Raulin, F., 2015. Optical constants of Titan aerosols and their tholins analogs: Experimental results and modeling/observational data, *Planet Space Sci.*, **109-110**, 159–174.

Brogi, M. & Line, M. R., 2019. Retrieving Temperatures and Abundances of Exoplanet Atmospheres with High-resolution Cross-correlation Spectroscopy, *ApJ*, **157**, 114.

Bromley, S. T., Gómez Martín, J. C., & Plane, J. M. C., 2016. Under what conditions does SiO_N nucleation occur? A bottom-up kinetic modelling evaluation, *Phys. Chem. Chem. Phys.*, **18**, 26913–26922.

Bromm, V. & Larson, R. B., 2004. The First Stars, *ARA&A*, **42**, 79–118.

Bromm, V., Yoshida, N., Hernquist, L., & McKee, C. F., 2009. The formation of the first stars and galaxies, *Nature*, **459**, 49–54.

Brooke, J. S. A., Bernath, P. F., Schmidt, T. W., & Bacskay, G. B., 2013. Line strengths and updated molecular constants for the C_2 Swan system, *J. Quant. Spectrosc. Radiat. Transf.*, **124**, 11 – 20.

Brooke, J. S. A., Bernath, P. F., Western, C. M., Sneden, C., Afsar, M., Li, G., & Gordon, I. E., 2016. Line strengths of rovibrational and rotational transitions in the $X\ ^2\Pi$ ground state of OH, *J. Quant. Spectrosc. Radiat. Transf.*, **168**, 142–157.

Buck, A. L., 1981. New Equations for Computing Vapor Pressure and Enhancement Factor, *J. Appl. Meteorol. Clim.*, **20**, 1527 – 1532.

Buehler, S. A., Brath, M., Lemke, O., Hodnebrog, Ø., Pincus, R., Eriksson, P., Gordon, I., & Larsson, R., 2022. A new halocarbon absorption model based on HITRAN cross-section data and new estimates of halocarbon instantaneous clear-sky radiative forcing, *J. Adv. Model. Earth Syst.*, **14**, e2022MS003239.

Bui, T. Q., Changala, P. B., Bjork, B. J., Yu, Q., Wang, Y., Stanton, J. F., Bowman, J., & Ye, J., 2018. Spectral analyses of trans- and cis-DOCO transients via comb spectroscopy, *Mol. Phys.*, **116**, 3710–3717.

Buldyreva, J. & Daneshvar, L., 2013. Extension of the non-markovian energy-corrected sudden model to the case of parallel and perpendicular infrared bands, *J. Chem. Phys.*, **139**, 164107.

Buldyreva, J., Bonamy, J., & Robert, D., 1999. Semiclassical calculations with exact trajectory for N_2 rovibrational Raman linewidths at temperatures below 300 K, *J. Quant. Spectrosc. Radiat. Transf.*, **62**, 321–343.

Buldyreva, J., Yurchenko, S. N., & Tennyson, J., 2022. Simple semiclassical model of pressure-broadened infrared/microwave linewidths in the temperature range 200–3000 K, *RASTI*, **1**, 43–47.

Buldyreva, J., Brady, R. P., & Yurchenko, S. N.and Tennyson, J., 2024a. Collisional broadening of molecular rovibronic lines, *J. Quant. Spectrosc. Radiat. Transf.*, **313**, 108843.

Buldyreva, J., Stehlin, K., Yurchenko, S. N., Guest, E. R., & Tennyson, J., 2024b. Semi-classical estimates of pressure-induced linewidths for infrared absorption by hot (exo)planetary atmospheres, *ApJS*.

Buldyreva, J. V., Gennadiev, N. A., & Filippov, N. N., 2013. Line-mixing in absorption bands of linear molecules diluted in high-density rare gases: Measurements and modeling for OCS-He, *J. Chem. Phys.*, **138**, 164117.

Burcat, A., Ruscic, B., Chemistry, & of Tech., T. I. I., 2005. Third millenium ideal gas and condensed phase thermochemical database for combustion (with update from active thermochemical tables), Tech. rep., Argonne National Lab. (ANL), Argonne, IL (United States).

Burgasser, A. J., Burrows, A., & Kirkpatrick, J. D., 2006. A Method for Determining the Physical Properties of the Coldest Known Brown Dwarfs, *ApJ*, **639**, 1095–1113.

Burke, U., Metcalfe, W. K., Burke, S. M., Heufer, K. A., Dagaut, P., & Curran, H. J., 2016. A Detailed Chemical Kinetic Modeling, Ignition Delay Time and Jet-Stirred Reactor Study of Methanol Oxidation, *Combust. Flame*, **165**, 125–136.

Burkholder, J., Sander, S., Abbatt, J., Barker, J., Cappa, C., Crounse, J., Dibble, T., Huie, R., Kolb, C., Kurylo, M., et al., 2020. Chemical kinetics and photochemical data for use in atmospheric studies; evaluation number 19, Tech. rep., Jet Propulsion Laboratory, Pasadena.

Burrows, A. & Volobuyev, M., 2003. Calculations of the far-wing line profiles of sodium and potassium in the atmospheres of substellar-mass objects, *ApJ*, **583**, 985–995.

Burrows, A., Dulick, M., Bauschlicher, C. W., Bernath, P. F., Ram, R. S., Sharp, C. M., & Milsom, J. A., 2005. Spectroscopic

constants, abundances, and opacities of the tih molecule, *ApJ*, **624**, 988–1002.

Bykov, A. D., Lavrentieva, N. N., & Sinitsa, L. N., 2004. Semi-empiric approach to the calculation of H_2O and CO_2 line broadening and shifting, *Mol. Phys.*, **102**, 1653–1658.

Cameron, W. D. & Bernath, P., 2022. Visible opacity of M Dwarfs and hot Jupiters: The TiO B $^3\Pi$-X $^3\Delta$ band system, *ApJ*, **926**, 39.

Campargue, A., Karlovets, E. V., Vasilchenko, S. S., & Turbet, M., 2023. The high resolution absorption spectrum of methane in the 10 800 - 14 000 cm^{-1} region: literature review, new results and perspectives, *Phys. Chem. Chem. Phys.*, **25**, 32778–32799.

Campbell, J. M., Klapstein, D., Dulick, M., Bernath, P. F., & Wallace, L., 1995. Infrared Absorption and Emission Spectra of SiO, *ApJS*, **101**, 237.

Castelli, F. & Kurucz, R. L., 2004. New grids of ATLAS9 model atmospheres, *arXiv*.

Cathonnet, M., Boettner, J. C., & James, H., 1982. Etude de l'oxydation et de l'auto-inflammation du méthanol dans le domaine de températures 500-600° C, *J. Chim. Phys.*, **79**, 475–478.

Catling, D. C. & Kasting, J. F., 2017. *Atmospheric Evolution on Inhabited and Lifeless Worlds*, Cambridge University Press, Cambridge, UK.

Cavalié, T., Rezac, L., Moreno, R., Lellouch, E., Fouchet, T., Benmahi, B., Greathouse, T. K., Sinclair, J. A., Hue, V., Hartogh, P., Dobrijevic, M., Carrasco, N., & Perrin, Z., 2023. Evidence for auroral influence on Jupiter's nitrogen and oxygen chemistry revealed by ALMA, *Nature Astronomy*, **7**, 1048–1055.

Cerezo, M., Arrasmith, A., Babbush, R., Benjamin, S. C., Endo, S., Fujii, K., McClean, J. R., Mitarai, K., Yuan, X., Cincio, L., & Coles, P. J., 2020. Variational Quantum Algorithms, *arXiv e-prints*, p. arXiv:2012.09265.

Chakraborty, S., Yurchenko, S. N., Georges, R., Simon, A., et al., 2024. Laboratory investigation of shock-induced dissociation of buckminsterfullerene and astrophysical insights, *A&A*, **681**, A39.

Chang, C., Patzer, A. B. C., Kegel, W. H., & Chandra, S., 2013. Small Fe bearing ring molecules of possible astrophysical interest: molecular properties and rotational spectra, *Astrophys. Space Sci.*, **347**, 315–325.

Chang, Y., Yang, J., Chen, Z., Zhang, Z., Yu, Y., Li, Q., He, Z., Zhang, W., Wu, G., Ingle, R. A., Bain, M., Ashfold, M. N. R., Yuan, K., Yang, X., & Hansen, C. S., 2020. Ultraviolet photochemistry of ethane: implications for the atmospheric chemistry of the gas giants, *Chem. Sci.*, **11**, 5089–5097.

Chang, Y., Ashfold, M. N. R., Yuan, K., & Yang, X., 2023. Exploring the vacuum ultraviolet photochemistry of astrochemically important triatomic molecules, *Natl. Sci. Rev.*, **10**, nwad158.

Changala, P. B., Spaun, B., Patterson, D., Doyle, J. M., & Ye, J., 2016. Sensitivity and resolution in frequency comb spectroscopy of buffer gas cooled polyatomic molecules, *Appl. Phys. B*, **122**, 292.

Changala, P. B., Weichman, M. L., Lee, K. F., Fermann, M. E., & Ye, J., 2019. Rovibrational quantum state resolution of the C_{60} fullerene, *Science*, **363**, 49–54.

Changeat, Q. & Yip, K. H., 2023. ESA-Ariel Data Challenge NeurIPS 2022: Introduction to exo-atmospheric studies and presentation of the Atmospheric Big Challenge (ABC) Database, *RASTI*, **2**, 45–61.

Changeat, Q., Edwards, B., Al-Refaie, A. F., Tsiaras, A., Skinner, J. W., Cho, J. Y. K., Yip, K. H., Anisman, L., Ikoma, M., Bieger, M. F., Venot, O., Shibata, S., Waldmann, I. P., & Tinetti, G., 2022. Five key exoplanet questions answered via the analysis of 25 hot-jupiter atmospheres in eclipse, *ApJS*, **260**, 3.

Changeat, Q., Skinner, J. W., Cho, J. Y.-K., Nättilä, J., Waldmann, I. P., Al-Refaie, A. F., Dyrek, A., Edwards, B., Mikal-Evans, T., Joshua, M., Morello, G., Skaf, N., Tsiaras, A., Venot, O., & Yip, K. H., 2024. Is the atmosphere of the ultra-hot Jupiter WASP-121 b variable?, *ApJS*, **270**, 34.

Charnay, B., Blain, D., Bézard, B., Leconte, J., Turbet, M., & Falco, A., 2021. Formation and dynamics of water clouds on temperate sub-Neptunes: the example of K2-18b, *A&A*, **646**, A171.

Chase, M., 1998. *NIST-JANAF Thermochemical Tables, 4th Edition*, American Institute of Physics.

Chen, J., Hua, T. P., Tao, L. G., Sun, Y. R., Liu, A. W., & Hu, S. M., 2018. Absolute frequencies of water lines near 790 nm with 10^{-11} accuracy, *J. Quant. Spectrosc. Radiat. Transf.*, **205**, 91–95.

Chen, M., Felmy, A. R., & Dixon, D. A., 2014. Structures and Stabilities of $(MgO)_n$ Nanoclusters, *J. Phys. Chem. A*, **118**, 3136–3146.

Chistikov, D. N., Finenko, A. A., Lokshtanov, S. E., Petrov, S. V., & Vigasin, A. A., 2019. Simulation of collision-induced absorption spectra based on classical trajectories and ab initio potential and induced dipole surfaces. I. Case study of N_2-N_2 rototranslational band, *J. Phys. Chem.*, **151**, 194106.

Cho, J. Y.-K., Skinner, J. W., & Thrastarson, H. T., 2021. Storms, variability, and multiple equilibria on hot jupiters, *ApJL*, **913**, L32.

Chowdhury, M. R., Garcia, G. A., Hrodmarsson, H. R., Loison, J.-C., & Nahon, L., 2024. Photoionization of nitrile-substituted naphthalene and benzene: Cation spectroscopy, photostability, and implications for photoelectric gas heating, *ApJ*, **963**, 29.

Chowdhury, P. K., Merer, A. J., Rixon, S. J., Bernath, P. F., & Ram, R. S., 2006. Low-N lines of the A $^6\Sigma^+$ - X $^6\Sigma^+$ (1,0) band of CrH, *Phys. Chem. Chem. Phys.*, **8**, 822–826.

Chubb, K. L., Joseph, M., Franklin, J., Choudhury, N., Furtenbacher, T., Császár, A. G., Gaspard, G., Oguoko, P., Kelly, A., Yurchenko, S. N., Tennyson, J., & Sousa-Silva, C., 2018a. MARVEL analysis of the measured high-resolution spectra of C_2H_2, *J. Quant. Spectrosc. Radiat. Transf.*, **204**, 42–55.

Chubb, K. L., Naumenko, O., Keely, S., Bartolotto, S., Macdonald, S., Mukhtar, M., Grachov, A., White, J., Coleman, E., Liu, A., Fazliev, A. Z., Polovtseva, E. R., Horneman, V.-M., Campargue, A., Furtenbacher, T., Császár, A. G., Yurchenko, S. N., & Tennyson, J., 2018b. MARVEL analysis of the measured high-resolution rovibrational spectra of $H_2^{32}S$, *J. Quant. Spectrosc. Radiat. Transf.*, **218**, 178 – 186.

Chubb, K. L., Rocchetto, M., Yurchenko, S. N., Min, M., Waldmann, I., Barstow, J. K., Molliére, P., Al-Refaie, A. F., Phillips, M., & Tennyson, J., 2020a. The ExoMolOP Database: Cross-sections and k-tables for Molecules of Interest in High-Temperature Exoplanet Atmospheres, *A&A*, **646**, A21.

Chubb, K. L., Tennyson, J., & Yurchenko, S. N., 2020b. ExoMol Molecular linelists – XXXVII: spectra of acetylene, *MNRAS*, **493**, 1531–1545.

Chubb, K. L., Stam, D. M., Helling, C., Samra, D., & Carone, L., 2023. Modelling reflected polarized light from close-in giant exoplanet WASP-96b using PolHEx (Polarization of hot exoplanets), *MNRAS*, **527**, 4955–4982.

Civiš, S., Pastorek, A., Ferus, M., Yurchenko, S. N., & Boudjema, N.-I., 2023. Infrared spectra of small radicals for exoplanetary spectroscopy: OH, NH, CN and CH: The state of current knowledge, *Molecules*, **28**, 3362.

Clark, V. H. J., Owens, A., Tennyson, J., & Yurchenko, S. N., 2020. The high-temperature rotation-vibration spectrum and rotational clustering of silylene (SiH_2), *J. Quant. Spectrosc. Radiat. Transf.*, **246**, 106929.

Cloutis, E. A., 2015. Mineral and rock sample database planetary spectrohotometer facility (PSF), Tech. rep., University of Winnipeg.

Coddington, I., Newbury, N., & Swann, W., 2016. Dual-comb spectroscopy, *Optica*, **3**, 414–426.

Coheur, P.-F., Bernath, P. F., Carleer, M., Colin, R., Polyansky, O. L., Zobov, N. F., Shirin, S. V., Barber, R. J., & Tennyson, J., 2005. A 3000 K laboratory emission spectrum of water, *J. Chem. Phys.*, **122**, 074307–074307.

Cole, R. K., Tran, H., Hoghooghi, N., & Rieker, G. B., 2023. Temperature-dependent CO_2 line mixing models using dual fre-

quency comb absorption and phase spectroscopy up to 25 bar and 1000 K, *J. Quant. Spectrosc. Radiat. Transf.*, **297**, 108488.

Coles, P. A., Yurchenko, S. N., Kovacich, R. P., Hobby, J., & Tennyson, J., 2019a. A variationally computed room temperature line list for AsH_3, *Phys. Chem. Chem. Phys.*, **21**, 3264–3277.

Coles, P. A., Yurchenko, S. N., & Tennyson, J., 2019b. ExoMol molecular line lists XXXV: a rotation-vibration line list for hot ammonia, *MNRAS*, **490**, 4638–4647.

Colin, R. & Bernath, P. F., 2010. Revised molecular constants and term values for the X $^2\Pi$ state of CH, *J. Mol. Spectrosc.*, **263**, 120–122.

CollisionDB, 2024. Collisiondb: A database of plasma collisional processes, https://amdis.iaea.org/db/collisiondb/.

Conrath, B. J., Gierasch, P. J., & Ustinov, E. A., 1998. Thermal structure and para hydrogen fraction on the outer planets from Voyager IRIS measurements, *Icarus*, **135**, 501–517.

Coppola, C. M., Lodi, L., & Tennyson, J., 2011. Radiative cooling functions for primordial molecules, *MNRAS*, **415**, 487–493.

Cossel, K. C., Gresh, D. N., Sinclair, L. C., Coffey, T., Skripnikov, L. V., Petrov, A. N., Mosyagin, N. S., Titov, A. V., Field, R. W., Meyer, E. R., Cornell, E. A., & Ye, J., 2012. Broadband velocity modulation spectroscopy of HfF^+: Towards a measurement of the electron electric dipole moment, *Chem. Phys. Lett.*, **546**, 1–11.

Coxon, J. A. & Hajigeorgiou, P. G., 2015. Improved direct potential fit analyses for the ground electronic states of the hydrogen halides: HF/DF/TF, HCl/DCl/TCl, HBr/DBr/TBr and HI/DI/TI, *J. Quant. Spectrosc. Radiat. Transf.*, **151**, 133–154.

Crawford, M. F., Welsh, H. L., & Locke, J. L., 1949. Infra-Red Absorption of Oxygen and Nitrogen Induced by Intermolecular Forces, *Phys. Rev.*, **75**, 1607–1607.

Cristallo, S., Straniero, O., Lederer, M. T., & Aringer, B., 2007. Molecular opacities for low-mass metal-poor AGB stars undergoing the third dredge-up, *AJ.*, **667**, 489–496.

Cubillos, P. E. & Blecic, J., 2021. The Pyrat Bay framework for exoplanet atmospheric modelling: a population study of Hubble/WFC3 transmission spectra, *MNRAS*, **505**, 2675–2702.

Cui, W., , Zhang, J., Schmidt, F., Cui, D., Huang, X., Li, T., & Tian, F., 2018. Simultaneous characterization of the atmospheres, surfaces, and exomoons of nearby rocky exoplanets, *Earth and Planetary Physics*, **2**, 247–256.

Curtis, D. B., Hatch, C. D., Hasenkopf, C. A., Toon, O. B., Tolbert, M. A., McKay, C. P., & Khare, B. N., 2008. Laboratory studies of methane and ethane adsorption and nucleation onto organic particles: Application to Titan's clouds, *Icarus*, **195**, 792–801.

Cybulski, H., Bielski, A., Ciurylo, R., Szudy, J., & Trawinski, R., 2013. Power-law temperature dependence of collisional broadening and shift of atomic and molecular rovibronic lines, *J. Quant. Spectrosc. Radiat. Transf.*, **120**, 90–103.

Darby-Lewis, D., Tennyson, J., Lawson, K. D., Yurchenko, S. N., Stamp, M. F., Shaw, A., Brezinsek, S., & JET Contributor, 2018. Synthetic spectra of BeH, BeD and BeT for emission modelling in JET plasmas, *J. Phys. B: At. Mol. Opt. Phys.*, **51**, 185701.

De Lucia, F. C. & Green, S., 1988. Recent advances in pressure broadening: experiments and theory, *J. Mol. Struct.*, **190**, 435–446.

de Oliveira, N., Joyeux, D., Roudjane, M., Gil, J.-F., Pilette, B., Archer, L., Ito, K., & Nahon, L., 2016. The high-resolution absorption spectroscopy branch on the VUV beamline DESIRS at SOLEIL, *J. Synchrotron Radiat.*, **23**, 887–900.

de Regt, S., Kesseli, A. Y., Snellen, I. A. G., Merritt, S. R., & Chubb, K. L., 2022. A quantitative assessment of the VO line list: Inaccuracies hamper high-resolution VO detections in exoplanet atmospheres, *A&A*, **661**, A109.

de Vanssay, E., Gazeau, M. C., Guillemin, J. C., & Raulin, F., 1995. Experimental simulation of Titan's organic chemistry at low temperature, *Planet Space Sci.*, **43**, 25–31.

Deguine, A., Petitprez, D., Clarisse, L., Gułmundsson, S., Outes, V., Villarosa, G., & Herbin, H., 2020. Complex refractive index of volcanic ash aerosol in the infrared, visible, and ultraviolet, *Appl. Opt.*, **59**, 884–895.

Delahaye, T., Landsheere, X., Pangui, E., Huet, F., Hartmann, J. M., & Tran, H., 2016. Measurements of H_2O-broadening coefficients of O_2 A-band lines, *J. Quant. Spectrosc. Radiat. Transf.*, **184**, 316–321.

Delahaye, T., Armante, R., Scott, N. A., Jacquinet-Husson, N., et al., 2021. The 2020 edition of the GEISA spectroscopic database, *J. Mol. Spectrosc.*, **380**, 111510.

D'Eu, J.-F., Lemoine, B., & Rohart, F., 2002. Infrared HCN Lineshapes as a Test of Galatry and Speed-Dependent Voigt Profiles, *J. Mol. Spectrosc.*, **212**, 96–110.

Devi, V. M., Benner, D. C., Sung, K., Brown, L. R., Crawford, T. J., Yu, S., Smith, M. A. H., Mantz, A. W., Boudon, V., & Ismail, S., 2016. Spectral line parameters including line shapes in the $2\nu_3$ Q branch of $^{12}CH_4$, *J. Quant. Spectrosc. Radiat. Transf.*, **177**, 152–169.

DeWitt, H. L., Trainer, M. G., Pavlov, A. A., Hasenkopf, C. A., Aiken, A. C., Jimenez, J. L., McKay, C. P., Toon, O. B., & Tolbert, M. A., 2009. Reduction in haze formation rate on prebiotic earth in the presence of hydrogen, *Astrobiology*, **9**, 447–453.

Di Biagio, C., Formenti, P., Balkanski, Y., Caponi, L., Cazaunau, M., Pangui, E., Journet, E., Nowak, S., Andreae, M. O., Kandler, K., Saeed, T., Piketh, S., Seibert, D., Williams, E., & Doussin, J.-F., 2019. Complex refractive indices and single-scattering albedo of global dust aerosols in the shortwave spectrum and relationship to size and iron content, *Atmos. Chem. Phys.*, **19**, 15503–15531.

Ding, X.-L., Xue, W., Ma, Y.-P., Wang, Z.-C., & He, S.-G., 2009. Density functional study on cage and noncage $(Fe_2O_3)_n$ clusters, *J. Phys. Chem.*, **130**.

Ding, Y., Strand, C. L., & Hanson, R. K., 2019. High-temperature mid-infrared absorption spectra of methanol (CH_3OH) and ethanol (C_2H_5OH) between 930 and 1170 cm^{-1}, *J. Quant. Spectrosc. Radiat. Transf.*, **224**, 396–402.

Diouf, M. L., Tóbiás, R., Simkó, I., Cozijn, F. M. J., Salumbides, E. J., Ubachs, W., & Császár, A. G., 2021. Network-based design of near-infrared lamb-dip experiments and the determination of pure rotational energies of $H_2^{18}O$ at kHz accuracy, *J. Phys. Chem. Ref. Data*, **50**, 023106.

Diouf, M. L., Tóbiás, R., van der Schaaf, T. S., Cozijn, F. M. J., Salumbides, E. J., Császár, A. G., & Ubachs, W., 2022. Ultra-precise relative energies in the (2 0 0) vibrational band of $H_2^{16}O$, *Mol. Phys.*, **120**, e2050430.

Dobrijevic, M., Hébrard, E., Loison, J. C., & Hickson, K. M., 2014. Coupling of oxygen, nitrogen, and hydrocarbon species in the photochemistry of Titan's atmosphere, *Icarus*, **228**, 324–346.

Dobrijevic, M., Loison, J. C., Hickson, K. M., & Gronoff, G., 2016. 1D-coupled photochemical model of neutrals, cations and anions in the atmosphere of Titan, *Icarus*, **268**, 313–339.

Dodangodage, R., Bernath, P. F., Zhao, J., & Billinghurst, B., 2020. Absorption cross sections for ethane broadened by hydrogen and helium in the 3.3 micron region, *J. Quant. Spectrosc. Radiat. Transf.*, **253**, 107131.

Dominik, C., Min, M., & Tazaki, R., 2021. OpTool: Command-line driven tool for creating complex dust opacities, Astrophysics Source Code Library, record ascl:2104.010.

Domysławska, J., Wójtewicz, S., Masłowski, P., Bielska, K., Cygan, A., Słowi'nski, M., Trawiński, R. S., Ciuryło, R., & Lisak, D., 2020. Line-shape analysis for high *J* R-branch transitions of the oxygen B band, *J. Quant. Spectrosc. Radiat. Transf.*, **242**, 106789.

Dorschner, J., Begemann, B., Henning, T., Jaeger, C., & Mutschke, H., 1995. Steps toward interstellar silicate mineralogy. II. Study of Mg-Fe-silicate glasses of variable composition., *A&A*, **300**, 503.

Draine, B. T. & Flatau, P. J., 1994. Discrete-dipole approximation for scattering calculations, *J. Opt. Soc. Am. A*, **11**, 1491–1499.

Draine, B. T. & Li, A., 2007. Infrared emission from interstellar dust. IV. The silicate-graphite-PAH model in the post-spitzer

era, *ApJ*, **657**, 810.

Drant, T., Garcia-Caurel, E., Perrin, Z., Sciamma-O'Brien, E., Carrasco, N., Vettier, L., Gautier, T., Brubach, J.-B., Roy, P., Kitzmann, D., & Heng, K., 2024. Optical constants of exoplanet haze analogs from 0.3 to 30 μm: Comparative sensitivity between spectrophotometry and ellipsometry*, *A&A*, **682**, A6.

Drouin, B. J., Benner, D. C., Brown, L. R., Cich, M. J., et al., 2017. Multispectrum analysis of the oxygen A-band, *J. Quant. Spectrosc. Radiat. Transf.*, **186**, 118–138.

Dubey, D., Grübel, F., Arenales-Lope, R., Molaverdikhani, K., Ercolano, B., Rab, C., & Trapp, O., 2023. Polycyclic aromatic hydrocarbons in exoplanet atmospheres - I. Thermochemical equilibrium models, *A&A*, **678**, A53.

Dubois, D., Iraci, L. T., Barth, E. L., Salama, F., Vinatier, S., & Sciamma-O'Brien, E., 2021. Investigating the condensation of benzene ($C6H_6$) in Titan's south polar cloud system with a combination of laboratory, observational, and modeling tools, *PSJ*, **2**, 121.

Dudaryonok, A. S. & Lavrentieva, N. N., 2018. Theoretical estimation of SO_2 line broadening coefficients induced by carbon dioxide in the 150-300 K temperature range, *J. Quant. Spectrosc. Radiat. Transf.*, **219**, 360–365.

Dudás, E., Vispoel, B., Gamache, R. R., Rey, M., Tyuterev, V. G., Nikitin, A. V., Kassi, S., Suas-David, N., & Georges, R., 2023. Non-LTE spectroscopy of the tetradecad region of methane recorded in a hypersonic flow, *Icarus*, **394**, 115421.

Dypvik, H., Hellevang, H., Krzesińska, A., Sætre, C., Viennet, J.-C., Bultel, B., Ray, D., Poulet, F., Loizeau, D., Veneranda, M., et al., 2021. The Planetary Terrestrial Analogues Library (PTAL)–An exclusive lithological selection of possible martian earth analogues, *Planet Space Sci.*, **208**, 105339.

Dyrek, A., Min, M., Decin, L., Bouwman, J., et al., 2024. SO_2, silicate clouds, but no CH_4 detected in a warm Neptune, *Nature*, **625**, 51–54.

Edwards, B. & Tinetti, G., 2022. The Ariel Target List: The Impact of TESS and the Potential for Characterizing Multiple Planets within a System, *AJ.*, **164**, 15.

Edwards, B., Mugnai, L., Tinetti, G., Pascale, E., & Sarkar, S., 2019a. An Updated Study of Potential Targets for Ariel, *AJ.*, **157**, 242.

Edwards, B., Rice, M., Zingales, T., Tessenyi, M., Waldmann, I., Tinetti, G., Pascale, E., Savini, G., & Sarkar, S., 2019b. Exoplanet spectroscopy and photometry with the twinkle space telescope, *Exp. Astron.*, **47**, 29–63.

Encrenaz, T., Coustenis, A., Gilli, G., Marcq, E., Molaverdikhani, K., Mugnai, L. V., Ollivier, M., & Tinetti, G., 2022. Observability of temperate exoplanets with Ariel, *Exp. Astron.*, **53**, 375–390.

Ercolano, B., Rab, C., Molaverdikhani, K., Edwards, B., Preibisch, T., Testi, L., Kamp, I., & Thi, W.-F., 2022. Observations of PAHs in the atmospheres of discs and exoplanets, *MNRAS*, **512**, 430–438.

Es-sebbar, E.-t. & Farooq, A., 2014. Intensities, broadening and narrowing parameters in the ν_3 band of methane, *J. Quant. Spectrosc. Radiat. Transf.*, **149**, 241–252.

Esposito, L. W., Barth, C. A., Colwell, J. E., Lawrence, G. M., et al., 2004. The Cassini Ultraviolet Imaging Spectrograph Investigation, *Space Sci. Rev.*, **115**, 299–361.

Fairman, C., Wakeford, H. R., & MacDonald, R. J., 2024. The importance of optical wavelength data on atmospheric retrievals of exoplanet transmission spectra.

Fakhardji, W., Boulet, C., Tran, H., & Hartmann, J.-M., 2022. Direct calculations of the CH_4+CO_2 far infrared collision-induced absorption, *J. Quant. Spectrosc. Radiat. Transf.*, **283**, 108148.

Fano, U., 1961. Effects of configuration interaction on intensities and phase shifts, *Phys. Rev.*, **124**, 1866–1878.

Farmer, C. B. & Houghton, J. T., 1966. Collision-induced Absorption in the Earth's atmosphere, *Nature*, **209**, 1341–1342.

Fateev, A., Clausen, S., Wang, Y., Owens, A., Tennyson, J., & Yurchenko, S. N., 2023. Experimental VUV cross sections of molecules: ExoMol database update, *J. Quant. Spectrosc. Radiat. Transf.*.

Fauchez, T., Rossi, L., & Stam, D. M., 2017. The O_2 A-band in the fluxes and polarization of starlight reflected by earth-like exoplanets, *ApJ*, **842**, 41.

Fernández-Milán, P., Borràs, V. J., Gonzélez-Vázquez, J., & Martín, F., 2023. Photoionization of the water molecule with XCHEM, *J. Phys. Chem.*, **158**, 134305.

Filippov, N. N., Asfin, R. E., Sinyakova, T. N., Grigoriev, I. M., Petrova, T. M., Solodov, A. M., Solodov, A. A., & Buldyreva, J. V., 2013. Experimental and theoretical studies of CO2 spectra for planetary atmosphere modelling: region 600–9650 cm-1 and pressures up to 60 atm, *Phys. Chem. Chem. Phys.*, **15**, 13826.

Finenko, A. A., Chistikov, D. N., Kalugina, Y. N., Conway, E. K., & Gordon, I. E., 2021. Fitting potential energy and induced dipole surfaces of the van der Waals complex CH_4–N_2 using non-product quadrature grids, *Phys. Chem. Chem. Phys.*, **23**, 18475–18494.

Finenko, A. A., Bézard, B., Gordon, I. E., Chistikov, D. N., Lokshtanov, S. E., Petrov, S. V., & Vigasin, A. A., 2022. Trajectory-based Simulation of Far-infrared Collision-induced Absorption Profiles of CH_4–N_2 for Modeling Titan's Atmosphere, *ApJS*, **258**, 33.

Fletcher, L. N., Gustafsson, M., & Orton, G. S., 2018. Hydrogen dimers in giant-planet infrared spectra, *ApJS*, **235**, 24.

Fleurbaey, H., Reed, Z. D., Adkins, E. M., Long, D. A., & Hodges, J. T., 2021. High accuracy spectroscopic parameters of the 1.27 μm band of O_2 measured with comb-referenced, cavity ring-down spectroscopy, *J. Quant. Spectrosc. Radiat. Transf.*, **270**, 107684.

Fleurbaey, H., Mondelain, D., Fakhardji, W., Hartmann, J.-M., & Campargue, A., 2022. Simultaneous collision-induced transitions in H_2O+CO_2 gas mixtures, *J. Quant. Spectrosc. Radiat. Transf.*, **285**, 108162.

Fleurbaey, H., Čermák, P., Campargue, A., Kassi, S., Romanini, D., Votava, O., & Mondelain, D., 2023. $12CO_2$ transition frequencies with kHz-accuracy by saturation spectroscopy in the 1.99-2.09 μm region, *Phys. Chem. Chem. Phys.*, **25**, 16319–16330.

Fleury, B., Benilan, Y., Venot, O., Henderson, B. L., Swain, M., & Gudipati, M. S., 2023. Experimental investigation of the photochemical production of hydrocarbons in warm gas giant exoplanet atmospheres, *ApJ*, **956**, 134.

Fleury, B., Poveda, M., Bénilan, Y., & Venot, O., 2023. High Temperature Measurement of Acetylene UV Absorption Cross Section for the Study of Hot Exoplanet Atmospheres, in *SF2A-2023: Proceedings of the Annual meeting of the French Society of Astronomy and Astrophysics*, pp. 377–380.

Flint, A. R. & Fortenberry, R. C., 2023. Formation and destruction of Si_6O_12 nanostructures in the gas phase: Applications to grain nucleation and water generation, *ACS Earth Space Chem.*, **7**, 2119–2128.

Foley, H., 1946. The pressure broadening of spectral lines, *Phys. Rev.*, **69**, 616–628.

Foltynowicz, A., Ban, T., Maslowski, P., Adler, F., & Ye, J., 2011. Quantum-noise-limited optical frequency comb spectroscopy, *Phys. Rev. Lett.*, **107**, 233002.

Foltynowicz, A., Rutkowski, L., Silander, I., Johansson, A. C., et al., 2021a. Measurement and assignment of double-resonance transitions to the 8900–9100-cm^{-1} levels of methane, *Phys. Rev. A*, **103**, 022810.

Foltynowicz, A., Rutkowski, L., Silander, I., Johansson, A. C., et al., 2021b. Sub-doppler double-resonance spectroscopy of methane using a frequency comb probe, *Phys. Rev. Lett.*, **126**, 063001.

Fortney, J., Robinson, T. D., Domagal-Goldman, S., et al., 2019. The need for laboratory measurements and ab initio studies to aid understanding of exoplanetary atmospheres, *Astro2020: Decadal Survey on Astronomy and Astrophysics*, **2020**, 146.

Fraine, J., Mayorga, L. C., Stevenson, K. B., Lewis, N. K., et al., 2021. The dark world: A tale of WASP-43b in reflected light

with HST WFC3/UVIS, *AJ.*, **161**, 269.

France, K., Loyd, R. O. P., Youngblood, A., Brown, A., et al., 2016. The muscles treasury survey. I. Motivation and overview, *ApJ*, **820**, 89.

Frohman, D. J., Bernath, P. F., & Brooke, J. S. A., 2016. Molecular line lists: The ro-vibrational spectra of NaF and KF, *J. Quant. Spectrosc. Radiat. Transf.*, **169**, 104–110.

Furtenbacher, T., Császár, A. G., & Tennyson, J., 2007. MARVEL: measured active rotational vibrational energy levels, *J. Mol. Spectrosc.*, **245**, 115–125.

Furtenbacher, T., Szabó, I., Császár, A. G., Bernath, P. F., Yurchenko, S. N., & Tennyson, J., 2016. Experimental Energy Levels and Partition Function of the $^{12}C_2$ Molecule, *ApJS*, **224**, 44.

Furtenbacher, T., Coles, P. A., Tennyson, J., Yurchenko, S. N., Yu, S., Drouin, B., Tóbiás, R., & Császár, A. G., 2020. Empirical rovibational energy of ammonia up to 7500 cm^{-1}, *J. Quant. Spectrosc. Radiat. Transf.*, **251**, 107027.

Gail, H. P. & Sedlmayr, E., 1999. Mineral formation in stellar winds. I. Condensation sequence of silicate and iron grains in stationary oxygen rich outflows, *A&A*, **347**, 594–616.

Gail, H.-P., Wetzel, S., Pucci, A., & Tamanai, A., 2013. Seed particle formation for silicate dust condensation by SiO nucleation, *A&A*, **555**, A119.

Galatry, L., 1961. Simultaneous effect of doppler and foreign gas broadening on spectral lines, *Phys. Rev.*, **122**, 1218–1223.

Galli, I., Pastor, P. C., Di Lonardo, G., Fusina, L., Giusfredi, G., Mazzotti, D., Tamassia, F., & De Natale, P., 2011. The ν_3 band of $^{14}C^{16}O_2$ molecule measured by optical-frequency-comb-assisted cavity ring-down spectroscopy, *Mol. Phys.*, **109**, 2267–2272.

Galli, I., Bartalini, S., Cancio Pastor, P., Cappelli, F., Giusfredi, G., Mazzotti, D., Akikusa, N., Yamanishi, M., & De Natale, P., 2013. Absolute frequency measurements of CO_2 transitions at 4.3 μm with a comb-referenced quantum cascade laser, *Mol. Phys.*, **111**, 2041–2045.

Gamache, R. R. & Vispoel, B., 2018. On the temperature dependence of half-widths and line shifts for molecular transitions in the microwave and infrared regions, *J. Quant. Spectrosc. Radiat. Transf.*, **217**, 440–452.

Gamache, R. R., Roller, C., Lopes, E., Gordon, I. E., Rothman, L. S., Polyansky, O. L., Zobov, N. F., Kyuberis, A. A., Tennyson, J., Yurchenko, S. N., Császár, A. G., Furtenbacher, T., Huang, X., Schwenke, D. W., Lee, T. J., Drouin, B. J., Tashkun, S. A., Perevalov, V. I., & Kochanov, R. V., 2017. Total Internal Partition Sums for 167 isotopologues of 53 molecules important in planetary atmospheres: application to HITRAN2016 and beyond, *J. Quant. Spectrosc. Radiat. Transf.*, **203**, 70–87.

Gamache, R. R., Vispoel, B., Rey, M., Nikitin, A., Tyuterev, V., Egorov, O., Gordon, I. E., & Boudon, V., 2021. Total internal partition sums for the HITRAN2020 database, *J. Quant. Spectrosc. Radiat. Transf.*, **271**, 107713.

Gandhi, S. & Madhusudhan, N., 2017. Retrieval of exoplanet emission spectra with HyDRA, *MNRAS*, **474**, 271–288.

Gandhi, S., Brogi, M., Yurchenko, S. N., Tennyson, J., Coles, P. A., Webb, R. K., Birkby, J. L., Guilluy, G., Hawker, G. A., Madhusudhan, N., Bonomo, A. S., & Sozzetti, A., 2020. Molecular cross-sections for high-resolution spectroscopy of super-Earths, warm Neptunes, and hot Jupiters, *MNRAS*, **495**, 224–237.

Gandhi, S., Kesseli, A., Zhang, Y., Louca, A., Snellen, I., Brogi, M., Miguel, Y., Casasayas-Barris, N., Pelletier, S., Landman, R., Maguire, C., & Gibson, N. P., 2023. Retrieval survey of metals in six ultrahot jupiters: Trends in chemistry, rain-out, ionization, and atmospheric dynamics, *AJ.*, **165**, 242.

Gao, H., Song, Y., Chang, Y.-C., Shi, X., Yin, Q.-Z., Wiens, R. C., Jackson, W. M., & Ng, C. Y., 2013. Branching Ratio Measurements for Vacuum Ultraviolet Photodissociation of $^{12}C^{16}O$, *J. Phys. Chem. A*, **117**, 6185–6195.

Gao, H., Song, Y., Jackson, W. M., & Ng, C.-Y., 2020a. Photodissociation branching ratios of $^{12}C^{16}O$ from 108000 cm^{-1} to 113200 cm^{-1} measured by two-color VUV-VUV laser pump-probe time-slice velocity-map ion imaging method: Observation of channels for producing O(1D), *Chin. J. Chem. Phys.*, **33**, 91–100.

Gao, P., Thorngren, D. P., Lee, E. K. H., Fortney, J. J., Morley, C. V., Wakeford, H. R., Powell, D. K., Stevenson, K. B., & Zhang, X., 2020b. Aerosol composition of hot giant exoplanets dominated by silicates and hydrocarbon hazes, *Nature Astronomy*, **4**, 951–956.

Gao, P., Wakeford, H. R., Moran, S. E., & Parmentier, V., 2021. Aerosols in exoplanet atmospheres, *J. Geophys. Res.: Planets*, **126**, e2020JE006655.

Garcia, G. A., de Miranda, B. K. C., Tia, M., Daly, S., & Nahon, L., 2013. DELICIOUS III: A multipurpose double imaging particle coincidence spectrometer for gas phase vacuum ultraviolet photodynamics studies, *Rev. Sci. Instrum.*, **84**.

Garcia, G. A., Tang, X., Gil, J.-F., Nahon, L., Ward, M., Batut, S., Fittschen, C., Taatjes, C. A., Osborn, D. L., & Loison, J.-C., 2015. Synchrotron-based double imaging photoelectron/photoion coincidence spectroscopy of radicals produced in a flow tube: OH and OD, *J. Chem. Phys.*, **142**, 164201.

García Muñoz, A., 2007. Formulation of molecular diffusion in planetary atmospheres, *Planet Space Sci.*, **55**, 1414–1425.

García Muñoz, A., Asensio Ramos, A., & Faure, A., 2024. NLTE modelling of water-rich exoplanet atmospheres. Cooling and heating rates, *Icarus*, **415**, 116080.

Gavilan, L., Carrasco, N., Hoffmann, S. V., Jones, N. C., & Mason, N. J., 2018. Organic Aerosols in Anoxic and Oxic Atmospheres of Earth-like Exoplanets: VUV-MIR Spectroscopy of CHON Tholins, *ApJ*, **861**, 110.

Geballe, T. R., Saumon, D., Golimowski, D. A., Leggett, S. K., Marley, M. S., & Noll, K. S., 2009. Spectroscopic detection of Carbon Monoxide in two late-type T dwarfs, *ApJ*, **695**, 844.

Georges, R., Thiévin, J., Benidar, A., Carles, S., Amyay, B., Louviot, M., Boudon, V., & Vander Auwera, J., 2019. High enthalpy source dedicated to quantitative infrared emission spectroscopy of gas flows at elevated temperatures, *Review of Scientific Instruments*, **90**, 093103.

Germann, M., Hjältén, A., Boudon, V., Richard, C., Krzempek, K., Hudzikowski, A., Głuszek, A., Soboń, G., & Foltynowicz, A., 2022. A methane line list with sub-mhz accuracy in the 1250 to 1380 cm^{-1} range from optical frequency comb fourier transform spectroscopy, *J. Quant. Spectrosc. Radiat. Transf.*, **288**, 108252.

Germann, M., Hjältén, A., Tennyson, J., Yurchenko, S. N., Gordon, I. E., Pett, C., Silander, I., Krzempek, K., Hudzikowski, A., Głuszek, A., Soboń, G., & Foltynowicz, A., 2024. Optical frequency comb Fourier transform spectroscopy of formaldehyde in the 1250 to 1390 cm^{-1} range: Experimental line list and improved MARVEL analysis, *J. Quant. Spectrosc. Radiat. Transf.*, **312**, 108782.

Gharib-Nezhad, E. & Line, M. R., 2019. The influence of H_2O pressure broadening in high-metallicity exoplanet atmospheres, *AJ.*, **872**, 27.

Gharib-Nezhad, E., Shayesteh, A., & Bernath, P. F., 2013. Einstein-A coefficients for rovibronic lines of the $A^2\Pi \rightarrow X^2\Sigma^+$ and $B'^2\Sigma^+ \rightarrow X^2\Sigma^+$ transitions of MgH, *MNRAS*, **432**, 2043–2047.

Gharib-Nezhad, E., Heays, A. N., Bechtel, H. A., & Lyons, J. R., 2019. H_2-induced pressure broadening and pressure shift in the P-branch of the ν_3 band of CH_4 from 300 to 655 K, *J. Quant. Spectrosc. Radiat. Transf.*, **239**, 106649.

Gharib-Nezhad, E., Iyer, A. R., Line, M. R., Freedman, R. S., Marley, M. S., & Batalha, N. E., 2021. EXOPLINES: Molecular absorption cross-section database for brown dwarf and giant exoplanet atmospheres, *ApJS*, **254**, 34.

Gharib-Nezhad, E. S., Batalha, N. E., Chubb, K., Freedman, R., Gordon, I. E., Gamache, R. R., Hargreaves, R. J., Lewis, N. K., Tennyson, J., & Yurchenko, S. N., 2024. The impact of spectral line wing cut-off: Recommended standard method with application to MAESTRO opacity database, *RASTI*, **3**, 44–55.

Ghysels, M., Vasilchenko, S., Mondelain, D., Béguier, S., Kassi, S., & Campargue, A., 2018. Laser absorption spectroscopy

of methane at 1000 K near 1.7 μm: A validation test of the spectroscopic databases, *J. Quant. Spectrosc. Radiat. Transf.*, **215**, 59–70.

Gobrecht, D., Cristallo, S., Piersanti, L., & Bromley, S. T., 2017. Nucleation of small silicon carbide dust clusters in AGB stars, *ApJ*, **840**, 117.

Gobrecht, D., Decin, L., Cristallo, S., & Bromley, S. T., 2018. A global optimisation study of the low-lying isomers of the alumina octomer $(Al_2O_3)_8$, *Chem. Phys. Lett.*, **711**, 138–147.

Gobrecht, D., Plane, J. M. C., Bromley, S. T., Decin, L., Cristallo, S., & Sekaran, S., 2022. Bottom-up dust nucleation theory in oxygen-rich evolved stars. I. Aluminium oxide clusters, *A&A*, **658**, A167.

Gobrecht, D., Hashemi, S. R., Plane, J. M. C., Bromley, S. T., Nyman, G., & Decin, L., 2023. Bottom-up dust nucleation theory in oxygen-rich evolved stars. II. Magnesium and calcium aluminate clusters, *A&A*, **680**, A18.

Godin, P. J., Ramirez, R. M., Campbell, C. L., Wizenberg, T., Nguyen, T. G., Strong, K., & Moores, J. E., 2020. Collision-induced absorption of ch$_4$ - co$_2$ and h$_2$ - co$_2$ complexes and their effect on the ancient Martian atmosphere, *J. Geophys. Res.: Planets*, **125**, e2019JE006357.

Gohle, C., Stein, B., Schliesser, A., Udem, T., & Hansch, T. W., 2007. Frequency comb Vernier spectroscopy for broadband, high-resolution, high-sensitivity absorption and dispersion spectra, *Phys. Rev. Lett.*, **99**, 263902.

Goldenstein, C. S., Jeffries, J. B., & Hanson, R. K., 2013. Diode laser measurements of linestrength and temperature-dependent lineshape parameters of H_2O-, co$_2$-, and n$_2$-perturbed h$_2$o transitions near 2474 and 2482 nm, *J. Quant. Spectrosc. Radiat. Transf.*, **130**, 100–111.

Goldflam, R., Green, S., & Kouri, D. J., 1977. Infinite order sudden approximation for rotational energy transfer in gaseous mixtures, *J. Chem. Phys.*, **67**, 4149–4161.

Gomez, F. M., Hargreaves, R. J., & Gordon, I. E., 2024. A hitran-formatted uv line list of s$_2$-containing transitions involving x $^3\sigma_g^-$, b $^3\sigma_u^-$, and b" $^3\pi_u$ electronic states, *MNRAS*, **528**, 3823–3832.

Gordon, I. E., Rothman, L. S., Hargreaves, R. J., et al., 2022. The HITRAN2020 molecular spectroscopic database, *J. Quant. Spectrosc. Radiat. Transf.*, **277**, 107949.

Gordon, R. G., 1966. Theory of the width and shift of molecular spectral lines in gases, *J. Chem. Phys.*, **44**, 3083–3089.

Gordon, S. & Mcbride, B. J., 1994. Computer program for calculation of complex chemical equilibrium compositions and applications, *NASA Lewis Research Center Cleveland, OH, United States*, **NASA-RP-1311**, 95N20180.

Gorman, M. N., Yurchenko, S. N., & Tennyson, J., 2019. ExoMol Molecular linelists – XXXVI. $X\ ^2\Pi - X\ ^2\Pi$ and $A\ ^2\Sigma^+ - X\ ^2\Pi$ transitions of SH, *MNRAS*, **490**, 1652–1665.

Goumans, T. P. M. & Bromley, S. T., 2012. Efficient nucleation of stardust silicates via heteromolecular homogeneous condensation, *MNRAS*, **420**, 3344–3349.

Grant, D., Lewis, N. K., Wakeford, H. R., Batalha, N. E., et al., 2023. JWST-TST DREAMS: Quartz Clouds in the Atmosphere of WASP-17b, *ApJL*, **956**, L32.

Grimm, S. L. & Heng, K., 2015. HELIOS-K: An ultrafast, open-source opacity calculator for radiative transfer, *ApJ*, **808**, 182.

Grimm, S. L., Malik, M., Kitzmann, D., Guzmán-Mesa, A., Hoeijmakers, H. J., Fisher, C., Mendonça, J. M., Yurchenko, S. N., Tennyson, J., Alesina, F., Buchschacher, N., Burnier, J., Segransan, D., Kurucz, R. L., & Heng, K., 2021. HELIOS-K 2.0 Opacity Calculator and Open-source Opacity Database for Exoplanetary Atmospheres, *ApJS*, **253**, 30.

Grosch, H., Fateev, A., & Clausen, S., 2015. UV absorption cross-sections of selected sulfur-containing compounds at temperatures up to 500°C, *J. Quant. Spectrosc. Radiat. Transf.*, **154**, 28–34.

Gruszka, M. & Borysow, A., 1997. Roto-translational collision-induced absorption of CO_2 for the atmosphere of venus at frequencies from 0 to 250 cm^{-1}, at temperatures from 200 to 800 K, *Icarus*, **129**, 172–177.

Guay, P., Genest, J., & Fleisher, A. J., 2018. Precision spectroscopy of H13CN using a free-running, all-fiber dual electro-optic frequency comb system, *Opt. Letters*, **43**, 1407–1410.

Guest, E. R., Tennyson, J., & Yurchenko, S. N., 2024. Modelling the Rotational Dependence of Line Broadening using Machine Learning, *J. Mol. Spectrosc.*, **401**, 111901.

Guillot, T., Fletcher, L. N., Helled, R., Ikoma, M., Line, M. R., & Parmentier, V., 2022. Giant Planets from the Inside-Out.

Guilluy, G., Sozzetti, A., Giacobbe, P., Bonomo, A. S., & Micela, G., 2022. On the synergy between Ariel and ground-based high-resolution spectroscopy, *Experimental Astronomy*, **53**, 655–677.

Guo, R., Teng, J., Dong, H., Zhang, T., Li, D., & Wang, D., 2021. Line parameters of the P-branch of (30012) ← (00001) $^{12}C^{16}O_2$ band measured by comb-assisted, Pound-Drever-Hall locked cavity ring-down spectrometer, *J. Quant. Spectrosc. Radiat. Transf.*, **264**, 107555.

Gustafsson, M. & Frommhold, L., 2001. Infrared absorption spectra of collisionally interacting He and H atoms, *ApJ*, **546**, 1168.

Gustafsson, M. & Frommhold, L., 2003. The H_2-H infrared absorption bands at temperatures from 1000 K to 2500 K, *A&A*, **400**, 1161–1162.

Hakalla, R., Niu, M. L., Field, R. W., Salumbides, E. J., Heays, A. N., Stark, G., Lyons, J. R., Eidelsberg, M., Lemaire, J. L., Federman, S. R., Zachwieja, M., Szajna, W., Kolek, P., Piotrowska, I., Ostrowska-Kopec, M., Kepa, R., de Oliveira, N., & Ubachs, W., 2016. VIS and VUV spectroscopy of $^{12}C^{17}O$ and deperturbation analysis of the A $^1\Pi$, v = 1—5 levels, *RSC Adv.*, **6**, 31588–31606.

Hansen, B. M. S. & Sterl Phinney, E., 1998. Stellar forensics - I. Cooling curves, *MNRAS*, **294**, 557–568.

Hapke, B., 1993. *Theory of reflectance and emittance spectroscopy*, Topics in Remote Sensing, Cambridge, UK: Cambridge University Press.

Haqq-Misra, J., Kopparapu, R., Fauchez, T. J., Frank, A., Wright, J. T., & Lingam, M., 2022. Detectability of Chlorofluorocarbons in the Atmospheres of Habitable M-dwarf Planets, *Planet. Sci. J.*, **3**, 60.

Hardy, P., Richard, C., Boudon, V., Khan, M. V., Manceron, L., & Dridi, N., 2023. High-resolution far-infrared spectroscopy and analysis of the ν3 and ν6 bands of chloromethane, *J. Quant. Spectrosc. Radiat. Transf.*, p. 108779.

Hargreaves, R. J., Hinkle, K. H., Bauschlicher, Charles W., J., Wende, S., Seifahrt, A., & Bernath, P. F., 2010. High-resolution 1.6 μm Spectra of FeH in M and L Dwarfs, *AJ.*, **140**, 919–924.

Hargreaves, R. J., Li, G., & Bernath, P. F., 2012. Ammonia line lists from 1650 to 4000 cm^{-1}, *J. Quant. Spectrosc. Radiat. Transf.*, **113**, 670–679.

Hargreaves, R. J., Buzan, E., Dulick, M., & Bernath, P. F., 2015. High-resolution absorption cross sections of C_2H_6 at elevated temperatures, *Mol. Astrophys.*, **1**, 20–25.

Hargreaves, R. J., Gordon, I. E., Rothman, L. S., Tashkun, S. A., Perevalov, V. I., Lukashevskaya, A. A., Yurchenko, S. N., Tennyson, J., & Müller, H. S., 2019. Spectroscopic line parameters of NO, NO_2, and N_2O for the HITEMP database, *J. Quant. Spectrosc. Radiat. Transf.*, **232**, 35–53.

Hargreaves, R. J., Gordon, I. E., Rey, M., Nikitin, A. V., Tyuterev, V. G., Kochanov, R. V., & Rothman, L. S., 2020. An accurate, extensive, and practical line list of methane for the HITEMP database, *ApJS*, **247**, 55.

Harper, O. J., Hassenfratz, M., Loison, J. C., Garcia, G. A., de Oliveira, N., Hrodmarsson, H. R., Pratt, S. T., Boye-Peronne, S., & Gans, B., 2019. Quantifying the photoionization cross section of the hydroxyl radical, *J. Chem. Phys.*, **150**, 141103.

Harper, O. J., Gans, B., Loison, J.-C., Garcia, G. A., Hrodmarsson, H. R., & Boyé-Péronne, S., 2021. Photoionization Cross Section of the NH_2 Free Radical in the 11.1–15.7 eV Energy Range, *J. Phys. Chem. A*, **125**, 2764–2769.

Harrison, J. J., 2018. New and improved infrared absorption cross

sections for trichlorofluoromethane (CFC-11), *Atmos. Meas. Tech.*, **11**, 5827–5836.

Hartmann, J. M., Boulet, C., & Robert, D., 2008. *Collisional effects on molecular spectra: Laboratory experiments and models, consequences for applications*, Elsevier Science, 1st edn.

Hartmann, J.-M., Boulet, C., Tran, H., & Nguyen, M. T., 2010. Molecular dynamics simulations for CO_2 absorption spectra. I. Line broadening and the far wing of the ν_3 infrared band, *J. Chem. Phys.*, **133**, 144313.

Hartmann, J.-M., Boulet, C., & Toon, G. C., 2017. Collision-induced absorption by N_2 near 2.16 μm: Calculations, model, and consequences for atmospheric remote sensing, *JGR-Atm*, **122**, 2419–2428.

Hartmann, J.-M., Boulet, C., Tran, D. D., Tran, H., & Baranov, Y., 2018. Effect of humidity on the absorption continua of CO_2 and N_2 near 4μm: Calculations, comparisons with measurements, and consequences for atmospheric spectra, *J. Phys. Chem.*, **148**, 054304.

Hartmann, J.-M., Tran, H., Armante, R., Boulet, C., Campargue, A., Forget, F., Gianfrani, L., Gordon, I., Guerlet, S., Gustafsson, M., Hodges, J. T., Kassi, S., Lisak, D., Thibault, F., & Toon, G. C., 2018. Recent advances in collisional effects on spectra of molecular gases and their practical consequences, *J. Quant. Spectrosc. Radiat. Transf.*, **213**, 178–227.

He, C., Hörst, S. M., Lewis, N. K., Moses, J. I., Kempton, E. M. R., Marley, M. S., Morley, C. V., Valenti, J. A., & Vuitton, V., 2019. Gas phase chemistry of cool exoplanet atmospheres: Insight from laboratory simulations, *ACS Earth Space Chem.*, **3**, 39–50.

He, C., Hörst, S. M., Radke, M., & Yant, M., 2022a. Optical Constants of a Titan Haze Analog from 0.4 to 3.5μm Determined Using Vacuum Spectroscopy, *Planet. Sci. J.*, **3**, 25.

He, C., Serigano, J., Hörst, S. M., Radke, M., & Sebree, J. A., 2022b. Titan atmospheric chemistry revealed by low-temperature N_2–CH_4 plasma discharge experiments, *ACS Earth Space Chem.*, **6**, 2295–2304.

He, C., Radke, M., Moran, S. E., Hörst, S. M., Lewis, N. K., Moses, J. I., Marley, M. S., Batalha, N. E., Kempton, E. M. R., Morley, C. V., Valenti, J. A., & Vuitton, V., 2024. Optical properties of organic haze analogues in water-rich exoplanet atmospheres observable with JWST, *Nature Astronomy*, **8**, 182–192.

He, J., Diamant, S. J. M., Wang, S., Yu, H., Rocha, W. R. M., Rachid, M., & Linnartz, H., 2022c. Refractive index and extinction coefficient of vapor-deposited water ice in the UV–vis range, *ApJ*, **925**, 179.

Heays, A. N., Bosman, A. D., & van Dishoeck, E. F., 2017. Photodissociation and photoionisation of atoms and molecules of astrophysical interest, *A&A*, **602**, A105.

Heays, A. N., de Oliveira, N., Gans, B., Ito, K., Boye-Peronnec, S., Douin, S., Hickson, K. M., Nahon, L., & Loison, J. C., 2018. High-resolution one-photon absorption spectroscopy of the D $^2\Sigma^- \leftarrow$ X $^2\Pi$ system of radical OH and OD, *J. Quant. Spectrosc. Radiat. Transf.*, **204**, 12–22.

Heays, A. N., Stark, G., Lyons, J. R., de Oliveira, N., Lewis, B. R., & Gibson, S. T., 2023. Ultraviolet photoabsorption in the B $^3\Sigma^-$ – X $^3\Sigma^-$ and C $^3\Pi$ – X$^3\Sigma^-$ band systems of SO sulphur isotopologues, *Mol. Phys.*, **121**, e2153092.

Hedges, C. & Madhusudhan, N., 2016. Effect of pressure broadening on molecular absorption cross sections in exoplanetary atmospheres, *MNRAS*, **458**(2), 1427–1449.

Heiter, U., Kupka, F., van 't Veer-Menneret, C., Barban, C., Weiss, W. W., Goupil, M.-J., Schmidt, W., Katz, D., & arrido, R., 2002. New grids of ATLAS9 atmospheres I: Influence of convection treatments on model structure and on observable quantities, *A&A*, **392**, 619–636.

Heller, S. R., McNaught, A., Pletnev, I., Stein, S., & Tchekhovskoi, D., 2015. InChI, the IUPAC International Chemical Identifier, *Journal of Cheminformatics*, **7**.

Helling, C., 2021. Clouds in exoplanetary atmospheres, in *ExoFrontiers*, 2514-3433, pp. 20–1 to 20–7, IOP Publishing.

Helling, C., Ackerman, A., Allard, F., Dehn, M., Hauschildt, P., Homeier, D., Lodders, K., Marley, M., Rietmeijer, F., Tsuji, T., & Woitke, P., 2008. A comparison of chemistry and dust cloud formation in ultracool dwarf model atmospheres, *MNRAS*, **391**, 1854–1873.

Helling, C., Samra, D., Lewis, D., Calder, R., Hirst, G., Woitke, P., Baeyens, R., Carone, L., Herbort, O., & Chubb, K. L., 2023. Exoplanet weather and climate regimes with clouds and thermal ionospheres: A model grid study in support of large-scale observational campaigns, *A&A*, **671**, A122.

Henning, T., Begemann, B., Mutschke, H., & Dorschner, J., 1995. Optical properties of oxide dust grains., *A&AS*, **112**, 143.

Henning, T., Il'in, V. B., Krivova, N. A., Michel, B., & Voshchinnikov, N. V., 1999. WWW database of optical constants for astronomy, *A&AS*, **136**, 405–406.

Herbort, O., Woitke, P., Helling, C., & Zerkle, A., 2020. The atmospheres of rocky exoplanets I. Outgassing of common rock and the stability of liquid water, *A&A*, **636**, A71.

Hewett, D., Bernath, P. F., Wong, A., Billinghurst, B. E., Zhao, J., Lombardo, N. A., Nixon, C. A., & Jennings, D. E., 2020. N_2 and H_2 broadened isobutane infrared absorption cross sections and butane upper limits on Titan, *Icarus*, **344**, 113460.

Hill, C., 2023. International Atomic and Molecular Code Centres Network: Virtual Atomic and Molecular Data Centres Consortium Annual Meeting: Summary Report of the 8th Biennial Technical Meeting of the IAEA Code Centres Network, INDC(NDS)-0897, Tech. rep., International Atomic Energy Agency.

Hill, C., Dipti, Heinola, K., & Haničinec, M., 2024. CollisionDB: A new database of atomic and molecular collisional processes with an interactive API, *Atoms*, **12**, 20.

Hindmarsh, W. R., Petford, A. D., & Smith, G., 1967. Interpretation of collision broadening and shift in atomic spectra, *Proc. R. Soc. Lond. Ser. A Math. Eng. Sci.*, **297**, 296–304.

Hinkle, K. H., Wallace, L., Ram, R. S., Bernath, P. F., Sneden, C., & Lucatello, S., 2013. The Magnesium Isotopologues of MgH in the A $^2\Pi$-X $^2\Sigma^+$ System, *ApJS*, **207**, 26.

Hjältén, A., Germann, M., Krzempek, K., Hudzikowski, A., Głuszek, A., Tomaszewska, D., Soboń, G., & Foltynowicz, A., 2021. Optical frequency comb Fourier transform spectroscopy of $^{14}N_2{}^{16}O$ at 7.8 μm, *J. Quant. Spectrosc. Radiat. Transf.*, **271**, 107734.

Hjältén, A., Foltynowicz, A., & Sadiek, I., 2023. Line positions and intensities of the ν_1 band of $^{12}CH_3I$ using mid-infrared optical frequency comb Fourier transform spectroscopy, *J. Quant. Spectrosc. Radiat. Transf.*, **306**, 108646.

Hobbs, R., Rimmer, P. B., Shorttle, O., & Madhusudhan, N., 2021. Sulfur chemistry in the atmospheres of warm and hot Jupiters, *MNRAS*, **506**, 3186–3204.

Hodges, J. N. & Bernath, P. F., 2017. Fourier Transform Spectroscopy of the $A\ ^3\Pi - X\ ^3\Sigma^-$ Transition of OH^+, *ApJ*, **840**, 81.

Hodges, J. N., Bittner, D. M., & Bernath, P. F., 2018. Improved Ultraviolet and Infrared Oscillator Strengths for OH^+, *ApJ*, **855**.

Hoeijmakers, H. J., Seidel, J. V., Pino, L., et al., 2020. Hot Exoplanet Atmospheres Resolved with Transit Spectroscopy (HEARTS) - IV. A spectral inventory of atoms and molecules in the high-resolution transmission spectrum of WASP-121 b, *A&A*, **641**, A123.

Holmberg, M. & Madhusudhan, N., 2024. Possible Hycean conditions in the sub-Neptune TOI-270 d, *A&A*, **683**, L2.

Hörst, S. M., Vuitton, V., & Yelle, R. V., 2008. Origin of oxygen species in titan's atmosphere, *J. Geophys. Res.: Planets*, **113**(E10).

Hörst, S. M., He, C., Lewis, N. K., Kempton, E. M. R., Marley, M. S., Morley, C. V., Moses, J. I., Valenti, J. A., & Vuitton, V., 2018a. Haze production rates in super-earth and mini-neptune atmosphere experiments, *Nature Astronomy*, **2**, 303–306.

Hörst, S. M., He, C., Ugelow, M. S., Jellinek, A. M., Pierrehumbert, R. T., & Tolbert, M. A., 2018b. Exploring the Atmosphere of

Neoproterozoic Earth: The Effect of O_2 on Haze Formation and Composition, *ApJ*, **858**, 119.

Hou, S. & Bernath, P. F., 2017. Line list for the MgF ground state, *J. Quant. Spectrosc. Radiat. Transf.*, **203**, 511 – 516.

Hou, S. & Bernath, P. F., 2018. Line list for the ground state of CaF, *J. Quant. Spectrosc. Radiat. Transf.*, **210**, 44 – 51.

Hrabina, J., Hosek, M., Rerucha, S., Cizek, M., Pilat, Z., Zucco, M., Lazar, J., & Cip, O., 2022. Absolute frequencies of $H^{13}C^{14}N$ hydrogen cyanide transitions in the 1.5-μm region with the saturated spectroscopy and a sub-kHz scanning laser, *Opt. Lett.*, **47**, 5704–5707.

Hrodmarsson, H. R. & Van Dishoeck, E. F., 2023. Photodissociation and photoionization of molecules of astronomical interest: Updates to the Leiden photodissociation and photoionization cross section database, *A&A*, **675**, A25.

Hrodmarsson, H. R., Garcia, G. A., Nahon, L., Loison, J.-C., & Gans, B., 2019. The absolute photoionization cross section of the mercapto radical (SH) from threshold up to 15.0 eV, *Phys. Chem. Chem. Phys.*, **21**, 25907–25915.

Hu, R., 2019. Information in the reflected-light spectra of widely separated giant exoplanets, *ApJ*, **887**, 166.

Hu, R., 2021. Photochemistry and spectral characterization of temperate and gas-rich exoplanets, *ApJ*, **921**, 27.

Huang, X., Schwenke, D. W., & Lee, T. J., 2015. Empirical infrared line lists for five SO_2 isotopologues: $^{32/33/34/36}S^{16}O_2$ and $^{32}S^{18}O_2$, *J. Mol. Spectrosc.*, **311**, 19–24.

Huang, X., Schwenke, D. W., & Lee, T. J., 2016. Ames $^{32}S^{16}O^{18}O$ line list for high-resolution experimental IR analysis, *J. Mol. Spectrosc.*, **330**, 101–111, Potentiology and Spectroscopy in Honor of Robert Le Roy.

Huang, X., Schwenke, D. W., & Lee, T. J., 2021. What It Takes to Compute Highly Accurate Rovibrational Line Lists for Use in Astrochemistry, *Acc. Chem. Res.*, **54**, 1311–1321.

Huang, X., Schwenke, D. W., Freedman, R. S., & Lee, T. J., 2022a. Ames-2021 CO_2 Dipole Moment Surface and IR Line Lists: Toward 0.1% Uncertainty for CO_2 IR Intensities, *J. Phys. Chem. A*.

Huang, X., Sung, K., Toon, G. C., Schwenke, D. W., & Lee, T. J., 2022b. A collaborative $^{14}NH_3$ IR spectroscopic analysis at 6000 cm^{-1}, *J. Quant. Spectrosc. Radiat. Transf.*, **280**, 108076.

Huang, X., Freedman, R. S., Tashkun, S., Schwenke, D. W., & Lee, T. J., 2023a. AI-3000K infrared line list for hot CO_2, *J. Mol. Spectrosc.*, **392**, 111748.

Huang, X., Schwenke, D. W., & Lee, T. J., 2023b. Highly Accurate Potential Energy Surface and Dipole Moment Surface for Nitrous Oxide and 296 K Infrared Line Lists for $^{14}N_2{}^{16}O$ and Minor Isotopologues, *Mol. Phys.*, p. e2232892.

Huebner, W. F., Keady, J. J., & Lyon, S. P., 1992. Solar photo rates for planetary atmospheres and atmospheric pollutants, *Astrophys. Space Sci.*, **195**, 1–294.

Humblicek, J., 1982. Optimized computation of the Voigt and complex probability functions, *J. Quant. Spectrosc. Radiat. Transf.*, **27**, 437–441.

Husser, T.-O., Wende-von Berg, S., Dreizler, S., Homeier, D., Reiners, A., Barman, T., & Hauschildt, P. H., 2013. A new extensive library of PHOENIX stellar atmospheres and synthetic spectra, *A&A*, **553**, A6.

Ibrahim, M. T. I., Alatoom, D., Furtenbacher, T., Csaszar, A. G., Yurchenko, S. N., Azzam, A. A. A., & Tennyson, J., 2024. MARVEL analysis of high-resolution rovibrational spectra of $^{13}C^{16}O_2$, *J. Comput. Chem.*, **45**, 969–984.

Imanaka, H., Khare, B. N., Elsila, J. E., Bakes, E. L., McKay, C. P., Cruikshank, D. P., Sugita, S., Matsui, T., & Zare, R. N., 2004. Laboratory experiments of Titan tholin formed in cold plasma at various pressures: implications for nitrogen-containing polycyclic aromatic compounds in Titan haze, *Icarus*, **168**, 344–366.

Innan, N., Al-Zafar Khan, M., & Bennai, M., 2023. Electronic Structure Calculations using Quantum Computing, *arXiv e-prints*, p. arXiv:2305.07902.

Irwin, A. W., 1981. Polynomial partition function approximations of 344 atomic and molecular species., *ApJS*, **45**, 621–633.

Irwin, P. G., Bowles, N., Braude, A. S., Garland, R., Calcutt, S., Coles, P. A., Yurchenko, S. N., & Tennyson, J., 2019. Analysis of gaseous ammonia (NH_3) absorption in the visible spectrum of Jupiter - update, *Icarus*, **321**, 572–582.

Irwin, P. G. J., Teanby, N. A., de Kok, R., Fletcher, L. N., Howett, C. J. A., Tsang, C. C. C., Wilson, C. F., Calcutt, S. B., Nixon, C. A., & Parrish, P. D., 2008. The NEMESIS planetary atmosphere radiative transfer and retrieval tool, *J. Quant. Spectrosc. Radiat. Transf.*, **109**, 1136 – 1150.

Ito, Y., Changeat, Q., Edwards, B., Al-Refaie, A., Tinetti, G., & Ikoma, M., 2022. Detectability of Rocky-Vapour atmospheres on super-Earths with Ariel, *Experimental Astronomy*, **53**(2), 357–374.

Iwakuni, K., 2022. Absolute frequency measurement of the $3\nu_1$ band of N_2O with comb-locked rapid scan spectroscopy using a multi-pass cell, *J. Mol. Spectrosc.*, **384**, 111571.

Iyer, A. R., Swain, M. R., Zellem, R. T., Line, M. R., Roudier, G., Rocha, G., & Livingston, J. H., 2016. A characteristic transmission spectrum dominated by h_2o applies to the majority of HST/WFC3 exoplanet observaitons, *ApJ*, **823**, 109.

Jablonski, A., 1937. Uber die wellenmechanische behandlung der linienverbreitung, *Acta Phys. Polon.*, **6**, 371–391.

Jablonski, A., 1945. General theory of pressure broadening of spectral lines, *Phys. Rev.*, **68**, 78–92.

Jacquinet-Husson, N., Armante, R., Scott, N. A., Chédin, A., et al., 2016. The 2015 edition of the GEISA spectroscopic database, *J. Mol. Spectrosc.*, **327**, 31–72.

Jaeger, C., Molster, F. J., Dorschner, J., Henning, T., Mutschke, H., & Waters, L. B. F. M., 1998. Steps toward interstellar silicate mineralogy. IV. The crystalline revolution, *A&A*, **339**, 904–916.

Jäger, C., Dorschner, J., Mutschke, H., Posch, T., & Henning, T., 2003. Steps toward interstellar silicate mineralogy - VII. Spectral properties and crystallization behaviour of magnesium silicates produced by the sol-gel method, *A&A*, **408**, 193–204.

Janson, M., Patel, J. Ringqvist, S. C., Lu, C., Rebollido, I., Lichtenberg, T., Brandeker, A., Angerhausen, D., & Noack, L., 2023. Imaging of exocomets with infrared interferometry, *A&A*, **671**, A114.

Janssen, L. J., Woitke, P., Herbort, O., Min, M., Chubb, K. L., Helling, C., & Carone, L., 2023. The sulfur species in hot rocky exoplanet atmospheres, *Astron. Nachr*, **344**, e20230075.

Jaziri, A. Y., Pluriel, W., Bocchieri, A., Panek, E., et al., 2024. ARES. VI. Viability of one-dimensional retrieval models for transmission spectroscopy characterization of exo-atmospheres in the era of JWST and Ariel, *A&A*, **684**, A25, Forthcoming article.

Jenkin, M. E., Valorso, R., Aumont, B., & Rickard, A. R., 2019. Estimation of rate coefficients and branching ratios for reactions of organic peroxy radicals for use in automated mechanism construction, *Atmos. Chem. Phys.*, **19**, 7691–7717.

Jeong, K. S., Chang, C., Sedlmayr, E., & Sülzle, D., 2000. Electronic structure investigation of neutral titanium oxide molecules Ti_xO_y, *J. Phys. B: At. Mol. Opt. Phys.*, **33**, 3417–3430.

Jäger, C., Il'in, V. B., Henning, T., Mutschke, H., Fabian, D., Semenov, D. A., & Voshchinnikov, N. V., 2003. A database of optical constants of cosmic dust analogs, *J. Quant. Spectrosc. Radiat. Transf.*, **79-80**, 765–774.

Jochims, H., Rühl, E., Baumgärtel, H., Tobita, S., & Leach, S., 1997. VUV peaks in absorption spectra and photoion yield curves of polycyclic aromatic hydrocarbons and related compounds, *Int. J. Mass Spectrom.*, **167-168**, 35–53, In Honour of Chava Lifshitz.

Jochims, H. W., Baumgaertel, H., & Leach, S., 1996. Photoionization quantum yields of polycyclic aromatic hydrocarbons., *A&A*, **314**, 1003–1009.

Jochims, H. W., Baumgärtel, H., & Leach, S., 1999. Structure-dependent photostability of polycyclic aromatic hydrocarbon cations: Laboratory studies and astrophysical implications, *ApJ*, **512**, 500.

John, T. L., 1988. Continuous absorption by the negative hydrogen

ion reconsidered, *A&A*, **193**, 189–192.

Johnson, J. W., Oelkers, E. H., & Helgeson, H. C., 1992. SUPCRT92: A software package for calculating the standard molal thermodynamic properties of minerals, gases, aqueous species, and reactions from 1 to 5000 bar and 0 to 1000 C, *Comput. Geosci.*, **18**, 899–947.

Kálmán, S., Szabó, G. M., Borsato, L., Bódi, A., Pál, A., & Szabó, R., 2023. Converting the sub-Jovian desert of exoplanets to a savanna with TESS, PLATO, and Ariel, *MNRAS*, **522**, 488–502.

Karhu, J., Tomberg, T., Senna Vieira, F., Genoud, G., Hänninen, V., Vainio, M., Metsälä, M., Hieta, T., Bell, S., & Halonen, L., 2019. Broadband photoacoustic spectroscopy of $^{14}CH_4$ with a high-power mid-infrared optical frequency comb, *Opt. Lett.*, **44**, 1142–1145.

Karkoschka, E., 1994. Spectrophotometry of the Jovian Planets and Titan at 300- to 1000-nm Wavelength: The Methane Spectrum, *Icarus*, **111**, 174–192.

Karlovets, E. V., Gordon, I. E., Konnov, D., Muraviev, A. V., & Vodopyanov, K. L., 2020. Dual-comb laser spectroscopy of CS_2 near 4.6 μm, *J. Quant. Spectrosc. Radiat. Transf.*, **256**, 107269.

Karlovets, E. V., Kassi, S., Tashkun, S. A., & Campargue, A., 2021. The absorption spectrum of nitrous oxide between 8325 and 8622 cm^{-1}, *J. Quant. Spectrosc. Radiat. Transf.*, **262**, 107508.

Karlovets, E. V., Tashkun, S. A., Kassi, S., & Campargue, A., 2022. An improved analysis of the N_2O absorption spectrum in the 1.18 μm window, *J. Quant. Spectrosc. Radiat. Transf.*, **278**, 108003.

Karman, T., Miliordos, E., Hunt, K. L. C., Groenenboom, G. C., & van der Avoird, A., 2015. Quantum mechanical calculation of the collision-induced absorption spectra of N_2-N_2 with anisotropic interactions, *J. Phys. Chem.*, **142**, 084306.

Karman, T., Koenis, M. A. J., Banerjee, A., Parker, D. H., Gordon, I. E., van der Avoird, A., van der Zande, W. J., & Groenenboom, G. C., 2018. O_2-O_2 and O_2-N_2 collision-induced absorption mechanisms unravelled, *Nature Chemistry*, **10**, 549–554.

Karman, T., Gordon, I. E., van der Avoird, A., Baranov, Y. I., et al., 2019. Update of the HITRAN collision-induced absorption section, *Icarus*, **328**, 160–175.

Kassi, S., Stoltmann, T., Casado, M., Daëron, M., & Campargue, A., 2018. Lamb dip CRDS of highly saturated transitions of water near 1.4 μm, *J. Chem. Phys.*, **148**.

Kassi, S., Guessoum, S., Acosta Abanto, J. C., Tran, H., Campargue, A., & Mondelain, D., 2021. Temperature Dependence of the Collision-Induced Absorption Band of O_2 Near 1.27 μm, *JGR-Atm*, **126**, e2021JD034860.

Kawashima, Y. & Min, M., 2021. Implementation of disequilibrium chemistry to spectral retrieval code ARCiS and application to 16 exoplanet transmission spectra - indication of disequilibrium chemistry for HD 209458b and WASP-39b, *A&A*, **656**, A90.

Kefala, K., Boudon, V., Yurchenko, S. N., & Tennyson, J., 2024. Empirical rovibrational energy levels for methane, *J. Quant. Spectrosc. Radiat. Transf.*, **316**, 108897.

Keller-Rudek, H., Moortgat, G. K., Sander, R., & Sörensen, R., 2013. The MPI-Mainz UV/VIS Spectral Atlas of Gaseous Molecules of Atmospheric Interest, *Earth Syst. Sci. Data*, **5**(2), 365–373.

Kéromnès, A., Metcalfe, W. K., Heufer, K. A., Donohoe, N., Das, A. K., Sung, C.-J., Herzler, J., Naumann, C., Griebel, P., Mathieu, O., Krejci, M. C., Petersen, E. L., Pitz, W. J., & Curran, H. J., 2013. An Experimental and Detailed Chemical Kinetic Modeling Study of Hydrogen and Syngas Mixture Oxidation at Elevated Pressures, *Combust. Flame*, **160**, 995–1011.

Khare, B., Sagan, C., Arakawa, E., Suits, F., Callcott, T., & Williams, M., 1984. Optical constants of organic tholins produced in a simulated Titanian atmosphere: From soft x-ray to microwave frequencies, *Icarus*, **60**, 127–137.

Kilpatrick, B. M., Cubillos, P. E., Stevenson, K. B., Lewis, N. K., Wakeford, H. R., et al., 2018. Community targets of JWST's Early Release Science program: Evaluation of WASP-63b, *AJ.*, **156**, 103.

Kitzmann, D. & Heng, K., 2017. Optical properties of potential condensates in exoplanetary atmospheres, *MNRAS*, **475**, 94–107.

Kitzmann, D., Heng, K., Oreshenko, M., Grimm, S. L., Apai, D., Bowler, B. P., Burgasser, A. J., & Marley, M. S., 2020. Helios-r2: A new bayesian, open-source retrieval model for brown dwarfs and exoplanet atmospheres, *ApJ*, **890**, 174.

Kitzmann, D., Stock, J. W., & Patzer, A. B. C., 2023. fastchem-cond: equilibrium chemistry with condensation and rainout for cool planetary and stellar environments, *MNRAS*, **527**, 7263–7283.

Knabe, K., Williams, P. A., Giorgetta, F. R., Radunsky, M. B., Armacost, C. M., Crivello, S., & Newbury, N. R., 2013. Absolute spectroscopy of N_2O near 4.5 μm with a comb-calibrated, frequency-swept quantum cascade laser spectrometer, *Opt. Express*, **21**, 1020–1029.

Kochanov, R. V., Gordon, I. E., Rothman, L. S., Wcisło, P., Hill, C., & Wilzewski, J. S., 2016. HITRAN Application Programming Interface (HAPI): A comprehensive approach to working with spectroscopic data, *J. Quant. Spectrosc. Radiat. Transf.*, **177**, 15–30.

Kochanov, R. V., Gordon, I. E., Rothman, L. S., Shine, K. P., Sharpe, S. W., Johnson, T. J., Wallington, T. J., Harrison, J. J., Bernath, P. F., Birk, M., Wagner, G., Le Bris, K., Bravo, I., & Hill, C., 2019. Infrared absorption cross-sections in HITRAN2016 and beyond: Expansion for climate, environment, and atmospheric applications, *J. Quant. Spectrosc. Radiat. Transf.*, **230**, 172–221.

Kocheril, P. A., Markus, C. R., Esposito, A. M., Schrader, A. W., Dieter, T. S., & McCall, B. J., 2018. Extended sub-Doppler resolution spectroscopy of the ν_3 band of methane, *J. Quant. Spectrosc. Radiat. Transf.*, **215**, 9–12.

Köhler, T., Mäder, H., & Nicolaisen, H.-W., 1995. Measurements of speed dependent relaxation rates using a microwave spectrometer with a circular waveguide. studies on nitrous oxide, *Mol. Phys.*, **86**, 287–300.

Köhler, T. M., Gail, H.-P., & Sedlmayr, E., 1997. Mgo dust nucleation in m-stars: calculation of cluster properties and nucleation rates., *A&A*, **320**, 553–567.

Köhn, C., Helling, C., Bødker Enghoff, M., Haynes, K., Sindel, J. P., Krog, D., & Gobrecht, D., 2021. Dust in brown dwarfs and extra-solar planets - VIII. TiO_2 seed formation: 3D monte carlo versus kinetic approach, *A&A*, **654**, A120.

Koike, C., Kaito, C., Yamamoto, T., Shibai, H., Kimura, S., & Suto, H., 1995. Extinction Spectra of Corundum in the Wavelengths from UV to FIR, *Icarus*, **114**, 203–214.

Kokaly, R. F., Clark, R. N., Swayze, G. A., Livo, K. E., Hoefen, T. M., Pearson, N. C., Wise, R. A., Benzel, W. M., Lowers, H. A., Driscoll, R. L., et al., 2017. Usgs spectral library version 7 data: Us geological survey data release, *United States Geological Survey (USGS): Reston, VA, USA*, **61**.

Koroleva, A. O., Kassi, S., Mondelain, D., & Campargue, A., 2023. The water vapor foreign continuum in the 8100-8500 cm^{-1} spectral range, *J. Quant. Spectrosc. Radiat. Transf.*, **296**, 108432.

Koroleva, A. O., Mikhailenko, S. N., Kassi, S., & Campargue, A., 2023. Frequency comb-referenced cavity ring-down spectroscopy of natural water between 8041 and 8633 cm^{-1}, *J. Quant. Spectrosc. Radiat. Transf.*, **298**, 108489.

Kowzan, G., Lee, K. F., Paradowska, M., Borkowski, M., Ablewski, P., Wojtewicz, S., Stec, K., Lisak, D., Fermann, M. E., Trawinski, R. S., & Maslowski, P., 2016. Self-referenced, accurate and sensitive optical frequency comb spectroscopy with a virtually imaged phased array spectrometer, *Opt. Letters*, **41**, 974–977.

Kowzan, G., Stec, K., Zaborowski, M., Wójtewicz, S., Cygan, A., Lisak, D., Masłowski, P., & Trawiński, R. S., 2017. Line positions, pressure broadening and shift coefficients for the second overtone transitions of carbon monoxide in argon, *J. Quant. Spectrosc. Radiat. Transf.*, **191**, 46–54.

Kowzan, G., Charczun, D., Cygan, A., Trawiński, R. S., Lisak, D., & Masłowski, P., 2019. Broadband Optical Cavity Mode Measurements at Hz-Level Precision With a Comb-Based VIPA

Spectrometer, *Sci. Rep.*, **9**, 8206.
Kramida, A., Ralchenko, Y., & Reader, J., 2013. NIST atomic spectra database – version 5, http://www.nist.gov/pml/data/asd.cfm.
Krenn, A. F., Lendl, M., Patel, J. A., Carone, L., et al., 2023. The geometric albedo of the hot Jupiter HD 189733b measured with CHEOPS, *A&A*, **672**, A24.
Krzempek, K., Tomaszewska, D., Gluszek, A., Martynkien, T., Mergo, P., Sotor, J., Foltynowicz, A., & Sobon, G., 2019. Stabilized all-fiber source for generation of tunable broadband fCEO-free mid-IR frequency comb in the 7–9 μm range, *Opt. Express*, **27**, 37435–37445.
Kuntz, M., 1997. A new implementation of the Humblicek algorithm for the calculation of the Voigt profile function, *J. Quant. Spectrosc. Radiat. Transf.*, **57**, 819–824.
Kurucz, R. L., 1995. The kurucz (smithsonian) atomic and molecular database, *Highlights of Astronomy*, **10**, 579–579.
Kurucz, R. L., 2011. Including all the lines, *Can. J. Phys.*, **89**, 417–428.
Kurucz, R. L., 2017. Including all the lines: data releases for spectra and opacities, *Can. J. Phys.*, **95**, 825–827.
Lafferty, W. J., Solodov, A. M., Weber, A., Olson, W. B., & Hartmann, J.-M., 1996. Infrared collision-induced absorption by n2 near 4.3μm for atmospheric applications: measurements and empiricalmodeling, *Appl. Opt.*, **35**, 5911–5917.
Lam, J., Amans, D., Dujardin, C., Ledoux, G., & Allouche, A.-R., 2015. Atomistic mechanisms for the nucleation of aluminum oxide nanoparticles, *J. Phys. Chem. A*, **119**, 8944–8949.
Lamperti, M., Gotti, R., Gatti, D., Shakfa, M. K., Cané, E., Tamassia, F., Schunemann, P., Laporta, P., Farooq, A., & Marangoni, M., 2020. Optical frequency metrology in the bending modes region, *Communications Physics*, **3**, 175.
Langford, S. R., Orr-Ewing, A. J., Morgan, R. A., Western, C. M., Ashfold, M. N. R., Rijkenberg, A., Scheper, C. R., Buma, W. J., & de Lange, C. A., 1998. The spectroscopy of high Rydberg states of ammonia, *JCP*, **108**(16), 6667–6680.
Langleben, J., Yurchenko, S. N., & Tennyson, J., 2019. ExoMol line list XXXIV: A Rovibrational Line List for Phosphinidene (PH) in its $X\,^3\Sigma^-$ and $a\,^1\Delta$ Electronic States, *MNRAS*, **488**, 2332.
Lavrentieva, N. N. & Dudaryonok, A. S., 2020. OCS-CO_2 line broadening coefficients and their temperature dependences for the Earth and Venus atmospheres, *Icarus*, **336**, 113452.
Lavvas, P. & Koskinen, T., 2017. Aerosol properties of the atmospheres of extrasolar giant planets, *AJ.*, **847**, 32.
Leconte, J., 2021. Spectral binning of precomputed correlated-k coefficients, *A&A*, **645**, A20.
Lecoq-Molinos, H., Gobrecht, D., Sindel, J. P., Helling, C., & Decin, L., 2024. Vanadium oxide clusters in substellar atmospheres: A quantum chemical study, *arXiv e-prints*, p. arXiv:2401.02784.
Lee, E., Helling, C., Giles, H., & Bromley, S. T., 2015. Dust in brown dwarfs and extra-solar planets. IV. Assessing TiO_2 and SiO nucleation for cloud formation modelling, *A&A*, **575**, A11.
Lee, E. K. H., Parmentier, V., Hammond, M., Grimm, S. L., Kitzmann, D., Tan, X., Tsai, S.-M., & Pierrehumbert, R. T., 2021. Simulating gas giant exoplanet atmospheres with Exo-FMS: comparing semigrey, picket fence, and correlated-k radiative-transfer schemes, *MNRAS*, **506**, 2695–2711.
Lefebvre-Brion, H. & Field, R. W., 2004. *Perturbations in the spectra of diatomic molecules: Revised and Enlarged Edition*, Elsevier B.V, P.O. Box 211, 1000AE Amsterdam, the Netherlands.
Lemaire, J. L., Heays, A. N., Eidelsberg, M., Gavilan, L., Stark, G., Federman, S. R., Lyons, J. R., & de Oliveira, N., 2018. Atlas of new and revised high-resolution spectroscopy of six CO isotopologues in the 101-115 nm range - Transition energies of the $v' = 0$, 1, 2, and 3 to $v'' = 0$ bands of the B $^1\Sigma^+$, C $^1\Sigma^+$ and E $^1\Pi$ to X $^1\Sigma^+$ states, related term values, and molecular constants, *A&A*, **614**, A114.
Lew, B. W. P., Roellig, T., Batalha, N. E., Line, M., et al., 2024. High-precision atmospheric characterization of a Y dwarf with JWST NIRSpec G395H spectroscopy: isotopologue, C/O ratio, metallicity, and the abundances of six molecular species.
Lewis, N. K., Wakeford, H. R., MacDonald, R. J., Goyal, J. M., et al., 2020. Into the UV: The atmosphere of the hot Jupiter HAT-P-41b revealed, *ApJL*, **902**, L19.
Li, G., Gordon, I. E., Hajigeorgiou, P. G., Coxon, J. A., & Rothman, L. S., 2013. Reference spectroscopic data for hydrogen halides, Part II: The line lists, *J. Quant. Spectrosc. Radiat. Transf.*, **130**, 284–295.
Li, G., Gordon, I. E., Rothman, L. S., Tan, Y., Hu, S.-M., Kassi, S., Campargue, A., & Medvedev, E. S., 2015. Rovibrational line lists for nine isotopologues of the CO molecule in the $X\,^1\Sigma^+$ ground electronic state, *ApJS*, **216**, 15.
Li, H.-Y., Tennyson, J., & Yurchenko, S. N., 2019. ExoMol molecular line lists XXXII: the rovibronic spectrum of MgO, *MNRAS*, **486**, 2351–2365.
Li, X., Qin, Z., & Liu, L., 2024. High-temperature molecular line list of hydroboron monoxide (hbo), *Phys. Chem. Chem. Phys.*, **26**, 12838–12843.
Lietzow, M. & Wolf, S., 2022. Polarimetric investigation of selected cloud compositions in exoplanetary atmospheres, *A&A*, **663**, A55.
Lindholm, E., 1945. The broadening of na lines by argon, *Arkiv Mat. Astron. Fysic*, **32**, 17.
Linsky, J. L., 1969. On the Pressure-Induced Opacity of Molecular Hydrogen in Late-Type Stars, *ApJ*, **156**, 989–1005.
Liu, G. L., Wang, J., Tan, Y., Kang, P., Bi, Z., Liu, A. W., & Hu, S. M., 2019. Line positions and N_2-induced line parameters of the 00^03–00^00 band of $^{14}N_2{}^{16}O$ by comb-assisted cavity ring-down spectroscopy, *J. Quant. Spectrosc. Radiat. Transf.*, **229**, 17–22.
Livingston Large, T. A. & Kliewer, C. J., 2024. Sensitive detection and imaging of H_2O density through Rydberg resonant femtosecond laser induced photofragmentation fluorescence, *J. Chem. Phys.*, **160**, 201102.
Lodge, M. G., Wakeford, H. R., & Leinhardt, Z. M., 2023. Aerosols are not spherical cows: using discrete dipole approximation to model the properties of fractal particles, *MNRAS*, **527**, 11113–11137.
Lodi, L., Yurchenko, S. N., & Tennyson, J., 2015. The calculated rovibronic spectrum of scandium hydride, ScH, *Mol. Phys.*, **113**, 1559–1575.
Loeb, A., 2010. *How did the first stars and galaxies form?*, Princeton University Press.
Lombardo, N. A., Nixon, C. A., Greathouse, T. K., Bézard, B., Jolly, A., Vinatier, S., Teanby, N. A., Richter, M. J., Irwin, P. J. G., Coustenis, A., & Flasar, F. M., 2019. Detection of propadiene on Titan, *ApJL*, **881**, L33.
López-Puertas, M., Dinelli, B. M., Adriani, A., Funke, B., García-Comas, M., Moriconi, M. L., D'Aversa, E., Boersma, C., & Allamandola, L. J., 2013. Large abundances of polycyclic aromatic hydrocarbons in Titan's upper atmosphere, *ApJ*, **770**, 132.
López-Puertas, M., nés Rodríguez, P. M., Pallé, E., Höpfner, M., Sánchez-López, A., García-Comas, M., & Funke, B., 2018. Aerosols and Water Ice in Jupiter's Stratosphere from UV-NIR Ground-based Observations, *AJ.*, **156**, 169.
Lu, Z., Chang, Y. C., Gao, H., Benitez, Y., Song, Y., Ng, C. Y., & Jackson, W. M., 2014. Communication: Direct measurements of nascent O(3P0,1,2) fine-structure distributions and branching ratios of correlated spin-orbit resolved product channels CO $(\tilde{a}^3\Pi; v)$ + O $(^3P_{0,1,2})$ and CO$(\tilde{X}^1\Sigma^+\tilde{X}^1\Sigma^+; v)$ + O$(^3P_{0,1,2})$ in VUV photodissociation of CO_2, *J. Chem. Phys.*, **140**, 231101.
Luo, P.-L., 2020. Long-wave mid-infrared time-resolved dual-comb spectroscopy of short-lived intermediates, *Opt. Lett.*, **45**, 6791–6794.
Lynas-Gray, A. E., Polyansky, O. L., Tennyson, J., Yurchenko, S. N., & Zobov, N. F., 2024. ExoMol Line Lists – LXII: Ro-Vibrational Energy Levels and Line-Strengths for the Propadienediylidene (C_3) electronic Ground-State, *MNRAS*.
Lynch, R., Gamache, R., & Neshyba, S., 1996. Fully complex implementation of the Robert–Bonamy formalism: Half widths

and line shifts of H_2O broadened by N_2, *J. Chem. Phys.*, **105**, 5711–5721.

Ma, Q., Tipping, R. H., & Boulet, C., 2007. Modification of the robert-bonamy formalism in calculating lorentzian half-widths and shifts, *J. Quant. Spectrosc. Radiat. Transf.*, **103**, 588–596.

Ma, Q., Boulet, C., & Tipping, R. H., 2013. Refinement of the Robert-Bonamy formalism: Considering effects from the line coupling, *J. Chem. Phys.*, **139**, 034305.

Ma, S., Ito, Y., Al-Refaie, A. F., Changeat, Q., Edwards, B., & Tinetti, G., 2023. Yunma: Enabling spectral retrievals of exoplanetary clouds, *AJ.*, **957**, 104.

MacDonald, R. J., 2023. POSEIDON: A Multidimensional Atmospheric Retrieval Code for Exoplanet Spectra, *JOSS*, **8**, 4873.

MacDonald, R. J. & Batalha, N. E., 2023. A catalog of exoplanet atmospheric retrieval codes, *RNAAS*, **7**, 54.

Mackowski, D. W. & Mishchenko, M. I., 1996. Calculation of the T matrix and the scattering matrix for ensembles of spheres, *J. Opt. Soc. Am. A*, **13**, 2266–2278.

Madhusudhan, N., Sarkar, S., Constantinou, S., Holmberg, M., Piette, A. A. A., & Moses, J. I., 2023. Carbon-bearing Molecules in a Possible Hycean Atmosphere, *ApJL*, **956**, L13.

Mahapatra, G., Helling, C., & Miguel, Y., 2017. Cloud formation in metal-rich atmospheres of hot super-Earths like 55 Cnc e and CoRoT7b, *MNRAS*, **472**, 447–464.

Malarich, N. A., Yun, D., Sung, K., Egbert, S., Coburn, S. C., Drouin, B. J., & Rieker, G. B., 2021. Dual frequency comb absorption spectroscopy of CH4 up to 1000 Kelvin from 6770 to 7570 cm^{-1}, *J. Quant. Spectrosc. Radiat. Transf.*, **272**, 107812.

Malaterre, C., ten Kate, I. L., Baqué, M., Debaille, V., Grenfell, J. L., Javaux, E. J., Khawaja, N., Klenner, F., Lara, Y. J., McMahon, S., Moore, K., Noack, L., Patty, C. L., & Postberg, F., 2023. Is there such a thing as a biosignature?, *Astrobiology*, **23**, 1213–1227, PMID: 37962841.

Malik, M., Grosheintz, L., Mendonça, J. M., Grimm, S. L., Lavie, B., Kitzmann, D., Tsai, S.-M., Burrows, A., Kreidberg, L., Bedell, M., Bean, J. L., Stevenson, K. B., & Heng, K., 2017. HELIOS: An Open-Source, GPU-Accelerated Radiative Transfer Code For Self-Consistent Exoplanetary Atmospheres, *ApJ*, **153**, 56.

Malloci, G., Joblin, C., & Mulas, G., 2007. On-line database of the spectral properties of polycyclic aromatic hydrocarbons, *Chem. Phys.*, **332**, 353–359.

Mant, B. P., Yachmenev, A., Tennyson, J., & Yurchenko, S. N., 2018. ExoMol molecular line lists - XXVII: spectra of C_2H_4, *MNRAS*, **478**, 3220 – 3232.

Mant, B. P., Chubb, K. L., Yachmenev, A., Tennyson, J., & Yurchenko, S. N., 2019. The Infrared Spectrum of PF_3 and the Analysis of Rotational Energy Clustering Effect, *Mol. Phys.*, **118**, e1581951.

Margenau, H., 1935. Theory of pressure effects of foreign gases on spectral lines, *Phys. Rev.*, **48**, 755–764.

Margenau, H., 1936. Note on pressure effects in band spectra, *Phys. Rev.*, **49**, 596–597.

Markus, C. R., Kocheril, P. A., & McCall, B. J., 2019. Sub-Doppler rovibrational spectroscopy of the ν_1 fundamental band of D_2H^+, *J. Mol. Spectrosc.*, **355**, 8–13.

Martin-Drumel, M.-A., Zhang, Q., Doney, K. D., Pirali, O., Vervloet, M., Tokaryk, D., Western, C., Linnartz, H., Chen, Y., & Zhao, D., 2023. The bending of C_3: Experimentally probing the l-type doubling and resonance, *J. Mol. Spectrosc.*, **391**, 111734.

Maslowski, P., Lee, K. F., Johansson, A. C., Khodabakhsh, A., Kowzan, G., Rutkowski, L., Mills, A. A., Mohr, C., Jiang, J., Fermann, M. E., & Foltynowicz, A., 2016. Surpassing the path-limited resolution of Fourier-transform spectrometry with frequency combs, *Phys. Rev. A*, **93**, 021802(R).

Masseron, T., Plez, B., Van Eck, S., Colin, R., Daoutidis, I., Godefroid, M., Coheur, P.-F., Bernath, P., Jorissen, A., & Christlieb, N., 2014. CH in stellar atmospheres: an extensive linelist, *A&A*, **571**, A47.

Maté, B., Lugez, C., Fraser, G. T., & Lafferty, W. J., 1999. Absolute intensities for the O_2 1.27μm continuum absorption, *JGR-Atm*, **104**, 30585–30590.

Mattioda, A. L., Hudgins, D. M., Boersma, C., Bauschlicher, C. W., Ricca, A., Cami, J., Peeters, E., de Armas, F. S., Saborido, G. P., & Allamandola, L. J., 2020. The NASA Ames PAH IR spectroscopic database: The laboratory spectra, *ApJS*, **251**, 22.

Mayor, M. & Queloz, D., 1995. A Jupiter-mass companion to a solar-type star, *Nature*, **378**, 355–359.

McElroy, M. B. & Donahue, T. M., 1972. Stability of the Martian atmosphere, *Science*, **177**, 986–988.

McKellar, A. R. W., 1988. Experimental Verification of Hydrogen Dimers in the Atmospheres of Jupiter and Saturn from Voyager IRIS Far-Infrared Spectra, *ApJL*, **326**, L75.

McKellar, A. R. W., 1989. Low-temperature infrared absorption of gaseous N_2 and $N_2 + H_2$ in the 2.0-2.5 μm region: Application to the atmospheres of Titan and Triton, *Icarus*, **80**, 361–369.

McKemmish, L. K., Yurchenko, S. N., & Tennyson, J., 2016. ExoMol line lists – XVIII. The high-temperature spectrum of VO, *MNRAS*, **463**, 771–793.

McKemmish, L. K., Masseron, T., Sheppard, S., Sandeman, E., Schofield, Z., Furtenbacher, T., Császár, A. G., Tennyson, J., & Sousa-Silva, C., 2017. MARVEL analysis of the measured high-resolution rovibronic spectra of $^{48}Ti^{16}O$, *ApJS*, **228**, 15.

McKemmish, L. K., Masseron, T., Hoeijmakers, J., Pérez-Mesa, V. V., Grimm, S. L., Yurchenko, S. N., & Tennyson, J., 2019. ExoMol Molecular line lists – XXXIII. The spectrum of Titanium Oxide, *MNRAS*, **488**, 2836–2854.

McKemmish, L. K., Syme, A. M., Borsovszky, J., Yurchenko, S. N., Tennyson, J., Furtenbacher, T., & Császár, A. G., 2020. An update to the MARVEL dataset and ExoMol line list for $^{12}C_2$, *MNRAS*, **497**, 1081–1097.

McKemmish, L. K., Bowesman, C. A., Kefala, K., Perri, A. N., Syme, A. M., Yurchenko, S. N., & Tennyson, J., 2024. A hybrid approach to generating diatomic line lists for high resolution studies of exoplanets and other hot astronomical objects: Updates to ExoMol MgO, VO and TiO line lists, *RASTI*.

Meerdink, S. K., Hook, S. J., Roberts, D. A., & Abbott, E. A., 2019. The ECOSTRESS spectral library version 1.0, *Remote Sensing of Environment*, **230**, 111196.

Melen, F., Grevesse, N., Sauval, A. J., Farmer, C. B., Norton, R. H., Bredohl, H., & Dubois, I., 1989. A new analysis of the vibration-rotation spectrum of CH from solar spectra, *J. Mol. Spectrosc.*, **134**, 305–313.

Melen, F., Sauval, A. J., Grevesse, N., Farmer, C. B., Servais, C., Delbouille, L., & Roland, G., 1995. A new analysis of the OH radical spectrum from solar infrared observations., *J. Mol. Spectrosc.*, **174**, 490–509.

Melin, S. T. & Sanders, S. T., 2018. H_2O absorption thermometry accuracy in the 7321-7598 cm^{-1} range studied in a heated static cell at temperatures up to 1723 K, *J. Quant. Spectrosc. Radiat. Transf.*, **214**, 1–7.

Melin, S. T., Sanders, S. T., & Nasir, E. F., 2020. Comparison of ExoMol simulated spectra for H_2O to high-temperature low-pressure gas cell measurements at 1723 K in the 7321-7598 cm−1 range, *J. Quant. Spectrosc. Radiat. Transf.*, **253**, 107079.

Mellor, T., Owens, A., Yurchenko, S. N., & Tennyson, J., 2022. ExoMol line lists – LI. Rvibronic molecular line list for thioformaldehyde (H_2CS), *MNRAS*, **520**, 1997–2008.

Melosso, M., Diouf, M. L., Bizzocchi, L., Harding, M. E., Cozijn, F. M. J., Puzzarini, C., & Ubachs, W., 2021. Hyperfine-resolved near-infrared spectra of $H_2{}^{17}O$, *J. Phys. Chem. A*, **125**, 7884–7890.

Menoux, V., Doucen, R. L., Boulet, C., Roblin, A., & Bouchardy, A. M., 1993. Collision-induced absorption in the fundamental band of N_2: temperature dependence of the absorption for N_2–N_2 and N_2–O_2 pairs, *Appl. Opt.*, **32**, 263–268.

Mikal-Evans, T., Sing, D. K., Barstow, J. K., Kataria, T., Goyal, J., Lewis, N., Taylor, J., Mayne, N. J., Daylan, T., Wakeford, H. R., Marley, M. S., & Spake, J. J., 2022. Diurnal variations in the stratosphere of the ultrahot giant exoplanet WASP-121b, *Nature Astronomy*, **6**, 471–479.

Miladi, M., Le Falher, J.-P., Roncin, J.-Y., & Damany, H., 1975. Pressure effects on the vibronic transitions of NH3 and NO, *J. Mol. Spectrosc.*, **55**, 81–87.

Miladi, M., Roncin, J.-Y., & Damany, H., 1978. Pressure induced configuration demixing in the electronic spectrum of NO, *J. Mol. Spectrosc.*, **69**, 260–280.

Millar, T. J., Walsh, C., Van de Sande, M., & Markwick, A. J., 2024. The UMIST Database for Astrochemistry 2022, *A&A*, **682**, A109.

Min, M., 2017. Random sampling technique for ultra-fast computations of molecular opacities for exoplanet atmospheres, *A&A*, **607**(A9), A9.

Min, M., Hovenier, J. W., & de Koter, A., 2005. Modeling optical properties of cosmic dust grains using a distribution of hollow spheres, *A&A*, **432**, 909–920.

Min, M., Ormel, C. W., Chubb, K., Helling, C., & Kawashima, Y., 2020. The ARCiS framework for Exoplanet Atmospheres: Modelling Philosophy and Retrieval, *A&A*, **642**, A28.

Mishchenko, M. I., Dlugach, J. M., & Liu, L., 2016. Applicability of the effective-medium approximation to heterogeneous aerosol particles, *J. Quant. Spectrosc. Radiat. Transf.*, **178**, 284–294.

Mitev, G. B., Taylor, S., Tennyson, J., Yurchenko, S. N., Buchachenko, A. A., & Stolyarov, A. V., 2022. ExoMol molecular line lists – XLIII: Rovibronic transitions corresponding to the close-lying X $^2\Pi$ and A $^2\Sigma^+$ states of NaO, *MNRAS*, **511**, 2349–2355.

Mitev, G. B., Yurchenko, S. N., & Tennyson, J., 2024. Predissociation dynamics of the hydroxyl radical (OH) based on a five-state spectroscopic model, *J. Chem. Phys.*, **160**, 144110.

Mizus, I. I., Alijah, A., Zobov, N. F., Kyuberis, A. A., Yurchenko, S. N., Tennyson, J., & Polyansky, O. L., 2017. ExoMol molecular line lists XX: a comprehensive line list for H_3^+, *MNRAS*, **468**, 1717–1725.

Mizus, I. I., Zobov, N. F., Pezzella, M., Boyarkin, O. V., Koshelev, M. A., Makarov, D. S., Yurchenko, S. N., Tennyson, J., & Polyansky, O. L., 2024. ExoMol Line Lists – LXIII: Ro-Vibrational Energy Levels and Line-Strengths HDO, *MNRAS*.

Mizushima, M., 1951. The theory of pressure broadening and its application to microwave spectra, *Phys. Rev.*, **83**, 94–103.

Mlawer, E. J., Payne, V. H., Moncet, J. L., Delamere, J. S., Alvarado, M. J., & Tobin, D. C., 2012. Development and recent evaluation of the MT_CKD model of continuum absorption, *Phil. Trans. Royal Soc. London A*, **370**, 2520–2556.

Mlawer, E. J., Turner, D. D., Paine, S. N., Palchetti, L., et al., 2019. Analysis of water vapor absorption in the far-infrared and submillimeter regions using surface radiometric measurements from extremely dry locations, *JGR-Atm*, **124**, 8134–8160.

Mlawer, E. J., Cady-Pereira, K. E., Mascio, J., & Gordon, I. E., 2023. The inclusion of the MT_CKD water vapor continuum model in the HITRAN molecular spectroscopic database, *J. Quant. Spectrosc. Radiat. Transf.*, **306**, 108645.

Mollière, P. & Snellen, I. A. G., 2019. Detecting isotopologues in exoplanet atmospheres using ground-based high-dispersion spectroscopy, *A&A*, **622**, A139.

Mollière, P., van Boekel, R., Bouwman, J., Henning, T., Lagage, P.-O., & Min, M., 2017. Observing transiting planets with JWST - prime targets and their synthetic spectral observations, *A&A*, **600**, A10.

Mollière, P., Wardenier, J. P., van Boekel, R., Henning, T., Molaverdikhani, K., & Snellen, I. A. G., 2019. petitRADTRANS - A Python radiative transfer package for exoplanet characterization and retrieval, *A&A*, **627**, A67.

Mondelain, D., Sala, T., Kassi, S., Romanini, D., Marangoni, M., & Campargue, A., 2015. Broadband and highly sensitive comb-assisted cavity ring down spectroscopy of CO near 1.57μm with sub-MHz frequency accuracy, *J. Quant. Spectrosc. Radiat. Transf.*, **154**, 35–43.

Mondelain, D., Kassi, S., & Campargue, A., 2019. Accurate Laboratory Measurement of the O_2 Collision-Induced Absorption Band Near 1.27 μm, *JGR-Atm*, **124**, 414–423.

Mondelain, D., Campargue, A., Fleurbaey, H., Kassi, S., & Vasilchenko, S., 2022. CRDS measurements of air-broadened lines in the 1.6 μm band of $^{12}CO_2$: Line shape parameters with their temperature dependence, *J. Quant. Spectrosc. Radiat. Transf.*, **288**, 108267.

Mondelain, D., Campargue, A., Fleurbaey, H., Kassi, S., & Vasilchenko, S., 2023. Line shape parameters of air-broadened $^{12}CO_2$ transitions in the 2.0 μm region, with their temperature dependence, *J. Quant. Spectrosc. Radiat. Transf.*, **298**, 108485.

Moos, H. W., McCandliss, S. R., & Kruk, J. W., 2004. FUSE: lessons learned for future FUV missions, in *UV and Gamma-Ray Space Telescope Systems*, vol. 5488, pp. 1 – 12, International Society for Optics and Photonics, SPIE.

Moran, S. E., Hörst, S. M., He, C., Radke, M. J., Sebree, J. A., Izenberg, N. R., Vuitton, V., Flandinet, L., Orthous-Daunay, F.-R., & Wolters, C., 2022. Triton haze analogs: The role of carbon monoxide in haze formation, *J. Geophys. Res.: Planets*, **127**, e2021JE006984.

Morley, C. V., Fortney, J. J., Marley, M. S., Visscher, C., Saumon, D., & Leggett, S. K., 2012. Neglected clouds in T and Y dwarf atmospheres, *ApJ*, **756**, 172.

Moses, J. I., Bézard, B., Lellouch, E., Gladstone, G., Feuchtgruber, H., & Allen, M., 2000. Photochemistry of Saturn's atmosphere: I. hydrocarbon chemistry and comparisons with ISO observations, *Icarus*, **143**, 244–298.

Moses, J. I., Fouchet, T., Bézard, B., Gladstone, G. R., Lellouch, E., & Feuchtgruber, H., 2005. Photochemistry and diffusion in Jupiter's stratosphere: Constraints from ISO observations and comparisons with other giant planets, *J. Geophys. Res.: Planets*, **110**, E08001.

Moses, J. I., Visscher, C., Keane, T. C., & Sperier, A., 2010. On the abundance of non-cometary HCN on Jupiter, *Faraday Discuss.*, **147**, 103–136.

Moses, J. I., Visscher, C., Fortney, J. J., Showman, A. P., Lewis, N. K., Griffith, C. A., Klippenstein, S. J., Shabram, M., Friedson, A. J., Marley, M. S., & Freedman, R. S., 2011. Disequilibrium Carbon, Oxygen, and Nitrogen Chemistry in the Atmospheres of HD 189733b and HD 209458b, *ApJ*, **737**, 15.

Moses, J. I., Fletcher, L. N., Greathouse, T. K., Orton, G. S., & Hue, V., 2018. Seasonal stratospheric photochemistry on Uranus and Neptune, *Icarus*, **307**, 124–145.

Mould, J. & Liebert, J., 1978. Infrared photometry and the atmospheric composition of cool white dwarfs, *ApJL*, **226**, L29–L33.

Mukherjee, S., Batalha, N. E., Fortney, J. J., & Marley, M. S., 2023. PICASO 3.0: A One-dimensional Climate Model for Giant Planets and Brown Dwarfs, *ApJ*, **942**, 71.

Muller, C., Michel, V., Scacchi, G., & Côme, G. M., 1995. THERGAS: a computer program for the evaluation of thermochemical data of molecules and free radicals in the gas phase, *J. Chem. Phys.*, **92**, 1154–1178.

Muñoz, A. G. & Isaak, K. G., 2015. Probing exoplanet clouds with optical phase curves, *Proc. Nat. Acad. Sci.*, **112**, 13461–13466.

Muñoz, A. G. & Schneider, P. C., 2019. Rapid escape of ultra-hot exoplanet atmospheres driven by hydrogen balmer absorption, *ApJL*, **884**, L43.

Muñoz, O., Moreno, F., Guirado, D., Dabrowska, D. D., Volten, H., & Hovenier, J. W., 2012. The Amsterdam–Granada Light Scattering Database, *J. Quant. Spectrosc. Radiat. Transf.*, **113**, 565–574.

Muraviev, A. V., Konnov, D., & Vodopyanov, K. L., 2020. Broadband high-resolution molecular spectroscopy with interleaved mid-infrared frequency combs, *Sci. Rep.*, **10**, 18700.

Nahon, L., de Oliveira, N., Garcia, G. A., Gil, J.-F., Pilette, B., Marcouille, O., Lagarde, B., & Polack, F., 2012. DESIRS: a state-of-the-art VUV beamline featuring high resolution and variable polarization for spectroscopy and dichroism at SOLEIL, *J. Synchrotron Radiat.*, **19**, 508–520.

Nassar, R. & Bernath, P., 2003. Hot methane spectra for astrophysical applications, *J. Quant. Spectrosc. Radiat. Transf.*, **82**, 279–292.

Ndengué, S., Quintas-Sánchez, E., Dawes, R., Blackstone, C. C., & Osborn, D. L., 2023. Temperature dependence of the electronic absorption spectrum of NO_2, *J. Phys. Chem. A*, **127**, 6051–6062.

Nikolaou, N., Waldmann, I. P., Tsiaras, A., Morvan, M., et al., 2023. Lessons learned from the 1st Ariel Machine Learning Challenge: Correcting transiting exoplanet light curves for stellar spots, *RASTI*, **2**, 695–709.

Niraula, P., de Wit, J., Gordon, I. E., Hargreaves, R. J., Sousa-Silva, C., & Kochanov, R. V., 2022. The impending opacity challenge in exoplanet atmospheric characterization, *Nature Astronomy*, **6**, 1287–1295.

Niraula, P., de Wit, J., Gordon, I. E., Hargreaves, R. J., & Sousa-Silva, C., 2023. Origin and Extent of the Opacity Challenge for Atmospheric Retrievals of WASP-39 b, *ApJL*, **950**, L17.

Nishiyama, A., Kowzan, G., Charczun, D., Ciuryło, R., Coluccelli, N., & Masłowski, P., 2024. Line-shape study of CO perturbed by N_2 with mid-infrared frequency comb-based Fourier-transform spectroscopy, *Measurement*, **227**, 114273.

Nixon, C. A., Jennings, D. E., Bézard, B., Vinatier, S., Teanby, N. A., Sung, K., Ansty, T. M., Irwin, P. G. J., Gorius, N., Cottini, V., Coustenis, A., & Flasar, F. M., 2013. Detection of propene Titan's stratosphere, *ApJL*, **776**, L14.

Nuth-III, J. A. & Ferguson, F. T., 2006. Silicates do nucleate in oxygen-rich circumstellar outflows: New vapor pressure data for SiO, *ApJ*, **649**, 1178.

Odintsova, T. A., Tretyakov, M. Y., Simonova, A. A., Ptashnik, I. V., Pirali, O., & Campargue, A., 2020. Measurement and temperature dependence of the water vapor self-continuum between 70 and 700 cm^{-1}, *Journal of Molecular Structure*, **1210**, 128046.

Odintsova, T. A., Serov, E. A., Balashov, A. A., Koshelev, M. A., Koroleva, A. O., Simonova, A. A., Tretyakov, M. Y., Filippov, N. N., Chistikov, D. N., Finenko, A. A., Lokshtanov, S. E., Petrov, S. V., & Vigasin, A. A., 2021. CO_2-CO_2 and CO_2-Ar continua at millimeter wavelengths, *J. Quant. Spectrosc. Radiat. Transf.*, **258**, 107400.

Okubo, S., Nakayama, H., Iwakuni, K., Inaba, H., & Sasada, H., 2011. Absolute frequency list of the v3-band transitions of methane at a relative uncertainty level of 10(-11), *Optics Express*, **19**, 23878–23888.

Orlando, J. J., Tyndall, G. S., Nickerson, K. E., & Calvert, J. G., 1991. The temperature dependence of collision-induced absorption by oxygen near 6 μm, *JGR-Atm*, **96**(D11), 20755–20760.

Ormel, C. W. & Min, M., 2019. ARCiS framework for exoplanet atmospheres - the cloud transport model, *A&A*, **622**, A121.

Owens, A. & Yurchenko, S. N., 2019. Theoretical rotation-vibration spectroscopy of cis- and trans-diphosphene (P_2H_2) and the deuterated species P_2HD, *J. Chem. Phys.*, **150**, 194308.

Owens, A., Yurchenko, S. N., Yachmenev, A., Thiel, W., & Tennyson, J., 2017. ExoMol molecular line lists XXII. The rotation-vibration spectrum of silane up to 1200 K, *MNRAS*, **471**, 5025–5032.

Owens, A., Yachmenev, A., Küpper, J., Yurchenko, S. N., & Thiel, W., 2018a. The rotation–vibration spectrum of methyl fluoride from first principles, *Phys. Chem. Chem. Phys.*, **21**, 3496–3505.

Owens, A., Yachmenev, A., Tennyson, J., Thiel, W., & Yurchenko, S. N., 2018b. ExoMol Molecular line lists XXIX: The rotation-vibration spectrum of methyl chloride up to 1200 K, *MNRAS*, **479**, 3002–3010.

Owens, A., Conway, E. K., Tennyson, J., & Yurchenko, S. N., 2020. ExoMol Molecular linelists – XXXVIII: High-temperature molecular line list of silicon dioxide (SiO_2), *MNRAS*, **495**, 1927–1933.

Owens, A., Tennyson, J., & Yurchenko, S. N., 2021. ExoMol line lists - XLI. High-temperature molecular line lists for the alkali metal hydroxides KOH and NaOH, *MNRAS*, **502**, 1128–1135.

Owens, A., Dooley, S., McLaughlin, L., Tan, B., Zhang, G., Yurchenko, S. N., & Tennyson, J., 2022a. ExoMol line lists – XLV. Rovibronic molecular line lists of calcium monohydride (CaH) and magnesium monohydride (MgH), *MNRAS*, **511**, 5448–5461.

Owens, A., Mitrushchenkov, A., Yurchenko, S. N., & Tennyson, J., 2022b. ExoMol line lists - XLVII. Rovibronic molecular line list of the calcium monohydroxide radical (CaOH), *MNRAS*, **516**, 3995–4002.

Owens, A., He, T., Hanicinec, M., Hill, C., Mohr, S., & Tennyson, J., 2023. LiDB: Database of molecular vibronic state radiative lifetimes for plasma processes, *Plasma Sources Sci. Technol.*, **32**, 085015.

Owens, A., , Yurchenko, S. N., & Tennyson, J., 2024a. ExoMol line lists - LVIII. High-temperature molecular line list of carbonyl sulphide (OCS), *MNRAS*, **530**, 4004–4015.

Owens, A., Wright, S. O. M., Pavlenko, Y., Mitrushchenkov, A., Koput, J., Yurchenko, S. N., & Tennyson, J., 2024b. ExoMol line lists - LI. Molecular line list for lithium hydroxide (LiOH), *MNRAS*, **527**, 731–738.

Palik, E. D., 2012. *Handbook of Optical Constants of Solids: Vol 2*, Academic Press.

Pannier, E. & Laux, C. O., 2019. RADIS: A nonequilibrium line-by-line radiative code for CO_2 and HITRAN-like database species, *J. Quant. Spectrosc. Radiat. Transf.*, **222-223**, 12–25.

Pastorek, A., Clark, V. H., Yurchenko, S. N., & Civiš, S., 2022. Time-Resolved Fourier Transform Infrared Emission Spectroscopy of NH Radical in the X $^3\Sigma^-$ Ground State, *J. Quant. Spectrosc. Radiat. Transf.*, **291**, 108332.

Patrascu, A. T., Tennyson, J., & Yurchenko, S. N., 2015. ExoMol molecular linelists - IX: The spectrum of AlO, *MNRAS*, **449**, 3613–3619.

Patzer, A. B. C., Chang, C., Sedlmayr, E., & Sülzle, D., 2005. A density functional study of small Al_xO_y (x, $y = 1 - 4$) clusters and their thermodynamic properties, *Eur. Phys. J. D*, **32**, 329–337.

Paulose, G., Barton, E. J., Yurchenko, S. N., & Tennyson, J., 2015. ExoMol Molecular linelists – XII. Line lists for eight isotopologues of CS, *MNRAS*, **454**, 1931–1939.

Pavlenko, Y. V., Yurchenko, S. N., McKemmish, L. K., & Tennyson, J., 2020a. Analysis of the TiO isotopologues in stellar optical spectra, *A&A*, **42**, A77.

Pavlenko, Y. V., Yurchenko, S. N., & Tennyson, J., 2020b. Analysis of first overtone bands of isotopologues of CO and SiO in stellar spectra, *A&A*, **633**, A52.

Pavlyuchko, A. I., Yurchenko, S. N., & Tennyson, J., 2015. ExoMol line lists XI: A Hot Line List for nitric acid, *MNRAS*, **452**, 1702–1706.

Peach, G., Yurchenko, S., Chubb, K., Baraffe, I., Phillips, M., & Tremblin, P., 2020. The resonance lines of sodium and potassium in brown dwarf spectra, *Contributions of the Astronomical Observatory Skalnaté Pleso*, **50**, 193–202.

Pearce, O., Yurchenko, S. N., & Tennyson, J., 2024. ExoMol line lists – LII. Line Lists for the Methylidyne Cation (CH^+), *MNRAS*, **527**, 10726–10736.

Perri, A. N. & McKemmish, L. K., 2024. Full spectroscopic model and trihybrid experimental-perturbative-variational line list for NH, *MNRAS*, **531**, 3023–3033.

Perri, A. N., Taher, F., & McKemmish, L. K., 2023. Full spectroscopic model and trihybrid experimental-perturbative-variational line list for ZrO, *MNRAS*, **524**, 4631–4641.

Petera, L., Knížek, A., Laitl, V., & Ferus, M., 2023. Decomposition of benzene during impacts in N_2-dominated atmospheres, *ApJ*, **945**, 149.

Pezzella, M., Yurchenko, S. N., & Tennyson, J., 2021. A method for calculating temperature-dependent photodissociation cross sections and rates, *Phys. Chem. Chem. Phys.*, **23**, 16390–16400.

Pezzella, M., Tennyson, J., & Yurchenko, S. N., 2022. ExoMol photodissociation cross-sections - I. HCl and HF, *MNRAS*, **514**, 4413–4425.

Phebus, B. D., Johnson, A. V., Mar, B., Stone, B. M., Colaprete, A., & Iraci, L. T., 2011. Water ice nucleation characteristics of JSC Mars-1 regolith simulant under simulated Martian atmospheric conditions, *J. Geophys. Res.: Planets*, **116**, E4.

Pickett, H. M., 1980. Effects of velocity avaraging on the shapes of

absorption lines, *J. Chem. Phys.*, **73**, 6090–6094.
Pierrehumbert, R. & Gaidos, E., 2011. Hydrogen Greenhouse Planets Beyond the Habitable Zone, *ApJS*, **734**, L13.
Pinhas, A. & Madhusudhan, N., 2017. On signatures of clouds in exoplanetary transit spectra, *MNRAS*, **471**, 4355–4373.
Pinkowski, N. H., Cassady, S. J., Strand, C. L., & Hanson, R. K., 2021. Quantum-cascade-laser-based dual-comb thermometry and speciation at high temperatures, *Meas. Sci. Technol.*, **32**, 035501.
Pollack, J. B., Hollenbach, D., Beckwith, S., Simonelli, D. P., Roush, T., & Fong, W., 1994. Composition and Radiative Properties of Grains in Molecular Clouds and Accretion Disks, *ApJ*, **421**, 615.
Polyanskiy, M. N., 2024. Refractiveindex.info database of optical constants, *Sci. Data*, **11**, 94.
Polyansky, O. L., Zobov, N. F., Viti, S., Tennyson, J., Bernath, P. F., & Wallace, L., 1997. Water on the Sun: line assignments based on variational calculations., *Science*, **277**, 346–348.
Polyansky, O. L., Kyuberis, A. A., Lodi, L., Tennyson, J., Ovsyannikov, R. I., & Zobov, N., 2017. ExoMol molecular line lists XIX: high accuracy computed line lists for $H_2{}^{17}O$ and $H_2{}^{18}O$, *MNRAS*, **466**, 1363–1371.
Polyansky, O. L., Kyuberis, A. A., Zobov, N. F., Tennyson, J., Yurchenko, S. N., & Lodi, L., 2018. ExoMol molecular line lists XXX: a complete high-accuracy line list for water, *MNRAS*, **480**, 2597–2608.
Postberg, F., Kempf, S., Schmidt, J., Brilliantov, N., Beinsen, A., Abel, B., Buck, U., & Srama, R., 2009. Sodium salts in E-ring ice grains from an ocean below the surface of Enceladus, *Nature*, **459**, 1098–1101.
Powell, D., Zhang, X., Gao, P., & Parmentier, V., 2018. Formation of Silicate and Titanium Clouds on Hot Jupiters, *ApJ*, **860**, 18.
Powell, D., Feinstein, A. D., Lee, E. K. H., Zhang, M., Tsai, S.-M., et al., 2024. Sulfur dioxide in the mid-infrared transmission spectrum of WASP-39b, *Nature*, **626**, 979–983.
Prajapat, L., Jagoda, P., Lodi, L., Gorman, M. N., Yurchenko, S. N., & Tennyson, J., 2017. ExoMol molecular line lists XXIII. Spectra of PO and PS, *MNRAS*, **472**, 3648–3658.
Pranjal, P., González-Vázquez, J., Bello, R. Y., & Martín, F., 2024. Resonant photoionization of CO_2 up to the fourth ionization threshold, *J. Phys. Chem. A*, **128**, 182–190.
Prlj, A., Ibele, L. M., Marsili, E., & Curchod, B. F. E., 2020. On the theoretical determination of photolysis properties for atmospheric volatile organic compounds, *J. Phys. Chem. Lett.*, **11**, 5418–5425.
Prlj, A., Marsili, E., Hutton, L., Hollas, D., Shchepanovska, D., Glowacki, D. R., Slavíček, P., & Curchod, B. F. E., 2022. Calculating photoabsorption cross-sections for atmospheric volatile organic compounds, *ACS Earth Space Chem.*, **6**, 207–217.
Ptashnik, I. V., McPheat, R. A., Shine, K. P., Smith, K. M., & Williams, R. G., 2011a. Water vapor self-continuum absorption in near-infrared windows derived from laboratory measurements, *JGR-Atm*, **116**, D16305,.
Ptashnik, I. V., Shine, K. P., & Vigasin, A. A., 2011b. Water vapour self-continuum and water dimers: 1. analysis of recent work, *J. Quant. Spectrosc. Radiat. Transf.*, **112**, 1286–1303.
PyValem, 2024. Pyvalem: a python package for parsing, validating, manipulating and interpreting the chemical formulas, quantum states and labels of atoms, ions and small molecules, https://github.com/xnx/pyvalem.
Qu, Q., Yurchenko, S. N., & Tennyson, J., 2021. ExoMol molecular line lists – XLII: Rovibronic molecular line list for the low-lying states of NO, *MNRAS*, **504**, 5768–5777.
Querry, M. R. & Wieliczka, D. M., 1988. Optical properties of selected minerals, metals, optical materials, soot, and liquids, in *DTIC ADA205188: Proceedings of the 1987 Scientific Conference on Obscuration and Aerosol Research*, vol. 180 of **Chemical Research, Development & Engineering Center**, pp. 117–128.
Rackham, B. V., Espinoza, N., Berdyugina, S. V., et al., 2023. The effect of stellar contamination on low-resolution transmission spectroscopy: needs identified by NASA's Exoplanet Exploration Program Study Analysis Group 21, *RAS Techniques and Instruments*, **2**, 148–206.
Ram, R. S. & Bernath, P. F., 2010. Revised molecular constants and term values for the $X\ ^3\Sigma^-$ and $A\ ^3\Pi$ states of NH, *J. Mol. Spectrosc.*, **260**, 115–119.
Ram, R. S., Brooke, J. S. A., Western, C. M., & Bernath, P. F., 2014. Einstein A-values and oscillator strengths of the $A\ ^2\Pi$ – $X\ ^2\Sigma^+$ system of CP, *J. Quant. Spectrosc. Radiat. Transf.*, **138**, 107–115.
Ramirez, R. M. & Kaltenegger, L., 2017. A Volcanic Hydrogen Habitable Zone, *ApJL*, **837**, L4.
Ranjan, S., Schwieterman, E. W., Harman, C., Fateev, A., Sousa-Silva, C., Seager, S., & Hu, R., 2020. Photochemistry of Anoxic Abiotic Habitable Planet Atmospheres: Impact of New H_2O Cross Sections, *ApJ*, **896**, 148.
Rautian, S. G. & Sobel'man, I. I., 1966. The effect of collisions on the doppler broadening of spectral lines, *Usp. Fiz. Nauk*, **90**, 209–236.
Rautian, S. G. & Sobel'man, I. I., 1967. The effect of collisions on the doppler broadening of spectral lines, *Sov. Phys. Usp.*, **9**, 701–716.
Reed, Z. D., Drouin, B. J., Long, D. A., & Hodges, J. T., 2021. Molecular transition frequencies of CO_2 near 1.6 μm with kHz-level uncertainties, *J. Quant. Spectrosc. Radiat. Transf.*, **271**, 107681.
Rees, M. J., 1976. Opacity-Limited Hierarchical Fragmentation and the Masses of Protostars, *MNRAS*, **176**, 483–486.
Régalia, L., Cousin, E., Gamache, R. R., Vispoel, B., Robert, S., & Thomas, X., 2019. Laboratory measurements and calculations of line shape parameters of the H_2O–CO_2 collision system, *J. Quant. Spectrosc. Radiat. Transf.*, **231**, 126–135.
Rengel, M., 2024. About the atomic and molecular databases in the planetary community - A contribution in the Laboratory Astrophysics Data WG IAU 2022 GA session, *IAU Symposium*, **371**, 87–91.
Rengel, M. & Adamczewski, J., 2023. Radiative transfer and inversion codes for characterizing planetary atmospheres: an overview, *Front. Astron. Space Sci.*, **10**.
Rey, M., 2022. Novel methodology for systematically constructing global effective models from ab initio based-surfaces: a new insight into high-resolution molecular spectra analysis, *J. Chem. Phys.*, **156**, 224103.
Rey, M., Nikitin, A. V., & Tyuterev, V. G., 2014a. Theoretical hot methane line list up T=2000 K for astrophysical applications, *ApJ*, **789**, 2.
Rey, M., Nikitin, A. V., & Tyuterev, V. G., 2014b. Accurate first-principles calculations for $^{12}CH_3D$ infrared spectra from isotopic and symmetry transformations, *J. Chem. Phys.*, **141**, 044316.
Rey, M., Delahaye, T., Nikitin, A. V., & Tyuterev, V. G., 2016a. First theoretical global line lists of ethylene ($^{12}C_2H_4$) spectra for the temperature range 50-700 K in the far-infrared for quantification of absorption and emission in planetary atmospheres, *A&A*, **594**, A47.
Rey, M., Nikitin, A. V., Babikov, Y. L., & Tyuterev, V. G., 2016b. TheoReTS – an information system for theoretical spectra based on variational predictions from molecular potential energy and dipole moment surfaces, *J. Mol. Spectrosc.*, **327**, 138–158.
Rey, M., Nikitin, A. V., & Tyuterev, V. G., 2017. Accurate theoretical methane line lists in the infrared up to 3000 K and quasicontinuum absorption/emission modeling for astrophysical applications, *ApJ*, **847**, 1.
Rey, M., Nikitin, A. V., Bézard, B., Rannou, P., Coustenis, A., & Tyuterev, V. G., 2018. New accurate theoretical line lists of $^{12}CH_4$ and $^{13}CH_4$ in the 0–13400 cm^{-1} range: Application to the modeling of methane absorption in Titan's atmosphere, *Icarus*, **303**, 114–130.
Rey, M., Viglaska, D., Egorov, O., & Nikitin, A. V., 2023. A

numerical-tensorial "hybrid" nuclear motion hamiltonian and dipole moment operator for spectra calculation of polyatomic nonrigid molecules, *J. Chem. Phys.*, **159**.

Richard, C., Gordon, I., Rothman, L., Abel, M., Frommhold, L., Gustafsson, M., Hartmann, J.-M., Hermans, C., Lafferty, W., Orton, G., Smith, K., & Tran, H., 2012. New section of the HITRAN database: Collision-induced absorption (CIA), *J. Quant. Spectrosc. Radiat. Transf.*, **113**, 1276–1285.

Richard, C., Boudon, V., & Rotger, M., 2020. Calculated spectroscopic databases for the VAMDC portal: New molecules and improvements, *J. Quant. Spectrosc. Radiat. Transf.*, **251**, 107096.

Richard, C., Asselin, P., & Boudon, V., 2022. High-resolution far-infrared synchrotron FTIR spectroscopy and analysis of the ν_7, ν_{19} and ν_{20} bands of trioxane, *J. Mol. Spectrosc.*, **386**, 111614.

Richard, C., Fathallah, O. B., Hardy, P., Kamel, R., Merkulova, M., Rotger, M., Ulenikov, O., & Boudon, V., 2024. CaSDa24: Latest updates to the Dijon calculated spectroscopic databases, *J. Quant. Spectrosc. Radiat. Transf.*, **327**, 109127.

Rimmer, P. B. & Helling, C., 2016. A chemical kinetics network for lightning and life in planetary atmospheres, *ApJS*, **224**, 9.

Rimmer, P. B., Ferus, M., Waldmann, I. P., Knížek, A., et al., 2019. Identifiable acetylene features predicted for young Earth-like exoplanets with reducing atmospheres undergoing heavy bombardment, *ApJ*, **888**, 21.

Rimmer, P. B., Majumdar, L., Priyadarshi, A., Wright, S., & Yurchenko, S. N., 2021. Detectable Abundance of Cyanoacetylene (HC_3N) Predicted on Reduced Nitrogen-rich Super-Earth Atmospheres, *ApJL*, **921**, L28.

Rinsland, C. P., Smith, M. A. H., Russell, J. M., Park, J. H., & Farmer, C. B., 1981. Stratospheric measurements of continuous absorption near 2400 cm^{-1}, *Appl. Opt.*, **20**, 4167–4171.

Rinsland, C. P., Smith, M. A. H., Seals Jr., R. K., Goldman, A., Murcray, F. J., Murcray, D. G., Larsen, J. C., & Rarig, P. L., 1982. Stratospheric measurements of collision-induced absorption by molecular oxygen, *J. Geophys. Res.: Ocean*, **87**, 3119–3122.

Ripamonti, E. & Abel, T., 2004. Fragmentation and the formation of primordial protostars: the possible role of collision-induced emission, *MNRAS*, **348**, 1019–1034.

Rivlin, T., Lodi, L., Yurchenko, S. N., Tennyson, J., & Le Roy, R. J., 2015. ExoMol line lists X: The spectrum of sodium hydride, *MNRAS*, **451**, 5153–5157.

Robert, D. & Bonamy, J., 1979. Short range force effects in semi classical molecular line broadening calculations, *J. Phys.*, **10**, 923–943.

Rocha, W. R. M., Rachid, M. G., Olsthoorn, B., van Dishoeck, E. F., McClure, M. K., & Linnartz, H., 2022. LIDA: The Leiden Ice Database for Astrochemistry, *A&A*, **668**, A63.

Rohart, F., Mäder, H., & Nicolaisen, H.-W., 1994. Speed dependence of rotational relaxation induced by foreign gas collisions: studies on CH_3F by millimeter coherent transients, *J. Chem. Phys.*, **101**, 6475–6486.

Rohart, F., Nguyen, L., Buldyreva, J., Colmont, J.-M., & Wlodarczak, G., 2007. Lineshapes of the 172 and 602 GHz rotational transitions of $HC^{15}N$, *J. Mol. Spectrosc.*, **246**, 213–227.

Roman, M. T., Kempton, E. M.-R., Rauscher, E., Harada, C. K., Bean, J. L., & Stevenson, K. B., 2021. Clouds in three-dimensional models of hot Jupiters over a wide range of temperatures. i. thermal structures and broadband phase-curve predictions, *ApJ*, **908**, 101.

Rooney, C. M., Batalha, N. E., Gao, P., & Marley, M. S., 2022. A new sedimentation model for greater cloud diversity in giant exoplanets and brown dwarfs, *ApJ*, p. 33.

Rose, J. P. & Berry, R. S., 1992. Towards elucidating the interplay of structure and dynamics in clusters: small KCl clusters as models, *J. Phys. Chem.*, **96**, 517–538.

Rothman, L. S., 2021. History of the HITRAN Database, *Nat. Rev. Phys.*, **3**, 302–304.

Rothman, L. S., Jacquemart, D., Barbe, A., Benner, D. C., Birk, M., Brown, L. R., Carleer, M. R., Chackerian Jr, C., Chance, K., Coudert, L. H. e. a., et al., 2005. The HITRAN 2004 molecular spectroscopic database, *J. Quant. Spectrosc. Radiat. Transf.*, **96**, 139–204.

Rothman, L. S., Gordon, I. E., Barber, R. J., Dothe, H., Gamache, R. R., Goldman, A., Perevalov, V. I., Tashkun, S. A., & Tennyson, J., 2010. HITEMP, the high-temperature molecular spectroscopic database, *J. Quant. Spectrosc. Radiat. Transf.*, **111**, 2139–2150.

Roueff, E., Abgrall, H., Czachorowski, P., Pachucki, K., Puchalski, M., & Komasa, J., 2019. The full infrared spectrum of molecular hydrogen, *A&A*, **630**, A58.

Royer, A., 1971. Expansion of the Spectrum in Powers of the Density in the Adiabatic Theory of Pressure Broadening, *Phys. Rev. A*, **3**, 2044.

Ruscic, B., Pinzon, R. E., von Laszewski, G., Kodeboyina, D., Burcat, A., Leahy, D., Montoy, D., & Wagner, A. F., 2005. Active Thermochemical Tables: thermochemistry for the 21st century, *J. Phys. Conf. Ser.*, **16**, 561.

Rutkowski, L., Foltynowicz, A., Schmidt, F. M., Johansson, A. C., Khodabakhsh, A., Kyuberis, A. A., Zobov, N. F., Polyansky, O. L., Yurchenko, S. N., & Tennyson, J., 2018. An experimental water line list at 1950 K in the 6250–6670 cm^{-1} region, *J. Quant. Spectrosc. Radiat. Transf.*, **205**, 213–219.

Ryabchikova, T., Piskunov, N., Kurucz, R. L., Stempels, H. C., Heiter, U., Pakhomov, Y., & Barklem, P. S., 2015. A major upgrade of the VALD database, *Phys. Scr.*, **90**, 054005.

Sadiek, I., Hjältén, A., Senna Vieira, F., Lu, C., Stuhr, M., & Foltynowicz, A., 2020. Line positions and intensities of the ν_4 band of methyl iodide using mid-infrared optical frequency comb Fourier transform spectroscopy, *J. Quant. Spectrosc. Radiat. Transf.*, **255**, 107263.

Sadiek, I., Hjältén, A., Roberts, F. C., Lehman, J. H., & Foltynowicz, A., 2023. Optical frequency comb-based measurements and the revisited assignment of high-resolution spectra of CH_2Br_2 in the 2960 to 3120 cm^{-1} region, *Phys. Chem. Chem. Phys.*, **25**, 8743–8754.

Saito, M., Yang, P., Ding, J., & Liu, X., 2021. A Comprehensive Database of the Optical Properties of Irregular Aerosol Particles for Radiative Transfer Simulations, *J. Atmos. Sci.*, **78**, 2089 – 2111.

Sakellaris, C. N., Miliordos, E., & Mavridis, A., 2011. First principles study of the ground and excited states of FeO, FeO^+, and FeO^-, *J. Phys. Chem.*, **134**, 234308.

Samuelson, R. E., Nath, N. R., & Borysow, A., 1997. Gaseous abundances and methane supersaturation in Titan's troposphere, *Planet Space Sci.*, **45**, 959–980.

Santagata, R., Tran, D. B. A., Argence, B., Lopez, O., et al., 2019. High-precision methanol spectroscopy with a widely tunable SI-traceable frequency-comb-based mid-infrared QCL, *Optica*, **6**, 411–423.

Saumon, D. & Jacobson, S. B., 1998. Pure Hydrogen Model Atmospheres for Very Cool White Dwarfs, *ApJ*, **511**, L107–L110.

Schaefer, L. & Fegley Jr., B., 2005. Silicon tetrafluoride on Io, *Icarus*, **179**, 252–258.

Schaefer, L., Lodders, K., & Fegley, Jr., B., 2012. Vaporization of the earth: Application to exoplanet atmospheres, *ApJ*, **755**, 41.

Schick, H. L., 1960. A Thermodynamic Analysis of the High-temperature Vaporization Properties of Silica, *Chem. Reviews*, **60**, 331–362.

Schmitt, B., Quirico, E., Trotta, F., & Grundy, W. M., 1998. Optical Properties of Ices from UV to Infrared, in *Solar System Ices*, vol. 227 of **Astrophysics and Space Science Library**, pp. 199–240, Kluwer.

Schmitt, B., Bollard, P., Garenne, A., Albert, D., Bonal, L., & Poch, O., 2018. SSHADE: The European solid spectroscopy database infrastructure, in *European Planetary Science Congress*, vol. 12.

Schneider, A. D., Carone, L., Decin, L., Jørgensen, U. G., Mollière, P., Baeyens, R., Kiefer, S., & Helling, C., 2022. Exploring the deep atmospheres of HD 209458b and WASP-43b using a non-gray general circulation model, *A&A*, **664**, A56.

Schroeder, P. J., Pfotenhauer, D. J., Yang, J., Giorgetta, F. R., Swann, W. C., Coddington, I., Newbury, N. R., & Rieker, G. B., 2017. High temperature comparison of the HITRAN2012 and HITEMP2010 water vapor absorption databases to frequency comb measurements, *J. Quant. Spectrosc. Radiat. Transf.*, **203**, 194–205.

Sciamma-O'Brien, E., Roush, T. L., Rannou, P., Dubois, D., & Salama, F., 2023. First optical constants of laboratory-generated organic refractory materials (tholins) produced in the NASA Ames COSmIC facility from the visible to the near infrared (0.4-1.6 μm): Application to Titan's aerosols, *PSJ*, **4**, 121.

Sciamma-O'Brien, E., Drant, T., & Wogan, N., 2024. In an exoplanet atmosphere far, far away, *Nat. Rev. Chem.*, **8**, 157–158.

Seager, S., Bains, W., & Hu, R., 2013. A biomass-based model to estimate the plausibility of exoplanet biosignature gases, *ApJ*, **775**, 104.

Seiff, A., Schofield, J. T., Kliore, A. J., Taylor, F. W., et al., 1985. Models of the structure of the atmosphere of Venus from the surface to 100 kilometers altitude, *Advances in Space Research*, **5**, 3–58.

Seinfeld, J. H. & Pandis, S. N., 2016. *Atmospheric Chemistry and Physics: From Air Pollution to Climate Change*, Wiley.

Selim, T., van der Avoird, A., & Groenenboom, G. C., 2022. Efficient computational methods for rovibrational transition rates in molecular collisions, *J. Phys. Chem.*, **157**, 064105.

Semenov, M., El-Kork, N., Yurchenko, S. N., & Tennyson, J., 2024. ExoMol Line Lists – LXIV: Empirical rovibronic spectra of phosphorous mononitride (PN) covering the IR and UV regions, *MNRAS*.

Serindag, D. B., Nugroho, S. K., Mollière, P., de Mooij, E. J. W., Gibson, N. P., & Snellen, I. A. G., 2021. Is TiO emission present in the ultra-hot Jupiter WASP-33b? a reassessment using the improved ExoMol TOTO line list, *A&A*, **645**, A90.

Shafer, R. & Gordon, R. G., 1973. Quantum scattering theory of rotational relaxation and spectral line shapes in H_2-He gas mixtures, *J. Chem. Phys.*, **58**, 5422–5443.

Sharp, C. M. & Burrows, A., 2007. Atomic and Molecular Opacities for Brown Dwarf and Giant Planet Atmospheres, *ApJS*, **168**, 140.

Sharp, C. M. & Huebner, W. F., 1990. Molecular Equilibrium with Condensation, *ApJS*, **72**, 417.

Sharpe, S. W., Johnson, T. J., Sams, R. L., Chu, P. M., Rhoderick, G. C., & Johnson, P. A., 2004. Gas-Phase Databases for Quantitative Infrared Spectroscopy, *Applied Spectroscopy*, **58**, 1452–1461.

Shayesteh, A., Henderson, R. D. E., Le Roy, R. J., & Bernath, P. F., 2007. Ground state potential energy curve and dissociation energy of MgH, *J. Phys. Chem. A*, **111**, 12495–12505.

Shi, X., Yin, Q.-Z., Gao, H., Chang, Y.-C., Jackson, W. M., Wiens, R. C., & Ng, C.-Y., 2017. Branching Ratios in Vacuum Ultraviolet Photodissociation of CO and N_2: Implications for Oxygen and Nitrogen Isotopic Compositions of the Solar Nebula, *ApJ*, **850**, 48.

Shine, K. P., Campargue, A., Mondelain, D., McPheat, R. A., Ptashnik, I. V., & Weidmann, D., 2016. The water vapour continuum in near-infrared windows – current understanding and prospects for its inclusion in spectroscopic databases, *J. Mol. Spectrosc.*, **327**, 193–208, New Visions of Spectroscopic Databases, Volume II.

Shipman, H. L., 1977. Masses, radii, and model atmospheres for cool white-dwarf stars, *ApJ*, **213**, 138–144.

Shulyak, D., Lara, L. M., Rengel, M., & Nèmec, N.-E., 2020. Stellar impact on disequilibrium chemistry and observed spectra of hot Jupiter atmospheres, *A&A*, **639**, A48.

Siciliani de Cumis, M., Eramo, R., Coluccelli, N., Galzerano, G., Laporta, P., & Cancio Pastor, P., 2018. Multiplexed direct-frequency-comb vernier spectroscopy of carbon dioxide $2\nu_1 + \nu_3$ ro-vibrational combination band, *J. Chem. Phys.*, **148**, 114303.

Silva de Oliveira, V., Silander, I., Rutkowski, L., Soboń, G., Axner, O., Lehmann, K. K., & Foltynowicz, A., 2024. Sub-doppler optical-optical double-resonance spectroscopy using a cavity-enhanced frequency comb probe, *Nature Communications*, **15**, 161.

Sindel, J. P., Gobrecht, D., Helling, C., & Decin, L., 2022a. Revisiting fundamental properties of TiO_2 nanoclusters as condensation seeds in astrophysical environments, *A&A*, **668**, A35.

Sindel, J. P., Gobrecht, D., Helling, C., & Decin, L., 2022b. VizieR Online Data Catalog: TiO_2 nanoclusters fundamental properties (Sindel+, 2022), *VizieR Online Data Catalog*, pp. J/A+A/668/A35.

Sindel, J. P., Helling, C., Gobrecht, D., Chubb, K. L., & Decin, L., 2023. Infrared spectra of TiO_2 clusters for hot Jupiter atmospheres, *A&A*, **680**, A65.

Skinner, J. W. & Cho, J. Y.-K., 2022. Modons on tidally synchronized extrasolar planets, *MNRAS*, **511**, 3584–3601.

Skinner, J. W., Nättilä, J., & Cho, J. Y.-K., 2023. Repeated Cyclogenesis on Hot-Exoplanet Atmospheres with Deep Heating, *Phys. Rev. Lett.*, **131**, 231201.

Smith, M., Benner, D. C., Predoi-Cross, A., & Devi, V. M., 2014. Air-and self-broadened half widths, pressure-induced shifts, and line mixing in the ν_2 band of $^{12}CH_4$, *J. Quant. Spectrosc. Radiat. Transf.*, **133**, 217–234.

Snels, M., Stefani, S., Boccaccini, A., Biondi, D., & Piccioni, G., 2021. A simulation chamber for absorption spectroscopy in planetary atmospheres, *Atmos. Meas. Tech.*, **14**, 7187–7197.

Song, Y., Gao, H., Chang, Y. C., Hammouténe, D., Ndome, H., Hochlaf, M., Jackson, W. M., & Ng, C. Y., 2016. Quantum-state dependence of product branching ratios in vacuum ultraviolet photodissociation of N_2, *ApJ*, **819**, 23.

Sousa-Silva, C., Al-Refaie, A. F., Tennyson, J., & Yurchenko, S. N., 2015. ExoMol line lists - VII. the rotation-vibration spectrum of phosphine up to 1500 K, *MNRAS*, **446**, 2337–2347.

Sousa-Silva, C., Petkowski, J. J., & Seager, S., 2019. Molecular simulations for the spectroscopic detection of atmospheric gases, *Physical Chemistry Chemical Physics (Incorporating Faraday Transactions)*, **21**, 18970–18987.

Spaun, B., Changala, P. B., Patterson, D., Bjork, B. J., Heckl, O. H., Doyle, J. M., & Ye, J., 2016. Continuous probing of cold complex molecules with infrared frequency comb spectroscopy, *Nature*, **533**, 517–520.

Spiering, F. R. & van der Zande, W. J., 2012. Collision induced absorption in the $a^1\Delta$ (v = 2) $\leftarrow X^3\Sigma_g^-$ (v = 0) band of molecular oxygen, *Phys. Chem. Chem. Phys.*, **14**, 9923–9928.

Spiering, F. R., Kiseleva, M. B., Filippov, N. N., van Kesteren, L., & van der Zande, W. J., 2011. Collision-induced absorption in the O_2 B-band region near 670 nm, *Phys. Chem. Chem. Phys.*, **13**, 9616–9621.

Sršeň, Š. & Slavíček, P., 2021. Optimal representation of the nuclear ensemble: Application to electronic spectroscopy, *J. Chem. Theory Comput.*, **17**, 6395–6404.

Sršeň, Š., von Lilienfeld, O., & Slavicek, P., 2023. Fast and accurate excited states predictions: Machine learning and diabatization, *ChemRxiv*.

Stam, D. M., 2008. Spectropolarimetric signatures of Earth-like extrasolar planets*, *A&A*, **482**, 989–1007.

Stankiewicz, K., Stolarczyk, N., Jóźwiak, H., Thibault, F., & Wcisło, P., 2021. Accurate calculations of beyond-voigt line-shape parameters from first principles for the He-perturbed HD rovibrational lines: A comprehensive dataset in the HITRAN DPL format, *J. Quant. Spectrosc. Radiat. Transf.*, **276**, 107911.

Stark, G., Herde, H., Lyons, J. R., Heays, A. N., de Oliveira, N., Nave, G., Lewis, B. R., & Gibson, S. T., 2018. Fourier-transform-spectroscopic photoabsorption cross sections and oscillator strengths for the S_2 B $^3\Sigma_u^-$ – X $^3\Sigma_g^-$ system, *J. Chem. Phys.*, **148**, 244302.

Stefani, S., Piccioni, G., Snels, M., Grassi, D., & Adriani, A., 2013. Experimental CO_2 absorption coefficients at high pressure and high temperature, *J. Quant. Spectrosc. Radiat. Transf.*, **117**, 21–28.

Stefani, S., Snels, M., Piccioni, G., Grassi, D., & Adriani, A., 2018. Temperature dependence of collisional induced absorption (CIA) bands of CO_2 with implications for venus' atmosphere, *J. Quant. Spectrosc. Radiat. Transf.*, **204**, 242–249.

Stefani, S., Piccioni, G., Snels, M., Biondi, D., & Boccaccini, A., 2022a. CO_2 collisional induced absorption (CIA) database, Open Acess INAF.

Stefani, S., Piccioni, G., Snels, M., Biondi, D., & Boccaccini, A., 2022b. Experimental absorption coefficients of carbon dioxide at high pressure and high temperature, Open Acess INAF.

Steffens, B. L., Sung, K., Malaska, M. J., Lopes, R. M. C., Toon, G. C., & Nixon, C. A., 2023. Mid-infrared cross-sections and pseudoline parameters for trans-2-butene (2-C_4H_8), *J. Quant. Spectrosc. Radiat. Transf.*, **310**, 108730.

Stock, J. W., Kitzmann, D., Patzer, A. B. C., & Sedlmayr, E., 2018. FastChem: A computer program for efficient complex chemical equilibrium calculations in the neutral/ionized gas phase with applications to stellar and planetary atmospheres, *MNRAS*, **479**, 865–874.

Stock, J. W., Kitzmann, D., & Patzer, A. B. C., 2022. FastChem 2 : an improved computer program to determine the gas-phase chemical equilibrium composition for arbitrary element distributions, *MNRAS*, **517**, 4070–4080.

Strand, C. L., Ding, Y., Johnson, S. E., & Hanson, R. K., 2019. Measurement of the mid-infrared absorption spectra of ethylene (C_2H_4) and other molecules at high temperatures and pressures, *J. Quant. Spectrosc. Radiat. Transf.*, **222**, 122–129.

Sumlin, B. J., Heinson, W. R., & Chakrabarty, R. K., 2018. Retrieving the aerosol complex refractive index using PyMieScatt: A Mie computational package with visualization capabilities, *J. Quant. Spectrosc. Radiat. Transf.*, **205**, 127–134.

Sung, K. & Varanasi, P., 2005. CO_2-broadened half-widths and CO_2-induced line shifts of $^{12}C^{16}O$ relevant to the atmospheric spectra of Venus and Mars, *J. Quant. Spectrosc. Radiat. Transf.*, **91**, 319–332.

Sung, K., Toon, G. C., Mantz, A. W., & Smith, M. A. H., 2013. FT-IR measurements of cold C_3H_8 cross sections at 7-15 μm for Titan atmosphere, *Icarus*, **226**, 1499–1513.

Sung, K., Toon, G. C., & Crawford, T. J., 2016a. N_2- and (H_2+He)-broadened cross sections of benzene (C_6H_6) in the 7-15 μm region for the Titan and jovian atmospheres, *Icarus*, **271**, 438–452.

Sung, K., Wishnow, E., Venkataraman, M., Brown, L. R., Ozier, I., Benner, D. C., Crawford, T. J., Mantz, A., & Smith, M.-A. H., 2016b. Progress in the measurement of temperature-dependent N_2-N_2 collision-induced absorption and H_2-broadening of cold and hot CH_4, in *AAS/Division for Planetary Sciences Meeting Abstracts #48*, vol. 48, p. 424.11.

Sung, K., Toon, G. C., Drouin, B. J., Mantz, A. W., & Smith, M. A. H., 2018. FT-IR measurements of cold propene (C_3H_6) cross-sections at temperatures between 150 and 299 K, *J. Quant. Spectrosc. Radiat. Transf.*, **213**, 119–132.

Sung, K., Devi, V. M., Benner, D. C., Drouin, B. J., Crawford, T. J., Mantz, A. W., & Smith, M. A. H., 2020. H_2-pressure broadening and frequency shifts of methane in the $\nu_2 + \nu_3$ band measured in the temperature range between 80 and 370 K, *J. Quant. Spectrosc. Radiat. Transf.*, **256**, 107264.

Suto, H., Sogawa, H., Tachibana, S., Koike, C., Karoji, H., Tsuchiyama, A., Chihara, H., Mizutani, K., Akedo, J., Ogiso, K., Fukui, T. & Ohara, S., 2006. Low-temperature single crystal reflection spectra of forsterite, *MNRAS*, **370**, 1599–1606.

Swain, M. R., Tinetti, G., Vasisht, G., Deroo, P., Griffith, C., Bouwman, J., Chen, P., Yung, Y., Burrows, A., Brown, L. R., Matthews, J., Rowe, J. F., Kuschnig, R., & Angerhausen, D., 2009. Water, Methane, and Carbon Dioxide Present in the Dayside Spectrum of the Exoplanet HD 209458b, *ApJ*, **704**, 1616–1621.

Syme, A.-M. & McKemmish, L. K., 2021. Full spectroscopic model and trihybrid experimental-perturbative-variational line list for CN, *MNRAS*, **505**, 4383–4395.

Szabó, G. M., Kálmán, S., Pribulla, T., Claret, A., Mugnai, L. V., Pascale, E., Waltham, D., Borsato, L., Garai, Z., & Szabó, R., 2022. High-precision photometry with Ariel, *Exp. Astron.*, **53**, 607–634.

Szudy, J. & Baylis, W. E., 1975. Unified Franck-Condon treatment of pressure broadening of spectral lines, *J. Quant. Spectrosc. Radiat. Transf.*, **15**, 641–668.

Szudy, J. & Baylis, W. E., 1996. Profiles of line wings and rainbow satellites associated with optical and radiative collisions, *Phys. Rep.*, **266**, 127–227.

Tan, Y., Kochanov, R. V., Rothman, L. S., & Gordon, I. E., 2019. Introduction of Water-Vapor Broadening Parameters and Their Temperature-Dependent Exponents Into the HITRAN Database: Part I—CO_2, N_2O, CO, CH_4, O_2, NH_3, and H_2S, *JGR-Atm*, **124**, 11,580–11,594.

Tan, Y., Skinner, F. M., Samuels, S., Hargreaves, R. J., Hashemi, R., & Gordon, I. E., 2022. H_2, He, and CO_2 Pressure-induced Parameters for the HITRAN Database. II. Line Lists of CO_2, N_2O, CO, SO_2, OH, OCS, H_2CO, HCN, PH_3, H_2S, and GeH_4, *ApJS*, **262**, 40.

Tancin, R. J. & Goldenstein, C. S., 2021. Ultrafast-laser-absorption spectroscopy in the mid-infrared for single-shot, calibration-free temperature and species measurements in low- and high-pressure combustion gases, *Opt. Express*, **29**, 30140.

Tancin, R. J., Chang, Z., Gu, M., Radhakrishna, V., Lucht, R. P., & Goldenstein, C. S., 2020. Ultrafast laser-absorption spectroscopy for single-shot, mid-infrared measurements of temperature, CO, and CH4 in flames, *Opt. Lett.*, **45**, 583.

Taylor, J. & Parmentier, V., 2023. Another look at the dayside spectra of WASP-43b and HD 209458b: Are there scattering clouds?, *MNRAS*, **526**, 2133–2140.

Taylor, R. H., Borysow, A., & Frommhold, L., 1988. Concerning the rototranslational absorption spectra of He-CH_4 pairs, *J. Mol. Spectrosc.*, **129**, 45–58.

Tazaki, R. & Tanaka, H., 2018. Light scattering by fractal dust aggregates. II. Opacity and asymmetry parameter, *ApJ*, **860**, 79.

Tóbiás, R., Furtenbacher, T., Simkó, I., Császár, A. G., Diouf, M. L., Cozijn, F. M. J., Staa, J. M. A., Salumbides, E. J., & Ubachs, W., 2020. Spectroscopic-network-assisted precision spectroscopy and its application to water, *Nature Communications*, **11**, 1708.

Tennyson, J., 2024. Empirical rovibronic energy levels of C_3, *Mol. Phys.*, **122**, e2276912.

Tennyson, J. & Yurchenko, S., 2018. The ExoMol Atlas of Molecular Opacities, *Atoms*, **6**, 26.

Tennyson, J. & Yurchenko, S. N., 2017. Laboratory spectra of hot molecules: Data needs for hot super-Earth exoplanets, *Mol. Astrophys.*, **8**, 1 – 18.

Tennyson, J. & Yurchenko, S. N., 2021. ExoMol at 10, *Astronomy & Geophysics*, **62**, 6.16–6.21.

Tennyson, J., Bernath, P. F., Campargue, A., Császár, A. G., et al., 2014. Recommended isolated-line profile for representing high-resolution spectroscopic transitions (IUPAC Technical Report), *Pure Appl. Chem.*, **86**, 1931–1943.

Tennyson, J., Yurchenko, S. N., Al-Refaie, A. F., Clark, V. H. J., Chubb, K. L., Conway, E. K., Dewan, A., Gorman, M. N., Hill, C., Lynas-Gray, A. E., Mellor, T., McKemmish, L. K., Owens, A., Polyansky, O. L., Semenov, M., Somogyi, W., Tinetti, G., Upadhyay, A., Waldmann, I., Wang, Y., Wright, S., & Yurchenko, O. P., 2020. The 2020 release of the ExoMol database: Molecular line lists for exoplanet and other hot atmospheres, *J. Quant. Spectrosc. Radiat. Transf.*, **255**, 107228.

Tennyson, J., Pezzella, M., Zhang, J., & Yurchenko, S. N., 2023. Data structures for photoadsorption within the ExoMol project, *RASTI*, **2**, 231–237.

Tennyson, J., Furtenbacher, T., Yurchenko, S. N., & Császár, A. G., 2024a. Empirical rovibrational energy levels for nitrous oxide, *J. Quant. Spectrosc. Radiat. Transf.*, **316**, 108902.

Tennyson, J., Yurchenko, S. N., Zhang, J., Bowesman, C. A., Brady, R. P., Buldyreva, J., Chubb, K. L., Gamache, R. R., Gorman,

M. N., Guest, E. R., Hill, C., Kefala, K., Lynas-Gray, A. E., Mellor, T. M., McKemmish, L. K., Mitev, G. B., Mizus, I. I., Owens, A., Peng, Z., Perri, A. N., Pezzella, M., Polyansky, O. L., Qu, Q., Semenov, M., Smola, O., Solokov, A., Somogyi, W., Upadhyay, A., Wright, S. O. M., & Zobov, N. F., 2024b. The 2024 release of the ExoMol database: molecular line lists for exoplanet and other hot atmospheres, *J. Quant. Spectrosc. Radiat. Transf.*, **326**, 109083.

Thalman, R. & Volkamer, R., 2013. Temperature dependent absorption cross-sections of O_2-O_2 collision pairs between 340 and 630 nm and at atmospherically relevant pressure, *Phys. Chem. Chem. Phys.*, **15**, 15371–15381.

Thibault, F., Menoux, V., Doucen, R. L., Rosenmann, L., Hartmann, J.-M., & Boulet, C., 1997. Infrared collision-induced absorption by O_2 near 6.4 μm for atmospheric applications: measurements and empirical modeling, *Appl. Opt.*, **36**, 563–567.

Thibault, F., Ivanov, S. V., Buzykin, O. G., Gomez, L., Dhyne, M., Joubert, P., & Lepere, M., 2011. Comparison of classical, semiclassical and quantum methods in hydrogen broadening of acetylene lines, *J. Quant. Spectrosc. Radiat. Transf.*, **112**, 1429–1437.

Tilly, J., Chen, H., Cao, S., Picozzi, D., Setia, K., Li, Y., Grant, E., Wossnig, L., Rungger, I., & Booth, G. H., 2022. The Variational Quantum Eigensolver: a review of recent research and best practices, *Phys. Rep.*, **986**, 1–128.

Tinetti, G., Vidal-Madjar, A., Liang, M.-C., Beaulieu, J.-P., Yung, Y., Carey, S., Barber, R. J., Tennyson, J., Ribas, I., Allard, N., Ballester, G. E., Sing, D. K., & Selsis, F., 2007. Water vapour in the atmosphere of a transiting extrasolar planet, *Nature*, **448**, 169–171.

Tinetti, G., Drossart, P., Eccleston, P., Hartogh, P., et al., 2018. A chemical survey of exoplanets with ARIEL, *Exp. Astron.*, **46**, 135–209.

Tinetti, G., Eccleston, P., Haswell, C., Lagage, P.-O., et al., 2021. Ariel: Enabling planetary science across light-years.

Ting, W.-J., Chang, C.-H., Chen, S.-E., Chen, H.-C., Shy, J.-T., Drouin, B. J., & Daly, A. M., 2014. Precision frequency measurement of n2o transitions near 4.5 μm and above 150 μm, *Journal of the Optical Society of America B*, **31**, 1954–1963.

Tipping, R. & Poll, J., 1985. Chapter 7 - Multipole Moments of Hydrogen and its Isotopes, in *Molecular Spectroscopy: Modern Research*, pp. 421–446, ed. Rao, K. N., Academic Press.

Tóbiás, R., Diouf, M. L., Cozijn, F. M. J., Ubachs, W., & Császár, A. G., 2024. All paths lead to hubs in the spectroscopic networks of water isotopologues $H_2^{16}O$ and $H_2^{18}O$, *Comms. Chem.*, **7**, 34.

Tobita, S., Leach, S., Jochims, H. W., Rühl, E., Illenberger, E., & Baumgärtel, H., 1994. Single- and double-ionization potentials of polycyclic aromatic hydrocarbons and fullerenes by photon and electron impact, *Can. J. Phys.*, **72**, 1060–1069.

Tonkov, M. V., Filippov, N. N., Bertsev, V. V., Bouanich, J. P., Van-Thanh, N., Brodbeck, C., Hartmann, J. M., Boulet, C., Thibault, F., & Le Doucen, R., 1996. Measurements and empirical modeling of pure CO_2 absorption in the 2.3-μm region at room temperature: far wings, allowed and collision-induced bands, *Appl. Optics*, **35**, 4863–4870.

Trafton, L. M., 1964. The Thermal Opacity in the Major Planets, *ApJ*, **140**, 1340.

Tran, H., Boulet, C., & Hartmann, J.-M., 2006. Line mixing and collision-induced absorption by oxygen in the A band: Laboratory measurements, model, and tools for atmospheric spectra computations, *JGR-Atm*, **111**, D15210.

Tran, H., Boulet, C., Stefani, S., Snels, M., & Piccioni, G., 2011. Measurements and modelling of high pressure pure CO_2 spectra from 750 to 8500 cm^{-1}. I—central and wing regions of the allowed vibrational bands, *J. Quant. Spectrosc. Radiat. Transf.*, **112**, 925–936.

Tran, H., Ngo, N. H., & Hartmann, J.-M., 2013. Efficient computation of some speed-dependent isolated line profiles, *J. Quant. Spectrosc. Radiat. Transf.*, **129**, 199–203.

Trees, V. J. H. & Stam, D. M., 2022. Ocean signatures in the total flux and polarization spectra of earth-like exoplanets, *A&A*, **664**, A172.

Tremblin, P., Amundsen, D. S., Mourier, P., Baraffe, I., Chabrier, G., Drummond, B., Homeier, D., & Venot, O., 2015. Fingering convection and cloudless models for cool brown dwarf atmospheres, *ApJ*, **804**, L17.

Tremblin, P., Amundsen, D. S., Chabrier, G., Baraffe, I., Drummond, B., Hinkley, S., Mourier, P., & Venot, O., 2016. Cloudless Atmospheres for L/T Dwarfs and Extrasolar Giant Planets, *ApJL*, **817**, L19.

Triaud, A. H. M. J., 2005. Private Communication.

Tsai, S.-M., Lyons, J. R., Grosheintz, L., Rimmer, P. B., Kitzmann, D., & Heng, K., 2017. VULCAN: An Open-source, Validated Chemical Kinetics Python Code for Exoplanetary Atmospheres, *ApJS*, **228**, 20.

Tsai, S.-M., Malik, M., Kitzmann, D., Lyons, J. R., Fateev, A., Lee, E., & Heng, K., 2021. A Comparative Study of Atmospheric Chemistry with VULCAN, *ApJ*, **923**, 264.

Tsai, S. M., Lee, E. K. H., Powell, D., et al., 2023. Photochemically produced SO_2 in the atmosphere of WASP-39b, *Nature*, **617**, 483–487.

Tsao, C. J. & Curnutte, B., 1962. Line-widths of pressure-broadened spectral lines, *J. Quant. Spectrosc. Radiat. Transf.*, **2**, 41–46.

Tsuji, T., 1973. Molecular abundances in stellar atmospheres. II., *A&A*, **23**, 411.

Turbet, M., Tran, H., Pirali, O., Forget, F., Boulet, C., & Hartmann, J.-M., 2019. Far infrared measurements of absorptions by CH_4 + CO_2 and H_2 + CO_2 mixtures and implications for greenhouse warming on early Mars, *Icarus*, **321**, 189–199.

Turbet, M., Boulet, C., & Karman, T., 2020. Measurements and semi-empirical calculations of CO_2 + CH_4 and CO_2 + H_2 collision-induced absorption across a wide range of wavelengths and temperatures. Application for the prediction of early Mars surface temperature, *Icarus*, **346**, 113762.

Tyuterev, V., Barbe, A., Mikhailenko, S., Starikova, E., & Babikov, Y., 2021. Towards the intensity consistency of the ozone bands in the infrared range: Ab initio corrections to the S&MPO database, *J. Quant. Spectrosc. Radiat. Transf.*, **272**, 107801.

Underwood, D. S., Tennyson, J., Yurchenko, S. N., Clausen, S., & Fateev, A., 2016a. ExoMol line lists XVII: A line list for hot SO_3, *MNRAS*, **462**, 4300–4313.

Underwood, D. S., Tennyson, J., Yurchenko, S. N., Huang, X., Schwenke, D. W., Lee, T. J., Clausen, S., & Fateev, A., 2016b. ExoMol line lists XIV: A line list for hot SO_2, *MNRAS*, **459**, 3890–3899.

Upadhyay, A., Conway, E. K., Tennyson, J., & Yurchenko, S. N., 2018. ExoMol Molecular linelists – XXV: A hot line list for silicon sulphide, SiS, *MNRAS*, **477**, 1520–1527.

VAMDC, 2014-. Virtual atomic and molecular data centres website, https://vamdc.eu/.

van den Bekerom, D. & Pannier, E., 2021. A discrete integral transform for rapid spectral synthesis, *J. Quant. Spectrosc. Radiat. Transf.*, **261**, 107476.

Vangvichith, M., Tran, H., & Hartmann, J.-M., 2009. Line-mixing and collision induced absorption for O_2-CO_2 mixtures in the oxygen A-band region, *J. Quant. Spectrosc. Radiat. Transf.*, **110**, 2212–2216.

Vaughan, S. R., Gebhard, T. D., Bott, K., Casewell, S. L., et al., 2023. Chasing rainbows and ocean glints: Inner working angle constraints for the Habitable Worlds Observatory, *MNRAS*, **524**, 5477–5485.

Veillet, R., Venot, O., Sirjean, B., Bounaceur, R., Glaude, P.-A., Al-Refaie, A., & Hébrard, E., 2024. An extensively validated C/H/O/N chemical network for hot exoplanet disequilibrium chemistry, *A&A*, **682**, A52.

Venot, O., Hebrard, E., Agundez, M., Dobrijevic, M., Selsis, F., Hersant, F., Iro, N., & Bounaceur, R., 2012. A chemical model for the atmosphere of hot Jupiters, *A&A*, **546**, A43.

Venot, O., Fray, N., Bénilan, Y., Gazeau, M. C., Hébrard, E., Larcher, G., Schwell, M., Dobrijevic, M., & Selsis, F., 2013. High-

temperature measurements of VUV-absorption cross sections of CO_2 and their application to exoplanets, *A&A*, **551**, A131.

Venot, O., Hebrard, E., Agundez, M., Decin, L., & Bounaceur, R., 2015. New chemical scheme for studying carbon-rich exoplanet atmospheres, *A&A*, **577**, A33.

Venot, O., Bénilan, Y., Fray, N., Gazeau, M. C., Lefèvre, F., Essebbar, E., Hébrard, E., Schwell, M., Bahrini, C., Montmessin, F., Lefèvre, M., & Waldmann, I. P., 2018a. VUV-absorption cross section of carbon dioxide from 150 to 800 K and applications to warm exoplanetary atmospheres, *A&A*, **609**, A34.

Venot, O., Drummond, B., Miguel, Y., Waldmann, I. P., Pascale, E., & Zingales, T., 2018b. A better characterization of the chemical composition of exoplanets atmospheres with ARIEL, *Exp. Astron.*, **46**, 101–134.

Venot, O., Cavalié, T., Bounaceur, R., Tremblin, P., Brouillard, L., & Lhoussaine Ben Brahim, R., 2020. New chemical scheme for giant planet thermochemistry - Update of the methanol chemistry and new reduced chemical scheme, *A&A*, **634**, A78.

Verstraete, L., Leger, A., D'Hendecourt, L., Defourneau, D., & Dutuit, O., 1990. Ionization cross-section measurements for two PAH molecules - Implications for the heating of diffuse interstellar gas, *A&A*, **237**, 436–444.

Vicentini, E., Maddaloni, P., Aiello, R., Gambetta, A., Coluccelli, N., Molteni, L. M., Castrillo, A., Gianfrani, L., De Natale, P., Laporta, P., & Galzerano, G., 2020. Absolute frequency metrology of the chf3 8.6-μm ro-vibrational spectrum at 10-11 level, *J. Quant. Spectrosc. Radiat. Transf.*, **248**, 106963.

Vigasin, A. & Mokhov, I., 2017. Greenhouse effect in planetary atmospheres caused by molecular symmetry breaking in intermolecular interactions, *Izv. Atmos. Ocean. Phys.*, **53**, 164–173.

Villanueva, G. L., Liuzzi, G., Aoki, S., Stone, S. W., Brines, A., Thomas, I. R., Lopez-Valverde, M. A., Trompet, L., Erwin, J., Daerden, F., Ristic, B., Smith, M. D., Mumma, M. J., Faggi, S., Kofman, V., Robert, S., Neary, L., Patel, M., Bellucci, G., Lopez-Moreno, J. J., & Vandaele, A. C., 2022. The Deuterium Isotopic Ratio of Water Released From the Martian Caps as Measured With TGO/NOMAD, *Geophys. Res. Lett.*, **49**, e2022GL098161.

Villanueva, G. L., Fauchez, T. J., Kofman, V., Alei, E., et al., 2024. Modeling Atmospheric Lines by the Exoplanet Community (MALBEC) version 1.0: A CUISINES radiative transfer intercomparison project, *The Planetary Science Journal*, **5**, 64.

Villanueva, G. L., Smith, M. D., Protopapa, S., Faggi, S., & Mandell, A. M., 2018. Planetary Spectrum Generator: An accurate online radiative transfer suite for atmospheres, comets, small bodies and exoplanets, *J. Quant. Spectrosc. Radiat. Transf.*, **217**, 86–104.

Vispoel, B. & Gamache, R. R., 2024. Modified Complex Robert-Bonamy calculations of line shape parameters for the CO_2-H_2O collision system, *J. Quant. Spectrosc. Radiat. Transf.*, **316**, 108896.

Visscher, C., Lodders, K., & Bruce Fegley, J., 2006. Atmospheric chemistry in giant planets, brown dwarfs, and low-mass dwarf stars. II. Sulfur and phosphorus, *ApJ*, **648**, 1181.

Visscher, C., Lodders, K., & Fegley, B., 2010. Atmospheric chemistry in giant planets, brown dwarfs, and low-mass dwarf stars. III. Iron, magnesium, and silicon, *ApJ*, **716**, 1060.

Viswanath, G., Narang, M., Manoj, P., Mathew, B., & Kartha, S. S., 2020. A statistical search for star–planet interaction in the ultraviolet using GALEX, *AJ.*, **159**, 194.

Vitali, F., Stefania, S., Piccioni, G., Snels, M., & Grassi, D., 2024. Experimental measurements of the Collision Induced Absorptions of H_2-H_2 and H_2-He in the 3600-5500 cm^{-1} spectral range from 120 to 500 K, *J. Quant. Spectrosc. Radiat. Transf.*, **In press**.

Viti, S., Polyansky, O. L., Zobov, N. F., Tennyson, J., Bernath, P. F., & Wallace, L., 1998. Hot Water on the Sun: Assignments via *ab initio* Line Lists, in *Cool Stars, Stellar Systems, and the Sun*, vol. 154 of **Astronomical Society of the Pacific Conference Series**, p. 718.

Voronin, B. A., Tennyson, J., Tolchenov, R. N., Lugovskoy, A. A., & Yurchenko, S. N., 2010. A high accuracy computed line list for the HDO molecule, *MNRAS*, **402**, 492–496.

Votava, O., Kassi, S., Campargue, A., & Romanini, D., 2022. Comb coherence-transfer and cavity ring-down saturation spectroscopy around 1.65 μm: kHz-accurate frequencies of transitions in the $2\nu_3$ band of $^{12}CH_4$, *Phys. Chem. Chem. Phys.*, **24**, 4157–4173.

Vuitton, V., Yelle, R., Klippenstein, S., Hörst, S., & Lavvas, P., 2019. Simulating the density of organic species in the atmosphere of Titan with a coupled ion-neutral photochemical model, *Icarus*, **324**, 120–197.

Wakeford, H. R. & Sing, D. K., 2015. Transmission spectral properties of clouds for hot jupiter exoplanets, *A&A*, **573**, A122.

Wakeford, H. R., Visscher, C., Lewis, N. K., Kataria, T., Marley, M. S., Fortney, J. J., & Mandell, A. M., 2016. High-temperature condensate clouds in super-hot Jupiter atmospheres, *MNRAS*, **464**, 4247–4254.

Wakeford, H. R., Sing, D. K., Stevenson, K. B., Lewis, N. K., Pirzkal, N., Wilson, T. J., Goyal, J., Kataria, T., Mikal-Evans, T., Nikolov, N., & Spake, J., 2020. Into the UV: A precise transmission spectrum of HAT-P-41b using Hubble's WFC3/UVIS G280 Grism, *AJ.*, **159**, 204.

Wakelam, V., Herbst, E., Loison, J.-C., Smith, I. W. M., et al., 2012. A kinetic database for astrochemistry (KIDA), *ApJS*, **199**, 21.

Wallace, L., Bernath, P., Livingston, W., Hinkle, K., Busler, J., Guo, B., & Zhang, K., 1995. Water on the Sun, *Science*, **268**, 1155–1158.

Wang, F., Changeat, Q., Tinetti, G., Turrini, D., & Wright, S. O. M., 2023a. Constraining the atmospheric elements in hot Jupiters with Ariel, *MNRAS*, **523**, 4365–4380.

Wang, J., Hu, C. L., Liu, A. W., Sun, Y. R., Tan, Y., & Hu, S. M., 2021. Saturated absorption spectroscopy near 1.57 μm and revised rotational line list of $^{12}C^{16}O$, *J. Quant. Spectrosc. Radiat. Transf.*, **270**, 107717.

Wang, R., Balciunaite, U., Chen, J., Yuan, C., Owens, A., & Tennyson, J., 2023b. NASA polynomial representation of molecular specific heats, *J. Quant. Spectrosc. Radiat. Transf.*, **306**, 108617.

Wang, Y., Owens, A., Tennyson, J., & Yurchenko, S. N., 2020a. MARVEL analysis of the measured high-resolution rovibronic spectra of the calcium monohydroxide radical (CaOH), *ApJS*, **248**, 9.

Wang, Y., Tennyson, J., & Yurchenko, S. N., 2020b. Empirical Line Lists in the ExoMol Database, *Atoms*, **8**, 7.

Wargnier, A., Gautier, T., Poch, O., Beck, P., Quirico, E., Buch, A., Drant, T., Perrin, Z., & Doressoundiram, A., 2023. Organic detection in the near-infrared spectral Phobos regolith laboratory analogue in preparation for the Martian Moon eXploration mission, *A&A*, **669**, A146.

Warren, S. G. & Brandt, R. E., 2008. Optical constants of ice from the ultraviolet to the microwave: A revised compilation, *JGR-Atm*, **113**, D14.

Wcisło, P., Thibault, F., Stolarczyk, N., Jóźwiak, H., et al., 2021. The first comprehensive dataset of beyond-Voigt line-shape parameters from ab initio quantum scattering calculations for the HITRAN database: He-perturbed H_2 case study, *J. Quant. Spectrosc. Radiat. Transf.*, **260**, 107477.

Weast, R. C., 1971. *Handbook of Chemistry and Physics, 52nd ed.*, Boca Raton: CRC Press.

Weichman, M. L., Changala, P. B., Ye, J., Chen, Z. J., Yan, M., & Picqué, N., 2019. Broadband molecular spectroscopy with optical frequency combs, *J. Mol. Spectrosc.*, **355**, 66–78.

Weininger, D., 1988. SMILES, a chemical language and information system. 1. Introduction to methodology and encoding rules, *J. Chem. Inf. Comput. Sci.*, **28**, 31–36.

Welbanks & JWST Transiting Exoplanet Community Early Release Science team, 2024. JWST Early Release Science: A Unified Near-Infrared Spectrum of WASP-39b, **To be submitted**.

Wende, S., Reiners, A., Seifahrt, A., & Bernath, P. F., 2010. Crires spectroscopy and empirical line-by-line identification of feh

molecular absorption in an m dwarf, *A&A*, **523**, A58.

Wenzel, G., Joblin, C., Giuliani, A., Rodriguez Castillo, S., Mulas, G., Ji, M., Sabbah, H., Quiroga, S., Peña, D., & Nahon, L., 2020. Astrochemical relevance of VUV ionization of large PAH cations*, *A&A*, **641**, A98.

Western, C. M., 2017. PGOPHER: A program for simulating rotational, vibrational and electronic spectra , *J. Quant. Spectrosc. Radiat. Transf.*, **186**, 221–242.

Western, C. M., Carter-Blatchford, L., Crozet, P., Ross, A. J., Morville, J., & Tokaryk, D. W., 2018. The spectrum of N_2 from 4,500 to 15,700 cm^{-1} revisited with PGOPHER, *J. Quant. Spectrosc. Radiat. Transf.*, **219**, 127–141.

Whiteford, N., Glasse, A., Chubb, K. L., Kitzmann, D., Ray, S., Phillips, M. W., Biller, B. A., Palmer, P. I., Rice, K., Waldmann, I. P., Changeat, Q., Skaf, N., Wang, J., Edwards, B., & Al-Refaie, A., 2023. Retrieval study of cool directly imaged exoplanet 51 Eri b, *MNRAS*, **525**, 1375–1400.

Wilkinson, M. D., Dumontier, M., Aalbersberg, I. J., Appleton, G., et al., 2016. The FAIR Guiding Principles for scientific data management and stewardship, *Sci. Data*, **3**.

Wilson, E. H. & Atreya, S. K., 2004. Current state of modeling the photochemistry of Titan's mutually dependent atmosphere and ionosphere, *J. Geophys. Res.: Planets*, **109**, E06002.

Wilzewski, J. S., Gordon, I. E., Kochanov, R. V., Hill, C., & Rothman, L. S., 2016. H_2, He, and CO_2 line-broadening coefficients, pressure shifts and temperature-dependence exponents for the HITRAN database. Part 1: SO_2, NH_3, HF, HCl, OCS and C_2H_2, *J. Quant. Spectrosc. Radiat. Transf.*, **168**, 193–206.

Wogan, N. F., Batalha, N. E., Zahnle, K. J., Krissansen-Totton, J., Tsai, S.-M., & Hu, R., 2024. JWST observations of K2-18b can be explained by a gas-rich mini-Neptune with no habitable surface, *ApJL*, **963**, L7.

Woitke, P. & Helling, C., 2004. Dust in brown dwarfs - III. Formation and structure of quasi-static cloud layers, *A&A*, **414**, 335–350.

Woitke, P., Helling, C., & Turner, G., 2017. Graphical comparison of mineral gibbs free energy data.

Woitke, P., Helling, C., Hunter, G. H., Millard, J. D., Turner, G. E., Worters, M., Blecic, J., & Stock, J. W., 2018. Equilibrium chemistry down to 100 K - impact of silicates and phyllosilicates on the carbon to oxygen ratio, *A&A*, **614**, A1.

Wong, A., Yurchenko, S. N., Bernath, P., Mueller, H. S. P., McConkey, S., & Tennyson, J., 2017. ExoMol Line List XXI: Nitric Oxide (NO), *MNRAS*, **470**, 882–897.

Wong, A., Bernath, P. F., Rey, M., Nikitin, A. V., & Tyuterev, V. G., 2019. Atlas of Experimental and Theoretical High-temperature Methane Cross Sections from T = 295 to 1000 K in the Near-infrared, *ApJS*, **240**, 4.

Wordsworth, R., Kalugina, Y., Lokshtanov, S., Vigasin, A., Ehlmann, B., Head, J., Sanders, C., & Wang, H., 2017. Transient reducing greenhouse warming on early Mars, *Geophys. Res. Lett.*, **44**, 665–671.

Worters, M., Millard, D., Hunter, G., Helling, C., & Woitke, P., 2017. Comparison catalogue of gas-equilibrium constants.

Wright, S. O. M., Waldmann, I., & Yurchenko, S. N., 2022. Non-local thermal equilibrium spectra of atmospheric molecules for exoplanets, *MNRAS*, **512**, 2911–2924.

Xu, E. & Tennyson, J., 2024. Empirical rovibrational energy levels for carbonyl sulphide, *Mol. Phys.*, **122**, e2279694.

Xue, B.-X., Barbatti, M., & Dral, P. O., 2020. Machine learning for absorption cross sections, *J. Phys. Chem. A*, **124**, 7199–7210.

Yadin, B., Vaness, T., Conti, P., Hill, C., Yurchenko, S. N., & Tennyson, J., 2012. ExoMol Molecular linelists: I The rovibrational spectrum of BeH, MgH and CaH the $X\,^2\Sigma^+$ state, *MNRAS*, **425**, 34–43.

Yang, D., Hu, X., Zhang, D. H., & Xie, D., 2018. An improved coupled-states approximation including the nearest neighbor Coriolis couplings for diatom-diatom inelastic collision, *J. Phys. Chem.*, **148**, 084101.

Yang, J., Irwin, P. G. J., & Barstow, J. K., 2023. Testing 2D temperature models in Bayesian retrievals of atmospheric properties from hot Jupiter phase curves, *MNRAS*, **525**, 5146–5167.

Ycas, G., Giorgetta, F. R., Baumann, E., Coddington, I., Herman, D., Diddams, S. A., & Newbury, N. R., 2018. High-coherence mid-infrared dual-comb spectroscopy spanning 2.6 to 5.2 μm, *Nature Photonics*, **12**, 202–208.

Yousefi, M. & Bernath, P. F., 2018. Line Lists for AlF and AlCl in the $X\,^1\Sigma^+$ Ground State, *ApJS*, **237**, 8.

Yousefi, M., Bernath, P. F., Dulick, M., Birk, M., & Wagner, G., 2021. Line parameters for hot methane ν_3 band broadened by H_2 from 296 to 1100 K., *J. Quant. Spectrosc. Radiat. Transf.*, **263**, 107557.

Yurchenko, S. N. & Tennyson, J., 2014. ExoMol line lists IV: The rotation-vibration spectrum of methane up to 1500 K, *MNRAS*, **440**, 1649–1661.

Yurchenko, S. N., Tennyson, J., Bailey, J., Hollis, M. D. J., & Tinetti, G., 2014. Spectrum of hot methane in astronomical objects using a comprehensive computed line list, *Proc. Nat. Acad. Sci.*, **111**, 9379–9383.

Yurchenko, S. N., Blissett, A., Asari, U., Vasilios, M., Hill, C., & Tennyson, J., 2016. ExoMol Molecular linelists – XIII. The spectrum of CaO, *MNRAS*, **456**, 4524–4532.

Yurchenko, S. N., Amundsen, D. S., Tennyson, J., & Waldmann, I. P., 2017. A hybrid line list for CH_4 and hot methane continuum, *A&A*, **605**, A95.

Yurchenko, S. N., Al-Refaie, A. F., & Tennyson, J., 2018a. ExoCross: A general program for generating spectra from molecular line lists, *A&A*, **614**, A131.

Yurchenko, S. N., Bond, W., Gorman, M. N., Lodi, L., McKemmish, L. K., Nunn, W., Shah, R., & Tennyson, J., 2018b. ExoMol Molecular linelists – XXVI: spectra of SH and NS, *MNRAS*, **478**, 270–282.

Yurchenko, S. N., Sinden, F., Lodi, L., Hill, C., Gorman, M. N., & Tennyson, J., 2018c. ExoMol Molecular linelists – XXIV: A new hot line list for silicon monohydride, SiH, *MNRAS*, **473**, 5324–5333.

Yurchenko, S. N., Szabo, I., Pyatenko, E., & Tennyson, J., 2018d. ExoMol Molecular line lists XXXI: The spectrum of C_2, *MNRAS*, **480**, 3397–3411.

Yurchenko, S. N., Smirnov, A. N., Solomonik, V. G., & Tennyson, J., 2019. Spectroscopy of YO from first principles, *Phys. Chem. Chem. Phys.*, **21**, 22794–22810.

Yurchenko, S. N., Mellor, T. M., Freedman, R. S., & Tennyson, J., 2020a. ExoMol molecular line lists XXXIX: Ro-vibrational molecular line list for CO_2, *MNRAS*, **496**, 5282–5291.

Yurchenko, S. N., Tennyson, J., Miller, S., Melnikov, V. V., O'Donoghue, J., & Moore, L., 2020b. ExoMol molecular line lists XL: Ro-vibrational molecular line list for the hydronium ion (H_3O^+), *MNRAS*, **497**, 2340–2351.

Yurchenko, S. N., Tennyson, J., Syme, A.-M., Adam, A. Y., Clark, V. H. J., Cooper, B., Dobney, C. P., Donnelly, S. T. E., Gorman, M. N., Lynas-Gray, A. E., Meltzer, T., Owens, A., Qu, Q., Semenov, M., Somogyi, W., Upadhyay, A., Wright, S., & Zapata Trujillo, J. C., 2022. ExoMol line lists – XLIV. Infrared and ultraviolet line list for silicon monoxide ($^{28}Si^{16}O$), *MNRAS*, **510**, 903–919.

Yurchenko, S. N., Nogué, E., Azzam, A. A. A., & Tennyson, J., 2023a. ExoMol line lists – IL. Rovibronic spectrum of aluminium monochloride (AlCl), *MNRAS*, **520**, 5183–5191.

Yurchenko, S. N., Szajna, W., Hakalla, R., Semenov, M., Sokolov, A., Tennyson, J., Gamache, R. R., Pavlenko, Y., & Schmidt, M. R., 2023b. ExoMol line lists – LIV: Empirical line lists for AlH and AlD and experimental emission spectroscopy of AlD in A 1Π (v = 0, 1, 2), *MNRAS*, p. stad3802.

Yurchenko, S. N., Bowesman, C. A., Brady, R. P., Guest, E. R., Kefala, K., Mitev, G. B., Owens, A., Perri, A. N., Pezzella, M., Smola, O., Solokov, A., Zhang, J., & Tennyson, J., 2024a. ExoMol Line Lists – LX: Molecular line list for the ammonia isotopologue $^{15}NH_3$, *MNRAS*, **533**, 3442–3456.

Yurchenko, S. N., Brady, R. P., Tennyson, J., Smirnov, A. N., Vasilyev, O. A., & Solomonik, V. G., 2024b. ExoMol line lists –

LIII. Empirical Rovibronic spectra Yttrium Oxide (YO), *MNRAS*, **527**, 4899–4912.

Yurchenko, S. N., Mellor, T., & Tennyson, J., 2024c. ExoMol line lists – LIX. High-temperature line list for N_2O, *MNRAS*.

Yurchenko, S. N., Owens, A., Kefala, K., & Tennyson, J., 2024d. ExoMol line lists – LVII. High accuracy ro-vibrational line list for methane (CH_4), *MNRAS*, **528**, 3719–3729.

Yurchenko, S. N., Szajna, W., Hakalla, R., Semenov, M., Sokolov, A., Tennyson, J., Pavlenko, Y., & Schmidt, M. R., 2024e. ExoMol line lists – LIV. Empirical line lists for AlH and AlD and Emission spectroscopy of AlD in $A\ ^1\Pi$ (v = 0, 1, 2), *MNRAS*, **527**, 9736–9756.

Yurkin, M. A. & Hoekstra, A. G., 2011. The discrete-dipole-approximation code adda: Capabilities and known limitations, *J. Quant. Spectrosc. Radiat. Transf.*, **112**, 2234–2247, Polarimetric Detection, Characterization, and Remote Sensing.

Zahnle, K., Marley, M. S., Morley, C. V., & Moses, J. I., 2016. Photolytic hazes in the atmosphere of 51 Eri b, *ApJ*, **824**, 137.

Zapata Trujillo, J. C. & McKemmish, L. K., 2022a. VIBFREQ1295: A new database for vibrational frequency calculations, *J. Phys. Chem. A*, **126**, 4100–4122.

Zapata Trujillo, J. C. & McKemmish, L. K., 2022b. Meta-analysis of uniform scaling factors for harmonic frequency calculations, *WIREs Comput. Mol. Sci.*, **12**, e1584.

Zapata Trujillo, J. C. & McKemmish, L. K., 2023. Model chemistry recommendations for scaled harmonic frequency calculations: A benchmark study, *J. Phys. Chem. A*, **127**, 1715–1735.

Zapata Trujillo, J. C., Syme, A.-M., Rowell, K. N., Burns, B. P., et al., 2021. Computational infrared spectroscopy of 958 phosphorus-bearing molecules, *Front. Astron. Space Sci.*, **8**.

Zeidler, S., Posch, T., Mutschke, H., Richter, H., & Wehrhan, O., 2011. Near-infrared absorption properties of oxygen-rich stardust analogs - the influence of coloring metal ions, *A&A*, **526**, A68.

Zeidler, S., Posch, T., & Mutschke, H., 2013. Optical constants of refractory oxides at high temperatures - mid-infrared properties of corundum, spinel, and α-quartz, potential carriers of the 13micron feature, *A&A*, **553**, A81.

Zeidler, S., Mutschke, H., & Posch, T., 2015. Temperature-dependent infrared optical constants of olivine and enstatite, *AJ.*, **798**, 125.

Zhan, Z., Seager, S., Petkowski, J. J., Sousa-Silva, C., Ranjan, S., Huang, J., & Bains, W., 2021. Assessment of Isoprene as a Possible Biosignature Gas in Exoplanets with Anoxic Atmospheres, *Astrobiology*, **21**, 765–792.

Zhang, J., Tennyson, J., & Yurchenko, S. N., 2024. PyExoCross: a Python program for generating spectra and cross-sections from molecular line lists, *RASTI*, **3**, 257–287.

Zhang, M., Chachan, Y., Kempton, E. M.-R., Knutson, H. A., & Chang, W. H., 2020. PLATON II: New capabilities and a comprehensive retrieval on HD 189733b transit and eclipse data, *AJ.*, **899**, 27.

Zhao, L., Kaiser, R. I., Xu, B., Ablikim, U., Ahmed, M., Evseev, M. M., Bashkirov, E. K., Azyazov, V. N., & Mebel, A. M., 2018. Low-temperature formation of polycyclic aromatic hydrocarbons in Titan's atmosphere, *Nature Astronomy*, **2**, 973–979.

Zhen, J., Castillo, S. R., Joblin, C., Mulas, G., Sabbah, H., Giuliani, A., Nahon, L., Martin, S., Champeaux, J.-P., & Mayer, P. M., 2016. VUV photo-processing of PAH cations: Quantitative study on the ionization versus fragmentation processes, *ApJ*, **822**, 113.

Zhou, J., Zhao, Y., Hansen, C. S., Yang, J., Chang, Y., Yu, Y., Cheng, G., Chen, Z., He, Z., Yu, S., Ding, H., Zhang, W., Wu, G., Dai, D., Western, C. M., Ashfold, M. N. R., Yuan, K., & Yang, X., 2020. Ultraviolet photolysis of H_2S and its implications for SH radical production in the interstellar medium, *Nature Comm.*, **11**, 1547.

Zimmer, K., Zhang, Y., Lu, P., Chen, Y., Zhang, G., Dalkilic, M., & Zhu, C., 2016. SUPCRTBL: A revised and extended thermodynamic dataset and software package of SUPCRT92, *Comput. Geosci.*, **90**, 97–111.

Zingales, T., Tinetti, G., Pillitteri, I., Leconte, J., Micela, G., & Sarkar, S., 2018. The ARIEL mission reference sample, *Exp. Astron.*, **46**, 67–100.

Zobov, N. F., Shirin, S. V., Ovsyannikov, R. I., Polyansky, O. L., Barber, R. J., Tennyson, J., Bernath, P. F., Carleer, M., Colin, R., & Coheur, P.-F., 2008. Spectrum of hot water in the 4750-13000 cm^{-1} wavenumber range (0.769-2.1μm), *MNRAS*, **387**, 1093–1098.

Zolot, A. M., Giorgetta, F. R., Baumann, E., Swann, W. C., Coddington, I., & Newbury, N. R., 2013. Broad-band frequency references in the near-infrared: Accurate dual comb spectroscopy of methane and acetylene, *J. Quant. Spectrosc. Radiat. Transf.*, **118**, 26–39.